GPS-AEROTRIANGULATION:
IN OBSERVATION SPACE

BY

OZSEN CORUMLUOGLU

B.Sc. (YU); M.Sc. (SU)

NEWCASTLE UNIVERSITY LIBRARY
---
097 51554 7

Thesis L6048

Thesis submitted for the Degree of
Doctor of Philosophy

Department of Geomatics
University of Newcastle upon Tyne
February 1998

ABSTRACT

The research completed on GPS-aerial triangulation has been focused on combining of GPS and photogrammetric data in the way using GPS derived antenna coordinates, so called as "combination in position space". Thus, these antenna coordinates are used, or replaced with the normal control points on the ground, as control points which have been moved into the air. It was noticed that it is necessary to use crossing strips and introduce drift parameters into the analytical aerial triangulation estimation to compensate the shifts which are seen in these coordinates, probably caused by cycle slips in the GPS data. GPS offered a good opportunity to supplement, or completely replace, the ground control required by aerial triangulation procedures by determining the positions of an antenna onboard the aircraft, at each moment of exposure, quickly, cheaply and accurately but with crossing strips, drift parameters and stand-by GPS data, postprocessed GPS data as GPS derived antenna coordinates.

This thesis offers a new method which is based on a combination of GPS dual frequency phase observations and photogrammetric measurements in a bundle estimation process, so called as "combination in observation space". Thus the new method leads to the solution of the redundancy problem facing the GPS users if the ambiguities and the point coordinates (or coordinate differences) together with the other parameters are to be solved for simultaneously. It also removes the need for cross strips to compensate for shifts in the antenna coordinates and provides a good basis for the determination of integer ambiguities and cycle slips thereby saving a lot of effort and time. To explain this concept, the thesis reviews the GPS double differencing processes based upon phase observations and analytical aerial triangulation estimation method with emphasis being laid upon estimation using bundles. Alongside these, error sources that are likely to affect the GPS and bundle measurements are discussed and the new combination method is explained. The ability of the combined system to solve for the perspective center coordinates and the attitude of the camera onboard the aircraft, the coordinates of object points and integer ambiguities and to determine cycle slips in the way it propagates several random errors were the focus of the simulated tests carried out. The tests revealed the high

potential of the combined system in relation to this. Although the system may be regarded as a reasonably sensitive method to solve for these parameters simultaneously as there are some cases where some of these parameters, especially integer ambiguities, cannot be solved for correctly or cycle slips cannot be detected. This is thought not to be a disadvantage of the method itself, but is rather due to weak geometry or insufficient observations with the small sample used.

The main conclusion from this work is that a combination of GPS and photogrammetry is indeed possible in observation space. The advantage in that cycle slips and integer ambiguities can be solved for (i.e. photogrammetry is contributing to GPS - not just the other way around as in the usual case) and additional photogrammetric data (in the form of cross strips) is not needed. The method has been to be successful even in the presence of severe multipath (up to 5 cm).

ACKNOWLEDGMENTS

I would like to express my sincere gratitude and thanks to those who helped me and to Professor Paul Cross for his supervision, help, supportive discussion and constant encouragement throughout my research and I truly feel I am indebted to them. A special thanks must go to Professor Paul Cross again for his kindness of proof reading and correcting of this thesis even after he left the Newcastle University.

My thanks are also due to Dr. Simon Corbett for his invaluable help during the research, to the other members of staff, to Mr. Ian Newton for their help, to the post-graduate colleagues, in particular, Dr. A.M. Ibrahim, Dr. M. Sahin, Dr. C. Mekik, Dr. R.N. Celik, Dr. Y.M.H. Al-Haifi and those of the geodesy group for their useful discussions and advice.

This research has been sponsored by the Turkish Government on behalf of the University of Selcuk, to whom all I am thankful for financing my scholarship and for giving me this opportunity to update and increase my knowledge.

Finally, I am greatly indebted to my father, mother, twin sister, brother and sister for their endlessly support and encouragement during the research years, to my wife Yasemin for her constant encouragement, patience and suffering and to my children R. Betul, R. Faruk, N. Hafsa and E. Fatih for their suffering during the research period, and it is to them whom I dedicate this thesis.

LIST OF CONTENTS

ABSTRACT i

ACKNOWLEDGEMENTS iii

LIST OF CONTENTS iv

1. INTRODUCTION 1

1.1 OVERVIEW 1

1.2 RESEARCH BACKGROUND AND TIIESIS OBJECTIVES 6

1.3 THESIS AIM AND METHODOLOGY 11

1.3.1 THE AIM 11

1.3.2 METHODOLOGY 11

2. FUNDAMENTALS OF AIRBORNE KINEMATIC GPS AND AERIAL PHOTOGRAPHY 13

2.1 INTRODUCTION 13

2.2 CONSTELLATION OF GPS 14

2.3 GPS MEASUREMENTS 14

2.3.1 PSEUDO-RANGE 15

2.3.2 CARRIER PHASE 15

2.3.2.1 Range Difference 17

2.4 GPS POSITIONING 18

2.4.1 THE NAVIGATION SOLUTION 18

2.4.2 GPS ERROR SOURCES 18

2.4.2.1 Satellite Error Sources 19

2.4.2.1.1 Ephemeris Errors 19

2.4.2.1.2 Satellite clock 20

2.4.2.1.3 Impact of SA and A-S 20

2.4.2.1.3.1 Selective Availability (SA) 20

2.4.2.1.3.2 Anti-spoofing (A-S) 21

2.4.2.2 Propagation Error Sources 21

2.4.2.2.1 The Ionospheric Error 22

2.4.2.2.2 The Tropospheric Error 22

2.4.2.2.3 Multipath 23

2.4.2.3 Receiver Error Sources 24

2.4.2.3.1 Antenna Error Sources 25
2.4.2.3.2 Receiver Clock Error Sources 25
2.4.2.3.3 Measurement Error 25
2.4.2.4 Error of Earth Surface Kinematics 26
2.4.2.5 Algorithmic Error Sources 26
2.4.2.5.1 Cycle Slip 26
2.4.2.5.2 Integer Ambiguity 27
2.4.2.6 Other Error Sources 28
2.5 DIFFERENTIAL GPS POSITIONING 28
2.5.1 THE DOUBLE DIFFERENCING OF PHASE OBSERVABLES 29
2.6 AERIAL TRIANGULATION 35
2.6.1 DEFINITION 35
2.6.2 ESTIMATION METHODS 36
2.6.2.1 Bundle Estimation 36
2.6.3 FACTORS AFFECTING THE ACCURACY OF AERIAL TRIANGULATION 40
2.6.3.1 Systematic Errors 40
2.6.3.1.1 Comparator Errors 41
2.6.3.1.2 The Principal point Displacement 42
2.6.3.1.3 Lens Distortions 42
2.6.3.1.4 Atmospheric Refraction 42
2.6.3.1.5 Earth Curvature 43
2.6.3.2 Other Factors 43
2.6.3.2.1 The Type of Camera 43
2.6.3.2.2 The Scale of Photography and Flying Height 44
2.6.3.2.3 Identification and Transfer of Points 44
2.6.3.2.4 Type of Photographic Coverage 45
2.6.3.2.5 Type of Triangulation and Instruments 45
2.6.3.2.6 Distribution and Accuracy of Control Points 46
2.6.3.2.7 The Use of Auxiliary Data 47
2.6.3.2.8 Screening Gross Errors 47
2.6.3.3 Random Errors 47

2.6.3.4 Gross Errors 48

3. COMBINATION OF AERIAL PHOTOGRAPHY AND GPS: IN OBSERVATION SPACE 49
3.1 INTRODUCTION 49
3.2 SPECIFIC PROBLEMS IN AIRBORNE GPS 51
3.2.1 Spatial Offset 51
3.2.2 Time Offset 53
3.2.3 Datum Problems 55
3.2.4 Data Flow 56
3.2.5 Initial Phase Ambiguity 56
3.2.6 Cycle Slips and Discontinuities 57
3.3 CURRENT APPLICATIONS IN PHOTOGRAMMETRY USING GPS 58
3.3.1 AIRCRAFT NAVIGATION AND PIN-POINTING 59
3.3.2 DETERMINATION OF CAMERA ATTITUDE AND POSITION 61
3.3.2.1 Determination of Camera Positions by Using GPS 62
3.3.2.1.1 Current Researches 63
3.3.2.2 Determination of Camera Attitude 68
3.3.2.2.1 Current Research 71
3.4 COMBINATION OF THE SYSTEMS IN BUNDLE BLOCK ESTIMATION. 71
3.4.1 Introduction 71
3.4.2 Least Squares Estimation 73
3.4.3 Observation equations 77
3.5 NEW APPROACH TO THE COMBINATION OF GPS AND PHOTOGRAMMETRIC DATA IN A BUNDLE ADJUSTMENT: COMBINATION IN OBSERVATION SPACE 86
3.5.1 Observation Equations 86

4. SOFTWARE DESIGN FOR COMBINATION OF GPS AND AERIAL PHOTOGRAMMETRY IN OBSERVATION SPACE 96
4.1 INTRODUCTION 96
4.2 MATHEMATICAL MODEL 96
4.3 STRUCTURE AND FLOW CHART 97

4.3.1 INPUT DATA FILES AND DATA SIMULATIONS 99
4.3.2 FORMATION OF MATRICES AND LEAST SQUARES ESTIMATION PROCESS 104
4.3.3 THE W-TEST 113
4.3.4 MARGINALLY DETECTABLE ERRORS 114
4.4 DATA SIMILATION 119
4.4.1 GENERATING RANDOM ERRORS 123
4.4.2 TEST DATA 124

5. CHAPTER FIVE 126
5.1 DEMONSTRATION THAT THE NEW COMBINED SYSTEM WORKS 126
5.1.1 TEST OBJECTIVES 126
5.1.2 TEST SET-UP 126
5.1.3 PROCEDURE 126
5.1.4 TEST RESULTS 127
5.1.5 DISCUSSION OF RESULTS 130
5.1.6 SUMMARY 133
5.2 DESCRIPTION OF THE MAXIMUM ERROR LEVELS IN THE NEW COMBINED SYSTEM 135
5.2.1 TEST OBJECTIVES 135
5.2.2 TEST SET-UP 135
5.2.3 PROCEDURE 135
5.2.4 TEST RESULTS 136
5.2.5 DISCUSSION OF RESULTS 141
5.2.6 SUMMARY 145

6. CHAPTER SIX 146
6.1 VARIATIONS IN RELIABILITY AND PRECISION OF THE SYSTEM ACCORDING TO THE SPECIFIED VARIOUS ERRORS IN PHOTO MEASUREMENTS AND PHASE OBSERVABLES 146
6.1.1 TEST OBJECTIVES 146
6.1.2 TEST SET-UP 146
6.1.3 TEST PROCEDURE 146

6.1.4 RESULTS OF THE TEST 147
6.1.5 DISCUSSION OF RESULTS 157
6.1.6 SUMMARY 162

6.2 VARIATIONS IN THE RELIABILITY AND PRECISION OF THE SYSTEM WITH ADDITIONAL AMBIGUITY PARAMETERS 164
6.2.1 Test Objectives 164
6.2.2 Test Set-up 164
6.2.3 Procedure 164
6.2.4 Results of the test 165
6.2.5 Discussion of Results 174
6.2.6 Summary 179

7. CHAPTER SEVEN 182
7.1 IDENTIFICATION OF CYCLE SLIPS AND PRECISION ANALYSIS OF THE SYSTEM 182
7.1.1 Test Objectives 182
7.1.2 Test Set-up 182
7.1.3 Test Procedure 183
7.1.4 Results of the test 183
7.2 Discussion of Results 193
7.3 Summary 197

8. CONCLUSIONS AND SUGGESTIONS FOR FURTHER WORK 199
8.1 SUMMARY 207

9. REFERENCES AND BIBLIOGRAPHY 209

A. DERIVATION OF COLLINEARITY EQUATIONS 216
A.1 PHOTOGRAMMETRIC COORDINATE SYSTEM 216
A.2 THREE DIMENSIONAL COORDINATE ROTATION 217
A.3 DEVELOPMENT OF THE COLLINEARITY CONDITION EQUATIONS . 221

B. LINEARIZATION OF THE MODIFIED COLLINEARITY EQUATIONS 224

CHAPTER ONE

1. INTRODUCTION

1.1 OVERVIEW

Kinematic methods, especially the methods using GPS, have been widely and rapidly applied into geodesy, photogrammetry and surveying disciplines and numerous applications in these areas currently takes their places in this newly opened field. The consistent build-up of the GPS satellites until the constellation reached its full operational capacity (FOC) on 17 July, 1995, the advances in GPS receiver technology, the developments in the ambiguity resolution techniques and the advances in radio communications have also combined to make GPS a competitive system to conventional survey methods when high productivity and accuracy are sought.

In the field of photogrammetry using conventional methods, it is necessary to carry out a ground control survey in order to deduce the position and orientation of each photograph so that the photographed object can be spatially defined. During any ground control survey it is almost always possible to experience great difficulties especially when the object is remote, hazardous or inaccessible. Reducing the amount of ground control and increasing the quality of the coordinates determined using analytical triangulation estimation methods, have also been two of the major goals of the photogrammetric community. To assist in this, one school of thought has been to integrate data obtained using auxiliary systems with those obtained from photogrammetric systems. If additional control, which is not as expensive as the determination of ground control points, is available and if this can give the accuracy generally obtained using ground control points, then the two goals are achieved.

During the past few years, two further developments have made a large impact on photogrammetric aerial triangulation estimation procedures. These are:

- Rapid development in the field of computer technology. e.g. the development of pentium chips.

- The introduction of the **G**lobal **P**ositioning **S**ystem (**GPS**).
- Digital techniques leading to automatic aerial triangulation measurement.

These two developments have led to the use of analytical aerial triangulation for the purpose of providing control points and the determination of the exterior orientation parameters very attractive. The capability of the measuring unit by the analytical plotters for image coordinate measurement are about to reach the one micron level of precision. The introduction of fast and reasonably cheap personal computers with large memory have also made it possible to process large data sets. GPS is expected to have a great influence on the analytical aerial triangulation procedures that are used now. So, according to the research carried out so far, GPS can be used to obtain:

- The coordinates of exposure stations at the instant of exposures.
- Attitude of the aircraft and, therefore, attitude of the aerial camera onboard the aircraft.
- Pin-pointed photographs and accurate overlaps as a result of accurate navigation.

As has been proven in the early research (e.g. as in Ackermann's (1994) and Corbett's (1994) works), the requirement for photogrammetric ground control especially in such cases as those mentioned above is removed by the use of GPS derived camera positions and orientations. This is the main reason of utilising GPS to help aerial photogrammery in recent applications. This early combination method for GPS and photogrammetry has also brought its own problems besides its advantages. As discussed by the researchers who studied this method, for example Ackermann (1992a and 1992b), in such method it is necessary to compensate some systematic errors by using drift parameters introduced into the bundle estimation as additional unknowns and further more by flying crossing strips or locating extra ground control points.

The applications of the Global Positioning System (GPS) on aerial triangulation studies in photogrammetry that use GPS derived antenna positions as controls points moved up into the air is well appreciated and documented over the few recent years. For more information see, for example, Ackermann (1994).

So, this currently adopted approach which only uses GPS derived camera coordinates can never be more than a one way process and one that has been shown by many

researchers to have inherent uncontrolled errors as mentioned above (hence the use of completely arbitrary drift-rate parameters).

In this research, an extremely novel approach is suggested as it will enable the photogrammetrically derived information to feed directly back into the raw GPS observables, so helping with integer ambiguities and identification of cycle slips by means of the method that allows the combination of GPS phase observables and photogrammetric observables in observation space instead of combining them in point space as has already been done by some researchers as discussed above. So, the main objective of this research is to develop a methodology which enables the combination of GPS dual frequency double differenced phase observables and photogrammetric coordinates in observation space in an adjustment for aerial triangulation purposes to produce the spatial position and orientation of a camera at each exposure and the coordinates of the object points, integer ambiguities and to correct any cycle slips that exist in the GPS data.

Before combining GPS and photogrammetric data in a combined GPS-aerial triangulation bundle estimation model, even in both methods, GPS data must be corrected for the time offset between the GPS time of fix and the instant of exposure and the photogrammetric equations, the so-called collinearity equations, used in the system must also be modified for the spatial offset between the phase center of the GPS antenna and the perspective center of the camera onboard the aircraft. The first problem can be overcame by using modern receivers with a photogrammetric timing option. When the coordinates of image points obtained from individual photographs (bundles) and the GPS phase data corrected for the time offset or obtained by the modern receiver with photogrammetric option are formulated to form a unified mathematical model, a combined system is said to have been set up. When the data of this system are processed simultaneously, a combined GPS-aerial triangulation bundle estimation is said to have been performed. The following explains the good reasons behind why such a combined system is set up.

In general:

- The measured photo coordinates of image points and the coordinates of the available ground control points and precision of all these points constitutes the

major required input data for any aerial triangulation bundle estimation process. The establishment of these ground control points is a significant part of the total cost of aerial triangulation, especially if the photographs are to be acquired and ground control determined in rugged mountainous areas with steep slopes or in remote rural areas with no road access as can be experienced in many underdeveloped countries where this costs can be treated as prohibitive. Areas with well established geodetic control should also be considered, especially if the area is of some size. The targeting work is time consuming and expensive too. According to Jacobsen (1993), these costs might be reach up to 60% of the overall cost of mapping using aerial triangulation.

- In most cases, the coordinates of the ground control points may be available but the precision information of the coordinates may not be available from the same firm. An access to all these information might sometimes be very difficult and special effort and time are needed (for security reasons, as an example). For this reason the provision of ground control points also constitutes the most time consuming part of the mapping process using aerial triangulation methods.

- The most important factors in aerial triangulation are quality, money and time. Also, the other activity consuming a large amount of time and money in any surveying mission is the determination of point coordinates. Therefore, an aerial triangulation is preferred instead of ground surveying methods. Its use substantially reduces the time consumed and the large financial cost by reducing the number of ground control points required for the photogrammetric process.

- Many parts of the world have not yet been mapped in detail suitable for planning. In the future it may be necessary to develop the planning and collection of relevant information for these areas in a short period of time.

- In the construction of infrastructures of a country such as highways, railways etc., time is the dominant factor because the basic information required for all planning stages should be available immediately. Provision of such information speedily will probably affect the economy of the country.

- In the past, there were no practical instruments and methods which could supply the data sufficiently accurately to fill the gap due to reduced or removed ground control.

In the cases where the new combined system is used:

- Using the new method to combine GPS and photogrammetric data will remove the need for the extra strip lines known as crossing strips. In the method using GPS derived camera coordinates it is necessary to fly these cross strips to save the system from the shifts appearing in the coordinates of the antenna on the plane caused by the systematic errors due most probably to incorrect ambiguities in the GPS data. The shifts are estimated by introducing drift parameters into the estimation process.
- In the new method it is unnecessary to introduce these drift parameters into the estimation process. The new system can also determine and then correct cycle slips in the GPS data.
- There is also no need to solve initial integer ambiguities by keeping the antenna onboard the aircraft stationary in the airport before take off. They can be estimated in the combined GPS-aerial triangulation bundle estimation.

Considering the previous research (e.g. as in Ackermann's (1994) and Corbett's (1994) works), four control points on the corners of a photogrammetric block can be required to establish the datum in most cases. However, the primary reason behind the application of the combined system is in general considerable reduction in the number of ground control points required. In addition to this it is suggested in the new combined system that the crossing strips is unnecessary. This will also save more money and time than being in the previous method. Since the essential motive powers behind the use of combined GPS-aerial triangulation bundle block estimation are economy and time.

Although standard code-based DGPS using post-processing methods has high accuracy potential, it is essential to use phase GPS in a relative mode with photogrammetric observations and to establish a reference station on the ground near to the area of photography. The two receivers, the one onboard the aircraft and the other at the reference station, are used to collect data simultaneously and at the same rate. Relative positioning eliminates or reduces most of the GPS errors, e.g. atmospheric delays and orbit errors, provided that the reference receiver is not too far away from the photogrammetric area (maximum 10-20 km depending on ionospheric conditions).

1.2 RESEARCH BACKGROUND AND THESIS OBJECTIVES

In the last decade, much research has been undertaken and also some of it is still underway, investigating the application of GPS into photogrammetry. These applications can be given as aircraft navigation for the determination of flight lines and especially in the aerial triangulation as GPS camera positioning, attitude determination and determination of ground control points and hence determination of chosen object points.

It is necessary to determine preplanned flight lines in order to prevent gaps in the photography being experienced during a flight mission. The most comprehensive devices which lets the pilot to follow the flight lines may be applied to visual navigation for verification purposes only by using GPS. In fact, determination of ground control points is not a part of photogrammetric process. It can be performed independently using classical GPS static survey methods.

In an aerial triangulation process performed for determination of the ground points' coordinates, the number of necessary ground control points may be reduced to some by the use of a combined system, e.g. it utilizes from GPS in the way as explained earlier. If such a system is available they can even be removed since ground control will only be necessary for the datum transformation between photogrammetric system and GPS. Likewise, in the combined method, the camera perspective centers derived from GPS are treated as control points moved up into the air. The attitude of the aircraft, and therefore the attitude of the camera can also be determined by setting up four GPS antenna onboard the plane and computing the rotation angles of the aircraft utilizing from the coordinates of these antennas.

There are a number of simulated studies and tests that have been carried out on GPS supported aerial triangulation (Ackermann (1992a, 1992b, 1994), Becker et al. 1993, Blankenberg 1995, Cannon et al. 1992, Colomina 1993, Corbett and Short 1993, Curry et al. 1993, Faig et al. 1989, Hogholen 1993, Jacobsen 1993, Merchant DC 1993). Thus GPS has already proved useful in photogrammetric applications.

However, most of the research has generally concentrated on the manner in which determination of the position of camera exposure stations is to be used instead of

ground control points in order to reduce the number of them, the attitude of the aircraft and precision and reliability analysis of the system. So, Ackermann as one of the first researchers has carried out a large amount of work on determination of camera perspective centers using differential kinematic GPS (DKGPS) positioning technique. When he compared coordinates of camera perspective centers derived from GPS and standard photogrammetry, he found some systematic errors causing a shift in these coordinates. To correct this shift Ackermann suggested the use of linear drift parameters. When he used a different set of drift parameters for each strip of photography, he discovered one of the main disadvantages of the combined system. Then he came up with a conclusion that it was necessary to fly extra flight lines or have extra ground control in order to have a solution. The systematic errors in the GPS positions changing from strip to strip, caused by unavoidable cycle slips during turn of the aircraft from one flight strip to the next can be determined in a combined adjustment based on only four control points at the block corners if the block is stabilized by at least two crossing strips. Also under conditions of usual production a ground accuracy at the level of approximately 10 cm or even better can be reached. So that, it is necessary to be careful also with smaller components of the solution which can cause a loss of accuracy like the interpolation of the projection centers as a function of time between the not synchronized GPS-recordings.

The work outlined in this thesis has attempted to overcome the problems, that have been experienced in GPS-aerotriangulation so far, by combining the GPS phase observations with photogrammetric coordinates in observation space. As results of this approach, cross strips would be unnecessary, identification of cycle slips would be fulfilled and those drift parameters would be removed from the combined bundle block estimation. Although there are also other opinions on the source of these drift parameters. One of them argues that these GPS drift parameters are cumulative effects of errors in the interior orientation of the metric camera and residual errors from coordinates transformation (Gruen et al. 1993). But the generally accepted opinion is that incorrect ambiguities and cycle slips are the sources of these errors.

The combined block adjustment should be made by the bundle solution. The iterative independent model block adjustment solution cannot be used. Even a 7-parameter independent model block adjustment solution should be avoided because this will lead to an unnecessary loss of accuracy.

For large scale mapping and height determination GPS-positioning has to be based on the carrier phases. This is because the accuracy obtained by the use of C/A code is limited to ±1m up to ±2m. All carrier phase GPS positioning needs a local reference station, which need not be provided by the organization carrying out the photogrammetry (e.g. national reference stations might be used if they are sufficiently close and have sufficiently high data rate).

The growing number of satellites makes the use of GPS kinematic positioning for photogrammetric purposes more easy. At least four satellites are required for three dimensional positioning. An alteration in the constellation of the satellites during a flight strip should not be a problem with the suggested method in this thesis as the number of redundant equations would be sufficient to gain the desired solution in most cases.

As mentioned above the combined block adjustment with GPS derived projection center coordinates has been well documented up to now. The techniques used in this method were more or less the same. The stripwise shifts and also often drifts have to be determined by additional unknowns (3-6 per strip). If the block is stabilized by two crossing strips, totally four ground control points are sufficient, i.e. one in each block corner. That means, GPS-positions are only used for interpolation within the strips. This also solves the datum problem between the WGS84 used for GPS and the local coordinate system. The differences in the results of the combined block adjustments were mainly explained by the number of used satellites, quality of the receivers which today do have less noise than some years ago and the quality of the independent check points.

An Inertial Navigation System (INS) can also be used in some airborne kinematic GPS positioning applications to enhance the accuracy and in order to reduce the number of unknowns in the combined adjustment. The high short term accuracy of INS can support the ambiguity resolution after loss of reference or multipath effect. In such a case not only a good relative accuracy but also good absolute accuracy can be reached and the number of unknowns can be reduced to only three shift parameters for the whole block. Since an INS is very expensive, they are not commonly used by the civilian community.

If GLONASS is available, it can be used together with the combined system. This new system with the increased number of satellites (e.g. even today at least 15 usable satellites) by the means of GLONASS improves the quality of airborne kinematic GPS-positioning. It means that the problem of cycle slips can also be solved more flexibly than today, and the maximal size of PDOP can be reduced to 2.83 which is much better than average value of 5.33 if just the GPS-satellites are used. But the problem of the different reference systems (WGS84 and the Soviet Geodetic System SGS85) and unsynchronized onboard time scales must be solved. A combined receiver can also be used to overcome this problems.

Corbett (1995) has focused his research on a single epoch ambiguity resolution algorithm to resolve the GPS phase ambiguities with one epoch of dual frequency GPS data to remove the drift parameters to compensate the shifts in the GPS derived camera coordinates. Four antenna onboard the aircraft were used in order to derive rotation angles of the camera. As these would lead the aerial triangulation process much easier than before with known rotation angles and perspective center coordinates. So that the only thing left to be solved by collinearity equations is the coordinates of new object points unless there is a remaining shift in the camera coordinates derived from GPS with single epoch ambiguity resolution. He has also carried out a study on the expected double difference phase residual due to multipathing caused by the airframe. It is in the order of ten millimeters, and at worst 0.1 L1 cycles. This will be a limit on the achievable accuracy, since it cannot be removed through differencing. Not all of this error will only go directly into position, but also the errors due to the additional double difference residuals "averaging out" in the least squares computation. In his research it is also stated that the correct single ambiguity resolution (and therefore the correct coordinates) for a pair of GPS antennas on the aircraft has been possible for between 70-90% of the time. For the rest of the observation period the ambiguities and the coordinates of the antennas have not been solved correctly. An increase in noise in the phase measurements, the distance from the known receiver, or the approximate positions are given as reasons to this. So, these are sufficient reasons to develop a method which will enable the combination of digital photogrammetric data with GPS phase measurements in order to make position and attitude solutions more robust.

As it is suggested in this thesis that most of the disadvantages experienced in the methods and the systems used in the past as explained above can be overcome by the new combination method with a newly developed bundle adjustment which uses GPS

dual frequency phase observations and photogrammetric coordinates to combine them in observation space. So the main aim of the thesis is to remove the cross strips or ground control which are necessary in the currently used GPS aerial triangulation although they are most cost effective factors in the aerial triangulation using GPS. These strips and the ground control are only necessary to compensate the shift in the camera positions probably caused by cycle slips. So that, the drift parameters added into the combined bundle block adjustment can then be removed.

If integer ambiguities and cycle slips in the GPS observations could correctly be solved for as in the suggested method, there would not be any necessity to solve for drift parameters, which are put into the adjustment because of the drift in the GPS-derived camera positions (due to initial ambiguities being incorrect), and therefore to fly cross strips or to have the ground control to compensate them. Although the drift in the camera positions derived using GPS data, no matter which method is applied, is a well known fact. In the new method, any initial ambiguity error in the GPS that would cause drift parameters can be determined. Also any cycle slips during the photogrammetric survey that cause shifts in the camera positions can be fixed and fed back into the raw GPS observations. Thus the camera positions are not affected by either drifts or sudden shifts.

Another point that needs to be mentioned here as a well known fact is that in accurate positioning, GPS carrier phase observations are utilized. However, the measured phase is ambiguous because of the unknown integer number of cycles at the beginning of observations which has to be determined. The problem facing the GPS users is the lack of the redundancy if the ambiguities and the point coordinates (or coordinate differences) together with the other parameters are to be solved for simultaneously. A combination of GPS and photogrammetric measurements would lead to the solution of the redundancy problem (generally, the photogrammetric observations are far more than the unknown parameters) and provide good grounds for the determination of integer ambiguities thereby saving a lot of effort and time generally spent on solving the ambiguities.

The goal of this work has been to achieve kinematic GPS supported aerial triangulation without cross strips. In order to do this, the following objectives can be identified for the research:

- In order to combine GPS dual frequency phase data and the photogrammetric data in a bundle adjustment, a new style of combined bundle adjustment must be developed. This has been done combining both types of data in observation space.
- To achieve this objective, it was essential that a software which applies the theory into practice be written.
- To solve the integer ambiguities during the adjustment process and so, remove the necessity for the solution of initial integer ambiguities that had to be done using the static GPS positioning technique before take off.
- To determine cycle slips and to eliminate their effects on the camera positions by correcting the raw phase observations when they are found.
- To investigate characteristics specific to the kinematic GPS aerotriangulation using the GPS and photogrammetric data combined in observation space.

1.3 THESIS AIMS AND METHODOLOGY

1.3.1 THE AIM

GPS became a wellknown fact in term of its application in to the phogrammetry during last decade. Currently adopted approach uses the coordinates of antenna mounted on the aircraft derived form postprocessed GPS data. If three or four antenna are available on the both wing and on the tail of the aircraft, these data can also be used to derive attitude of the aircraft. To work with this method it is necessary to introduce drift parameters into the least squares estimation to solve for them and also necessary to fly cross strips or to add ground control at the each ends of photogrammetric block in order to compensate these systematic drift errors probably caused by cycle slips in GPS data. Thus, these constitute the main limitations in the currently adopted method. If there would be a method which can remove these necessities, then the GPS aerial triangulation using this method will provide more economic, efficient and quality products. In connection with this idea, the main aim of this thesis became to develop a method which is capable of producing results at least as good as those produced by current method without using cross strips or ground control by combining GPS dual frequency double difference phase observations and photo coordinates of object points.

1.3.2 METHODOLOGY

To fulfill this aim, the stages below are adopted:

- Priori GPS and photogrammetric data which the simulated data will be based on has been collected.
- GPS data has been modified for the time offset to have the data at the time of each exposure. This has been performed by an interpolation between two consecutive GPS data epoch which are closest to the each exposure time.
- Simulated data has been fixed for both systems, GPS and photogrammetry.
- An algorithm which is capable of combining GPS dual frequency double difference phase observations and photo coordinates in observation space and using photogrammetric collinearity equations modified for spatial offset between the antenna and the camera onboard the aircraft and GPS double difference equations has been developed to perform a GPS-earotriangulation bundle estimation without drift parameters and also for the system without cross strips.
- A research software has been developed to perform this algorithm.
- Using the software the new combined system has been tested under various conditions. Then its liability, performance, reliability and capacity indicators have been obtained.

CHAPTER TWO

2. FUNDAMENTALS OF AIRBORNE KINEMATIC GPS AND AERIAL PHOTOGRAPHY

2.1 INTRODUCTION

There are four different fields relating to photogrammetry in GPS positioning:

- determination of ground control points;
- survey flight navigation and pin-point photography;
- sensor positioning (for multispectral scanners, rather/laser profilers or scanners, video cameras or other airborne sensors for geophysics, meteorology, etc.);
- aerial triangulation (Ackermann 1992).

This chapter is not concerned with survey navigation, pin-point photography, non-imaging sensor orientation or with the determination of ground control points by GPS which is considered as belonging to geodesy. The chapter will mostly concentrate on aerial triangulation, and only briefly mention pin-point photography and non-imaging sensor orientation.

To produce accurate maps by the use of aerial photography, it is required that the photographs be scaled to reference points that are visible in the photographs. To fulfill the function of aerial photography the spatial relationship of the reference points must be known. The control points as reference points can be defined by locating a mark directly on each point before the flight takes place.

The establishment of the necessary ground control points including the placement of reference markers (premarks) are the main costs in producing accurate photogrammetric maps. In some cases, these processes can comprise more than half the total costs of map production.

Although the use of Global Positioning System (GPS) surveying methods have cut down these costs, there still remains the cost of placing and maintaining the point reference markers. Producing accurate maps without ground control points is theoretically possible by using the camera perspective centers as control points moved up into the air provided spatial position and orientation of each of the photographs can be determined at the instant of exposure. Recent availability of GPS kinematic surveying methods has made this technique a viable possibility with an extremely high benefit/cost ratio.

2.2 CONSTELLATION OF GPS

Some features of GPS positioning are now discussed. Block II/IIA of the GPS satellite constellation met the requirement for Full Operational Capability (FOC) which was formally declared by the U.S. Air Force Space Command (AFSC) on the date of July 17, 1995, after completion of the experimental phase. Requirements include 24 operational satellites (Block II/IIA) functioning in their assigned orbits at about 20200 km altitude with about two revolutions per day and successful testing completed for operational military functionality. So, 5 to 10 satellites should eventually be visible at any time from practically anywhere on earth.

2.3 GPS MEASUREMENTS

All satellites continuously broadcast electromagnetic signals to make range measurements available. These signals are transmitted in two electromagnetic carrier waves, L1 and L2, with frequencies of 1575.42 MHz and 1227.60 MHz, which correspond to wavelengths of 19 cm and 24 cm, respectively. Both of them are modulated by pseudo-noise (PN) sequences. There are different codes, known as C/A (coarse or clear acquisition) code (on L1) and P (precision) code (on L1 and L2). The code measurements are generally called pseudo-ranges while the carrier phase measurements are simply called phase measurements. There are three main type of measurements that can be made on the GPS signals (Canadian GPS Associates, 1986). These are:

- Pseudo-ranges,
- Carrier phase,
- Range difference.

2.3.1 PSEUDO-RANGE

The range computed by multiplying the time difference between emission and reception of a signal by the speed of light is contaminated by the satellite and receiver clock errors and hence the name pseudo-range is called. This requires very high synchronization and time accuracy of both clocks. Apart from the clock errors, the pseudo-range measurements give direct distances. The internal precision as standard errors is of the order of 0.3 m (P code), 3 m (C/A code without SA (refer to section 2.4.2.1.3.1 in this chapter)), or 30 m (C/A code with SA). The essential point is that pseudo-range is generally used to perform real time positioning.

2.3.2 CARRIER PHASE

There is second type of range measurement which based on carrier waves. They can be used directly for code-free ranging by phase measurements. In GPS for aerial triangulation, phase observations are normally used in differential mode, for accuracy reason.

The carrier phase at a given instant of time (t) is the difference between the phase of the incoming satellite carrier signal and the phase of a constant frequency signal generated in the receiver. Although their precision is generally considered to be in the order of 1 percent of λ, less than 2 mm, an accuracy better than 0.1 mm can be achieved with most modern receivers. Phase measurements refer only to the last incoming cycle of a sine wave. Therefore, it is a fraction of a cycle and is affected by the offset in time between the receiver and satellite clock. Total number of phase consists of the measured fractional part, an integer count of phase cycles since an initial time (t_0), which the receiver is locked onto a satellite, to the time of measurement (t) and an unknown integer number of cycles (N) at the initial time (t_0). So, total phase is known except the unknown number of cycles at the initial time. This

unknown number of cycles is called as integer ambiguity (N). For a certain receiver and certain satellite, as long as lock to the satellite is maintained during the observation period, the number of cycles (N) at the initial time (t_0) is a constant. (i.e. there is only one integer ambiguity per satellite per receiver). It is only the initial phase ambiguity, at beginning of the phase observation process, which has to be determined and solved for by an additional unknowns. If a loss of lock to a satellite due to an obstruction of the signal is occurred, then the reception of the signal is interrupted. When the signal lock is resumed, the fractional part of the measured phase remains the same but the integer number of cycle does not and a new integer ambiguity results.

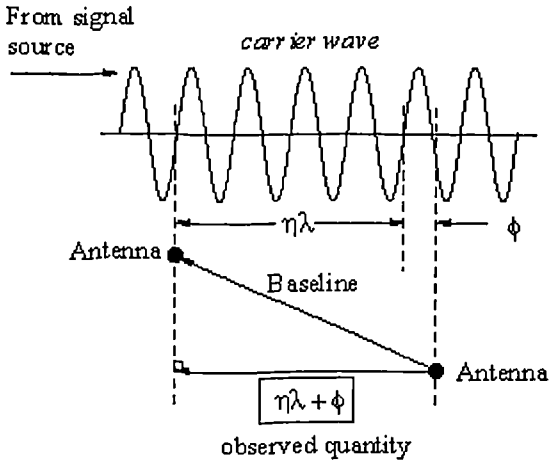

Figure 2.1 Differential GPS carrier phase measurement

The mathematical model of a carrier phase observable in length unit (Leick, 1995) can be represented as:

$$\Phi_A^j(t) = \rho_A^j(t) + d\rho^j + d\rho_{sa} + c\,(dt - dT) + \lambda N - d_{ion}(t) + d_{trop}(t) + d_A(t) + d^j(t) + \varepsilon_{\phi_{mult}}(t) + \varepsilon_\phi \qquad (2.1)$$

where:

$\Phi_A^j(t)$ is the carrier beat phase observable

$\rho_A^j(t)$ is the geometric distance between satellite j and receiver A at epoch t

$d\rho^j$ is the orbital error for satellite j

$d\rho_{sa}$	is the error due to SA
c	is the speed of light in vacuum ($\approx 3*10^8$ *m/sec*)
dt	is the receiver clock offset from GPS time
dT	is the satellite clock offset from GPS time
λ	is the carrier wavelength (c/f), where c is the speed of light in vacuum and f is the frequency of the corresponding carrier wave
N	is the initial phase integer ambiguity
$d_{ion}(t)$	is the ionospheric delay
$d_{trop}(t)$	is the tropospheric delay
$d_A(t)$	is the receiver hardware phase delay
$d^i(t)$	is the satellite hardware phase delay
$\varepsilon_{\phi_{mult}}(t)$	is the multipathing effects on the carrier phase
ε_ϕ	is the receiver noise

2.3.2.1 Range Difference

Range difference called integrated Doppler is a change in range over a certain interval of time (e.g. two epochs) and can be obtained from either the change of code phase or carrier phase. It can be interpreted as the change of phase or range since some initial epoch utilizing the fact that the frequency received by a receiver is different from that emitted by the satellite, due to the relative motion of the satellite with respect to the receiver, and the received frequency is said to have been Doppler shifted. This frequency shift would lead to a phase change which, in turn, can be converted into range difference since the time of lock onto the satellite. This range difference can be used for real-time velocity determination (Hofmann-Wellenhof et al, 1995). Therefore it is very useful for navigation.

2.4 GPS POSITIONING

2.4.1 THE NAVIGATION SOLUTION

For normal navigation GPS positioning simply based on range measurements. If a GPS receiver observes signals simultaneously from at least three satellites the distance between the antennas on the satellites and the antenna where the receiver was connected can be calculated using either pseudo-range or phase measurements by distance intersection/trilateration provided that coordinates of the antennas on the satellites are known. In practice, the clock error of the receiver is also treated as an additional unknown because of its large magnitude. Therefore it is necessary to measure pseudo-ranges simultaneously to at least four satellites to determine position of the receiver and its momentary clock error. This process describes the standard navigation solution. It is also valid for phase measurement if the initial phase ambiguities have been solved separately.

The internal range measuring precision Q_s by pseudo-range or phase observations is propagated into the precision of positioning by the computational algorithm of distance intersection. The result depends on the geometry of the satellite constellation which is expressed by the factor PDOP* = $(Q_{xx}+ Q_{yy}+ Q_{zz})^{1/2}$. Thus precision of the derived position is described as PDOP x Q_s (Ackermann 1992). In good and acceptable constellations, the values of PDOP are in the order of 3 to 6.

2.4.2 GPS ERROR SOURCES

In practice, GPS measurements, both pseudo-ranges and carrier phases, experience various errors classified as below:

- Satellite : ephemeris, clock, SA, and A-S
- Propagation : ionosphere, troposphere, multipath

---

* Positional dilution of precision

- Receiver : antenna , clock, measurement error
- Earth : Earth surface kinematics
- Algorithmic : cycle-slip, ambiguity

2.4.2.1 Satellite Error Sources

Mathematical algorithms are used to extrapolate the parameters, clock and orbit, to some future time. These algorithms, the way they are implemented and rate of data transfer between the satellites and the segments involved are the main sources of the satellite errors. If not corrected, the orbital errors will appear as position errors of similar magnitudes (Abidin HZ, 1993).

2.4.2.1.1 Ephemeris Errors

The satellite orbits are determined using the Monitor Station smoothed measurements. Modeling of the forces accurately acting on the satellite is not easy from these measurements. However, to calculate the position of the receiver by pseudo-range or phase measurements it is necessary to know position of the satellite accurately. Thus the satellites broadcast an Navigation Message consisting Keplerian-type parameters. Errors in these parameters cause the use of wrong information to calculate the positions of the satellite and /or receiver.

Typically, an error of 1 ppm in satellite orbit produces a maximal error of 1 ppm in baseline. The error of broadcast orbit is of the order of 0.5 ppm (Remondi and Hoffmann-Wellenhof, 1989). However, with SA activated, broadcast orbit errors can in theory reach 5 ppm (Tolman et al., 1990). Post-computed precise orbits better than 0.1 ppm (Beutler, 1992) reduce, to a negligible level, the impact of satellite orbit error on short baselines.

2.4.2.1.2 Satellite clock

The stability of satellite clocks is another factor affecting the precision of the system. These clock errors may not be perfectly synchronized to GPS time and may drift away from the standard GPS time system. Humidity and temperature variations can cause higher order drifts which can be neglected over short periods but not for long periods (Canadion GPS Association, 1986).

Satellite clocks are dithered if selective availability is turned on. According to Rocken and Meertens (1991), clock dithering (at ±2 Hz) has no significant effect on relative positioning as long as the receiver clocks are synchronized to better than 10 msec.

2.4.2.1.3 Impact of SA and A-S

There are two process imposed by the DoD to deny some GPS users full access of the system capabilities. They are known as Selective Availability **(SA)** and as Anti-Spoofing **(AS).**

2.4.2.1.3.1 Selective Availability (SA)

Selective Availability (SA) denies precise positioning by corruption of the GPS signal structure. It is composed of two components:

- corruption of broadcast navigation message and
- rapid "dithering" or oscillations of the frequency standards in the satellites.

The first component of SA is of little consequence to scientific users because in precise millimeter applications the orbits of the GPS satellites are computed from carrier measurements much more accurately than even the precise ephemeris available from the DoD. Also the dynamics of the GPS satellites are well enough understood that these orbits can be integrated forward in time by several days with accuracies better than the (uncorrupted) broadcast ephemeris except when there are thruster

firings on the GPS satellites. The second component currently also has little effect when differential (either real-time or post-processing) techniques are used. While the effects of SA are almost totally eliminated in differential positioning, the rapid fluctuations in satellite clocks do complicate the process of removing slips in the number of carrier phase cycles accumulated by the receiver and SA makes it nearly impossible to use averaged phase measurements (normal points) with a much lower sampling rate. In real-time navigation problems, SA limits accuracy of navigation, although for aircraft this is not a major problem since the position of an aircraft can generally only be controlled to within about 100 m. This is also not a problem for the applications which postprocessing is applied. Because this error can be corrected by a precise orbit data, for the satellites utilized, had within few days after from the mission day.

2.4.2.1.3.2 Anti-spoofing (A-S)

Anti-spoofing (AS) is meant to stop false signals from corrupting military receivers, but as a consequence of the system used, AS denies access to the P-code. AS is implemented by modulating the P-code with an additional code (the W-code), and because only the P-code (with the W-code modulation) is superimposed on the L2 frequency, some type of codeless tracking of L2 is required when AS is turned on. The prime consequence of AS is loss of accuracy in both range measurements and phase measurements. For aircraft applications, this loss of accuracy (about 1000-fold for L2 tracking) is particularly severe because of the dynamics of the aircraft and the usually high multipath environment on the aircraft. In particular, results of the quality can only be obtained by coherently averaging the L2 signal for about 1 second. This is an acceptable compromise for a static receiver, but in an aircraft leads to frequent loss of lock on the L2 signal.

2.4.2.2 Propagation Error Sources

These errors affects the propagation of the signal as it travels from the satellite to the receiver.

2.4.2.2.1 The Ionospheric Error

The primary source of error is the ionospheric time delay (the code information is delayed and therefore the determined pseudo-range is longer than it should be). The main factor causing the ionospheric time delay is the total number of electron encountered by the signal on its travel from the satellite to the receiver. The electron density* is a function of many parameters among which are: magnetic activity, season, time of the day, location and satellite direction (Gervaise et.al, 1985). Even with GPS high frequency signals, large delaying effects can be expected when low elevation satellites are observed since these travel for a long period in the ionosphere. In kinematic GPS positioning of an aircraft, errors of up to 20 cm could result from this effect (Georgiadou and Kleusberg, 1988a; Kleusberg, 1991). The effect of this error can be minimized by using ionospheric models with single frequency receivers, with dual frequency receivers it may be minimized or completely eliminated by forming the so-called ionospheric-free linear combination of L1 and L2 carrier phases. This combination which leads to an observable with a three times higher noise than the L1 observables, ionospheric correction to the L1 observation from deterministic ionospheric model may be applied on short baselines. Such a model has been developed by Wild et al. (1989) and Georgiadou (1990) who has shown that the remaining ionospheric effect on baselines was below 0.2 ppm. For further details, the reader is referred to Hofmann-Wellenhof et.al (1995).

2.4.2.2.2 The Tropospheric Error

Troposphere consists of two main parts: a wet part and dry part (Canadian GPS associates, 1986). The dominant effect is in the dry part where propagation of a signal is independent of radio wave frequencies of up to 15 GHz. The wet term depends on the atmospheric conditions along the path of the signal which is in general not the same as the surface conditions. Tropospheric refraction, especially the wet path delay induced from the water vapor content, is one of the most difficult errors to model. For

---

* Total number of electrons in one cubic meter

example, each 1 mm of relative tropospheric zenith delay mismodeling creates an error of 3 mm in the baseline height component (Santerre, 1991). So, it is a function of the distance traveled by the signal through the troposphere (de Jong, 1991). The distance traveled by the signal before reaching the receiver is a function of the elevation of the satellite. The lower the elevation, the longer distance the signal travels and the largest tropospheric effect it experiences. Large height differences or local meteorological phenomena (e.g., temperature inversions) lead to errors significant even on short baselines. Estimation of a tropospheric delay parameter can take into account unmodeled tropospheric error. However, at present, there are various models that use surface meteorological data to account for errors from this source. e.g. Hopfield and Saataminen models.

2.4.2.2.3 Multipath

One of the major error sources of GPS in a reflective environment is multipathing. Multipath error comes into existence if the emitted satellite signal arrives at the receiver via more than one path. Main sources of the multipath are the reflective surfaces, such as an aircraft, near by the antenna connected to the receiver or on the satellite. Multipath is not a random error source. It depends on the geometry orbit to satellite and cannot be removed by differencing. However it distorts both the code and the carrier phase measurement, carrier phases are less affected than code pseudo-ranges because it is also frequency dependent (Leick, 1995).

A general model cannot be formed for the multipathing effect because of the different situations under which observations are carried out. However, because it is geometry dependent, it could be detected by comparing the data obtained from successive observing days because errors from this source show a cyclic behavior and repeat from day to day for a static receiver (Georgiadou and Kleusberg 1988b, Cross 1994). Except for multipathing and ionospheric delay, all other major sources of error are frequency independent (Canadian GPS Association 1986, Hofmann-Wellenhof et al.

1992) and therefore they influence code and carrier phase by the same amount. If the effects of ionosphere are removed from code ranges and carrier phases and corresponding double differences are formed, all the effects, except of multipathing, will be considerably reduced and the remaining errors, apart from the noise level, thus reflect the multipathing effect.

Satellite multipath which occurs when the transmitted signal is reflected off from a part of the satellite, before being directed to Earth, were almost negligible according to a presentation by Czopek and Shollenberger at the Institution of Navigation conference in Salt Lake City in 1994. It is now commonly accepted by most researchers that there is no satellite multipathing.

An antenna could be designed with certain characteristics for satellites near the horizon having an ability to filter the actual signal from multipathing effects and considering that from geometrical point of view, signals received from low elevation satellites are affected by multipathing more than those received from high elevation satellites. If such an antenna is used in kinematic GPS involving the use of aircraft where the environment is highly dynamic, it causes problems. In that case, some of the satellites may be masked off and the aircraft might be affected by drag in order to filter the multipathing effect from received signal (Braasch 1992).

Its magnitude may reach maximum to one quarter of the carrier wavelength (i.e., 5 cm on L1) (Georgiadou and Kleusberg 1988) according to the survey environment. Corbett (1994) also stated in his thesis that the expected double difference phase residual due to multipathing caused by airframe of an aircraft, is in the order of ten millimeters, and at worst 0.1 L1 cycles (or 19 millimeters).

2.4.2.3 Receiver Error Sources

Accuracy of positioning using GPS is influenced at a significant level by the accuracy of used receiver which measures the phase, signal or both. These error sources may be reviewed in three subtitles as follow:

2.4.2.3.1 Antenna Error Sources

Antenna phase offset and variation are the major sources of antenna errors. Phase center of an antenna is that the point to which the GPS signal measurement is referred. Since the antenna cannot be produced as a perfect device, in general this point is not certainly identical with the physical center of the antenna. This offset depends on the satellite elevation and direction and on the intensity of the satellite signal (Hofmann-Wellenhof et al. 1992). The precision of an antenna depends on variation of the antenna phase center, not on the offset because the latter is generally constant and can be determined to be corrected. Modeling the variation of an antenna phase center is fairly difficult because it differs from an antenna to another. Therefore, it is difficult to confirm the effects of antenna errors on measurements. There are some suggestions such as calibration of antenna phase center variation in anechoic chambers to drop down the effect of this error to the mm-level (Tranquilla, Colpitts 1989). Also Geiger (1990) stated that relative phase center variations of "identical" antenna is usually less than 5 mm.

2.4.2.3.2 Receiver Clock Error Sources

The clock in the receiver is not stable. So this instability becomes another source of the errors in GPS. Some receivers have relatively cheap and not so accurate clocks than other. In addition to these advantages, they have also an ability to correct clock errors using pseudo-range measurements. Since this error affects all the observables in an epoch, the use of differential GPS methods for the measurements in each individual epoch will remove the receiver clock error. It can also be modeled and solved for. If proper electronics are used in designing the receivers, then this error source can be considerably minimized or may be completely eliminated.

2.4.2.3.3 Measurement Error

Measurement error is the difference between the actual measurement, and one that would be made using perfect instrumentation.

It is usually caused by physical effects which have no predictable pattern, may be treated statistically or have a pattern that could be predicted if we had sufficient data and a good enough model about the processes involved. The followings can be given as examples to this kind of errors. So, they are systematical errors caused by the imperfection of receiver firmware's code correlation model and firmware's tracking loop model and arisen as electronic channel biases which vary with temperature and randomly appeared errors as electronic noise and finite clock instability by random atomic motion and sampling error by finite bandwidth smoothes out signal.

2.4.2.4 Error of Earth Surface Kinematics

However, it is not the subject to the kinematic positioning and concerns static positioning, because the changes in the motion of the earth and the earth surface in time causes that sort of errors. If a stationary receiver are used even in kinematic GPS for long period of time, again it should be taken into consideration.

2.4.2.5 Algorithmic Error Sources

Cycle slips and ambiguities are the major sources of potential blunders in any mission utilizing GPS.

2.4.2.5.1 Cycle Slip

If tracking of the satellite signal is momentarily lost during a certain time of observation since the signal has been blocked from reaching the antenna by some physical obstruction, fractional phase measurement after re-acquisition of the signal is the same as if tracking had been maintained. However, the integer number of cycle is different (King et at. 1987). Cycle slips may occur at both frequency while using dual frequency receiver, then the problem becomes more complicated. Therefore, dual frequency measurements are tested using L1 and L2 simultaneously for better identifying a cycle slip. The sources of a cycle slip (losing or gaining an integer number of cycles) may be divided into two main categories:

Observation sources;

- high noise from multipathing or/and ionospheric effect,
- low satellite elevation (high noise, low signal strength),
- signal obstruction (kinematic observations most vulnerable).

Receiver sources;

- weak signals may allow interferences to be magnified by the receiver,
- limitations of internal processing of the signal,
- rotations of the antenna (again, kinematic observations in aircraft and rover vessels).

2.4.2.5.2 Integer Ambiguity

At the beginning of a survey when a receiver is turned on, the fractional beat phase, which is the difference between the satellite emitted carrier signal and a receiver generated replica signal, is measured and an integer counter initialized. Each observed new signal wave which is changed from 0 to 2 π increments the number of the counter by one. The accumulated phase (Φ^a) during an epoch is sum of this integer count (n) and the fractional phase ($\Delta\Phi$). But the initial integer number (N) of cycles between satellite and the receiver is not known. As long as the signal lock is not lost, this integer phase ambiguity (N) remains constant. So the expression 2.2 represents the final situation of the phase(Φ).

$$\Phi = \Delta\Phi + n + N \qquad (2.2)$$

If a long observation break occurs for any satellite or if a new satellite comes to the horizon, new integer ambiguities are introduced. The ideal integer ambiguities consists of integer numbers, but some time it may not come out as an integer number from processing, especially for long baselines. In addition, if the ionosphere-free linear combination is used, the combined ambiguities are no longer integer numbers. Once the ambiguities are initialized and solved, then the data processing is re-performed once more by fixing them. Several ambiguity resolution techniques can be found in

practice, e.g. (Corbett 1995), (Teunissen 1995), (Blewitt 1989), (Bock 1986), (Hatch and Larson 1985), (Melbourne 1985), (Wubbena 1985).

Since resolution of the ambiguities is not the main object of this thesis, investigating or/and reviewing of the current techniques will not be given. The reader is referred to Hoffmann-Wellenhof et.at (1994) and Leick (1995) for further details.

2.4.2.6 Other Error Sources

These error sources could be wrongly formed stochastic model (e.g. using incorrect weight matrix for least-squares), offset in the coordinate of fixed station (e.g. Santerre 1991) has shown that each 10 m of offset in the height of the fixed station mainly produced a 0.4 ppm error in horizontal baseline components being proportional to baseline length) and relative cable delay in the missions which are required to use long cable lines to connect the antenna to the receiver because of some restrictions.

2.5 DIFFERENTIAL GPS POSITIONING

Using point positioning with a single receiver, the coordinates of a single point can be determined within the errors mentioned in section 2.4. In this point positioning a single receiver observes GPS signals (code and/or carrier phase) from normally four or more satellites. If two receiver are used, differential positioning becomes possible, and code and/or phase observables from at least four same satellites are simultaneously collected by the receivers at two sites. In general, the receiver mounted on the known site is stationary.

Certain errors in GPS, such as atmospheric refraction, are common to all receivers provided that the extent of the area where the receivers are deployed is limited. If the condition (small area) is fulfilled, then the errors mentioned in section 2.4 are correlated except the multipathing, the epsilon component of SA, the antenna phase center variation and the receiver noise. When observations are differenced, then these errors will cancel or otherwise their effect is considerably reduced. Therefore, the data

processing from two sites results with the better accuracy than in the case of point positioning.

By the use of differential GPS positioning techniques, the coordinates of an unknown point are determined with respect to a known point. If simultaneous observations are made at both points. Assuming that such simultaneous observations are made at the two points A and B to satellites j and k. If $\varphi_A{}^J$ is the phase to satellite j from station A then:

- single difference $$\nabla\varphi_{AB}^{j} = \varphi_A^j - \varphi_B^j \qquad (2.3)$$
- double difference $$\nabla\Delta\varphi_{AB}^{jk} = (\varphi_A^j - \varphi_B^j) - (\varphi_A^k - \varphi_B^k) \qquad (2.4)$$
- triple difference

$$\delta\nabla\Delta\varphi_{AB}^{jk}(t_{i+1}) = \{(\varphi_A^j - \varphi_B^j) - (\varphi_A^k - \varphi_B^k)\}^{t(i)} - \{(\varphi_A^j - \varphi_B^j) - (\varphi_A^k - \varphi_B^k)\}^{t(i+1)} \qquad (2.5)$$

Each one of these differencing techniques comes with its advantages. The satellite clock error term and orbit error vanish by the means of use of single differencing, since they will be constant for both receivers. Receiver clock error terms are removed as well if double differencing is used. Using triple differencing , as well as removing both satellite and receiver clock errors and orbit errors, the integer ambiguity term is also removed, since this is constant over time (assuming there are no cycle slips). Over short baselines (less than 20-30 km) each differencing techniques will reduce the ionospheric and tropospheric effects since the signals will follow similar paths in the atmosphere.

2.5.1 THE DOUBLE DIFFERENCING OF PHASE OBSERVABLES

"The most commonly adopted strategy is to difference with respect to both satellites and" two receiver sites "to produce the so-called *double difference* observable" (Cross 1994). The use of double differencing technique gives much more redundant observations than single differencing technique. So, this leads to the use of the least-squares procedure more efficiently. "The least-squares procedure is usually adopted to force the integer ambiguity parameters to take integer values. Another

commonly adopted strategy is to form *triple difference* observation equations, i.e. to difference with respect to time, satellites and" two receiver sites. "This process does not yield results of the highest quality (one reason being that the integer ambiguities are no longer solved for, and it is not possible to force them to integer values)" (Cross 1994). From the statements in this paragraph, it is obvious the necessity to the use of double differencing technique in the least-squares procedure as a best method to estimate the coordinates of unknown point and the integer ambiguities accurately.

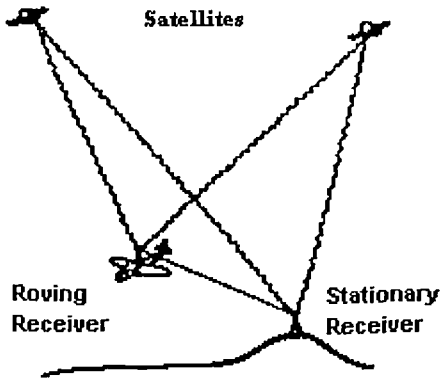

Figure 2.2 Airborne double differencing

In general, airborne differential GPS (ADGPS) positioning involves differencing strategies. The most used one, double differencing, will be discussed in brief. Equation 2.4 is a basic expression for double differencing. A more complete one should be given in order to form a true model. This primarily involves the expansion of the clock term. If there is 1 nanosecond timing error, being considered the speed of light ($3x10^8$ ms^{-1}), this timing error will cause 30 cm distance error. So, that is why modeling of the clocks is so important. The double difference equation including clock terms is written as following:

$$\begin{aligned}\nabla\Delta\varphi_{AB}^{jk} = &-f/c\{\rho_A^k - \rho_B^k - \rho_A^j + \rho_B^j\} + N_{AB}^{kj} \\ &-f/c(\dot{\rho}_A^k - \dot{\rho}_B^k - \dot{\rho}_A^j + \dot{\rho}_B^j)(\frac{\delta t_A + \delta t_B}{2}) \\ &-f/2c(\dot{\rho}_A^k + \dot{\rho}_B^k - \dot{\rho}_A^j - \dot{\rho}_B^j)(\delta t_A - \delta t_B) \\ &+f.A + \varepsilon\end{aligned} \qquad (2.6)$$

where ρ_A^j and $\dot{\rho}_A^j$ are respectively the range and the rate of change of range from antenna A to satellite j. N_{AB}^{kj} is the double differenced integer ambiguity term involving receivers A and B to k and j. The receiver clock errors of receivers A and B are denoted in terms of common clock error, $\frac{\delta t_A + \delta t_B}{2}$ and relative shift (offset), $\delta t_A - \delta t_B$. A and ε are respectively term of atmospheric delay and noise term. If the ranges in equation 2.6 are expanded and the terms are rearranged, it becomes:

$$
\begin{aligned}
&-\frac{f}{c}\{[(X_A - X^k)^2 + (Y_A - Y^k)^2 + (Z_A - Z^k)^2]^{1/2} - \\
&[(X_B - X^k)^2 + (Y_B - Y^k)^2 + (Z_B - Z^k)^2]^{1/2} - \\
&[(X_A - X^j)^2 + (Y_A - Y^j)^2 + (Z_A - Z^j)^2]^{1/2} + \\
&[(X_B - X^j)^2 + (Y_B - Y^j)^2 + (Z_B - Z^j)^2]^{1/2}\} + N_{AB}^{jk} \\
&= \\
&\varphi_A^k - \varphi_B^k - \varphi_A^j + \varphi_B^j \\
&+ \\
&\frac{f}{c}(\dot{\rho}_A^k - \dot{\rho}_B^k - \dot{\rho}_A^j + \dot{\rho}_B^j)t_{AB} \\
&+ \\
&\frac{f}{2c}(\dot{\rho}_A^k + \dot{\rho}_B^k - \dot{\rho}_A^j - \dot{\rho}_B^j)\Delta t_{AB} \\
&+ \\
&trop_A^k - trop_B^k - trop_A^j + trop_B^j \\
&+ \\
&ion_A^k - ion_B^k - ion_A^j + ion_B^j \\
&+ \\
&\text{(eart rotation correction)} \\
&+ \\
&\text{Noise}
\end{aligned}
\qquad (2.7)
$$

X_A, Y_A, Z_A and X_B, Y_B, Z_B are the coordinates of the antennas at both sides, A and B

X^k, Y^k, Z^k and X^j, Y^j, Z^j are the coordinates of the satellites k and j.

In Equation 2.7 clock error terms are negligible for short baselines (e.g. 10 km) and no large clock synchronization errors (Remondi 1984). Lachapelle *et al* (1992) also suggest that the terms of atmospheric delays are small or negligible over short

distances (e.g. < 10-20 km). However, if the height difference between the base and roving receiver is large (e.g. >100*m*), the double difference tropospheric residuals (if they were not modeled or computed) will have a significant effect on the accuracy of the final solution. Double differencing of the observables yields high precision results as a consequence of eliminating or reducing common mode bias errors (e.g. orbital errors, satellite and receiver clock errors, and atmospheric delays) while it magnifies the magnitude of the uncommon biases (e.g. multipathing effects) and receiver noises by a factor of 2 (Lachapelle *et al*, 1992) and their correlated nature (Remondi, 1985). According to the statements above and making an assumption such that in GPS supported aerial triangulation, the tropospheric delay has been modeled well, then Equation 2.7 can simply be given as:

$$
\begin{aligned}
-\frac{f}{c}\{&[(X_A - X^k)^2 + (Y_A - Y^k)^2 + (Z_A - Z^k)^2]^{1/2} - \\
&[(X_B - X^k)^2 + (Y_B - Y^k)^2 + (Z_B - Z^k)^2]^{1/2} - \\
&[(X_A - X^j)^2 + (Y_A - Y^j)^2 + (Z_A - Z^j)^2]^{1/2} + \\
&[(X_B - X^j)^2 + (Y_B - Y^j)^2 + (Z_B - Z^j)^2]^{1/2}\} + N_{AB}^{jk} \\
&= \\
&\varphi_A^k - \varphi_B^k - \varphi_A^j + \varphi_B^j \\
&+ \\
&\text{Noise (+ multipathing)}
\end{aligned}
\qquad (2.8)
$$

Since the double difference observable equations are not linear equations they can not be solved directly. Therefore, the linearised form of the double difference observation equations is what is solved in a least squares geometrical adjustment sense, see Cross (1983) for linearising the mathematical model of an observation equation. The mathematical mode of the linearised double difference observable, which contains the unknown baseline components and double difference initial ambiguities, can be shown mathematically as:

$$A\,x = b + v \qquad (2.9)$$

where:

A is the design matrix

x is the vector of unknowns

b is vector of double difference residuals

v is vector of adjustment residuals

The design matrix A contains the partial derivatives of the distance between the GPS receiver's antenna and satellite with respect to the unknown parameters.

With full GPS constellation, a satellite configuration of 10 satellites above 15° mask angle may be available over some particular parts of the world for short periods of time. One epoch measurements from 10 satellites (i, j, .., r) collected simultaneously by two receivers (A & B) lead to forming 9 double differences with 12 unknowns (3 for the baseline components and 9 for the double difference ambiguities) for the single frequency receiver case or 18 double difference equations with 21 unknowns for the case of dual frequency receivers (3 for baseline components, 9 for L1 and 9 for L2 ambiguities).

Double difference observation equations are associated with a correlation matrix (C_l), due to the mathematical differencing between observables. The contents of the matrices A and C_l and the vectors x, b and v can be shown as follows.

$$A = \begin{pmatrix} \frac{\partial \rho_{AB}^{ij}}{\partial X_B} & \frac{\partial \rho_{AB}^{ij}}{\partial Y_B} & \frac{\partial \rho_{AB}^{ij}}{\partial Z_B} & \frac{\partial \rho_{AB}^{ij}}{\partial N_{AB}^{ij}} & .. & 0 \\ \frac{\partial \rho_{AB}^{ik}}{\partial X_B} & \frac{\partial \rho_{AB}^{ik}}{\partial Y_B} & \frac{\partial \rho_{AB}^{ik}}{\partial Z_B} & 0 & .. & 0 \\ .. & .. & .. & .. & .. & 0 \\ \frac{\partial \rho_{AB}^{ir}}{\partial X_B} & \frac{\partial \rho_{AB}^{ir}}{\partial Y_B} & \frac{\partial \rho_{AB}^{ir}}{\partial Z_B} & .. & .. & \frac{\partial \rho_{AB}^{ir}}{\partial N_{AB}^{ir}} \end{pmatrix} \qquad (2.10)$$

The partial derivative coefficients of the design matrix are derived as follows:

$$\frac{\partial \rho_{AB}^{ij}}{\partial X_B} = -\left[\frac{X_{0B} - X^i}{\rho_B^i}\right] + \left[\frac{X_{0B} - X^j}{\rho_B^j}\right] ; \quad \frac{\partial \rho_{AB}^{ij}}{\partial Y_B} = -\left[\frac{Y_{0B} - Y^i}{\rho_B^i}\right] + \left[\frac{Y_{0B} - Y^j}{\rho_B^j}\right] ;$$

$$\frac{\partial \rho_{AB}^{ij}}{\partial Z_B} = -[\frac{Z_{0B} - Z^i}{\rho_B^i}] + [\frac{Z_{0B} - Z^j}{\rho_B^j}], \quad \cdots \quad ; \quad \frac{\partial \rho_{AB}^{ij}}{\partial N_{AB}^{ij}} = \cdots = \frac{\partial \rho_{AB}^{ir}}{\partial N_{AB}^{ir}} = 1$$

The content of the correlation matrix C_l is given by

$$C_l = \begin{bmatrix} 4 & 2 & .. & 2 \\ 2 & 4 & .. & .. \\ .. & .. & .. & .. \\ .. & .. & .. & 4 \end{bmatrix} \qquad (2.11)$$

with a corresponding a priori weight matrix $W = C_l^{-1}$ (2.12)

Correlation derivation over various observing and processing considerations (e.g. multi-epoch, multi-receiver and multi-baseline mode) can be found in the literature (e.g. Leick 1995, Hofmann-Wellenhof et al 1994, Khalid 1990).

The vector of unknowns ($\hat{\mathbf{x}}$) can be shown in the form:

$$\hat{\mathbf{x}} = \begin{pmatrix} dX_{AB} \\ dY_{AB} \\ dZ_{AB} \\ .. \\ N_{AB}^{ir} \end{pmatrix} \qquad (2.13)$$

The right hand side of equation 2.9 can be represented in a vector form as follows:

$$b = \begin{pmatrix} b_1 \\ b_2 \\ .. \\ b_9 \end{pmatrix} \qquad (2.14)$$

where

$b_1 = \Phi_{AB}^{ij} - \rho_{AB}^{ij}/\lambda$; $b_2 = \Phi_{AB}^{ik} - \rho_{AB}^{ik}/\lambda$; $b_3 = \Phi_{AB}^{il} - \rho_{AB}^{il}/\lambda$, and so on.

Clearly, a straight forward solution of these observation equations is impossible as the number of unknowns is greater than the number of equations (i.e. there is no redundancy). Therefore, measurements from more than one epoch are required to provide sufficient or even redundant observation equations (with no cycle slips or have been accounted for) to solve for the involved parameters. The commonly recommended observation session length is at least half to an hour. This is not because of the need for the whole data set but to allow for a change in satellite geometry (i.e. to have a system of normal equations with different coefficient values, otherwise the equations are ill-conditioned), so the ambiguities are resolvable.

2.6 AERIAL TRIANGULATION

2.6.1 DEFINITION

Aerial triangulation can be defined (Wolf 1983) as "the process of determining X, Y and Z ground coordinates of individual points based on measurements from photographs". Both aerial and terrestrial photographs can be used for triangulation purposes. Nowadays aerial triangulation is applied in a variety of fields (e.g. mapping, cadastral engineering and geodetic applications of photogrammetry).

Aerial triangulation procedures can be classified into three groups according to the small data units, the bundle, the model or the strip. The bundle consists of one photograph only, the model consists of two consecutive photographs taken along the flight line with a common forward overlap between them and the strip consists of one or more models. The procedure can be performed either using analogue, semi-analytical or full analytical methods. Further information about these methods can be found in the common photogrammetric literature.

2.6.2 ESTIMATION METHODS

After the availability of "electronic computers", many programmetrists were encouraged to develop numerical methods for aerial photogrammetry. While developing such a method, the main problem was handling and solving large sets of equations in a large number of unknowns. By developments so far, the numerical procedures of aerial triangulation block estimation and the corresponding software have been optimized to the extent that large blocks with a large number of photographs can be efficiently adjusted in either main frame or personal computers.

The existing block estimation programs may be classified into three groups:

- Polynomial estimation (programs using the technique require strip coordinates as input),
- Independent model estimation (programs for this method require model coordinates, including those of the perspective centers, as input),
- Bundle estimation (for bundle estimation programs, photo coordinates are needed as input).

Theoretically, the bundle estimation should give the highest accuracy especially when the self-calibration technique is applied. For this reason (and because of that it is the technique used in this research), in the next section, analytical bundle estimation technique will be explained, without going into too much detail. The reader is referred to literature (e.g. Wolf 1983) for further details on each technique mentioned above.

2.6.2.1 Bundle Estimation

Smallest unit is the bundle, in this method. The position and orientation of all the bundles in the block or strip are estimated in space simultaneously to achieve the best possible intersection of all conjugate rays of each points on the ground (e.g. figure 2.3

shows single bundle resection of the rays) and fit to the given control points using collinearity equations (figure 2.4 represents collinearity condition*).

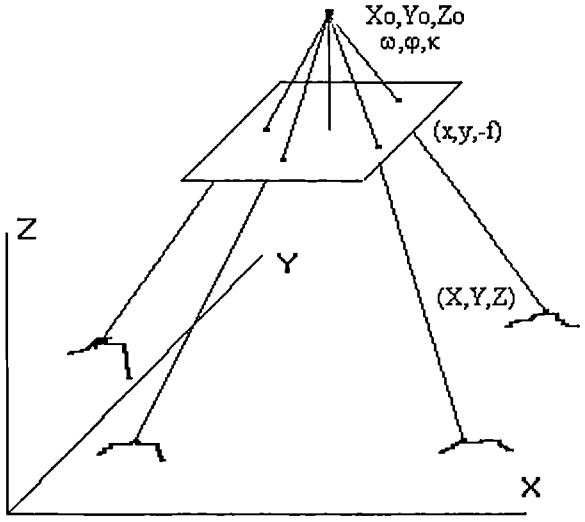

Figure 2.3 Single bundle resection

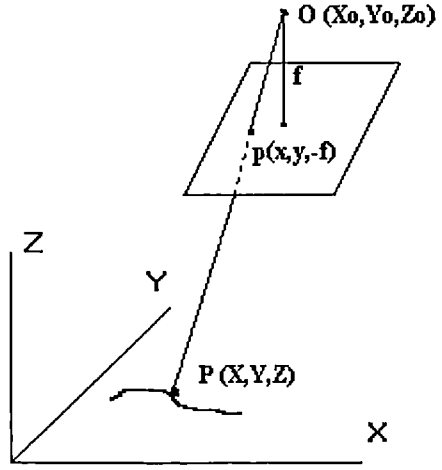

Figure 2.4 Collinearity condition

From a theoretical point of view, this method is the most accurate one compared with the other two estimation methods as mentioned before. The following reasons can be given for this:

---

* Collinearity is the condition that the exposure station, O(Xo,Yo,Zo), any object point, P(X,Y,Z), and its photo image, p(x,y,-f), all lie along a straight line.

- The collinearity equations used in the bundle estimation represents the actual situation without any serious approximations.

- The instruments used to measure the photo image coordinates as comparators, or analytical plotters have relatively small instrumental errors. Standard deviations of less than 3 μm at photo scale could easily be achieved by an experienced operator.

- Since the photo coordinates are used as input data in the bundle estimation to obtain the unknown spatial coordinates of the measured object points and the orientation parameters of each bundle, the relative and absolute orientations are generally not required. Thus, the residual errors resulting from performing these orientations would no longer exist. This will considerably save time, therefore, lower cost and an increase in accuracy.

The relation between image and ground coordinates can be written as:

$$\begin{bmatrix} X_i \\ Y_i \\ Z_i \end{bmatrix} = \lambda_{ij} R_j \begin{bmatrix} x_{ij} \\ y_{ij} \\ -f \end{bmatrix} + \begin{bmatrix} X_{oj} \\ Y_{oj} \\ Z_{oj} \end{bmatrix} \qquad (2.15)$$

where:

$[X_i\ Y_i\ Z_i]^T$ are the ground coordinates of the ith point

$[X_{oj}\ Y_{oj}\ Z_{oj}]^T$ are the ground coordinates of the jth exposure station

$[x_{ij}\ y_{ij}]^T$ are the photo coordinates of the ith points in the jth photograph

λ_{ij} is the scale factor for the ith point in the jth photograph

$\mathbf{R_j}$ is the rotation matrix associated with the jth photograph

f is the camera principal distance.

Taking $\begin{bmatrix} X_{oj} & Y_{oj} & Z_{oj} \end{bmatrix}^T$ to left hand side, multiplying both sides by $\frac{1}{\lambda_{ij}} R_j^T$ (R_j is orthogonal) and dividing the first and second rows by the third, Equations (2.15) take forms as:

$$x_{ij} = -f \frac{r_{11}(X_i - X_{oj}) + r_{12}(Y_i - Y_{oj}) + r_{13}(Z_i - Z_{oj})}{r_{31}(X_i - X_{oj}) + r_{32}(Y_i - Y_{oj}) + r_{33}(Z_i - Z_{oj})} \qquad (2.16)$$

$$y_{ij} = -f \frac{r_{21}(X_i - X_{oj}) + r_{22}(Y_i - Y_{oj}) + r_{23}(Z_i - Z_{oj})}{r_{31}(X_i - X_{oj}) + r_{32}(Y_i - Y_{oj}) + r_{33}(Z_i - Z_{oj})} \qquad (2.17)$$

where $r_{11}, r_{12},...,r_{33}$ are the elements of rotation matrix R_j^T.

These observation equations are not linear and therefore their linearised forms have to be used in an estimation procedure. The full linearised equations can be found in Appendix B. In matrix form, the linearised observation equations could be written as:

$$A_{ij} \begin{bmatrix} \Delta\omega \\ \Delta\varphi \\ \Delta\kappa \\ \Delta X_0 \\ \Delta Y_0 \\ \Delta Z_0 \end{bmatrix} + B_{ij} \begin{bmatrix} \Delta X \\ \Delta Y \\ \Delta Z \end{bmatrix} = \begin{bmatrix} b_{x_{ij}} \\ b_{y_{ij}} \end{bmatrix} \qquad (2.18)$$

where:

$\mathbf{A}_{ij}$ and $\mathbf{B}_{ij}$ are design matrices containing the partial derivatives of the functions corresponding to the ith point with respect to the unknown rotation and position of the jth photograph and the unknown ground coordinates of the ith ground point respectively.

$\begin{bmatrix} b_{x_{ij}} & b_{y_{ij}} \end{bmatrix}^T$ is a vector containing the differences between observed x and y photo coordinates of the ith image point measured on the photo and calculated x and y photo coordinates of the same point using approximate values.

Two equations of the form above will therefore be produced for each point from each photo in which the point appears. These equations will slightly change depending on the type of observed photo point (e.g. full control, plan, height or tie point).

These observed photo coordinates will generally be affected by various systematic errors. The known ones have to be accounted for before using the photo coordinates in equations 2.15 and 2.16.

2.6.3 FACTORS AFFECTING THE ACCURACY OF AERIAL TRIANGULATION

In any measurements there will be errors in the magnitude of which depend on the observer, the used instrument, the environment which the measurement is carried out or a combination of some or all of these factors. To obtain satisfactory results, either the effects of these errors are removed, or at least minimized, or they have to be accounted in the mathematical models.

These errors can be classified into three main groups according to the way they affect the results. They are:

- systematic errors,
- random errors, and
- gross errors.

2.6.3.1 Systematic Errors

The collinearity equations are used in the bundle estimation or in any other areas of photogrammetry, making an assumption that the photograph has been taken with a

perfect camera containing a perfect lens with a negative held flat in the focal plane, and in which the object space, defined by three dimensional Cartesian coordinate system, is a vacuum allowing light rays to travel in straight lines from the object to its image on the negative through the perspective center. This situation will never be experienced in practice and, therefore, deviations from this ideal situation must be accounted for.

The major systematic errors are:

- comparator errors.
- principal point displacement,
- lens distortions,
- atmospheric refraction,
- Earth curvature, and
- film deformations.

2.6.3.1.1 Comparator Errors

There are three major factors causing these comparator errors being exist:

The comparator axes are

- not being exactly orthogonal,
- not having the same scale along them, and
- not being parallel to the photo axes

when the measurements were performed. These effects are normally accounted for by use of a six parameter affine transformation. This transformation accounts for the film deformations, the non-perpendicular of the comparator axes, the translations between the comparator and the fiducial systems, and the scale changes. The transformation equations can be found in the literature (Wolf 1983).

2.6.3.1.2 The Principal point Displacement

The indicated principal point does not generally coincide with the calibrated principal point. Therefore, the measured coordinates of all points should be corrected for this difference to bring them to an origin at the calibrated principal point. To do this, the off-set between these two points is calculated and then added to the coordinates of all measured points.

2.6.3.1.3 Lens Distortions

The effect of lens distortions appears as a displacement of the points from their true positions. It is a function of the radial distance of the point from the principal point and is generally divided into two categories as following:

- radial (symmetric), and
- tangential (asymmetric) distortions.

The radial lens distortion is the more serious of the two. Most commonly, the method of approximating the radial lens distortion is to use polynomial involving only odd powers of the radial distance from the principal points, e.g. $\Delta r = k_1 r + k_2 r^3 + k_3 r^5 + ...$ where r is the radial distance. The coefficients, $k_{1,2,3,...,n}$, can be obtained from a least squares best fit to a curve of known radial distortions at varying radial distances.

The tangential distortion is usually of smaller magnitude than the radial element. In aerial triangulation using analogue instruments, it is found very difficult to compensate for and as a result, it is usually disregarded. In analytical aerial triangulation also, it is often regarded as being insignificant.

2.6.3.1.4 Atmospheric Refraction

A ray of light coming from an object on the earth surface to the camera lens in an aircraft passing through the atmosphere does not follow a straight line because of changing density of the atmosphere. It is refracted away from the vertical. With well

flown aerial photography using modern aerial cameras, the topographic nadir and principal points approximately coincide. Therefore, the effect of atmospheric refraction is similar to that of the radial lens distortion. This error is very difficult to model and, therefore, atmospheric model are used to derive corrections for the measured photo coordinates as be used in GPS to model atmospheric layers.

2.6.3.1.5 Earth Curvature

Photogrammetric measurements are taken on a plane which are not similar with those in surveying. Especially heights of points are not measured along a direction normal to the curved surface of the earth. Therefore, the images of points are displaced inward towards to the principal point.

2.6.3.2 Other Factors

Regardless of the method of estimation used, the following are the most important factors which are affecting the accuracy:

2.6.3.2.1 The Type of Camera

Super-wide angle (SA) cameras have large base to height ratio compared to normal angle cameras. So, the large base to height ratio gives good ray intersections at ground points. But, in practice, SA cameras are not anticipated because large inclinations of the light rays create some geometrical distortions especially when the film is not flattened properly. When normal angle cameras are used, base to height ratio is small but geometrical effects due to the non-flatness of the film and the effects of refraction and curvature are smaller. The wide angle camera is used as a compromise between the normal and super-wide angle cameras. Some cameras are provided with a reseau while the others are having four or eight fiducial marks. So that the camera should give best results because it allows proper modeling of the various systematic errors.

2.6.3.2.2 The Scale of Photography and Flying Height

Photography are classified as small, medium and large scale photography in literature due to the scales used. While smallest photo scale is used in a photography maximum flying height can reach approximately 12 km. The important problem regarding the photo scale (especially at large photo scales) and flying height is the image movement resulted by the movement of aircraft during exposure. The amount of image movement depends on the speed of the aircraft during the photographic mission, the scale of photography, and the camera shutter speed. The higher the speed of the aircraft, the slower the shutter speed, and larger the scale of photography the larger is the effect of image motion as haze, poor image quality at the corners of the photographs. For good image quality it is necessary the use of high resolution emulsions. The high resolution emulsions require long exposure time. So, this means large image motion and then errors in the forward overlap, in particular, at high flying speeds. Nowadays, using of modern cameras built in Forward Motion Compensation (FMC) system and gyro stabilizer can cope with this problem regardless of the flying height and the scale of the photography.

2.6.3.2.3 Identification and Transfer of Points

The accuracy in identifying and measuring aerial triangulation points have a strong effect on the accuracy of results. This depends on the type of the measured point; whether it is a signalized, natural or artificial point. The signalized points are most preferred points between them. Measurements of such points can be done with an accuracy of few microns. The accuracy of point transfer from one photo to another can be the decisive factor on the level of accuracy in aerial triangulation. Recently, analytical plotters removed the need for point marking. Once, a point is measured in one photograph, its position is registered and can be refound as many times as it is needed on the other photographs. Therefore, if natural and artificial points are used in aerial triangulation with analytical plotters, the accuracy of their positions will be as accurate as signalized points.

2.6.3.2.4 Type of Photographic Coverage

In general, 60% ±5% forward and 20% ±5% side overlap of strips are used under normal circumstances. For high precision work, such a geodetic network densification, 60% forward and side overlaps may be used. Although the use of these size of overlaps is more expensive, because of nearly twice the number of photographs will be taken, the resulting aerial triangulation will be extremely strong because each pass point will be imaged on as many as nine different photographs whereby some of the errors tend to compensate and the geometry of the block will be stronger. This also helps in detecting obvious gross errors in the observations which can then be deleted or corrected in a pre-estimation process.

2.6.3.2.5 Type of Triangulation and Instruments

It is obvious that the accuracy of the measurements will be influenced by the used triangulation procedure and the type of used instrument which differ from one manufacturer to another and from one model to another.

On the one hand, analytical aerial triangulation is more accurate than analogue and semi-analytical methods of aerial triangulation because analytical methods can more effectively eliminate, or at least reduce, the systematic distortions explained in section 2.6.3.1 earlier. Analytical techniques are also free from the optical and mechanical limitations imposed by stereo plotters.

On the other hand, stereo plotters have traditionally rated into four categories according to their measurement capabilities. These are:

- analytical stereo plotters, capable of measuring accuracy of 2 μm,
- first order stereo plotters, capable of making measurements to an accuracy of 3-10 μm,
- second order stereo plotters, capable of measuring accuracy of 10-20 μm, and
- third order stereo plotters with measuring accuracy of about 30 μm.

Analytical plotters are superior than the other plotters for various reasons:

- Because they do not form model points by intersection of projected light rays, optical and mechanical errors from these sources are not introduced.
- Any combination of the systematic errors can effectively corrected by them.
- They can take advantage of redundant observations and incorporate the method of least squares estimation.

First order plotters are rarely used nowadays, having being replaced by analytical plotters. Second or third order plotters should not be used for the accurate mapping proposes or determination of coordinates of new points. However, in many countries they are still widely used.

2.6.3.2.6 Distribution and Accuracy of Control Points

The determination procedure of control points directly affects the accuracy of their coordinates. Second or third order triangulation and barometric leveling or trigonometric heighting are sufficient for small scale mapping. But for large scale mapping, first or second order triangulation are generally used with spirit leveling. Nowadays, the use of GPS to fix control points and to provide camera positions are main subjects in aerial photography. Regardless of the method of control provision, these control points are selected according to the certain distribution rules throughout the block. These rules are:

- full control points (X,Y,Z) around the perimeter of the block with a point every 5, or more models, and
- height control points every 5, or more, models across the strips.

In general, the closer these points to one another, the higher is the expected accuracy.

2.6.3.2.7 The Use of Auxiliary Data

The use of statoscope or Airborne Profile Recorder (APR) for height control improves the results of block adjustment. Recently, GPS has provided quicker, cheaper, easier and more precise auxiliary data than the others. So, it introduces further improvement in the results. The determination of the proper weight is the most important matter in the use of auxiliary data combined with photogrammetric and terrestrial data in a simultaneous estimation.

2.6.3.2.8 Screening Gross Errors

It is necessary to eliminate gross errors for the accuracy reason. This is one of the big challenges in aerial triangulation procedures. The cleaner the data set, the more precise the results that they will likely be obtained.

The readers are referred to the literature (Wolf 1983, Burnside 1979, Amer 1978) for further details about the aerial triangulation procedures.

2.6.3.3 Random Errors

They obey the laws of probability. In this concept, they have an equal chance of being positive as being negative and their magnitudes are also subject to random events. Therefore, they generally have a tendency to cancel one another. Even if systematic and gross errors have been removed, random errors still remain. They can not be removed by applying corrections to observations or refining the estimation model.

To deal with random errors in photogrammetry and surveying disciplines, as well as any other disciplines, least squares estimation is used extensively for many good reasons:

- When it is compared with the other estimation techniques, it is relatively easy to understand, easy to implement and interpret the results of its outcome for decision making.

- Normal distribution does not really matter to apply least squares estimation to measurements.
- On average, the expectations of parameters estimated from a least square process are equal to their true values.
- It gives minimum variances for determined parameters and for quantities derived from these parameters.

2.6.3.4 Gross Errors

Gross errors sometimes referred to as blunders, outliers or mistakes can arise from an incorrect measuring or recording procedure or from the observer or the computer software used. These are usually considered to be the most serious errors in any surveying application, since their sizes are relatively large. For this reason, they should be avoided or eliminated, otherwise results obtained from an estimation process deviate from their true values.

There are several definitions about gross error by various authors. One of them has been stated by Cross et al (1993) that "When carrying out a statistical test for outliers a so-called test statistic is computed. The PDF of the statistic is known and, if its value is so high that it can only be expected to be exceeded in (say) 1% of cases, it is assumed that the observation must have been generated by another process. (i.e. it is centered about a different mean) and is highlighted as a possible outlier (for probable rejection)".

The last interpretation of an outlier or gross error given by Cross et al (1993) is the most widely used interpretation. It follows the so-called mean-shift model where it is assumed that the mean of an observation is shifted when a gross error is present but the shape of its distribution is not altered. i.e. it is still normally distributed with a given variance. This mean-shift model has the advantage of allowing statistical tests to be applied. It is for this reason that the mean-shift model has found good support in methods and techniques dealing with gross error detection.

CHAPTER THREE

3. COMBINATION OF AERIAL PHOTOGRAPHY AND GPS: IN OBSERVATION SPACE

3.1 INTRODUCTION

Nowadays, for various purposes such as those mentioned in the introduction section of the previous chapter, the application of GPS into photogrammetry has become a well known subject among surveyors. Photogrammetry generally involves making measurements from photographs. In addition to measurements from photographs, photogrammetry uses position of points on the ground which have been positioned from ground measurements or from remotely-sensed satellite-based measurements (e.g. GPS). So, one of the major steps in any photogrammetric work is to acquire the photographs. While taking photographs it is required that the flight lines have been pre-determined. By the means of navigating the aircraft into these pre-determined flight lines, it is actually the camera on board directed from one exposure station to another to obtain the pre-planned photographs. After having the photographs, they will be used to reconstruct the actual situations when they were taken. To do this, relative and absolute orientation of the photographs are required to form the models using analog or analytical methods. This process will allow measurements to be made on the models. To carry out the absolute orientation of each model, at least five ground control points (two plan and three height) with known coordinates in the ground coordinate system are needed. There are two possibilities to provide these points. They are

- to use traditional or modern (e.g. GPS) geodetic methods before photography (i.e. this method requires an extensive amount of time consuming and costly field work), or
- the use of aerial triangulation which gives an advantage to replace some of these points with some other points (pass and tie points).

During the absolute orientation, the main requirement is the determination of nine unknown parameters which are interior (inner) parameters (coordinates of principal point and camera principal distance) and exterior (outer) orientation parameters (exposure station coordinates in the ground coordinate system, X_0, Y_0 and Z_0, and the three angles, ω, φ and κ, necessary to rotate the image coordinate system to the ground coordinate system). Interior orientation parameters are usually determined from camera calibration. Exterior orientation requires existence of control points with known coordinates. They can be determined directly during flight if appropriate instruments are available on the board. These instruments include Inertial Navigation System (INS), periscopes, NASA's Attitude Reference System (ARS), Airborne Profile Recorder (APR), statoscope, ...etc. These systems have showed their limited success due to their relatively high cost and/or insufficient reliability both in the results obtained using them and in their operation (Corten 1984, Leatherdale 1988, Becker and Barriere 1993, Schade and Cramer 1994). On the other hand, GPS fulfills the requirements of high precision, universal availability, system reliability, ease of data collection, and low data collection cost while determining all, or some, of the exterior orientation parameters and providing control to be used in estimation procedures using aerial triangulation.

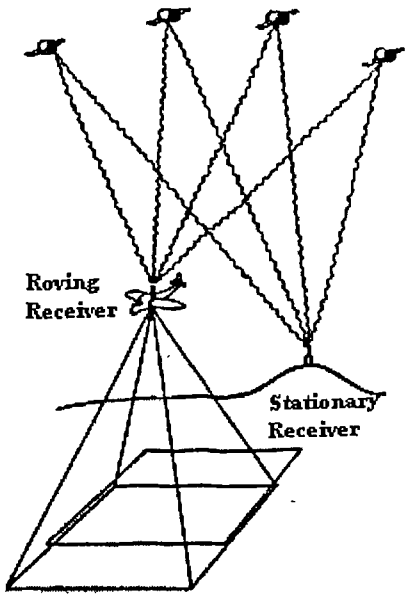

Figure 3.1 Relative airborne GPS

Today exposure station coordinates are determined efficiently and accurately with this GPS technology. The weakness in this method is its inability to determine the rotation angles (ω, φ, κ) with an acceptable accuracy. Therefore, aerial triangulation cannot be eliminated. But, the coordinates of exposure stations determined using GPS give an advantage to reduce the number of ground control points. So, these points can be replaced with most of the ground control points in a bundle adjustment. It is also necessary to utilize from relative techniques using the phase observables for high precision applications. During this process, two GPS receivers are required. One of them is placed on a known site (stationary receiver), the other one is onboard the aircraft (roving receiver) during the photo mission (figure 3.1). Both receivers observe carrier phase data simultaneously at the same rate during the flight. After the flight, the data collected is ready to be evaluated. But, before postprocessing, there are several complicating factors to be considered. In this concept, it is necessary to determine the spatial offset between the GPS-antenna phase center and the entrance nodal point of the camera, and the time offset between a GPS-epoch (a group of observations at a specific time) and each exposure. It is also necessary to detect and correct the cycle slips in the phase observations, and the unknown ambiguities have to be determined. In addition, the results from the adjustment should normally be transformed from WGS84 to the local ground coordinate system.

In the following sections, a summary of the research which has already been done on how to integrate GPS with photogrammetry will be discussed and then our new approach to this integration. But first, the factors mentioned above will be explained.

3.2 SPECIFIC PROBLEMS IN AIRBORNE GPS

3.2.1 SPATIAL OFFSET

One of the major complicating factors is the spatial offset between the phase center of GPS antenna onboard and the perspective center of the camera in the aircraft. During the flight, this spatial offset varies depending on the aircraft rotations with respect to the ground coordinate system. It is required to compensate for this offset during the

photo mission. Thus, the rotations will be the same with the rotations of the aircraft as if the camera (ω, φ, κ) in the ground coordinate system. Then the offset will depend on these rotations only. These rotations can also be estimated in the bundle block adjustment. If they are not measured, during the flight mission, by the means of appropriate instruments pre-installed to the aircraft such as the instruments mentioned section 3.1.

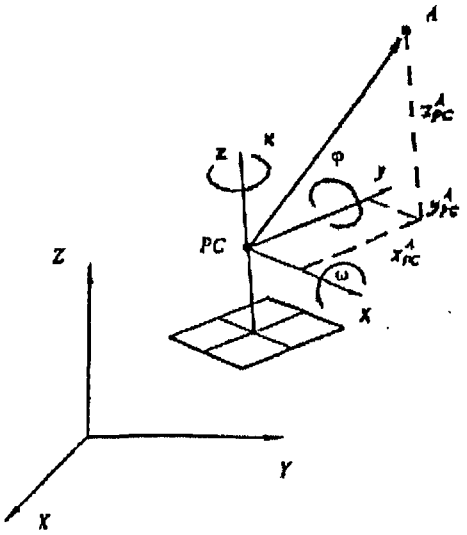

Figure 3.2 Spatial Offset (A = antenna, PC = perspective center)

Components of the offset vector, also called eccentricity vector, in the image coordinate system have to be known in the combined adjustment to correct this offset. In practice, several methods exist for the determination of this offset vector. One method whose achievable accuracies is better than ± 1 cm is based on terrestrial photogrammetry (Blankenberg, 1993). Another method is to use normal surveying techniques, e.g. theodolite and tape or EDM. This method is based on intersections from sides surrounding the aircraft. Horizontal directions, zenith distances and distances are measured from each side. Then, the vector from the principal point to the antenna phase center is estimated by a network adjustment where the fiducial marks define the image coordinate system. The sought vector from the nodal entrance to the antenna is found by simple algebra.

Introduction of this offset into the observation equation used in the combined adjustment will be given in the following sections.

One difficulty while determining this offset is the necessity that the camera has to be fixed to the aircraft. Ideally the crab-settings should be kept constant during the flight, but this is not a limitation if the crab-setting can be recorded, either manually or automatically. This registration is also done by a stabilization camera mount.

If the GPS antenna is mounted directly above the camera, the crab angle will hardly affect the eccentricity vector (Ackerman 1992). In this situation, the offset vector will still be changed by depending on tilt corrections of the antenna. The effect of the tilt correction is small with this antenna position, but not negligible for large image scales. It can also be investigated that they are introduced and solved for in the new combined adjustment. Then this limitation is no longer a problem and the camera will be free to tilt.

3.2.2 TIME OFFSET

GPS data can be obtained at constant intervals in a sequence defined by measuring rate of GPS-receivers, e.g. once per second, not at time of the camera exposure, to be more precise, not at the mid-time of the exposure. However this rate can be customized manually by the user. Therefore, an offset depending on the time difference between these two events occurs from the sought position of the camera.

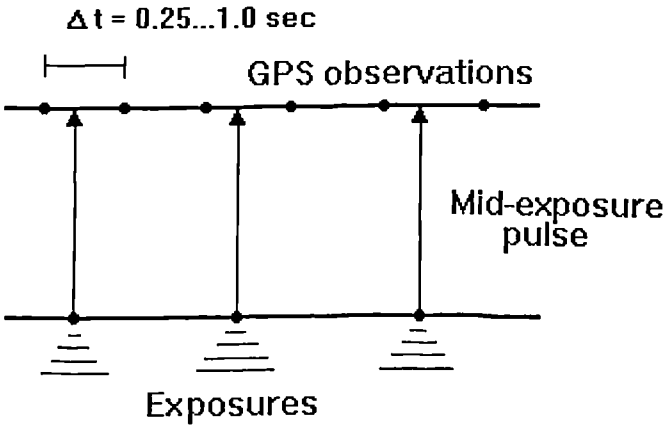

Figure 3.3 Time offset

This problem can be solved in three ways:

- The mid-time of exposure is recorded, and the sought position of the camera can be estimated through interpolation between the two consecutive GPS-positions.
- The shutter of the camera is released by a pulse from the GPS receiver. The time offset is then eliminated or at least minimized.
- A mid-exposure pulse send by the camera to the receiver can drive the measurements made in the receiver.

In the first method, it is required that each exposure is recorded in the time frame of the GPS receiver. Modern cameras are designed to emit very accurate mid exposure time pulse, e.g. in the Wild RC20 camera this emitted pulse has a maximal deviation of $\pm$ 52 μs from the exact mid point of exposure. This deviation causes a negligible 5 mm forward motion in a ground speed of 100m/s of an aircraft. The pulse is sent to GPS receiver and recorded in the time frame of the receiver. Therefore time tags of the exposure and the GPS observations are referred to the same time frame. This time tagging is only possible if the GPS receiver has a photogrammetric option.

The antenna positions at the instant of exposures can be derived easily by interpolating the closest GPS positions. Therefore the exposure time has to be recorded in the GPS time base, this is not a problem with the newest cameras (e.g. RMK TOP, LMK 2000 and RC30). The other cameras have to be equipped with a diode for the registration of the instant of exposure (Jacobsen 1991) and the time delay between exposure time recording and the instant of exposure has to be determined as a function of the exposure time. Several interpolation formulas have been suggested, e.g. ordinary linear interpolation (Ackermann 1992), lagrange interpolation of third order (Frieb 1991) or least square matching. This should be based on information about the flight path of the aircraft, which may be different depending upon turbulence of the atmosphere - depending upon the height above ground and the weather conditions. Since the camera moves 50 m between two GPS epochs if the aircraft ground speed is around 100m/s, it is readily be seen that the interpolation interval is quite wide. Therefore the interpolated position may deviate several cm from the true position. The results can be improved if the camera is triggered close to a GPS registration.

Several GPS receivers emit a pulse which can be used to trigger a camera. But the receivers can emit the pulse at a constant rate. In aerial triangulation constant overlap is usually required within the strips. This can only be obtained if time interval between two subsequent exposures can be varied.

If a navigation system based on GPS (e.g. code measurements) is used in the aircraft and the camera connected to this system it is also possible to assure proper overlap between images. The navigation system will combine the camera position with other data (flight plan, elevation model, etc.) and decide when to trigger the camera. The trigger pulse is emitted simultaneously with the closest GPS epoch. The camera performs the exposure, and emits the mid-exposure pulse to the GPS receiver for recording. This is necessary because the unsynchronized clocks in the two GPS receivers and the delay in the camera shutter still makes interpolation necessary. But, the small deviations will be negligible.

An inexpensive receiver will be sufficient for the navigational purposes. But a precise geodetic dual frequency receiver should be used for the positioning of the camera.

The third method is not realistic, because there is no receiver available to perform measurements at specific epochs. It would also be difficult to obtain simultaneous observations from the two receivers (stationary and roving). It is necessary for single or double differencing.

3.2.3 DATUM PROBLEMS

GPS uses the global datum WGS84, while the ground coordinate system is usually referred to a national datum. According to the various national datum, the ellipsoids used are most likely different in shape and size and in position. Even if spatial orientation of an ellipsoid is well-defined, there might be small differences and the local network might be inhomogeneous. Therefore, the network of local area often has scale and rotation errors, when compared to the national datum.

Heights are usually referred to the geoid. But, the spatial coordinate differences between the reference receiver and the roving receiver are related to the WGS84 ellipsoid, and usually the geoid and the ellipsoid form an angle at the reference site (deflection of the vertical).

The results from the GPS positioning are the coordinates of the antenna in the WGS84 reference system while the mapping is often performed in the national reference system. So, it is required to transform these coordinates to the mapping reference system. When some points with known coordinates in both systems are available, the transformation can be done using Helmert transformation (seven parameters) if the deflection is constant in the mission area. An explanation of three-dimensional similarity transformation can be found in literature (e.g. Hofmann-Wellenhof al. et 1983).

If an *a priori* transformation of the coordinates is impossible, then it is necessary to do this transformation in the combined adjustment.

3.2.4 DATA FLOW

The process of GPS supported photogrammetry requires a considerable volume of data to be recorded onboard and at the stationary receiver during flight, unlike geodetic operations. The data recorded and stored may amount to 20 or more Mbytes (Ackermann 1992).

3.2.5 INITIAL PHASE AMBIGUITY

Precise positioning by GPS requires use of phase observations. While processed phase observations for GPS supported aerial triangulation, it is necessary to solve initial phase ambiguities before the kinematic positioning starts. In the case of one stationary receiver and one roving receiver onboard the aircraft, the initial ambiguity problem may be solved by stationary recording before take-off and/or after landing. There are two possibilities being used in practice, either use a known baseline, i.e. both receivers start at known GPS points, or determine an initial baseline from a known GPS point,

which stationary receiver's antenna was set on, to the other fixed antenna on the stationary aircraft. Simultaneous stationary observations at the both sites are required to continue for about one hour in order to obtain a precise baseline determination. In fact, recent ambiguity solution techniques (e.g. fast ambiguity solution technique) reduced the time necessary to solve initial ambiguities to several minutes.

Using the new combination method, there will be no necessity to solve for the initial ambiguities before kinematic positioning starts. As these ambiguities are solved for in the estimation process simultaneously together with the other unknowns in the new combined model.

3.2.6 CYCLE SLIPS AND DISCONTINUITIES

Phase measurements have to be maintained without any interruption during the flight mission (including the stationary recordings before take off and after landing) in order to calculate the trajectory of the aircraft. This is the general requirement in the current applications for GPS supported aerial triangulation so far unless one of on the fly ambiguity resolution techniques is used. Unfortunately, at any time a signal interruption can happen throughout the flight. There are several reason causing the signal interruption known as following:

- Interruption of signal. The signal from a satellite may be interrupted because of some kind of reason, for example, being cut off by the wing and fuselage of an airplane while turning. Especially, during a 180^{o} turn with a large banking angle a signal after another may be interrupted.
- Cycle slips. It happens, sometimes without any apparent cause. It comes up as a slip of the full cycle counts in the receiver by a few up to possibly thousands of cycles, although the phase observables still seem to be continuous on first sight. If not corrected they result in jumps in the trajectory. The reasons of cycle slips may be a matter of receiver design, multiple path effect or discontinuities in the ionosphere. They should not happen any more, but apparently they still do.

- Constellation changes. During an observation period of up to several hours, some satellite move out of sight, some come up. Hence the number and the constellations of the satellites are changing and jumping in and out.

Most GPS software can handle such disturbances. The problem is not too severe if at least four or five satellite remain in sight and thus allow recalling of interrupted signals. The main problem is that the phase ambiguities have to be reassessed. There are a number of concepts to solve this problem depending on the remaining information. If only two or three satellites or none at all remain undisturbed, the problem is more severe. Because the phase ambiguities cannot be exactly recovered after an interruption. So, the problem is serious, asking for more sophisticated software, especially in connection with kinematic camera positioning and the determination of precise aircraft trajectories or different approaches to the integration of GPS and photogrammetry for aerial mapping as that in this thesis it is suggested and opened to researches possibly to be made in the future.

3.3 CURRENT APPLICATIONS IN PHOTOGRAMMETRY USING GPS

A large amount of research on integration of GPS and aerial photography has generally been focused onto the works carried out in order to provide accurate navigation and precise positions of the exposure stations and the attitudes of the aerial photographs. Better to divide these applications into four areas according to their application fields in photogrammetry (Ackermann 1992):

- Aircraft navigation and pin-point photography.
- Determination of camera attitude and position.
- Determination of ground control points.
- Determination of antenna positions to be used in combined GPS aerial triangulation estimation procedures.

Since determination of ground control points is mainly based on field work, it concerns geodesy and will not be discussed here. Ground points are currently located with an accuracy of 1-2 ppm, or better if GPS is used which is well within the requirement of mapping for all photo scales.

3.3.1 AIRCRAFT NAVIGATION AND PIN-POINTING

In an aerial triangulation process, it is necessary to navigate aircraft from one pre-planned exposure station to another and to obtain recognizable land marks from the aircraft, so called "*pin*-pointing". There are several factors, which affect the aircraft navigation, such as the speed and altitude of the aircraft. If the aircraft flies quickly, this will reduce the time between the measurements of navigation information and their computation, display and recording. The altitude must also well defined in navigation.

Navigation can be classified in four divisions (Corten 1984):

- Contact navigation or pilotage.
- Deduced (Dead) Reckoning (DR).
- Position fixing.
- Integrated systems.

Contact navigation needs the pilot to visually guide the aircraft tracing along the recognizable features, such as roads, rivers, or along a visually defined path on a map. Deduced reckoning is an interpolation of a known position to some future time by means of direction and distance or speed and time. Point positioning is the determination of the position of an aircraft by observing the recognizable landmarks (pin-pointing), using two or more lines of positions, such as rail roads or rivers, or using resection from three or more known points as in position fixing by GPS. If several navigation methods are available, it is possible to integrate their outputs into one or more computers and then to produce a single output to the pilot or auto-pilot. Using the output produced from one of the navigation systems above, calculations,

such as actual position of the aircraft, time estimate for the next exposure, destination heading, ...etc. are carried out by the navigation computer. Then these calculations can be used to control the auto pilot to direct the camera to predetermined locations where photographs are taken.

The use of GPS in aircraft navigation and pin-point positioning has become a standard procedure (Jacobsen 1993, Becker and Barriere 1993, Landau et al. 1994). Aircraft navigation with GPS only needs one receiver onboard the aircraft and to collect the C/A code. Under selective availability, deviations from the pre-defined positions of exposure stations are possible in about 70 meters, 80% of the time (Jacopsen 1993). These deviations can be reduced to less than 5 meters at 95% of the times using DGPS (Ackroyd and Lorimer 1990). This is sufficient even for large scale mapping. It is simple in principle that application of GPS into aircraft navigation and pin-point positioning. In the market, recent navigation systems are equipped with a computer onboard the aircraft which lets the user store the actual flight plan (Becker and Barriere 1993, Landau et al. 1994). The position of the aircraft can be calculated, continuously, as the aircraft moves along the flight line. Then these calculated positions with the course of the aircraft and deviations from the actual flight line can graphically be displayed to the pilot to carry out the necessary adjustment required. At the same time, the computer can send a message to trigger the camera to take photos at points within specified deviations from the pre-planned positions. An accurate regular photographic overlap and pin-point photography can be carried out safely with no gaps and strips with good lateral overlap (sidelap). In practice, however, the directing and positioning of an aircraft or taking of a photograph at the right place at the right time using GPS is unpredictable, since the required conditions for accurate GPS point positioning are different from those needed for a good quality photography. On the one hand, aerial photography depends on factors such as weather conditions, snow cover, clouds, vegetation, security, safety regulations, ...etc.. On the other hand, GPS, being a military program, has been designed to sometimes deny its civilian users to accurately determine their real time positions by the means of selective availability (SA) whereby the signal received by the civilian user is altered to degrade the accuracy to about 100 meters 95% of the time. Other factors include the satellites geometry, elevation angles of the available satellites and the atmospheric conditions. These errors affect the

position of the aircraft as well as the actual location of the photographs. To obtain pin-pointed photography and accurate navigation, DGPS should be used. The differential mode eliminates most biases common to the two receivers and yields positions accurate enough even for large scale photography.

3.3.2 DETERMINATION OF CAMERA ATTITUDE AND POSITION

The use of photogrammetry for mapping and coordinate determination purposes is the economical way if its cost is compared with those for ground surveying methods. To use modern methods such as GPS for ground surveying can reduce the cost but not as much as in the current photogrammetric processes. In fact, photogrammetry needs some ground points to link photographic points to the national networks. It is also possible to reduce the number of ground control points required for photogrammetric process by using photogrammetric methods of block estimation. It is even possible to reduce it to under four control points by flying cross strips, but then the accuracy is usually not sufficient. The use of additional observations, which is not as expensive as establishment and measurement of ground control points and can give the accuracy usually obtained using ground control points. However, the experiences in the past show that the additional observations obtained using some instruments, such as the horizon camera, stethoscope, APR, and radar altimeter are either not accurate enough or not reliable enough and/or the methods used to obtain them are too expensive or too complicated. For these reasons, most of these instruments were not used by all countries except a few of them (Leatherdale 1988). When GPS become an important issue in surveying agenda, photogrammetrists were encouraged to use GPS to accurately determine the position of the exposure stations and camera attitude at the time of exposure for aerial triangulation purposes. The estimation using blocks of photography can therefore be carried out without ground control points, unless the block requires transforming to a national or local coordinate system.

3.3.2.1 Determination of Camera Positions by Using GPS

The provision of ground control for photogrammetry, even the use of GPS is one of the most time consuming and expensive operation in photogrammetry. In most projects it is responsible for 30%-60% of the overall cost of mapping (Jacopsen 1993, Mrstik and Kusevic 1994). Control points are necessary for the purpose of exterior orientation of the photographs. One of the principal goals for the mapping companies using photogrammetry is to reduce the amount of ground control points, whose positions are determined by traditional or modern surveying methods, using GPS derived exposure stations, as control points moved up into the air. The exposure stations can be determined within a decimeter using GPS carrier phase in a kinematic differential mode or within one meter using GPS pseudo-ranges (Curry and Schuckman 1993, Schwards et al. 1993). They can then be used as control (i.e. as aerial control points) in photogrammetric estimation procedures. The use of exposure stations as control points in photogrammetric estimation process will greatly reduce, or even eliminate the need for ground control in aerial triangulation.

In aerial photography supported by GPS, two receivers are required of which one is mounted on the ground as a "known" point, so called stationary receiver and the other one is carried aboard the aircraft, so called roving receiver, in order to utilize advantages of DGPS. These two receivers simultaneously collect GPS phase data from at least four satellites at the same rate. After post-processing of the data, the exposure station coordinates can then be determined with an accuracy of 5 centimeters, at the 2σ level for all three coordinates, using dual frequency receivers for distances of up to 30 km (Landau et al. 1994). There are various factors affecting the accuracy level as following:

- The degree of accuracy of ambiguity resolution.
- The transformation accuracy from GPS reference frame (WGS84) to the used ground coordinate system or reverse.
- The measuring accuracy of the offset vector between the GPS antenna and the camera onboard the aircraft.

- The used interpolation techniques to provide the time synchronization between GPS epochs and each exposure.
- The time spent on the flying mission and the distance between the "known" site and the area of photography.

Before reaching the accuracies mentioned above, in the procedure of aerial photography using GPS, the following factors (i.e. those mentioned in chapter two) must first be considered:

- relative phase processing for precise GPS positioning,
- geodetic coordinate transformation,
- time synchronization, and
- antenna offset.

After these reductions, precise GPS coordinates of the exposure station of the camera may be obtained. In addition to these reductions, it is required that initial ambiguity solution has to be done. The required initial ambiguity solution can be obtained by starting from a known GPS determined baseline. The determination of a GPS baseline, before take-off, used to take at least one hour of stationary recordings to the same satellites by both receivers. That situation has been eased, recently, as the GPS observing windows got larger and more sophisticated processing algorithms have reduced the recording time to perhaps 10 minutes or less.

3.3.2.1.1 Current Research

A large amount of research has been completed on determination of camera positions using GPS for aerial photogrammetry. Some of them will be summarized in the following paragraphs.

There are several works which have been done on GPS photogrammetry in Europe. For examples, the tests have been made by ITC, Enschede, the Netherlands (Cortes, Heimes 1989), the IGN, St. Mande, France (Brossier, Millon 1990), the

Rijkswaterstaat, Delft, the Netherlands (van der Vegt, Boswinkel, Witmer 1988), Continental Shelf and Petroleum Technology Research Institute, Norway (Andersen 1989), the University FAF, Munich together with Rheinbraun, Koln, Germany (Hein 1989) and University of Hannover, Germany (Jacobsen 1990 and Jacobsen, Li 1990).

In these tests, quality of kinematic GPS positioning has been checked against the locations of projection centers determined by block adjustment. Systematic errors, in any case, have been present up to several meters. A drift in the antenna positions depending upon time has been in most of the data sets. After elimination of the systematic errors of the GPS positions the r.m.s. differences have reached between ± 4 cm in the case of a relative GPS positioning and ± 60 cm in the case of absolute GPS positioning.

In fact, the combination of GPS and photogrammetric measurements have been widely used for aerial triangulation to reduce or even eliminate ground control points. Lapine (1992) reports that aerial triangulation can be done without any control provided that the satellite signals are not blocked during the flight mission. He also suggests that the offset vector between the GPS antenna and the camera perspective center has to be determined through a calibration procedure and the integer ambiguity can be initialized from a known reference point, before the flight mission. In order to determine the antenna position at the instant of each exposure, Alobaida (1993) indicates that linear functions or cubic splines can commonly be used as interpolation techniques. For any signal interruption (in fact, it is always possible in GPS aerial triangulation) during GPS data collection, Euler and Landau (1992) and Schade (1992) developed different algorithms for recovering the ambiguity through filtering and prediction techniques, and recently by using dual frequency receivers.

Ackermann who carried out large amount of work is one of the first researchers studied on GPS supported aerial triangulation. Ackermann's work has mainly been focused on deriving of the perspective centers of the vertical aerial cameras using relative kinematic GPS positioning. He found that there was some systematic errors causing a shift in the coordinates of camera perspective centers derived from GPS

when they were compared with those derived from standard aerial triangulation (Ackermann 1992b). Ackermann then used drift parameters to correct GPS derived camera perspective center coordinates affected by these systematic errors.

Ackermann (1992) also states that there are no propagation errors in the block of photography and as a conclusion, the accuracy of the blocks of photography depends on the drift parameters to be applied for the GPS derived coordinates during the adjustment procedure, slightly GPS accuracy, the ground control and block size when GPS derived camera positions are used.

The concept of drift parameters is subject to an argument among the researchers dealing with GPS supported photogrammetry. If the initial ambiguities were solved incorrectly and held fixed over a period of time, the result of this will be the shift in the coordinates of antenna and this shift may be corrected by drift parameters in the photogrammetric adjustment. So, on the one hand, this is not a GPS drift error, they come up because initial ambiguities are incorrect. Therefore, the solution for these drift errors caused by incorrect initial ambiguity can be treated as a solution to the problem of initial ambiguity resolution and then they may be solved in the photogrammetric adjustment. On the other hand, Gruen, Cocard and Kahle (1993) argued that "so-called GPS drift parameters are cumulative effects of errors in the interior orientation of the metric camera and residual errors from coordinate transformation".

Ackermann (1992) indicates that a linear set of drift parameters are sufficient and if a loss of lock to satellites occurred, a new set of drift parameters should be introduced into the adjustment for each strip of photography.

Theoretically, the requirement for ground control points is removed if GPS supported aerial triangulation is used, except the need for datum transformation. Four control points in the corners of the block are usual use of ground control points in the GPS supported aerial triangulation, although three are theoretical. Four control points are also not sufficient if drift parameters are introduced as additional unknown into the

adjustment, especially if a new set of drift parameters are used for each strip (Ackermann 1992). This requirement for more control points is caused by the singularity problem associated with the adjustment of the block of photography. This can be overcome using vertical ground control points at the each end of each strip of photography or flying two cross lines additionally at the each end of the block of photography. This is the main disadvantage of using drift parameters in the photogrammetric adjustment as suggested in the Ackermann method.

Ackermann used a flight test of twelve strips containing one hundred and forty photographs to demonstrate the presence of drift errors. He has individually tested each strip and compared the root mean square differences between the GPS and conventional aerial triangulation. The differences without using drift corrections were of the order of 86-370 millimeters, the root mean square differences were reduced to 41-84 millimeters when the drift parameters were added to the adjustment.

The test results in Ackermann's work (1992) for six strips, each containing twenty one photographs (i.e. twenty models), four ground control points located in the corners of the block, and a line of vertical control points at each end of the block indicates that GPS supported aerial triangulation may be considered viable technique for most medium and small scale mapping. Since they require block accuracy of the order of $2\,\sigma_0 \cdot s$ to $5\,\sigma_0 \cdot s$ (where s is the scale of photography, σ_0 is the standard deviation of the image coordinates) and the GPS controlled aerial triangulation offers respectively root mean square of horizontal and vertical standard deviation less than $1.0\,\sigma_0 \cdot s$ and $1.5\,\sigma_0 \cdot s$ with no drift parameters, $1.7\,\sigma_0 \cdot s$ and $1.7\,\sigma_0 \cdot s$ with one set of parameters for the block and $2.1\,\sigma_0 \cdot s$ and $2.3\,\sigma_0 \cdot s$ with one set of drift parameters per strip.

Table 3.1 taken from Ackermann (1994) also shows a list of GPS block adjustments which have been carried out by Inpho GmbH, Stuttgart, between summer 1991 and the end of 1993. In all projects, GPS aerial triangulation was applied, characterized by no GPS initialization, L1 phase observation and C/A code pseudo-ranges, one stationary receiver and all blocks with two or more cross strips.

Project	Photoscale	Photographs	Strips	Control Points	Block size (km)	σ_0 (μm)	Theoretical accuracy (in σ_0) plan/height	Absolute accuracy on check points (in σ_0) plan/height
Guinea	1:30000	346	11+4	29	45x90	9	1.2/2.0	
Germany 1	1:8000	90	5+2	4	6x8	6.3		1.3/2.2
Germany 2	1:7500	50	4+2	4	5x6	4.8	1.3/2.5	1.8/2.3
Germany 3	1:7500	70	6+2	4	7x7	4.5	1.2/2.6	1.6/2.8
Germany 4	1:7500	55	4+2	4	6x5.5	4	1.2/2.6	1.6/2.6
USA 1	1:8700	415	14+3	12	16x25	6.4	1.1/1.8	1.8/2.6
Germany 5	1:6200	1633	39+6	34	23x33	7.8	1.3/3.0	
USA 2	1:42000	78	6	4	35x35	7.5	1.2/2.3	
USA 3	1:34000	106	7	4	35x40	8	1.6/2.2	
USA 4	1:41000	65	5	4	35x30	8	1.2/2.7	
Canada 1	1:6100	159	8+2	12	7.6x7.6	6.9	0.9/1.6	1.8/1.9
UAE 1	1:28000	249	10+2	38	38x25	9.1	0.9/1.8	
Germany 6	1:5000	44	4+3	4	2x2	4.8	0.7/1.4	0.44/1.8
UAE 2	1:28000	12	1	4	15x5	8.5		
Middle East 1	1:50000	143	4+3	6	133x33	7.4	0.8/1.4	1.1/1.3
Middle East 2	1:50000	136	4+3	6	130x33	7	0.8/1.6	1.5/1.9
USA 5	1:24000	86	5+3	6	35x21	6.1	1.1/2.1	
USA 6	1:38000	185	6+4	8	150x30	6	1.1/1.9	
Canada 2	1:31000	57	4+1	6	45x12	7.1	1.7/3.5	
New Zealand 1	1:22000	72	5+2	4	19x17	5.9	1.3/2.2	
UAE 3	1:28000	64	4+2	4	26x20	8.6	1.8/2.6	
UAE 4	1:27000	16	3	7	13x10	5.6	1.6/3.5	
USA 7	1:14000	183	9+2	4	20x20	6.1	1.2/2.3	1.5/2.4
					Average =	6.8 $\overline{\sigma_0}$	1.2/2.3	1.5/2.2

Table 3.1 Parameters of some GPS supported aerial triangulation projects

As can be seen from Table 3.1, the overall r.m.s accuracies of adjusted blocks amount to $1.2\,\overline{\sigma_0}$ in horizontal and $2.3\,\overline{\sigma_0}$ vertical coordinates. The accuracy range of $0.8\,\overline{\sigma_0}$ to $1.8\,\overline{\sigma_0}$ in X,Y and of $1.4\,\overline{\sigma_0}$ to $3.5\,\overline{\sigma_0}$ in Z demonstrates that the deviation of the theoretical accuracy of individual blocks from the general expectation ($1.5\,\overline{\sigma_0}$ / $2.0\,\overline{\sigma_0}$) can be considerable. Nevertheless, the general high accuracy level of the GPS blocks is ascertained.

The empirical r.m.s errors at the check points range from $1.1\,\overline{\sigma}_0$ to $1.8\,\overline{\sigma}_0$ in X,Y and from $1.3\,\overline{\sigma}_0$ to $2.8\,\overline{\sigma}_0$ in Z. The empirical results confirm in general that expected high accuracy level of GPS blocks is obtainable under practical operational conditions.

Many researchers, e.g. Schade (1993), Curry and Schuckman (1993), Jacopsen (1993) and Blankenberg (1994) also demonstrate that the use of GPS derived camera exposure stations in aerotriangulation is a practical solution to enable the reduction of necessary ground control. In the works of Schade (1993) and Blankenberg (1994), they compare the results computed using traditional aerial triangulation, and using GPS camera positions and then conclude that there is no significant accuracy difference, and therefore it is possible to reduce the number of ground control points.

3.3.2.2 Determination of Camera Attitude

The position determination of the camera involving the direct solution of the six unknown coordinates can be treated separately from the determination of the camera attitude in respect to the solution of the three rotation angles (i.e. ω,ϕ,κ). If the position and the orientation of the aircraft are known, together with the transformation parameters between the GPS antenna and camera perspective center positions, then the position and the orientation of the camera may be obtained. This effectively reduces the number of unknown parameters and increases the redundancy in the adjustment. By mounting three or more antenna on the aircraft, these three unknown rotations therefore camera attitude may be computed utilizing from GPS measurements. There are several methods in practice used for the attitude determination. One of them will be discussed in the following paragraphs.

The determination of the camera attitude involves the rotation transformation between a coordinate system fixed in space and a body coordinate system (van Graas and Braasch 1991). In the aerial triangulation procedure, the space coordinate system is usually typical local coordinate system in which the x-axis points towards East, the y-axis towards North and the z-axis vertically upwards. Body coordinate system relates to an aircraft fixed coordinate system in which the x-axis points along the fuselage, the

y-axis along the wing and the z-axis downwards through the plane. Figure 3.4 shows the relation between these two coordinate systems and the rotation angles.

In order to derive camera attitude at the instant of each exposure, the two coordinate system may be related using the positions of the antennas on the aircraft derived from GPS and transformed into the local coordinate system and into the airframe coordinate system. The antenna coordinates in the airframe coordinate system must be determined prior to flight, either using a conventional geodetic surveying methods or a GPS static survey. For each epoch the two coordinate systems are related by:

$$X^s = R\,X^a \qquad (3.1)$$

where:

X^s is the vector of coordinates in the space (i.e. local) coordinate system
X^a is the vector of coordinates in the airframe (i.e. body) coordinate system
R is a rotation matrix.

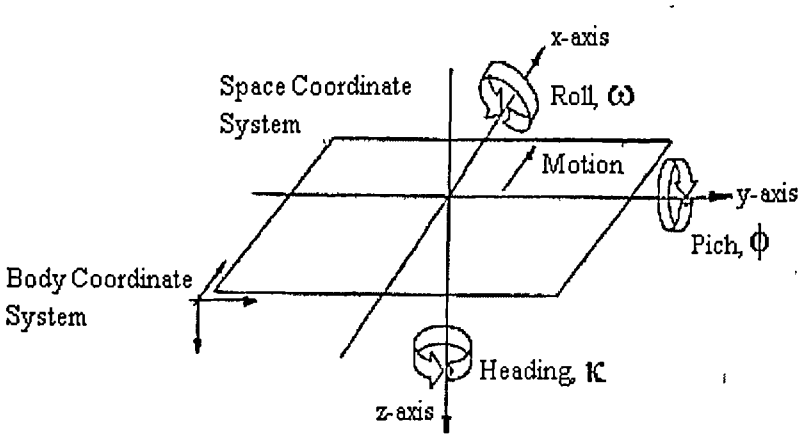

Figure 3.4 Attitude Angles (taken from Corbett 1994)

The rotation matrix contains nine direction cosines relating the two coordinate system one another, and is a function of the rotation angles, i.e. ω,ϕ and κ, which the photograph rotated relative to the ground coordinates system at the time of exposure. The rotation matrix known as the Euler rotation matrix may be shown (e.g. Kraus 1993) by:

$$R = \begin{bmatrix} \cos\phi\cos\kappa & \sin\omega\sin\phi\cos\kappa + \cos\omega\sin\kappa & -\cos\omega\sin\phi\cos\kappa + \sin\omega\sin\kappa \\ -\cos\phi\sin\kappa & -\sin\omega\sin\phi\sin\kappa + \cos\omega\cos\kappa & \cos\omega\sin\phi\sin\kappa + \sin\omega\cos\kappa \\ \sin\phi & -\sin\omega\cos\phi & \cos\omega\cos\phi \end{bmatrix} \quad (3.2)$$

Then the individual attitude angles may be computed such that:

$$\phi = \sin^{-1}(R_{31})$$

$$\omega = \sin^{-1}\left(-\frac{R_{32}}{\cos\phi}\right) \quad (3.3)$$

$$\kappa = \cos^{-1}\left(\frac{R_{11}}{\cos\phi}\right)$$

As can be seen from equations 3.3, Euler angles are not a robust solution since the rotations around the x and y axis may not be calculated where $\phi = \pm 90^{\circ}$. van Graas and Brassch (1991) therefore suggest quaternions (refer to Griffiths and Hilton (1970) for detail) to use for pithiness, efficiency and stability.

The another problem is the flexing of some part of aircraft body, e.g. flexing of the wings or the tail, because of aerodynamic forces during flight. The baselines between the antenna are therefore no more constant by the time being. These inconsistencies may be compensated by modeling them using complete dynamic analysis, Kalman filtering or empirical methods.

There is also a large amount of research, which has been carried out for attitude determination, using multi antenna GPS interferometry techniques. Interested readers are referred to Brown (1992), Nesbo and Canter (1990), Quinn (1993), Rath and Ward (1989), Roth (1986) and van Graas and Braasch (1991).

3.3.2.2.1 Current Research

One example of research concentrating on attitude determination in GPS supported aerial triangulation has been undertaken by Schade et al. (1993). Schade et al. (1993) have compared GPS derived attitude parameters with those derived from standard analytical photogrammetric procedures. During the GPS derived attitude determination process, the Ashtech 3DF (three dimension direction finder) receiver with a twenty four channel single frequency capacity that may be connected to four antenna has been used. It may output attitude information at a rate of 1 Hz (Ashtech 1991) during an interferometric process.

The difference between the GPS solution and the standard photogrammetric solution was of the order of twenty minutes of arc for each attitude angles (Schade et al. 1993). Although it is known, as a priori knowledge, that the orientation of the camera may typically be computed to better than one minute of arc using standard photogrammetric aerial triangulation method. Therefore Schade et al. (1993) conclude that GPS derived attitude parameters may be used for medium to small scale mapping, or starting values for integrated data processing in analytical plotting instruments.

3.4 COMBINATION OF THE SYSTEMS IN BUNDLE BLOCK ESTIMATION

3.4.1 INTRODUCTION

In the traditional bundle estimation the inputs are the image coordinates of object points and ground control points. If the elements of exterior orientations of the photographs are known these image coordinates can be transformed into object space coordinates. It is crucial to know the coordinates of some control points in order to solve exterior orientation elements of each photo (inverse photogrammetry) if they are not known. Interior orientation parameters are usually assumed known, from camera calibration. The observation equations of photogrammetric system are derived from three dimensional coordinate transformation between object space coordinates and

image space coordinates using collinearity principles (see section 2.6.2.1 of Chapter Two). The basic assumption of the collinearity condition is that if a light ray from an object point to a point in the film plane passes through the atmosphere and the camera lens system, the path of such a light ray will be a straight line. The line can then be defined by the object space coordinates, camera lens entrance node coordinates (perspective center) and the image coordinates. This is formation of the first order photogrammetric model.

In practice a first order model cannot ideally be formed since the image coordinates are distorted by some systematic effects, such as film deformations, camera lens distortion, atmospheric refraction, earth curvature, ...etc. (see section 2.6.3 of Chapter Two). So, this is called as second order model. Since these errors, the observed image coordinates are corrected before using them in the estimation process.

In the third order model assumption, it is assumed that some systematic effects are still present in the second order model. Therefore, these are modeled and introduced into the observation equations as additional parameters to be solved for.

It is only recently that the GPS derived camera air stations have been utilized in aerial triangulation. The GPS data, after reduction of antenna and time offsets, refer to the coordinate of perspective centers of the aerial photographs. They represent observations of the position parameters of the exterior camera orientation elements. It is therefore expedient approach to treat GPS camera positioning data as additional observations, and merge them, properly weighted, with photogrammetric aerial triangulation data into combined block adjustment. This is essentially the same approach that was formerly referred to as block adjustment with auxiliary (camera orientation) data. The aerial triangulation observations are assumed to be same as in the conventional aerial triangulation with standard tie points* distribution.

---

* Pass points which tie strips together

3.4.2 LEAST SQUARES ESTIMATION

Least square estimation used in photogrammetry, surveying and other disciplines has many advantages, such as:

- If it is compared with other estimation techniques, it is relatively easy to understand, implement and interpret the results of its outcome for decision making.
- Normal distribution is not necessary for the errors in the measurements.
- The expected parameters through the least square estimation process are on average equal to their true values.
- It gives minimum variances for estimated parameters and the quantities derived from this parameters.

In order to utilize from these benefits of least squares technique, the functions that relate to the unknown parameters have to be correctly formulated. The functional relationship between the parameters and the observables is generally called the mathematical or functional model. The stochastic model, which describes the stochastic properties of observed quantities, should also be correctly formulated. It is important to estimate correctly the variances and covariances of the observations. They should be correctly estimated, unless both the stochastic and functional models are wrong. If there is a failure in the estimation process of the variances of observations, this will lead to a wrong weight matrix being used in the estimation process. If it happened, in general, the estimated parameters and the residuals of observations will not be affected but their covariance matrices will be under estimated or over estimated by the same factor.

There is a relationship between a set of observations ℓ having true values $\bar{\ell}$ and a set of required parameters $\bar{x}$ as described in the following function:

$$F(\bar{x}) = \bar{\ell} \qquad (3.4)$$

This functional relationship relates the observations and parameters to be estimated in a simplified form which is commonly known as observation equations method of least squares.

If v is a vector containing the true residuals of the observations, then:

$$\bar{\ell} = \ell + v \qquad (3.5)$$

Assuming that x_0 is an approximation to $\bar{x}$ and applying Taylor's theorem to (3.4) to a first order and using (3.5), functional model can be constituted as following:

$$F(\bar{x}) = F(x_0) + \frac{\partial F}{\partial \bar{x}}(\bar{x} - x_0) = \ell + v \qquad (3.6)$$

Writing x for ($\bar{x}$ - x_0), b for (ℓ - $F(x_0)$) and rearranging, it is obtained:

$$A\,x = b + v \qquad (3.7)$$

where:

$$A = \begin{bmatrix} \frac{\partial F_1}{\partial x_1} & \frac{\partial F_1}{\partial x_2} & \cdots & \cdots & \frac{\partial F_1}{\partial x_m} \\ \frac{\partial F_2}{\partial x_1} & \frac{\partial F_2}{\partial x_2} & \cdots & \cdots & \frac{\partial F_2}{\partial x_m} \\ \cdots & \cdots & \cdots & \cdots & \cdots \\ \cdots & \cdots & \cdots & \cdots & \cdots \\ \frac{\partial F_n}{\partial x_1} & \frac{\partial F_n}{\partial x_2} & \cdots & \cdots & \frac{\partial F_n}{\partial x_m} \end{bmatrix} \qquad (3.8)$$

b is the vector containing the observed values minus the functions calculated using the approximate values.

Equation (3.7) is the linearized form of the functional model (3.4). Taking the covariance matrix of the observations, generally regarded as uncorrelated in

photogrammetric problems, as C_ℓ then the weight matrix of the observations is given by:

$$W = \frac{1}{\sigma_0^2} C_\ell^{-1} \qquad (3.9)$$

σ_0^2 is a dimensionless quantity usually called the unit variance, the reference variance or the variance factor. It is considered to be theoretically known either from long experience with the instruments used or from applied methods and techniques of measurements or from both. Since observations in photogrammetry are assumed as uncorrelated regarding to one another, the diagonal elements of weight matrix are usually defined as following (other elements of weight matrix are zero):

$$p_i = \frac{1}{(S_i)^2} \qquad (3.10)$$

where:

p_i is the weight of the ith observation and

$(S_i)^2$ is the square of the standard deviation or variance of the observation.

The least squares solution of equation (3.7) is given by (Cross 1983) as:

$$\hat{x} = (A^T W A)^{-1} A^T W b = N^{-1} A^T W b \qquad (3.11)$$

and

$$\hat{v} = A\hat{x} - b \qquad (3.12)$$

After a least square solution, the variances of the parameters estimated as the results, the variances of the residuals and the variances of the least squares estimates of the observations could easily be extracted from their respective covariance matrices,

obtained via the law of propagation of variances and covariance. They are not proven here. For further details, the reader is referred to Cross (1983).

The covariance matrix of estimated parameters, $C_{\hat{x}}$, is given by:

$$C_{\hat{x}} = N^{-1} \qquad (3.13)$$

That of least squares residuals, $C_{\hat{v}}$, is given by:

$$C_{\hat{v}} = (W^{-1} - AN^{-1}A^T) \qquad (3.14)$$

That of least squares estimate of observed quantities, $C_{\hat{\ell}}$, is given by:

$$C_{\hat{\ell}} = AN^{-1}A^T = W^{-1} - C_{\hat{v}} \qquad (3.15)$$

The unit variance after least squares estimation is generally given the term *a posteriori* unit variance and is given by:

$$\hat{\sigma}_0^2 = \frac{\hat{v}^T W \hat{v}}{n-m} = \frac{\hat{v}^T W \hat{v}}{u} \qquad (3.16)$$

In all above equations ((3.4) through (3.16)):

n: Number of observations.

m: Number of unknown parameters.

ℓ: Vector of observations (n x 1).

$\bar{\ell}$: Vector of true values of observations (n x 1).

A: Design matrix (n x m).

$\bar{x}$: Vector of true values of unknown parameters (m x 1).

x_0: Vector of approximate values of unknown parameters (m x 1).

$\hat{x}$: Vector of least squares estimates of unknown parameters (m x 1).

b: Vector of absolute terms (observed values - computed values) (n x 1).

v: Vector of true residuals (n x 1).

$\hat{v}$: Vector of least squares residuals (n x 1).

W: Weight matrix of observations (n x n).

u: Degrees of freedom (redundancy).

From (3.11) and (3.12) it can be written:

$$\begin{aligned} \hat{v} &= AN^{-1}A^{T}Wb - b = (AN^{-1}A^{T}W - I)b \\ &= (AN^{-1}A^{T} - W^{-1})Wb \\ &= -(W^{-1} - AN^{-1}A^{T})Wb \end{aligned} \qquad (3.17)$$

A direct relationship between residuals and observations could be obtained by substituting (3.14) into (3.17) to get:

$$\hat{v} = -C_{\hat{v}}Wb \qquad (3.18)$$

3.4.3 OBSERVATION EQUATIONS

The fundamental mathematical model used for the photogrammetric data in combined adjustment is a set of collinearity equations extracted from the principle of collinearity. With collinearity principles, the light rays sharing the same perspective center form a bundle. As a result of this, a bundle of rays passing through the same perspective center can mathematically be related to the ground coordinate system. The collinearity equations have the form given in section 2.6.2.1 of Chapter Two and recalled here as:

$$\begin{bmatrix} X_i \\ Y_i \\ Z_i \end{bmatrix} = \lambda_{ij} R_j \begin{bmatrix} x_{ij} \\ y_{ij} \\ -f \end{bmatrix} + \begin{bmatrix} X_{oj} \\ Y_{oj} \\ Z_{oj} \end{bmatrix} \qquad (2.15)$$

where:

$[X_i \; Y_i \; Z_i]^T$ are the ground coordinates of the ith object point,

$[X_{0j} \; Y_{0j} \; Z_{0j}]^T$ are the coordinates of the perspective center of the jth photograph,

$[x_{ij} \; y_{ij}]^T$ are the image coordinates of the ith points in the jth photograph,

f is the focal distance of the camera,

λ_{ij} is the scale factor with respect to the ith point in the jth photograph,

R_j is the rotation matrix of the jth photograph.

As can be seen from the equation above that when dealing with individual photographs it is required that the object space coordinates must be known. However, when more than one photograph is used and points common to adjacent photographs are measured, a strip or block of photographs is formed and connections between the individual photographs can be made by forcing the rays from conjugate image points to intersect at a common point (object). This condition eliminates the need to have object space coordinates for each photo points and, at the same time creates strong connections between adjacent photographs. Because many conjugate points can be measured in a strip or block, connections can be made between photographs using a limited number of control points. These control points are not necessarily required to be ground points.

Equations (2.15) cannot be used as they stand because for each point in each photograph there is a different scale factor λ_{ij}. To eliminate this scale factor, both sides of equation (2.15) are multiplied by $\frac{1}{\lambda_{ij}} R_j^T$ (R_j is an orthogonal matrix) and dividing the first and second rows by the third to get:

$$x_{ij} = -f \frac{r_{11}\Delta X + r_{12}\Delta Y + r_{13}\Delta Z}{r_{31}\Delta X + r_{32}\Delta Y + r_{33}\Delta Z} \qquad (3.19)$$

$$y_{ij} = -f \frac{r_{21}\Delta X + r_{22}\Delta Y + r_{23}\Delta Z}{r_{31}\Delta X + r_{32}\Delta Y + r_{33}\Delta Z} \qquad (3.20)$$

where:

$$\Delta X = X_i - X_{0j}$$
$$\Delta Y = Y_i - Y_{0j}$$
$$\Delta Z = Z_i - Z_{0j}$$

Equation (3.19) and (3.20) constitute the first order mathematical model of the photogrammetric bundle block estimation. The results of the bundle block estimation include estimates of the perspective center location, attitude of each photograph and the coordinates of all pass and tie points, whose image coordinates are used in the estimation process, in the ground coordinate system.

In an aerial triangulation estimation procedure, it is common using bundles to treat the coordinates of the available ground control points as stochastic variables. Their available coordinates are then used as measured quantities with appropriate weights. For each ground control points k, following observation equations are applied:

$$\begin{bmatrix} X_g \\ Y_g \\ Z_g \end{bmatrix}_k = \begin{bmatrix} \tilde{X}_g \\ \tilde{Y}_g \\ \tilde{Z}_g \end{bmatrix}_k + \begin{bmatrix} v_X \\ v_Y \\ v_Z \end{bmatrix}_k \qquad (3.21)$$

where:

$\begin{bmatrix} X_g & Y_g & Z_g \end{bmatrix}_k^T$ are the required ground coordinates of control points k.

$\begin{bmatrix} \tilde{X}_g & \tilde{Y}_g & \tilde{Z}_g \end{bmatrix}_k^T$ are the *a priori* "known" ground coordinates of control points k.

$\begin{bmatrix} v_X & v_Y & v_Z \end{bmatrix}_k^T$ are the residuals of the ground coordinates of control points k.

To introduce GPS observations into the combined adjustment, it is assumed that GPS observations are interpolated at the time of exposure of the photographs. For each camera position the observed GPS antenna coordinates are then introduced as additional observations via equations of the form (3.22).

$$\begin{bmatrix} X_G \\ Y_G \\ Z_G \end{bmatrix}_j + \begin{bmatrix} v_X \\ v_Y \\ v_Z \end{bmatrix}_j = \begin{bmatrix} X_0 \\ Y_0 \\ Z_0 \end{bmatrix}_j \qquad (3.22)$$

where:

$\begin{bmatrix} X_G & Y_G & Z_G \end{bmatrix}_j^T$ are the coordinates of the jth GPS derived camera perspective center.

$\begin{bmatrix} X_0 & Y_0 & Z_0 \end{bmatrix}_j^T$ are the coordinates of the jth camera perspective center.

$\begin{bmatrix} v_G & v_G & v_G \end{bmatrix}_j^T$ are the residuals of the jth camera perspective center.

Equation such as those above cannot directly be included into the estimation model because the camera perspective center and the GPS antenna phase center cannot occupy the same point in space. There is an offset between the antenna phase center and the camera perspective center. This offset should be accounted for either by direct measurements or by introducing its components into the estimation process as further unknown parameters. The latter solution poses computational problems since the normal equation matrix will be singular or very nearly so (Ackermann 1990, Ackermann and Schade 1993, Frieβ 1990). Even when direct measurements are made to determine the offset between the antenna phase center and the camera perspective center, there are some operational problems. If the camera is operated in a locked-down mode, the components of the offset vector are constant in the camera coordinate system. In practice, however, the camera is usually not locked down on its mount during the flight mission and consequently its orientations changes with respect to the aircraft. It is frequently tilted and/or rotated to compensate for the crab angle of the aircraft with regard to the planned flight line. Consequently, the components of the offset vector in the camera coordinate system changes. There are two possibilities to solve this problem:

1. If the GPS antenna mounted vertically above the aerial camera, then the horizontal components of the offset vector will be zero or at least small enough to ignore. Empirical results have shown that, with the GPS antenna in that position, the

camera tilts and the crab angle will have a little effect on the results (Ackermann (1992a, 1992b), Frieβ 1991).

2. If the GPS antenna can not be mounted vertically above the camera, the actual alignment of the camera relative to the aircraft fixed coordinate system has to be determined using a special device such as an inertial navigation system.

Both solutions bring with their disadvantages. The disadvantages of the first solution are:

- Some gaps between the strips can be found resulting from failure to follow the predetermined flight lines due, for example, to strong cross winds. However, with the present navigation systems utilizing GPS such as the Hauts-Monts Inc. automated flight navigation system (Mrstik and Kusevic 1994) and the T flight software package (Becker and Barriere 1993), the possibility of gaps between strips occurring is a rare one.
- With the proposed antenna position, multipathing is more likely.
- A signal interruption causing cycle slips can happen during turns of the aircraft because of shadowed satellites. However, this problem can be solved by resolving the ambiguities using single epochs.

The second solution brings up its own disadvantages. First it needs extra equipment. This equipment also has its own limitations and its purchase and maintenance will add to the total cost of the system.

In this research, locked down mode for the camera had been adopted. Thus, the offset vector can be resolved into components parallel to the axes, which are now fixed with respect to the aircraft. The rotation matrix that relates the image space to the object space can now operate to relate the GPS antenna phase center to the camera perspective center.

Recalling Figure (3.1) in section 3.2.1 of this Chapter, perspective center is taken to be the origin of the camera coordinate system. *XYZ* is the ground coordinate system, *xyz* is

the camera coordinate system, the camera perspective center coordinates with respect to the ground system will be X_0, Y_0 and Z_0, x_a, y_a and z_a are the offset vector components in the camera coordinate system and ω, φ and κ are rotations about x, y and z camera axes respectively.

The transformation relating the offset vector components between the jth perspective center coordinates and the GPS derived coordinates of the antenna at the instant of exposure of the jth photograph can be written as:

$$\begin{bmatrix} X_0 \\ Y_0 \\ Z_0 \end{bmatrix}_j = \begin{bmatrix} X_A \\ Y_A \\ Z_A \end{bmatrix}_j - R_j \begin{bmatrix} x_a \\ y_a \\ z_a \end{bmatrix} \qquad (3.23)$$

Substitution of equations (3.23) into (2.15) yields

$$\begin{bmatrix} X_i \\ Y_i \\ Z_i \end{bmatrix} = \lambda_{ij} R_j \begin{bmatrix} x_{ij} \\ y_{ij} \\ -f \end{bmatrix} + \begin{bmatrix} X_A \\ Y_A \\ Z_A \end{bmatrix}_j - R_j \begin{bmatrix} x_a \\ y_a \\ z_a \end{bmatrix} \qquad (3.24)a$$

or:

$$\lambda_{ij} R_j \begin{bmatrix} x_{ij} \\ y_{ij} \\ -f \end{bmatrix} = \begin{bmatrix} X_i \\ Y_i \\ Z_i \end{bmatrix} - \begin{bmatrix} X_A \\ Y_A \\ Z_A \end{bmatrix}_j + R_j \begin{bmatrix} x_a \\ y_a \\ z_a \end{bmatrix} \qquad (3.24)b$$

Multiplying both sides of equation (3.24)b by $\frac{1}{\lambda_{ij}} R_j^T$, noting that R_j is an orthogonal matrix, expanding results as three equations and dividing the first and the second equation by the third, yield the modified first order photogrammetric bundle estimation model. For a point i in photo j and an antenna coordinates at the instant of exposure of photo j, the equations take the form:

$$x_{ij} = -f\frac{r_{11}\Delta\tilde{X} + r_{12}\Delta\tilde{Y} + r_{13}\Delta\tilde{Z} + x_a}{r_{31}\Delta\tilde{X} + r_{32}\Delta\tilde{Y} + r_{33}\Delta\tilde{Z} + z_a} \qquad (3.25)$$

$$y_{ij} = -f\frac{r_{21}\Delta\tilde{X} + r_{22}\Delta\tilde{Y} + r_{23}\Delta\tilde{Z} + y_a}{r_{31}\Delta\tilde{X} + r_{32}\Delta\tilde{Y} + r_{33}\Delta\tilde{Z} + z_a} \qquad (3.26)$$

where:

$\Delta\tilde{X} = X_i - X_A^j$, $\Delta\tilde{Y} = Y_i - Y_A^j$, and $\Delta\tilde{Z} = Z_i - Z_A^j$

$[\, x_a \;\; y_a \;\; z_a \,]^T$ are the antenna offset vector components in the camera coordinate system, and

X_A^j, Y_A^j and Z_A^j are the GPS derived antenna coordinates at the instant of exposure of the jth photograph.

Now, GPS derived coordinates can be introduced as stochastic variables. For the GPS antenna associated with jth photograph, the following observation equations are applied:

$$\begin{bmatrix} X_A \\ Y_A \\ Z_A \end{bmatrix}_j = \begin{bmatrix} \tilde{X}_A \\ \tilde{Y}_A \\ \tilde{Z}_A \end{bmatrix}_j + \begin{bmatrix} v_{\tilde{X}} \\ v_{\tilde{Y}} \\ v_{\tilde{Z}} \end{bmatrix}_j \qquad (3.27)$$

where:

$\left[\tilde{X}_A \;\; \tilde{Y}_A \;\; \tilde{Z}_A\right]_j^T$ are the *a priori* estimated antenna coordinates at the instant of exposure of jth photograph,

$\left[v_{\tilde{X}} \;\; v_{\tilde{Y}} \;\; v_{\tilde{Z}}\right]_j^T$ are the residuals of the GPS derived antenna coordinates,

and the other quantities are as defined before.

Equations (3.21), (3.25), (3.26) and (3.27) constitute the general observation equations in the combined GPS-aerial triangulation bundle block estimation. However, equations (3.25) and (3.26) are non-linear. Before using them in the estimation process, they have to be linearized. Linearization processes of these equations are given in Appendix B. The linearization will results in the following observation equation:

$$\mathbf{A X + B Y + C Z} = (\mathbf{x} - \mathbf{x}_c) + v_1 \qquad (3.28)$$

Equations (3.21) and (3.27) are already linear and can be written as:

$$\mathbf{I Y} = (\tilde{\mathbf{X}}_A - \mathbf{X}_{Ac}) + v_2 \qquad (3.29)$$

$$\mathbf{I Z} = (\tilde{\mathbf{X}}_g - \mathbf{X}_{gc}) + v_3 \qquad (3.30)$$

where:

A, B and C — are design matrices containing the partial derivatives of the observed image coordinates with respect to the unknown orientation elements, antenna coordinates and the ground coordinates of the observed image points respectively.

X, Y and **Z** — are vectors for the corrections to be added to the approximate values of the orientation elements, antenna coordinates and the ground coordinates of the observed image points.

$\mathbf{x}_c$ — is a vector containing the computed coordinates of the observed image points.

$\mathbf{x}$ — is a vector containing the observed photo coordinates, corrected for all systematic errors and for the principle point displacement.

$\mathbf{X}_{gc}$ — is a vector containing the computed values of the *a priori* estimated ground control point coordinates and generally taken to be equal to $\tilde{\mathbf{X}}_G$.

$\mathbf{X}_{Ac}$ — is a vector containing the computed values of the *a priori* estimated GPS antenna coordinates and generally taken to be equal to $\tilde{\mathbf{X}}_A$.

v_1, v_2 and v_3 are the residuals associated with the observed image coordinates, the *a priori* estimated antenna coordinates and the *a priori* estimated ground control point coordinates respectively.

$\tilde{X}_g$ and $\tilde{X}_A$ are the vectors as defined earlier.

If the linearized observation equations of the combined GPS aerial triangulation bundle block estimation are written in matrix form, it may be formed as following:

$$\begin{bmatrix} A & B & C \\ 0 & I & 0 \\ 0 & 0 & I \end{bmatrix} \begin{bmatrix} X \\ Y \\ Z \end{bmatrix} = \begin{bmatrix} b_1 \\ b_2 \\ b_3 \end{bmatrix} + \begin{bmatrix} v_1 \\ v_2 \\ v_3 \end{bmatrix} \qquad (3.31)$$

where

$$b_1 = x - x_c$$
$$b_2 = \tilde{X}_A - X_{Ac}$$
$$b_3 = \tilde{X}_g - X_{gc}$$

Least squares may be applied to solve for equations (3.31) and to determine the corrections $\hat{X}, \hat{Y}$ and $\hat{Z}$ to be added to the approximate values to obtain the least square estimates of the unknown parameters. The unknowns in the least square estimation are:

- the orientation elements $\hat{\omega}, \hat{\phi}$ and $\hat{\kappa}$ of each photograph,
- the antenna coordinates associated with each photograph at the instant of exposure, and
- the coordinates of the observed image points in the ground coordinates system.

3.5 NEW APPROACH TO THE COMBINATION OF GPS AND PHOTOGRAMMETRIC DATA IN A BUNDLE ADJUSTMENT: COMBINATION IN OBSERVATION SPACE

All the procedures for combined GPS-aerial triangulation bundle estimation explained in the previous section are based on the integration of GPS and photogrammetric data in the position space. As a new method and new approach to the integration of these systems, it may be suggested that GPS and photogrammetric data are combined in an observation space. Therefore, the cycle slips may no longer be a serious problem and the cross strips are not necessary in the GPS supported aerial triangulation. Also this new approach to the combination of GPS and photogrammetric data will increase the number of observation equations in the least squares bundle estimation, therefore the redundancy of the whole system.

In this method, the inputs are also the same as those described in the previous section, i.e. image coordinates of ground points, image coordinates of ground control points and ground coordinates of some control points (may be at the corner of the block). These control points are only required for datum transformation in GPS supported aerial triangulation. But, GPS controlled strip triangulation as in this research with a strip of four photographs cannot be carried out without ground control, because all exposure stations are along a single strip line. Therefore, at least two control points were utilized in the strip.

3.5.1 OBSERVATION EQUATIONS

Observation equations can be divided into two major parts. The first part consists of photogrammetric collinearity equations as usual, second part uses double difference phase observation equations for dual frequency phase observables. The general form of the entire observation equation will then be as following:

$$A\,x = b + v \qquad (3.32)a$$

where:

$$A = \begin{bmatrix} A_{pho} \\ A_{GPS} \end{bmatrix} \text{ and } b = \begin{bmatrix} b_{pho} \\ b_{GPS} \end{bmatrix} \qquad (3.32)b$$

The collinearity equations are derived from a three dimensional transformation of object space coordinates to image space coordinates utilizing the principle of collinearity as mentioned in section 2.4.1 of Chapter Two. The collinearity equations can also be recalled here as described in the same section such as:

$$\begin{bmatrix} X_i \\ Y_i \\ Z_i \end{bmatrix} = \lambda_{ij} R_j \begin{bmatrix} x_{ij} \\ y_{ij} \\ -f \end{bmatrix} + \begin{bmatrix} X_{oj} \\ Y_{oj} \\ Z_{oj} \end{bmatrix} \qquad (2.15)$$

These equations must be modified in order to include different scale factors for each point in each photograph and the offset vector components that provide a relation between GPS observables obtained by GPS antenna on the plane and the image coordinates measured on the photographs as photogrammetric abservables. The modified collinearity equations may be given as in the 2.4.1 section of Chapter Two. So, for a point i in photo j, the equations with the coordinates reduced to antenna location at the instant of exposure of photo j take the form as following:

$$x_{ij} = -f \frac{r_{11}\Delta\tilde{X} + r_{12}\Delta\tilde{Y} + r_{13}\Delta\tilde{Z} + x_a}{r_{31}\Delta\tilde{X} + r_{32}\Delta\tilde{Y} + r_{33}\Delta\tilde{Z} + z_a} \qquad (3.33)$$

$$y_{ij} = -f \frac{r_{21}\Delta\tilde{X} + r_{22}\Delta\tilde{Y} + r_{23}\Delta\tilde{Z} + y_a}{r_{31}\Delta\tilde{X} + r_{32}\Delta\tilde{Y} + r_{33}\Delta\tilde{Z} + z_a} \qquad (3.34)$$

The results of new combined bundle strip (could be a block as well) estimation include estimates of antenna phase center locations according to camera perspective center positions, attitude of each photographs and the coordinates of all ground points, whose image coordinates are used in the estimation process, in the ground coordinate system.

Photogrammetric observables can be set up as mentioned above in the combined system.

In the GPS part, double differencing are applied to the GPS phase observables to be used in the new combined estimation model in order to eliminate or reduce the effect of some systematic errors experienced in GPS. The GPS double difference phase observations can now be introduced to the observation equations of the new system using double difference equations for GPS phase measurements as described earlier in section 2.5.1:

$$
\begin{aligned}
&-\frac{f}{c}\{[(X_A - X^k)^2 + (Y_A - Y^k)^2 + (Z_A - Z^k)^2]^{1/2} - \\
&\quad [(X_B - X^k)^2 + (Y_B - Y^k)^2 + (Z_B - Z^k)^2]^{1/2} - \\
&\quad [(X_A - X^j)^2 + (Y_A - Y^j)^2 + (Z_A - Z^j)^2]^{1/2} + \\
&[(X_B - X^j)^2 + (Y_B - Y^j)^2 + (Z_B - Z^j)^2]^{1/2}\} + N_{AB}^{jk} \\
&\qquad = \\
&\qquad \varphi_A^k - \varphi_B^k - \varphi_A^j + \varphi_B^j \\
&\qquad + \\
&\qquad \text{Noise (+ multipathing)}
\end{aligned}
\tag{2.8}
$$

where:

X_A, Y_A, Z_A and X_B, Y_B, Z_B	are the coordinates of the both antennas, stationary antenna A and roving antenna B
X^k, Y^k, Z^k and X^j, Y^j, Z^j	are the coordinates of the satellites k and j.
f and c	are frequency of the phase and speed of the light in the vacuum respectively.
N_{AB}^{jk}	is double differenced phase ambiguity.
φ_A^j	is the phase measurement at the site A to the satellite j.

The corrections for the errors caused by the other error sources have not been added to Equation (2.8) because of their negligible sizes in certain conditions as explained in

section 2.5.1 of Chapter Two. Therefore it was simplified in order to study the new combined estimation model.

If a dual frequency receiver is available, L1 and L2 phase measurements are obtained and then equation (2.8) should be formed for L1 and L2 phase observations separately.

$$
\begin{aligned}
&-\frac{f_{L1}}{c}\{[(X_A - X^k)^2 + (Y_A - Y^k)^2 + (Z_A - Z^k)^2]^{1/2} - \\
&\quad [(X_B - X^k)^2 + (Y_B - Y^k)^2 + (Z_B - Z^k)^2]^{1/2} - \\
&\quad [(X_A - X^j)^2 + (Y_A - Y^j)^2 + (Z_A - Z^j)^2]^{1/2} + \\
&[(X_B - X^j)^2 + (Y_B - Y^j)^2 + (Z_B - Z^j)^2]^{1/2}\} + {}^{(L1)}N_{AB}^{jk} \\
&\qquad = \\
&\quad {}^{(L1)}\varphi_A^k - {}^{(L1)}\varphi_B^k - {}^{(L1)}\varphi_A^j + {}^{(L1)}\varphi_B^j \\
&\qquad + \\
&\quad \text{Noise (+ multipathing)}
\end{aligned}
\qquad (3.35)
$$

and

$$
\begin{aligned}
&-\frac{f_{L2}}{c}\{[(X_A - X^k)^2 + (Y_A - Y^k)^2 + (Z_A - Z^k)^2]^{1/2} - \\
&\quad [(X_B - X^k)^2 + (Y_B - Y^k)^2 + (Z_B - Z^k)^2]^{1/2} - \\
&\quad [(X_A - X^j)^2 + (Y_A - Y^j)^2 + (Z_A - Z^j)^2]^{1/2} + \\
&[(X_B - X^j)^2 + (Y_B - Y^j)^2 + (Z_B - Z^j)^2]^{1/2}\} + {}^{(L2)}N_{AB}^{jk} \\
&\qquad = \\
&\quad {}^{(L2)}\varphi_A^k - {}^{(L2)}\varphi_B^k - {}^{(L2)}\varphi_A^j + {}^{(L2)}\varphi_B^j \\
&\qquad + \\
&\quad \text{Noise (+ multipathing)}
\end{aligned}
\qquad (3.36)
$$

The results from GPS observations in the estimation model include estimates of the locations of the antenna on the aircraft and double difference phase ambiguities whose number depends on the number of observed satellites for the each phase type, i.e. L1

and L2. In order to provide convenient GPS observables to be used in conjunction with photogrammeric measurements, the GPS observables have to be interpolated into those at the instant of each exposure using linear or polynomial interpolation techniques.

Equations from (3.33) through (3.36) constitute the general observation equations of the new combined GPS-aerial triangulation bundle block estimation model as shown in equation (3.32)a. Since these observation equations are non-linear. They have to be linearized before using them in the estimation process. The linearisasion process for these equations is shown in Appendix B. So, the linearized equations result in the following observation equations:

$$A\,X + B_{Pho}\,Y + C\,Z = (x - x^0) + v_{Pho} \qquad (3.37)$$

$$B_{GPS}\,Y + I\,N = (\varphi - \varphi^0) + v_{GPS} \qquad (3.38)$$

In Equations (3.37) and (3.38):

A, B_{Pho} and C are design matrix elements containing the partial derivatives of the observed image coordinates with respect to the unknown orientation elements of the camera and antenna coordinates on the aircraft and the ground coordinates of the observed image points respectively.

B_{GPS} and I are also design matrix elements containing the partial derivatives of the double difference GPS phase observables with respect to the unknown antenna coordinates and the double difference phase ambiguities respectively. I is also block unit matrix formed for the ambiguities.

X, Y, Z and N are corrections to be added to the approximate values of the orientation elements, the antenna coordinates, the ground coordinates of the observed image points and the double difference phase ambiguities respectively.

x^0, x are as defined earlier.

φ^0 is a vector containing the computed phase measurements.

φ is a vector containing the observed phase measurements, corrected for all systematic errors

v_{Pho} and v_{GPS} are the residuals associated with the observed image coordinates and the observed double difference phase measurements respectively.

The linearized observation equations of the new combined GPS-aerial triangulation bundle block estimation can then be written, in matrix form, as following:

$$\begin{bmatrix} A & B_{Pho} & C & 0 \\ 0 & B_{GPS} & 0 & I \end{bmatrix} \begin{bmatrix} X \\ Y \\ Z \\ N \end{bmatrix} = \begin{bmatrix} b_{Pho} \\ b_{GPS} \end{bmatrix} + \begin{bmatrix} v_{Pho} \\ v_{GPS} \end{bmatrix} \qquad (3.39)a$$

or:

$$D\Delta = b + v \qquad (3.39)b$$

Where:

$$A = \begin{bmatrix} \frac{\partial F_{Pho(x)}}{\partial(\omega,\phi,\kappa)} \\ \frac{\partial F_{Pho(y)}}{\partial(\omega,\phi,\kappa)} \end{bmatrix}; B_{Pho} = \begin{bmatrix} \frac{\partial F_{Pho(x)}}{\partial(X_A,Y_A,Z_A)} \\ \frac{\partial F_{Pho(y)}}{\partial(X_A,Y_A,Z_A)} \end{bmatrix}; C = \begin{bmatrix} \frac{\partial F_{Pho(x)}}{\partial(X,Y,Z)} \\ \frac{\partial F_{Pho(y)}}{\partial(X,Y,Z)} \end{bmatrix};$$

$$B_{GPS} = \begin{bmatrix} \frac{\partial F_{GPS(L1)}}{\partial(X_A,Y_A,Z_A)} \\ \frac{\partial F_{GPS(L2)}}{\partial(X_A,Y_A,Z_A)} \end{bmatrix};$$

I is the unit matrix for the dual frequency double difference phase ambiguities;

$$X=\begin{bmatrix} d\omega \\ d\phi \\ d\kappa \end{bmatrix};\quad Y=\begin{bmatrix} dX_A \\ dY_A \\ dZ_A \end{bmatrix};\quad Z=\begin{bmatrix} dX \\ dY \\ dZ \end{bmatrix};\quad N=\begin{bmatrix} dN_{L1} \\ dN_{L2} \end{bmatrix};$$

$$b_{Pho}=\begin{bmatrix} x+(f\frac{R_1\Delta X}{R_3\Delta X})^0 \\ y+(f\frac{R_2\Delta X}{R_3\Delta X})^0 \end{bmatrix};\quad b_{GPS}=\begin{bmatrix} \varphi_{L1}-\varphi_{L1}^0 \\ \varphi_{L2}-\varphi_{L2}^0 \end{bmatrix};$$

$$\nu_{Pho}=\begin{bmatrix} \nu_x \\ \nu_y \end{bmatrix};\quad \nu_{GPS}=\begin{bmatrix} \nu_{L1} \\ \nu_{L2} \end{bmatrix}.$$

The elements of the design matrix which consists of A, B_{Pho} and C can be found in Appendix B and the elements of B_{GPS} are given in section 2.5.1 of Chapter Two. Using least squares, equation (3.24)b can then be solved for the corrections for the unknowns (i.e. $\hat{X},\hat{Y},\hat{Z}$ and $\hat{N}$) to be added to their respective *a priori* approximate values to obtain the least squares estimates of these unknown parameters.

While processing the least squares estimation method to solve for the unknown parameters, the weight matrix may be formed as below:

$$W = \begin{bmatrix} W_{Pho} & 0 \\ 0 & W_{GPS} \end{bmatrix} \qquad (3.40)$$

W_{Pho} is a diagonal matrix and consists of $\sigma_1^2,\sigma_2^2,\ldots,\sigma_{2n}^2$ variances of 2n observations, it can be given by:

$$W_{Pho}=\begin{bmatrix} 1/\sigma_1^2 & & & \\ & 1/\sigma_2^2 & & \\ & & \ddots & \\ & & & 1/\sigma_{2n}^2 \end{bmatrix}=\begin{bmatrix} w_1 & & & \\ & w_2 & & \\ & & \ddots & \\ & & & w_{2n} \end{bmatrix}$$

where:

w_1, w_2, ..., w_{2n} are the weights of the observations. Since the photogrammetric coordinate measurements are equally weighted observations. The final form of the W_{pho} will be as following:

$$W_{Pho} = \begin{bmatrix} 1/\sigma^2_{pho} & & & \\ & 1/\sigma^2_{pho} & & \\ & & \ddots & \\ & & & 1/\sigma^2_{pho} \end{bmatrix} = \begin{bmatrix} w_{pho} & & & \\ & w_{pho} & & \\ & & \ddots & \\ & & & w_{pho} \end{bmatrix} \quad (3.41)a$$

W_{GPS} is also diagonal matrix with only a difference from W_{Pho} above. It is block diagonal. When being used double difference process for GPS phase observations, the observations in an epoch regarding to the type of used phase are only correlated. Other observations in other epochs and of other type of phase are not correlated each other. Therefore, W_{GPS} can be formed as:

$$W_{GPS} = \begin{bmatrix} W^{GPS}_{L1\ 1.epo} & & & & & & \\ & W^{GPS}_{L2\ 1.epo} & & & & & \\ & & W^{GPS}_{L1\ 2.epo} & & & & \\ & & & W^{GPS}_{L2\ 2.epo} & & & \\ & & & & \ddots & & \\ & & & & & W^{GPS}_{L1\ n.epo} & \\ & & & & & & W^{GPS}_{L2\ n.epo} \end{bmatrix} \quad (3.41)b$$

$W^{GPS}_{L1\ i.epo}$ and $W^{GPS}_{L2\ i.epo}$ are equal to equation (2.12), thus they can be given by:

$$W^{GPS}_{L1\ i.epo} = W^{GPS}_{L2\ i.epo} = \begin{bmatrix} 4 & 2 & .. & 2 \\ 2 & 4 & .. & .. \\ .. & .. & .. & .. \\ .. & .. & .. & 4 \end{bmatrix}^{-1} \quad (3.41)c$$

where

$$i = 1,2,3,...,n$$

The unknown parameters derived from the least squares estimation will also be as following:

- The orientation elements $\hat{\omega}, \hat{\phi}$, and $\hat{\kappa}$ of each photograph.
- The antenna coordinates associated with each photograph at the instant of exposure.
- The coordinates of the observed image points in the ground coordinate system.
- Double difference integer ambiguities according to the types of observed phases, i.e. L1 and/or L2.

After solving the unknowns, the coordinates of the antenna on the aircraft as one of outcomes of the new system must be projected to the camera perspective center by the means of offset vector components and the solved camera attitude at the each exposure time. This process only requires a simple coordinate transformation from body reference frame to the ground coordinates system. The relationship between these two coordinate systems can be given by the following equation:

$$\begin{bmatrix} \tilde{X}_0 \\ \tilde{Y}_0 \\ \tilde{Z}_0 \end{bmatrix}_j = R_{WGS84}^{LOCAL} \left(\begin{bmatrix} \tilde{X}_A - X_O \\ \tilde{Y}_A - Y_O \\ \tilde{Z}_A - Z_O \end{bmatrix}_j + R_j^{WGS84} \begin{bmatrix} x_a \\ y_a \\ z_a \end{bmatrix} \right) \qquad (3.42)$$

where

$\begin{bmatrix} \tilde{X}_0 & \tilde{Y}_0 & \tilde{Z}_0 \end{bmatrix}_0^T$ is the vector which consists of camera perspective center coordinates at the instant of jth exposure with respect to the local ground coordinates system,

$\begin{bmatrix} \tilde{X}_A & \tilde{Y}_A & \tilde{Z}_A \end{bmatrix}_j^T$ is the vector which consists of antenna phase center coordinates derived from the new combined bundle

estimation at the instant of jth exposure with respect to the ground coordinates system,

$[X_O \quad Y_O \quad Z_O]^T$ is the vector which consists of the coordinates of local coordinate system origin with respect to WGS84 coordinates system,

R_j^{WGS84} is the rotation matrix, whose elements were derived from the new combined bundle estimation, between the body reference frame and WGS84 reference frame at the jth exposure,

R_{WGS84}^{LOCAL} is the rotation matrix between the local coordinate system and WGS84 coordinate system.

After the coordinate transformation, It is also necessary to find out the attitude of the aircraft, and therefore rotations of the photographs, with respect to the local coordinate system. To do this, the collinearity equations (3.33 and 3.34) are used. At least, two points with known local coordinates are sufficient to solve for the rotations of each photograph with respect to the local coordinate system. These two points are also adequate to set up a least squares estimation.

CHAPTER FOUR

4. SOFTWARE DESIGN FOR COMBINATION OF GPS AND AERIAL PHOTOGRAMMETRY IN OBSERVATION SPACE

4.1 INTRODUCTION

The software designed within this research for a combined GPS and aerial triangulation system in observation space utilizes observations from GPS receivers (one is stationary and the other one is roving on an aircraft) and observations measured by an analytical stereoplotter on photographs, as inputs. It yields an estimation of three dimensional relative positions for camera perspective centers and for object points in ground coordinates system, an estimation of camera attitude and an estimation of double difference integer ambiguities. It also identifies and fixes cycle slips if there are some in GPS phase observations. The GPS observations used in the program is the double difference phase observations, since they are the only GPS observations that retain the integer nature of ambiguity biases. These double difference observations have been obtained for both L1 and L2 phases.

This chapter describes how to combine GPS phase observations and photogrammetric measurements in observation space to solve for the unknowns by using a bundle least squares estimation technique in a computer environment. So, a computer program has been written in quick C in order to examine this new approach. It outlines the measurements in the both systems and the new combined model used and therefore alternatively put forward a new combined model being different than those used in the researches so far. In this concept it suggests a combination of GPS and photogrammetric observations in the observation space.

4.2 MATHEMATICAL MODEL

The basic data form which the unknown parameters can be computed are the observations. For GPS supported aerial triangulation, the unknowns are camera

attitude, camera perspective center coordinates and coordinates of object points in local coordinate system and double difference ambiguities, and the observations are determined by the sensors used within the system, see table 4.1.

Sensor	Observables
GPS receiver	Phase measurements for the stationary and the roving antennae (L1 and L2)
Aerial camera	Photo coordinates of the object and control points

Table 4.1 Observations in the new combination of GPS and aerial photography

Mathematical relationships can be defined between the observations, observational errors and unknown parameters. The mathematical model, linking observations to unknown parameters, (so called functional model) describes the geometrical relationship between them plus any corrections required to the observations i.e. scaling factors, drifts etc. In section 3.5.1 of Chapter Three the complete mathematical models adopted in this research for GPS and photogrammetric observations are presented.

4.3 STRUCTURE AND FLOW CHART

In this program written in C, all the data files are accessed using FOPEN statement, while the software constants are introduced into the program in a header file which consists of DEFINE statements. Moreover, arrays and variables required by many subroutines and function (so called subroutine) prototypes are held in the main header file. The main header file and the file consisting of DEFINE statements are separate single files. Another header file which consists of the structures defined for a group of related data items of different types under one name is also held as a single file.

Since the program here was constructed for the propose of research, simulated data for both GPS and photogrammetric observations was used. Therefore, while developing the program this situation was taken into the consideration.

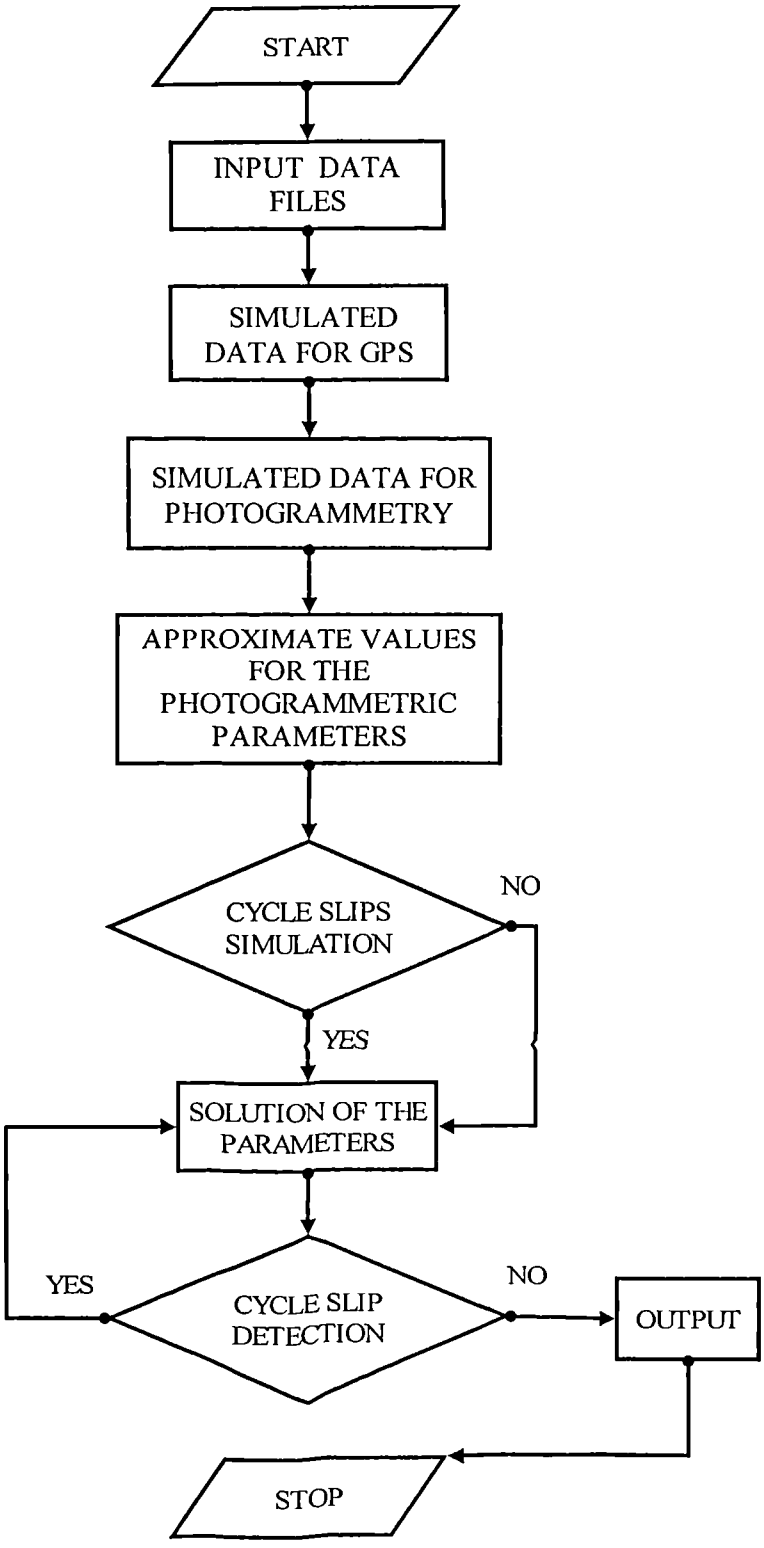

Figure 4.1 Program main flow chart

The structure of the program is based upon following program modules, which are shown in diagram form in Figure (4.1).

- Input of data files and test parameter's file.
- Simulation of GPS observations.
- Simulation of photogrammetric observations.
- Assigning approximate values to photogrammetric parameters.
- Simulation of cycle slip if it will be tested.
- The solution of the parameters.
- Cycle slip detection if there is any.
- Coordinate transformation.

In the following sections more detailed flow charts are given in where they are relevant. As it is seen from Figure (4.1) that the input data files must be read first.

4.3.1 INPUT DATA FILES AND DATA SIMULATIONS

The input of data must be the first step of the program. In this concept, there are several files to be read by the program.

- First the data files produced in RINEX (Receiver INdependent EXchange) format containing GPS data are read for both receivers separately, and then
- the program reads the other files, which are constituted for each photograph separately, containing the photo coordinates of the measured control and object points and the numbers of these points.
- Another input file read is the file containing the coordinates of chosen ground control points which are used when approximate values of the unknown parameters in photogrammetric system are computed.
- The last file is the file constituted for the exposure times and to enter a different set of test parameters at each individual run of the program.

After reading and assigning of the photo coordinates (x and y) of each object and control point stored in the files constituted for the photos, which the point appears on, to the

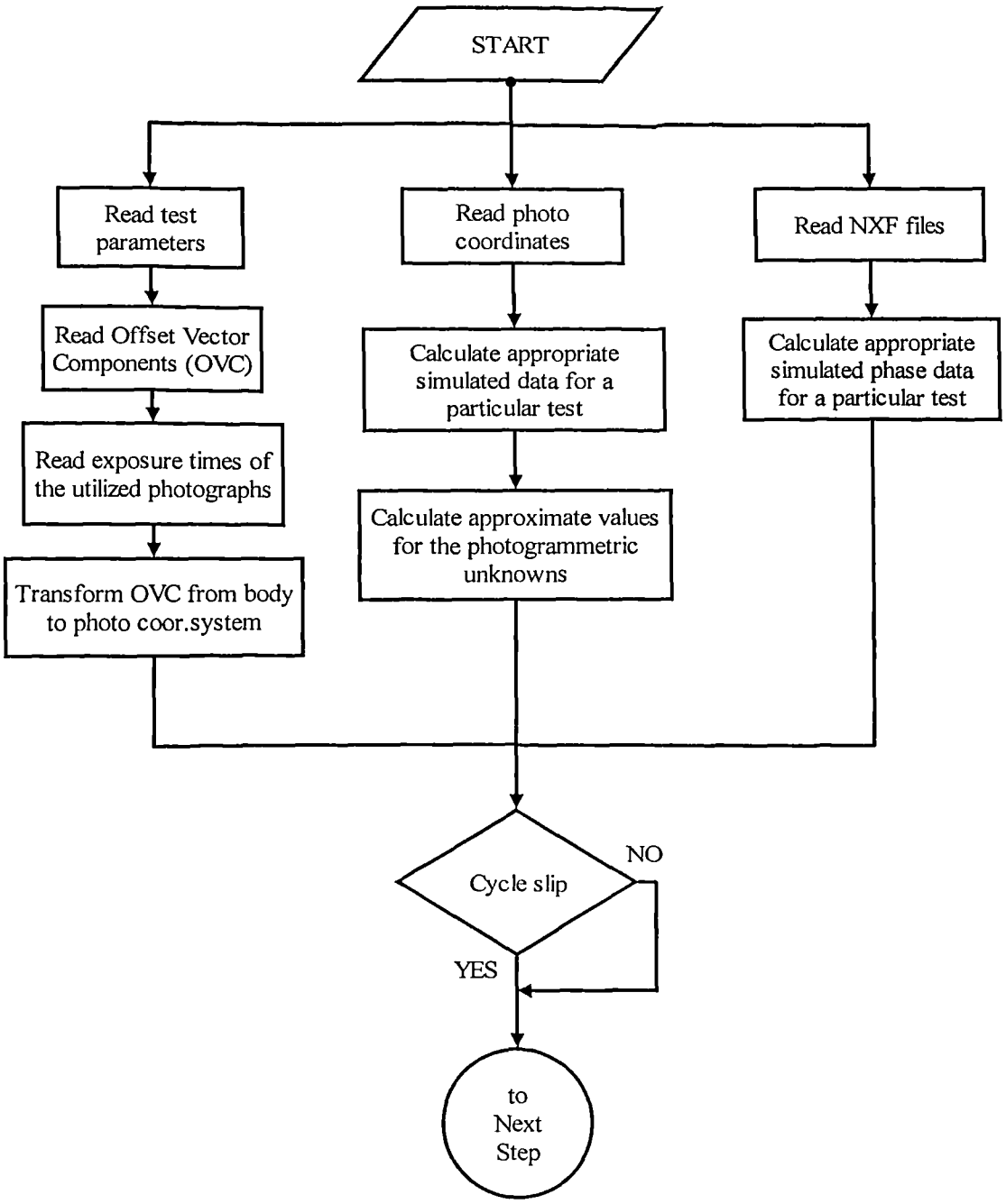

Figure 4.2 Reading procedures of GPS and photogrammetric data and of some parameters

appropriate elements of a STRUCTURE, randomly generated errors which are convenient to the requirements of the test experienced are added to the photo coordinates read from these files to form the simulated photo coordinates of each object and control points.

The program can also read NXF files produced for both stationary and roving receivers to store the coordinates of each satellite in view at each epoch to be used and it also reads phase observations, i.e. in each type, and pseudo-range measurements to each satellites. But they have not actually been utilized from in the program, since the simulated data is used in the research. The epochs utilized and stored in the modified NXF files were the epochs at the each exposure time, interpolated from two consecutive epochs in normal NXF files produced by RINTONXF* software. The simulated data constituted as phase observations was acquired in four steps as follows:

- The first, antenna coordinates derived by employing the offset vector components and the camera perspective center coordinates used in the formation of the simulated photogrammetric data were utilized to compute the distances between the location of the antenna on the aircraft and the coordinates of each satellite in view at each exposure time.
- The second, randomly generated errors as noises and/or multipath were included to these distances to form the pseudo-ranges and then to compute the phase observations to be made up.
- The third, these pseudo-ranges were divided by the wavelength of the phases used, i.e. L1 and L2. Therefore, artificial phase observations without integer ambiguities were obtained by this way.
- The fourth, to obtain the phase observations in a way how they are experienced in the practice after correcting the systematic errors, which they have and can nowadays be modeled using available techniques or are negligible under some certain conditions, randomly generated integer ambiguities were added to these third order phase observations without integer ambiguities.

If a test was set up to study any case with cycle slips, gross errors as cycle slips have to be entered to the appropriate simulated phase observations formed as those at the fourth step above as well. To fulfill this, one or two phase observations in the same or different epoch for the same or different phase (depending on structure of the test set up) were chosen and then cycle slips were added to these observations. For the tests

* This software which was developed by Surveying department in Newcastle Upon Tyne University exchanges a RINEX file to a NXF file.

not studying cycle slips, this step was skipped to carry out the rest of the test process without any cycle slips.

After the data to be used in the next steps of the program is read and simulated in the ways explained as above, approximate values were calculated and assigned to those photogrammetric unknowns:

- the orientation angles of each photograph, and
- the coordinates of the camera perspective center at each exposure.

In this concept the following equations and assumptions were utilized from:

- $\bar{\omega} = \bar{\varphi} = 0$ (This assumption is reasonable for vertical photography).
- $\bar{Z}_0$ can be assumed to be equal to the flying height
- $\bar{\kappa}, \bar{X}_0$ and $\bar{Y}_0$ can be obtained by linear conformal transformation using x_i, y_i, X_i and Y_i as following:
  - Determine the values of a, b, C_x and C_y by least squares solution using the following equations

$$\begin{bmatrix} X_i \\ Y_i \end{bmatrix} = \begin{bmatrix} x_i & -y_i & 1 & 0 \\ y_i & x_i & 0 & 1 \end{bmatrix} \begin{bmatrix} a \\ b \\ C_x \\ C_y \end{bmatrix} \qquad (4.1)$$

  - $\left.\begin{matrix} \bar{X}_0 \approx C_x \\ \bar{Y}_0 \approx C_y \end{matrix}\right\}$ are the camera perspective center coordinates on the ground
  - $\bar{\kappa} \approx \tan^{-1}(\frac{b}{a})$

Since the above assumption is only valid for near vertical photographs. They have been used in the research and they were good enough at producing of reasonable approximate values for the unknowns mentioned above. Another way to obtain them might be to utilize from a map and GPS pseudo-range measurements.

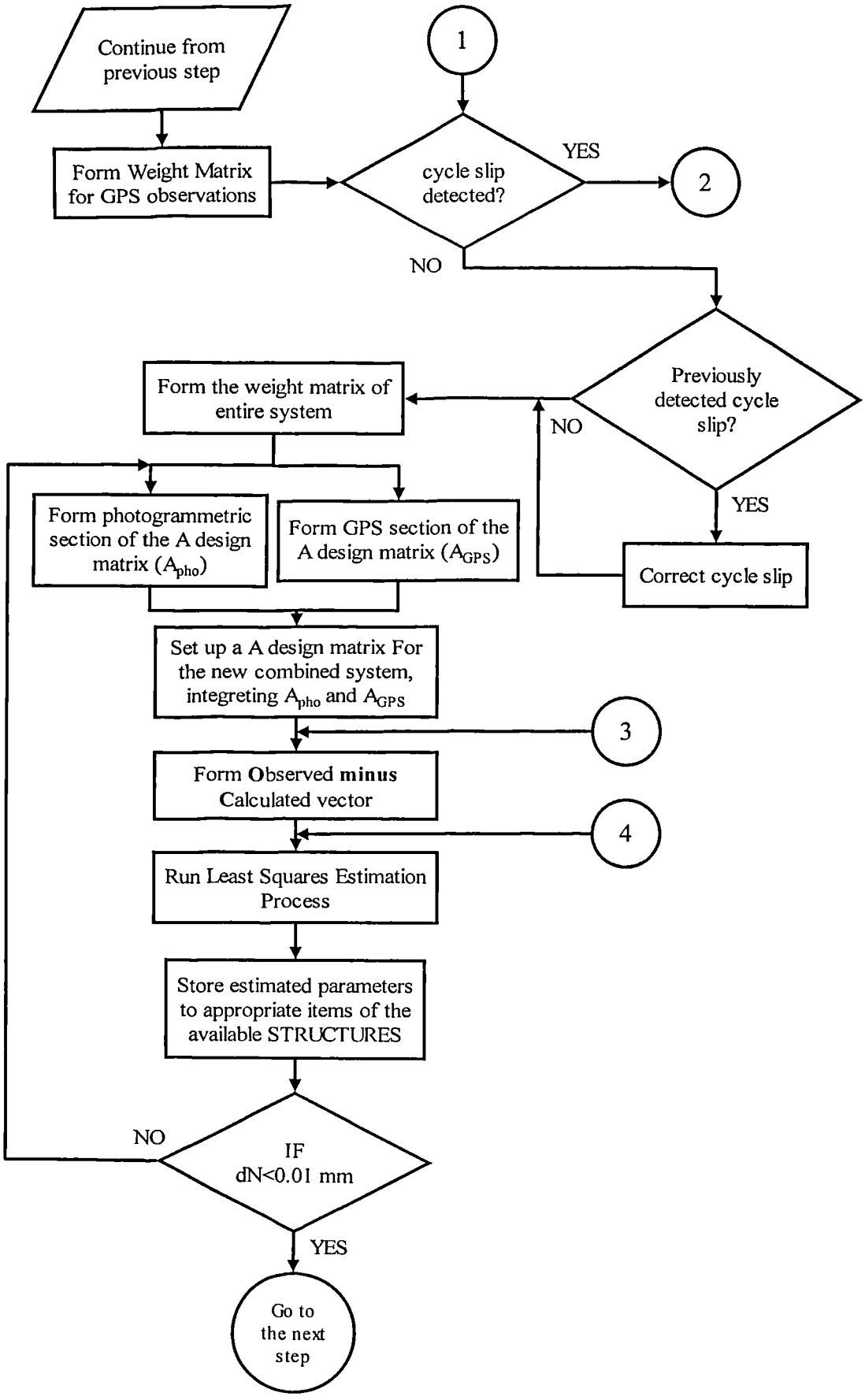

Figure 4.3 Formation of the matrices and Least Squares Estimation Processes

The approximate coordinates of each object points were then computed using the least squares estimation process. The equations used in this process are as following:

$$\begin{bmatrix} x_{ij} \\ y_{ij} \\ -f \end{bmatrix} = \frac{1}{\bar{\lambda}_{ij}} \bar{R}_j \begin{bmatrix} \bar{X}_i - \bar{X}_0 \\ \bar{Y}_i - \bar{Y}_0 \\ \bar{Z}_i - \bar{Z}_0 \end{bmatrix} \qquad (4.2)$$

$$x_{ij} = -f \frac{\bar{r}_{11}^j \Delta\bar{X} + \bar{r}_{12}^j \Delta\bar{Y} + \bar{r}_{13}^j \Delta\bar{Z}}{\bar{r}_{31}^j \Delta\bar{X} + \bar{r}_{32}^j \Delta\bar{Y} + \bar{r}_{33}^j \Delta\bar{Z}} \qquad (4.3)$$

$$y_{ij} = -f \frac{\bar{r}_{21}^j \Delta\bar{X} + \bar{r}_{22}^j \Delta\bar{Y} + \bar{r}_{23}^j \Delta\bar{Z}}{\bar{r}_{31}^j \Delta\bar{X} + \bar{r}_{32}^j \Delta\bar{Y} + \bar{r}_{33}^j \Delta\bar{Z}} \qquad (4.4)$$

where:

$\Delta\bar{X} = \bar{X}_i - \bar{X}_0^j$, $\Delta\bar{Y} = \bar{Y}_i - \bar{Y}_0^j$ and $\Delta\bar{Z} = \bar{Z}_i - \bar{Z}_0^j$

$\bar{X}_0^j, \bar{Y}_0^j$ and $\bar{Z}_0^j$ are the approximate coordinates of camera perspective center at the instant of jth photograph.

$\bar{r}_{11}^j, \bar{r}_{12}^j, \bar{r}_{13}^j, \ldots, \bar{r}_{33}^j$ are elements of rotation martix ($\bar{R}_j$) computed using approximate orientation angles of jth photograph.

x_{ij}, y_{ij} and f are as those described earlier.

After the use of initial approximate values for the quantities above, the coordinate of object points are derived by the least squares estimation.

4.3.2 FORMATION OF MATRICES AND LEAST SQUARES ESTIMATION PROCESS

During the formation of weight matrix for GPS phase observations, correlation matrix 2.11 introduced in section 2.5.1 of the chapter two was the matrix utilized. First, its inverse matrix was computed and then this inverse matrix was placed as the number of used phase type as for each epoch to form the section for GPS observations in the

weight matrix of new combined system. Therefore, in the weight matrix this section was represented in a block diagonal form consisting of those elements shown by Equations 3.40, 3.41b and 3.41c in chapter three. The other elements of this section are zero. To form the photogrammetric section of the weight matrix is easier than GPS one. Since the photogrammetric section only takes value for its diagonal elements not for the others. The others are also zero. Each diagonal element in this section was the same with the others and calculated by using Equations 3.10 and 3.41a in chapter Three. In the weight matrix of the whole combined system, the photogrammetric section took first place and then GPS section as in the functional model, i.e. the photographic observations were given first place and then to the GPS observations.

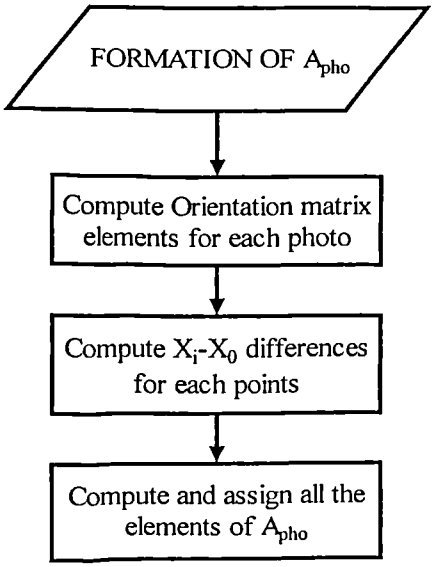

Figure 4.4 Formation of design matrix A_{pho}

The rotation matrix used in the computation process of its elements was the rotation marix shown in Equation 3.2 in this chapter. As a next step, computation process of the coordinate differences between the coordinates of each ground and object points and the coordinates of camera perspective centers took place in the program. The values used in these computations are the initially assigned approximate quantities to all unknowns in the photogrammetric section of the new combined system.

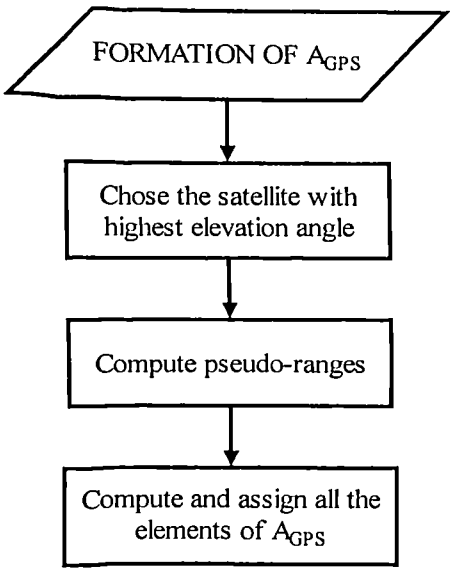

Figure 4.5 Formation of design matrix A_{GPS}

During double differencing process, it is required that the satellite with highest elevation angle must be chosen as a reference satellite. To sort this out, using the determined common satellites between the base and roving site, the elevation angle (and azimuth) to each common satellite is computed by projecting the instantaneous roving receiver-satellite position vector onto the orthogonal axes of the local coordinate system. The mathematics involved can be shown as follows.

The relationship between the Cartesians (X, Y and Z) and geodetic coordinates (λ, φ and h) of a particular point (p) the reference ellipsoid is given by

$$\begin{bmatrix} X \\ Y \\ Z \end{bmatrix} = \begin{bmatrix} (N+h)\cos\varphi \ \cos\lambda \\ (N+h)\cos\varphi \ \sin\lambda \\ (\frac{b^2}{a^2}N+h) \ \sin\varphi \end{bmatrix} \qquad (4.5)$$

where:

N is the radius of curvature along the prime vertical

h is the geodetic height along the normal line

a and b are the semi-major and semi-manor axis of the reference ellipsoid

N can be obtained from the following relationship

$$N = \frac{a^2}{\sqrt{a^2 \cos^2 \varphi + b^2 \sin^2 \varphi}} \qquad (4.6)$$

The geodetic latitude can be computed from the following

$$\varphi = \tan^{-1}\left(\frac{Z + e^2 N \sin\varphi}{\sqrt{X^2 + Y^2}}\right) \qquad (4.7)$$

where:

e^2 is the first eccentricity of the reference ellipsoid, which may be given by

$$e^2 = 2f' - f'^2 \qquad (4.8)$$

where f' is the flattening of the reference ellipsoid, which can be given by

$$f' = \frac{a-b}{a} \qquad (4.9)$$

Equation 4.7 is iterated where φ on the right hand side is initialised by the following value.

$$\varphi = \tan^{-1}\left(\frac{Z}{\sqrt{X^2 + Y^2}}\right) \qquad (4.10)$$

and the geodetic longitude is then computed from

$$\lambda = \tan^{-1}\left(\frac{Y}{X}\right) \qquad (4.11)$$

and the geodetic height is given by

$$h = \left(X \sec\lambda \ \sec\varphi\right) - N \qquad (4.12)$$

The GPS receiver-satellite Cartesian vector components (ΔX, ΔY and ΔZ) expressed in a local coordinates frame (e, n and z') centred at the receiver's antenna can be shown from the following expressions (Kleusberg, 1995).

$$\begin{bmatrix} e \\ n \\ z' \end{bmatrix} = R_X\,(90-\varphi) R_Z (90+\lambda) \begin{bmatrix} \Delta X \\ \Delta Y \\ \Delta Z \end{bmatrix} \qquad (4.13)$$

where R_X and R_Z denote the rotation matrices with respect to the observer's latitude and longitude by the angles (90-φ) and (90+λ) of a right-handed coordinate system around the X-axis and Z-axis, respectively. The resultant rotation matrix is given as follows.

$$R_{xz} = \begin{pmatrix} -\sin\lambda & \cos\lambda & 0 \\ -\sin\varphi\cos\lambda & -\sin\varphi\sin\lambda & \cos\varphi \\ \cos\varphi\cos\lambda & \cos\varphi\sin\lambda & \sin\varphi \end{pmatrix} \qquad (4.14)$$

The azimuth of the line to a particular satellite is then computed as follows

$$\alpha = \tan^{-1}(e/n) \qquad (4.15)$$

while the elevation angle (*e. a.*) to the satellite is computed from the following relationship

$$e.a = \sin^{-1}(z'/s) \qquad (4.16)$$

where

$$s = \sqrt{n^2 + e^2 + z'^2} \qquad (4.17)$$

After determination of the satellite with highest attitude, double difference equations were constituted as functional model for GPS section of the new system. To substitute this model into a least square estimation the partial derivatives (refer to Appendix B)

with respect to every unknown parameter were derived. Pseudo-ranges from the antennas on both sides to every common satellite are required to compute the coefficients of the derivatives referred to the antenna coordinates. Therefore, these pseudo-ranges were computed in the next step. Then the elements of A design matrix where A_{GPS} will stand in were the next computation using the pseudo-ranges.

After completing the computation process of the elements of both photogrammetric and GPS section in A design matrix of new system, integration of both, A_{pho} and A_{GPS}, was fulfilled in this matrix known as A design matrix.

As can be seen from the flow chart in figure 4.3, the next step is the computation to find out observed minus computed values. During this process, the following equations were used:

$$\vec{b} = \begin{bmatrix} \vec{b}_{pho} \\ \vec{b}_{GPS} \end{bmatrix} \qquad (4.18)$$

$\vec{b}_{pho}$ describing the photogrammetric section of the b vector in equation 4.18 may be expressed as following:

$$\vec{b}_{pho} = \vec{x} - \vec{x}^{c} \qquad (4.19)$$

and

$$\vec{x} = \begin{bmatrix} x_{ij} & y_{ij} \end{bmatrix}^{T} \qquad \vec{x} = \begin{bmatrix} x_{11} & y_{11} & \cdots & x_{mn} & y_{mn} \end{bmatrix}^{T}$$

$$\vec{x}^{c} = \begin{bmatrix} x_{ij}^{c} & y_{ij}^{c} \end{bmatrix}^{T} \qquad \vec{x}^{c} = \begin{bmatrix} x_{ij}^{c} & y_{ij}^{c} & \cdots & x_{mn}^{c} & y_{mn}^{c} \end{bmatrix}^{T}$$

where $\bar{x}$ and $\bar{y}$ consist of the observed coordinates of every object points in each photograph, e.g. x_{ij} and y_{ij} are the observed coordinates of ith point in the jth photograph.

Similarly, $\bar{x}^c$ and $\bar{y}^c$ consist of the computed values for photo coordinates of the points derived from the *a priori* estimated values for photogrammetric unknowns by using the equations below.

$$x_{ij}^c = -f\frac{\tilde{r}_{11}\Delta\tilde{X}_{ij} + \tilde{r}_{12}\Delta\tilde{Y}_{ij} + \tilde{r}_{13}\Delta\tilde{Z}_{ij} + x_a}{\tilde{r}_{31}\Delta\tilde{X}_{ij} + \tilde{r}_{32}\Delta\tilde{Y}_{ij} + \tilde{r}_{33}\Delta\tilde{Z}_{ij} + z_a} \qquad (4.20)a$$

$$y_{ij}^c = -f\frac{\tilde{r}_{21}\Delta\tilde{X}_{ij} + \tilde{r}_{22}\Delta\tilde{Y}_{ij} + \tilde{r}_{23}\Delta\tilde{Z}_{ij} + y_a}{\tilde{r}_{31}\Delta\tilde{X}_{ij} + \tilde{r}_{32}\Delta\tilde{Y}_{ij} + \tilde{r}_{33}\Delta\tilde{Z}_{ij} + z_a} \qquad (4.20)b$$

where:

$$\Delta\tilde{X}_{ij} = \tilde{X}_i - \tilde{X}_A^j,\ \Delta\tilde{Y}_{ij} = \tilde{Y}_i - \tilde{Y}_A^j,\ \Delta\tilde{Z}_{ij} = \tilde{Z}_i - \tilde{Z}_A^j$$

$\tilde{X}_A^j, \tilde{Y}_A^j$ and $\tilde{Z}_A^j$ are the *a priori* estimated coordinates of the antenna on the aircraft at the instant of exposure of jth photograph.

$\tilde{X}_i, \tilde{Y}_i$ and $\tilde{Z}_i$ are the *a priori* estimated coordinates of the object points.

$\tilde{r}_{11}, \tilde{r}_{12}, \tilde{r}_{13}, \ldots, \tilde{r}_{33}$ are elements of the orientation matrix R computed from the *a priori* estimated orientation angles.

x_{ij}^c and y_{ij}^c are the computed coordinates of the observed image point i in the jth photograph.

Then $\vec{b}_{GPS}$ describing the GPS section of the b vector as in equation 4.18 may also be expressed as the following:

$$\vec{b}_{GPS} = \lambda_{L1,L2}(\vec{\varphi} - \vec{\varphi}^c) \qquad (4.21)$$

where $\vec{\varphi}$ is a vector that consists of observed double difference phases for L1 and L2, e.g. as following:

$$\varphi^{jmk}_{AB\,L1} = \varphi^{j}_{B\,L1}{}^{m} - \varphi^{j}_{B\,L1}{}^{k} - \varphi^{j}_{A\,L1}{}^{m} + \varphi^{j}_{A\,L1}{}^{k} \qquad \varphi^{jmk}_{AB\,L2} = \varphi^{j}_{B\,L2}{}^{m} - \varphi^{j}_{B\,L2}{}^{k} - \varphi^{j}_{A\,L2}{}^{m} + \varphi^{j}_{A\,L2}{}^{k},$$

$\vec{\varphi}^{c}$ is another vector that consists of double difference phases computed by using the *a priori* est' nated GPS antenna coordinates at each exposure and ambiguities as in the following equations:

$$\begin{aligned}\varphi^{jmk\,c}_{AB\,L1} = \frac{1}{\lambda_{L1}}\{&[(\tilde{X}^{j}_{A} - X^{j}_{k})^2 + (\tilde{Y}^{j}_{A} - Y^{j}_{k})^2 + (\tilde{Z}^{j}_{A} - Y^{j}_{k})^2]^{1/2} - \\ &[(\tilde{X}^{j}_{B} - X^{j}_{k})^2 + (\tilde{Y}^{j}_{B} - Y^{j}_{k})^2 + (\tilde{Z}^{j}_{B} - Y^{j}_{k})^2]^{1/2} - \\ &[(\tilde{X}^{j}_{A} - X^{j}_{m})^2 + (\tilde{Y}^{j}_{A} - Y^{j}_{m})^2 + (\tilde{Z}^{j}_{A} - Y^{j}_{m})^2]^{1/2} + \\ &[(\tilde{X}^{j}_{B} - X^{j}_{m})^2 + (\tilde{Y}^{j}_{B} - Y^{j}_{m})^2 + (\tilde{Z}^{j}_{B} - Y^{j}_{m})^2]^{1/2}\} + N^{mk}_{L1\,AB}\end{aligned} \qquad (4.22)a$$

and

$$\begin{aligned}\varphi^{jmk\,c}_{AB\,L2} = \frac{1}{\lambda_{L2}}\{&[(\tilde{X}^{j}_{A} - X^{j}_{k})^2 + (\tilde{Y}^{j}_{A} - Y^{j}_{k})^2 + (\tilde{Z}^{j}_{A} - Y^{j}_{k})^2]^{1/2} - \\ &[(\tilde{X}^{j}_{B} - X^{j}_{k})^2 + (\tilde{Y}^{j}_{B} - Y^{j}_{k})^2 + (\tilde{Z}^{j}_{B} - Y^{j}_{k})^2]^{1/2} - \\ &[(\tilde{X}^{j}_{A} - X^{j}_{m})^2 + (\tilde{Y}^{j}_{A} - Y^{j}_{m})^2 + (\tilde{Z}^{j}_{A} - Y^{j}_{m})^2]^{1/2} + \\ &[(\tilde{X}^{j}_{B} - X^{j}_{m})^2 + (\tilde{Y}^{j}_{B} - Y^{j}_{m})^2 + (\tilde{Z}^{j}_{B} - Y^{j}_{m})^2]^{1/2}\} + N^{mk}_{L2\,AB}\end{aligned} \qquad (4.23)b$$

where:

$\tilde{X}^{j}_{B}, \tilde{Y}^{j}_{B}$ and $\tilde{Z}^{j}_{B}$	are the *a priori* estimated coordinates of the antenna on the ground at the instant of exposure of jth photograph.
$\tilde{X}^{j}_{k}, \tilde{Y}^{j}_{k}$, $\tilde{Z}^{j}_{k}$ and $\tilde{X}^{j}_{m}, \tilde{Y}^{j}_{m}$, $\tilde{Z}^{j}_{m}$	are respectively the *a priori* estimated coordinates of satellites k and m at the instant of exposure of jth photograph.
$N^{mk}_{L1\,AB}$ and $N^{mk}_{L2\,AB}$	are the ambiguities for L1 and L2 phases respectively.

$\varphi^{j\,mk}_{AB\,L1}$ and $\varphi^{j\,mk}_{AB\,L2}$ are respectively observed values for L1 and L2 double difference phases at the instant of exposure of jth photograph.

$\varphi^{j\,c\,mk}_{AB\,L1}$ and $\varphi^{j\,c\,mk}_{AB\,L2}$ are respectively the computed L1 and L2 double difference phases at the instant of exposure of jth photograph.

After computing and assigning the elements of all matrices and vectors in equations (3.32)a and (3.32)b, the entire new combined system is ready to be processed by least squares estimation. Therefore, as a next step a least squares estimation process took place in the program as shown in the flow chart in figure 4.3. During the least square estimation process, some common subroutines written in the Geomatics department of Newcastle upon Tyne University were used to calculate multiplication, subtraction, inversion, etc. of matrices and vectors. After each run of the least squares estimation, the corrections produced for the unknowns were added to the *a priori* estimated values of these unknowns. Thus new estimated values for the unknowns were obtained. Then the corrections produced at the last iteration were used as a decision making criterion for the next iteration which would only take place if any one of the corrections is greater than 1% of accepted smallest unit for each specific type of the unknowns estimated in the new combined system. So, a new iteration became necessary where any one of the corrections was not able to satisfy this criterion. Each new iteration of the least squares estimation were restarted from the forming of the design matrix A as shown in figure 4.3. The iterations were stopped when all of the corrections were sufficiently small.

After the iteration processes of the least squares estimation, the estimated values of the unknowns are obtained. Then coordinates of the object and control points whose photo coordinates were measured on the photos where they appear are stored in an output file. Thus they can be used to see the deviations in the coordinates before any cycle slip correction.

The ambiguities resulting from the least squares estimation do not have integer values in the first place. Therefore they are rounded to the nearest integers. Before passing to statistical testing, all calculated coordinates were transformed into the local coordinate system by utilizing the equations from (4.5) to (4.17) and then stored in a file.

4.3.3 THE W-TEST

The residuals derived from the least squares estimation are commonly used for the detection of outliers. Therefore, before running a statistical test, the least squares residuals of the observations which are major materials of a statistical test are computed by the equation below as described earlier:

$$v = Ax - b$$

But, using the residuals basically are not satisfactory where an interpretation is necessary for the detection of outliers. So, a better method must be chosen to detect outliers. A test called as *normalised residuals* (w_i) developed by Baarda (1968) was the method chosen in tests. Cross (1990) also derives and describes the following formula for the test (i.e. w).

$$\hat{w}_i = \frac{-e_i^T W \hat{v}}{(e_i^T W C_{\hat{v}} W e_i)^{1/2}} \qquad (4.24)$$

where

$\hat{v}$ is the vector of least squares residuals

W is the observation weight matrix

$C_{\hat{v}}$ is the covariance matrix of the least squares residuals

Before setting up this formula for a w statistical test, first of all it is necessary to form a covariance matrix of residuals. In the program, equation (4.25) were used to compute this matrix.

$$C_{\hat{v}} = W^{-1} - A(A^T WA)^{-1} A^T \qquad (4.25)$$

4.3.4 MARGINALLY DETECTABLE ERRORS

If an outlier has a large chance of being detected (i.e. 80%) in the w-test, it is defined as "marginally detectable" error. So, a probability of 80% shows the limit case of an outlier that could be detected.

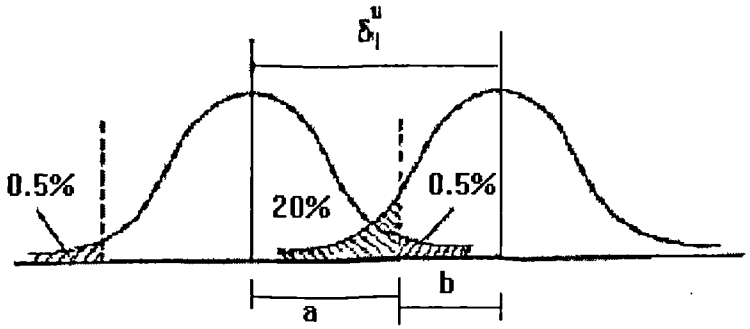

Figure 4.6 Two Gaussian PDF

Figure 4.6 which is a graphic of two Gaussian PDF's (Probability Density Function) shows the limit case of an outlier that may be detected with a probability of 80%. In order to compute the *marginally detectable error* in the normalised residuals it is defined as the bias δ_i, according to a power of the test of 80%.

The bias in the normalised residuals δ_i can be calculated by:

$$\delta_i = a + b \qquad (4.26)$$

a and b parameters in equation 4.26 can be found in the distribution tables. For more explanation the readers can refer to Cross (1983).

The foundvalues for these parameters from the distribution tables are:

$$\delta_i = 2.576 + 0.840 = 3.416$$

So, now "what bias in the ith observation will cause a bias in its normalised residual of 3.416?" is the question to be answered. This bias is the Marginally Detectable Error in the ith observation for parameters α = 1% and β = 20%. The marginally detectable error in the ith observation is computed by using the equation below:

$$MDE_i = \frac{\delta_i}{(e_i^T W C_{\hat{v}} W e_i)^{1/2}} \qquad (4.27)$$

In the program, equation 4.27 was used to compute the marginally detectable errors in the observations. These values can then be used as decision making criterion for the reliability analyzes of the combined system under various conditions.

In the next step, the program seeks whether or not there is an outlier in any one of the phase observations comparing the w values of them computed as described earlier in section 4.3.2 and the quantity derived from the table in a way similar to that in MDE process. If any outlier is detected, the program goes to point 1 and then point 2 as shown in figures 4.3 and 4.7. At this stage, as can be seen in figure 4.8, the program checks if there is cycle slip previously detected. If there is no previously detected bais in the observation as a cycle slip, only A design matrix is modified, considering the observation in that a cycle slip was detected. Then the program follows the next steps, that were explained earlier, after forming the design matrix A as being in the normal least squares estimation process. If we go back to point two, there is another possibility that there can be a previously detected cycle slip. If so, it becomes necessary to modify all the matrices and vectors (i.e. W, A and O-C) required for the least squares estimation in order to remove the observation infected by the cycle slip from among them. Before this process starts, previously detected cycle slip is corrected. Then rest of the process takes place as stated in figures 4.8 and 4.3 respectively.

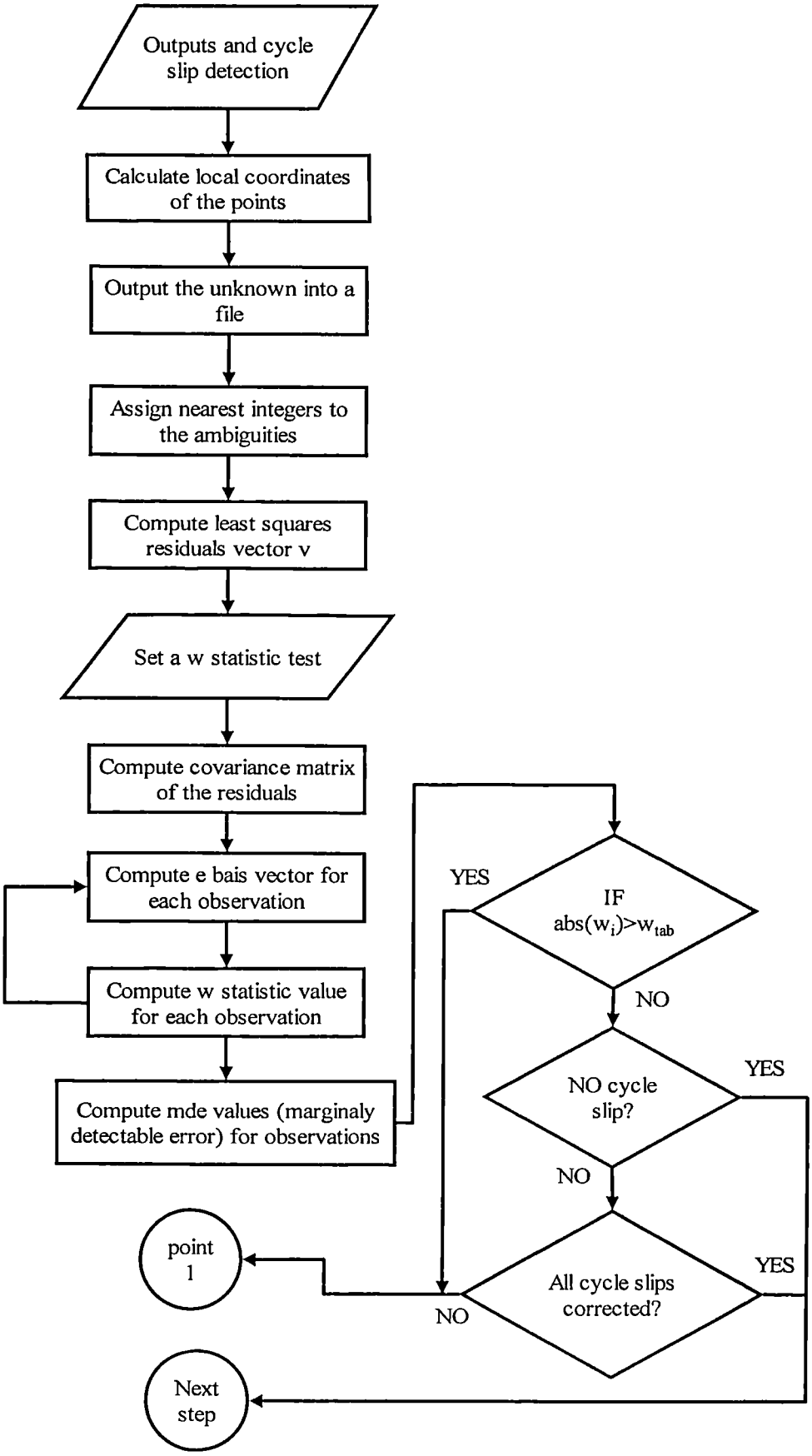

Figure 4.7 Minor outputs and statistical test flow chart

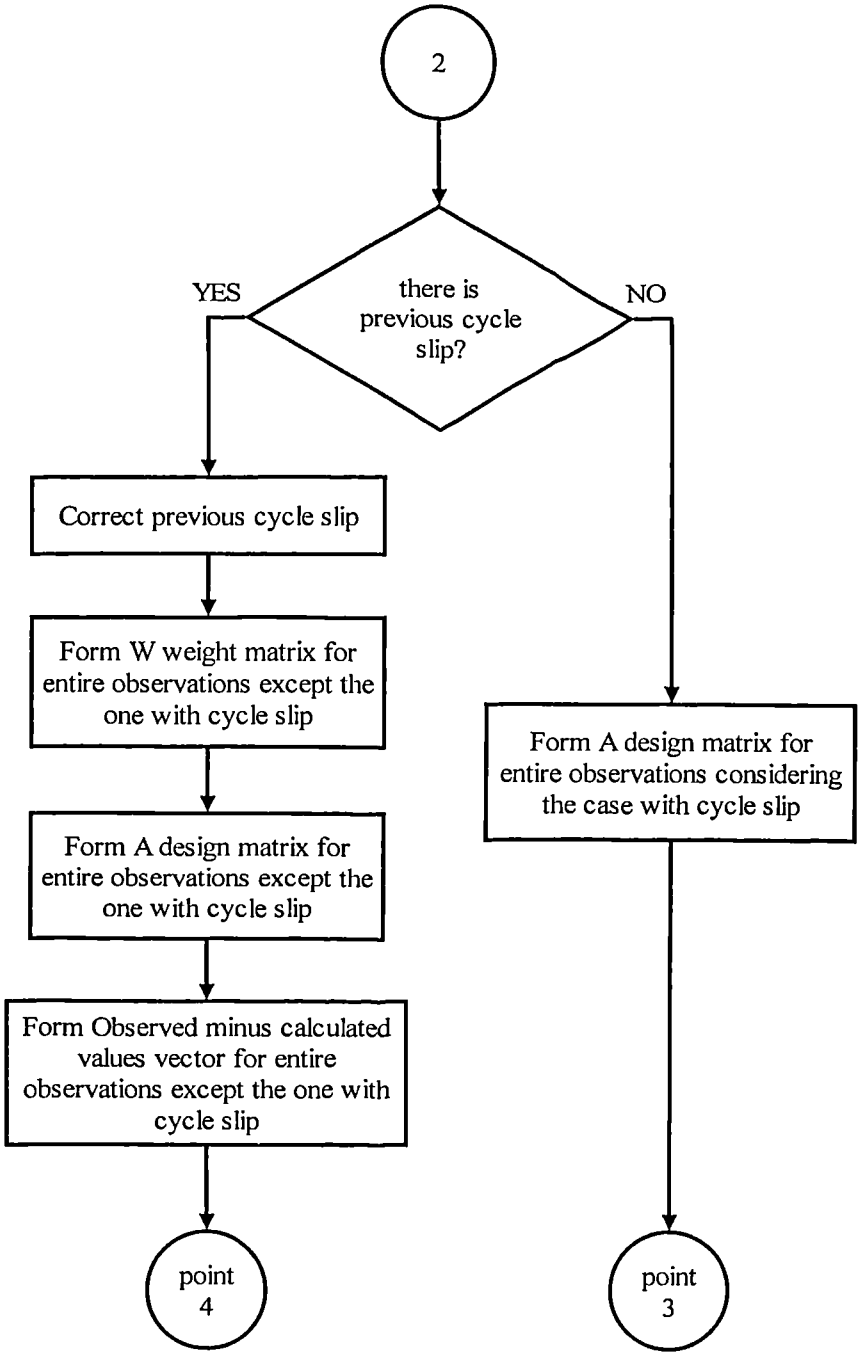

Figure 4.8 Formation of the matrices and vectors flow chart in the case with cycle slips

If we go back to the first IF statement in figure 4.7 which is for comparison of the w_i values of the observations and the w_{tab} value obtained from table, the another possibility to be experienced whilst running this statement is that all of the normalised residuals of the observations pass the test. This happens if there is no bias in the observations e.g. in the case without cycle slips and it also happens even if there are cycle slips in the observations and if all of these cycle slips were solved and corrected.

Therefore in the next two steps these two case are sought by the program. By the first IF statement the program seeks whether there is no cycle slip which was previously detected. If the answer is negative to this question then the program passes to the second IF statement. This means that there is cycle slip in the observations which was previously detected but no cycle slip in the present case. So it must be corrected and then the program must seek whether there is another cycle slip in the observations except this detected one. To follow this the program returns to point 1 shown in figure 4.3. At this state, there is also another possibility which must be mentioned here. It is so that there can be only one cycle slip in the entire observations. However this cycle slip is not solved until the current step. At that point the program passes to the next IF statement to seek this situation. Then it corrects the cycle slip and follows the procedures for formation of the matrices and the vector and the least squares estimation as shown in the follow chart in figure 4.3. This last process is given place in the program in order to obtain unknown parameters that were cleaned from the possible biases. Thus, the performance of the new combined system can be represented well.

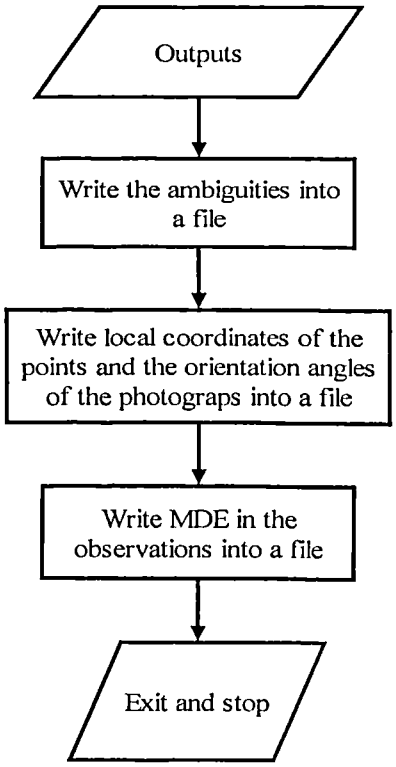

Figure 4.9 Outputs flow chart

To evaluate the outcomes obtained at the end of the last processes of the program explained above, they are written in a file as shown in figure 4.9. These processes are the last processes of the program. Therefore after finishing these processes, the program is stopped.

4.4 DATA SIMILATION

In order to formulate a stochastic model to describe a real phenomenon it is required to have a model that is realistic a replica of the actual situation and one whose mathematical analysis is feasible. Continuous advancements in the development of fast and inexpensive computation power can now easily facilitate the efficient analysis of these models by means of simulation study.

Most of the work in photogrammetric activities are carried out to satisfy the needs of clients by considering that the outcomes should be within the technical specifications. These technical specifications generally concentrate on the results and the quality of the results and not on the specific methods of obtaining them. The clients simply want good results in a form that satisfies their specifications and their definition of quality and at a reasonable cost in a relatively short time. It therefore depends on use of a system which is most efficient and economical to meet these demands. With regard to this, the tests carried out were based on the assumption that GPS phase observations would be used. In conjunction with these GPS phase observations, the specifications given by the **R**oyal **I**nstitution of **C**hartered **S**urveyors of Great Britain (**RICS**) (RICS, 1988) would also be used. In the RICS document, the accuracy of plan control for mapping at scales ranging between 1:1000 and 1:10000 is defined as a maximum tolerance of one part in 20000 and a relative tolerance between adjacent control points of ±0.06 m root mean square error at map scale. In the same document, it is required that height control points should be in sympathy with existing bench marks, or reference bench mark, to better than one third of contour interval (maximum tolerance) and adjacent height control points should be in sympathy to better than one tenth of the contour interval.

Generally, the mapping scale and contour interval required for any photography are supplied by the client. The organization responsible for carrying out the photography then keeps these in mind in order to meet the specification. With regard to this, it is

assumed that various mapping scales would be used ranging from 1:500 to 1:20000. As they are shown in Table 6.7(a).

Using modern instruments in the photogrammetric field as diapositive and the modern analytical plotters, the measurement precision of the image points can be raised up to the order of better than 1 μm.

By considering and keeping in mind all the information above, various test were carried out in order to test the new combined system. The performance of the new combined system is obtained by determining the quality of the parameters estimated under various test conditions. This will also be an indicator of how well the parameters estimated using the new combined system can be determined. The two criteria used to determine the quality of the estimated parameters are:

- The assessment of the ability of the new combined system on the detection of gross errors as cycle slips in GPS phase measurements, and
- The assessment of the effects of random errors in the observations on the parameters in the complete combined model. i.e. a measure of manner that the new combined system propagates random errors (i.e. precision).

The photogrammetric data were generated by computing the observations identified as x and y photo coordinates of all image points, i.e. x_{ij} and y_{ij}, using equations 2.16 and 2.17 in section 2.6.2.1 of chapter Two, that also constitute the photogrammetric model under known certain conditions. The condition to be satisfied here is the collinearity condition by providing the coordinates of the antenna onboard the aircraft with respect to the camera perspective center and the rotation elements of the camera at the each exposure, the ground coordinates of object points and the principal distance of camera lens. It was assumed that all measurements were made in mono-comparator mode and each image points were measured only once during the measurement process. Then the random numbers were generated and added to the computed photo coordinates. Therefore the final result at the end of this process were photogrammetric observations which are clear from systematic errors.

Although the recent GPS geodetic receiver technologies, which have been dramatically improved by the advances in electronics, are capable of extracting the code and phase

observables with resolution and accuracy of up to 0.01 of a cycle (or much better), the measured carrier phase pseudoranges (from L1 and L2) are in error by the ambiguous whole number of complete cycles (commonly known as initial phase integer ambiguities as described in chapter two) between the emitting point in the satellite and the receiver-antenna's phase-center at the instant of receiver phase locks on the satellite. Phase-locking on all satellites above a particular mask angle results in producing different initial ambiguities equal to the number of observed satellites. Following the initial phase lock, the receiver records the number of complete carrier cycles between two successive epochs in addition to the code pseudoranges and carrier phases.

The process is continued until the GPS signal between the receiver's antenna and one or more of the involved satellites is blocked, due to masked receiver-satellite-intervisibility or fading in signal strength (caused by high ionospheric activities or severe multipathing effects). When the receiver resumes phase lock on that satellite, the current measured phase is related to the previous recorded phase prior to loss of phase lock by an unknown number of integer cycles. Such phase data is commonly said to suffer from cycle slips. Cycle slips may occur many times in one observation session, depending on the dynamics as well as the environment of the roving (unknown) receiver(s); whereas cycle slips generated at the fixed base receiver are rarely common apart from those which may result due to receiver's software or hardware failure. This is due to the requirement of the base antenna to be attached to a reference tripod or pillar in a clear environment. As a consequence of cycle slips, two carrier phase related problems occur.

- The first problem is represented by the unknown number of complete cycles between the epochs of losing and resuming phase lock on satellite(s).
- The second problem is represented by the unknown initial phase ambiguities between the satellite and the receiver's antenna at the instant of resuming phase lock. Solving one of the previous problems will cancel the other.

As far as the carrier phase observables are concerned, the system inherited initial phase integer ambiguities are the largest biases imposed on the carrier phase pseudoranges. Biases due to cycle slips could range from one cycle to thousands of cycles. However,

determining the correct number of initial integer ambiguities converts phase pseudoranges to very precise observables.

The noises or random errors in GPS observables generally result from imperfect generating and recording mechanisms, i.e. the noises are inherited in the nature of the measurements (Leick, 1995). Random errors follow the normal distribution in which the probability of negative errors occurring is equal to the probability of positive errors occurring, and small values are more common than large values. The measurement noise can be something between 1-3*m* for C/A-code (about 10 *cm* for new C/A-code receivers with narrow correlating techniques), 10-20 *cm* for P(Y)-code and 3-10 *mm* for the carrier phases (Lachapelle *et al*, 1992).

According to Nolan *et al* (1992), the system noises are relatively constant, due to their independence on external factors (e.g. observing site environment and atmospheric activities). These errors can be investigated through carrying out some tests on the receivers (e.g. zero baseline tests).

Phase observations to each satellite was computed using the range calculated from the antenna coordinates on the plane, which were derived from the coordinates of the exposure station with the components of the antenna offset assumed to be geodetically determined, and the coordinates of the satellite at the time of exposure. Keeping all the explanations above about GPS error characters in mind, random numbers were generated to obtain artificial integer ambiguities, cycle slips and noises. Afterwards appropriate values required for each specific test were added to the computed ranges. Then in order to make up the GPS phase observations, these computed pseudo-ranges were divided by the wavelengths of the signals used in the system (i.e. wavelength of L1 and L2).

All observations were regarded as uncorrelated except those which are double difference phase observations for the same phase in the same epoch. The a priori reference factor was assumed to be equal to unity for the photogrammetric measurements and the weights were computed according to this assumption for photo measurements and the correlation between the phase observables as described in section 2.5.1 of chapter two. The generated data, as described above, were used in the various tests given in the following three chapters.

The main objective of the test carried out in this research is to assess the capability of the new combined system on the determination of the unknowns correctly under normal and noisy conditions and under the conditions with cycle slips in the GPS phase observations.

In the new combined system, the parameters to be determined, as in classical aerial triangulation block estimation procedures except those integer ambiguities coming from GPS, are:

- The ground coordinates of new points, generally pass, tie and, possibly check points and their standard deviations.
- Spatial coordinates of exposure stations and their standard deviations.
- Attitude of the camera at the instant of each exposure and standard deviations.

The precision of above parameters are also required by the clients. Therefore as a secondary objective, precision of the parameters that would be obtained from the combined system were also computed to see whether they would conform to the specifications laid down in Table 6.7(a).

4.4.1 GENERATING RANDOM ERRORS

To study the behavior of the new combined system with biased data and quantify the tolerable noise level for the phase and the photogrammetric data an algorithm that generates random errors has been integrated with the new combined GPS-aerial triangulation technique.

Random errors can be produced by a random number generator. Random error generators are mathematical equations, which generate numbers in random consequences. There is a diversity of random number generators in common use. Each generator has its own characteristics and areas of application. For the simulation work carried out in this research, the random number generator that generates normally distributed numbers has been utilized. Two numbers y_1 and y_2 can be randomly obtained using the following relationship as given in Press *et al* (1992):

$$y_1 = \sqrt{2\ln(x_1)}\ \cos(2\pi\ x_2) \qquad (4.28)$$

$$y_2 = \sqrt{2\ln(x_1)}\ \sin(2\pi\, x_2) \qquad (4.29)$$

where x_1 and x_2 are two random numbers in the range 0 to 1. The x_1 and x_2 random numbers are generated from the C-random library function for the C programming language. The C-random number library function actually generates random number between 0 and 2^{15}-1, i.e. between 0 and 32767. These generated random numbers y_1 and y_2 using equations 4.28 and 4.29 were then scaled to be in the range ± 1. The outputs from y_1 and y_2 have a bell-shaped Gaussian distribution with most of the generated figures distributed evenly around the zero value.

The random numbers generated for the phase observations were further scaled by decimal figures and added to the L1 and L2 raw phase data to simulate the phase observations with the appropriate noises. In addition to this the integer numbers were calculated from other randomly generated values to simulate the L1 and L2 phase data with the integer ambiguities. In order to simulate the photo measurements with the appropriate noises other random number were also generated and added to the raw photo observations, i.e. to the calculated photo coordinates of the points on the photographs. The investigations on the behavior of the new combined system with various random error sizes applied over various conditions are given in the following chapters.

4.4.2 TEST DATA

In the absence of real data, it is necessary to simulate the photogrammetric coordinate and dual frequency GPS phase measurements in the way mentioned above. In this concept two kind of simulated data were then used in the system, i.e. :

- Double difference GPS dual frequency phase observations, and
- Image coordinates of the points appeared in the photographs.

For the seek of simplicity, the systematic errors in the both kind of simulated data were assumed to be removed or modeled well.

The photogrammetric part of the combined system consists of a strip of four consecutive photographs, and uses 2 or 3 control points. In the GPS part 6 satellites and L1 and L2 phase observations are used. There are two receivers, one is mounted onboard the aircraft, and the other one is located of a known station on the ground

about 20 km away. These L1 and L2 phase observations to 6 satellites constituted 10 double difference equations for each epoch, i.e. 5 for L1 and 5 for L2. According to the number of photographs used in the research an interpolation was performed between two consecutive epochs to find out the 4 epochs of GPS data set at the exposure times of these 4 photographs. 60% overlap, a flying height of approximately 450 m, a camera focal length of 152.4 mm, and average terrain elevation of 100 m were used for the simulation according to the used photographs taken during Corbert & Short's study (1994). The standard error estimates used in the simulation were 2, 5 and 10 μm for photo coordinates and 2, 5 and 10 cm for dual frequency double difference GPS phase observations in the sample test given here. 2 cm error for GPS observations describes the multipath case to be met on the aircraft (Corbert 1994).

The perturbations used in the simulations were generated by using a normally distributed random number generator and standard error estimates of all the measured quantities.

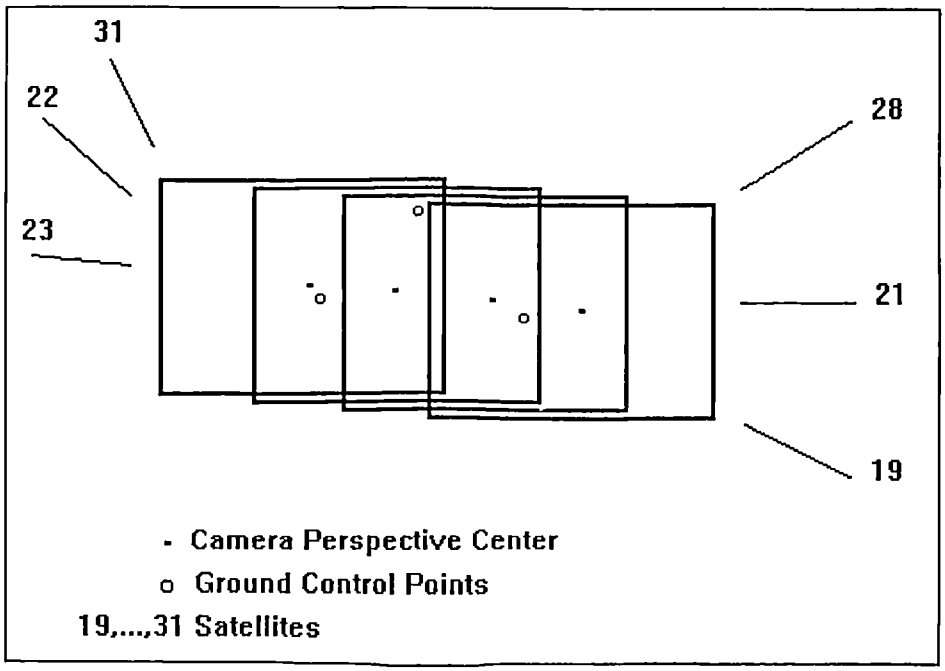

Figure 4.10 The used sample

5. CHAPTER FIVE

5.1 DEMONSTRATION THAT THE NEW COMBINED SYSTEM WORKS

5.1.1 TEST OBJECTIVES

Test objective is

- To show that the combination of photogrammetry and GPS is possible in observation space and that systems are mutually beneficial.

5.1.2 TEST SET-UP

Different numbers of control points (2 and 3) were used.

5.1.3 PROCEDURE

In order to show whether or not the combined system can deliver what is expected from it, under normal circumstances, say phase abservables with errors of standard deviation of 2 cm, photogrammetric coordinates with the errors of standard deviation of 10 μm, and without any cycle slips, the following parameters were produced throughout the bundle adjustment combined with GPS double difference phase observation equations :

- Coordinates of the antenna positions at the each exposure time, coordinates of new ground points, orientation elements of the camera and ambiguities for dual frequency double difference phases were separately computed for the cases of two and three control points.

- Deviations from the true values for each parameter were obtained to indicate whether or not the approach works as a new way of combining both photogrammetric and global positioning systems.
- Marginally detectable errors in the photo coordinates of ground control points and new ground points and GPS phase abservables were separately calculated for both cases with two and three ground control points.
- The standard deviation of each parameter is utilized to evaluate the precision of the estimated parameters.

5.1.4 TEST RESULTS

Table 5.1 shows the root mean square deviations from the coordinates of the true camera perspective center at the each exposure time and from the coordinates of the true object points before and after ambiguity fixing (BAF) (AAF) for the cases using two different number of ground control points.

	Exposure Stations Coordinates (cm)				New Ground Point's Coordinates (cm)			
	Plan (BAF)	Plan (AAF)	Height (BAF)	Height (AAF)	Plan (BAF)	Plan (AAF)	Height (BAF)	Height (AAF)
2 Ground cont. points	8.17	1.31	2.03	2.46	3.60	3.37	8.08	6.92
3 Ground cont. points	12.31	1.11	3.81	2.29	3.66	3.07	8.85	6.47

Table 5.1 r.m.s. errors from true values

Figure (5.1)a and b, respectively, are graphical representations of the root mean square errors in plan position and height of camera perspective center points and new ground points using photo scale of 1:3000 according to camera lens of 152 mm for each different number of ground control points (two and three).

Figure (5.2)a, b and table 5.2(a), (b), respectively, are graphical and numerical representations of the standard deviations from true value of the orientation elements, in the cases of 3 and 2 ground control points.

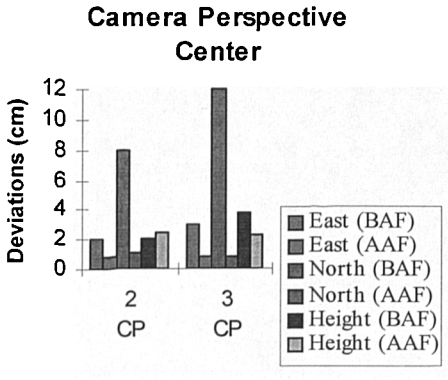

Figure (5.1)a r.m.s. errors in the camera positions in local coordinate system

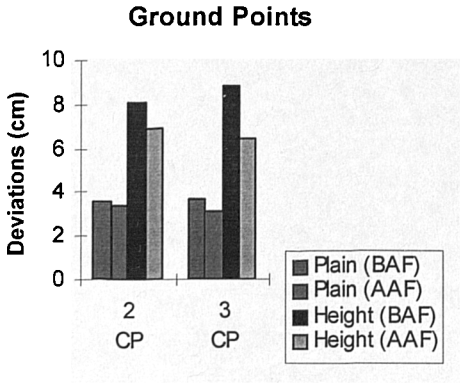

Figure (5.1)b r.m.s. errors in the coordinates of object points in local coordinate system

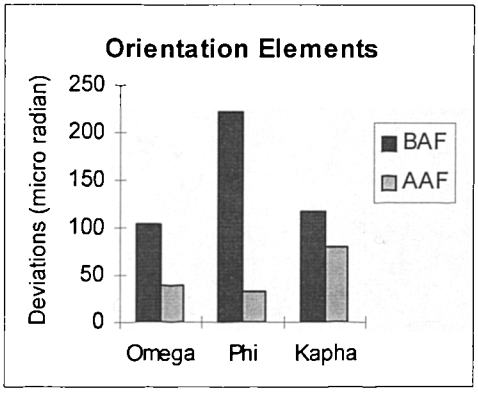

Figure (5.2)a Standard deviations from true orientation elements. With 3 ground control points.

(mili radian)	Before Ambiguity Fixing	After Ambiguity Fixing
Omega	1.05E+02	3.82E+01
Phi	2.22E+02	3.24E+01
Kappa	1.18E+02	7.94E+01

Table 5.2 (a) Standard deviations from true values of orientation elements

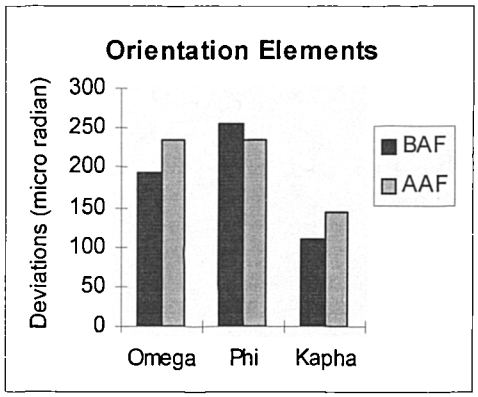

Figure (5.2)b Standard deviations from true orientation elements. With 2 ground control points.

(mili radian)	Before Ambiguity Fixing	After Ambiguity Fixing
Omega	193.48	233.60
Phi	254.92	233.77
Kappa	110.23	144.53

Table 5.2 (b) Standard deviations from true values of orientation elements

Figure (5.3)a and b, respectively, display the magnitude of the deviations, in units of cycles, from true ambiguities before ambiguity fixing in the cases of 3 and 2 ground control points.

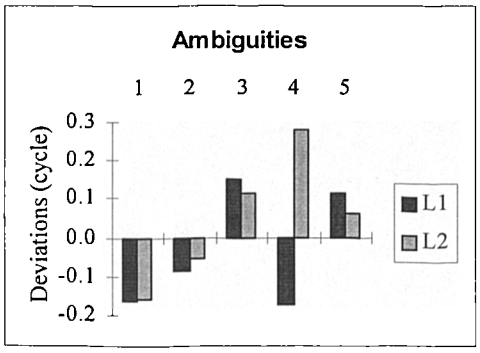

Figure (5.3)a Deviations from true ambiguities just before ambiguity fixing in the case of 3 control points

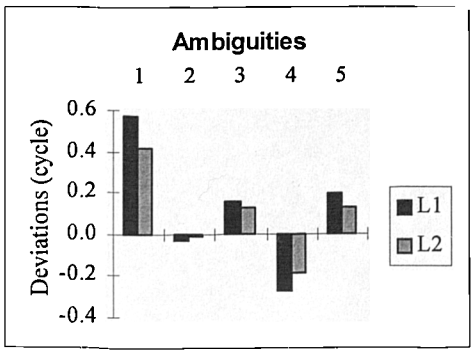

Figure (5.3)b Deviations from true ambiguities just before ambiguity fixing in the case of 2 control points

Figure (5.4) and table 5.3, respectively, represent graphically and numerically magnitude of the largest marginally detectable errors in GPS double difference phase observables, the coordinates of ground control points and new ground points for both cases of 2 and 3 ground control points.

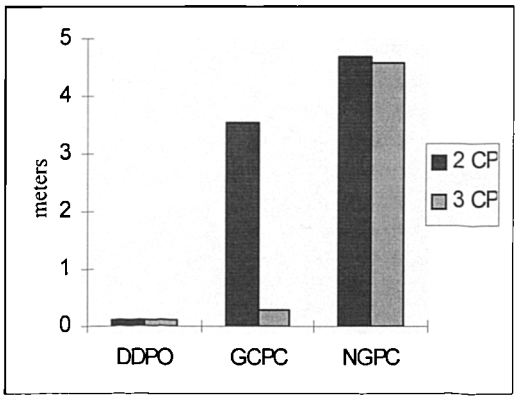

Figure (5.4) Largest marginally detectable errors

(meters)	2 control points version	3 control points version
GPS phase observables	0.117	0.115
Ground control point coords.	3.549	0.272
New ground point coords.	4.665	4.574

Table 5.3 Largest marginally detectable errors

5.1.5 DISCUSSION OF RESULTS

The results produce a good insight into the precision structures of the new bundle system combined with GPS dual frequency double difference phase observables, especially when using three ground control points, even if under the limited conditions of the currently used sample which consists of a strip with only four photos and four epochs. They also clearly show an improvement in the coordinates of new ground points and a much better improvement in the coordinates of camera perspective center, particularly after the ambiguities are fixed.

Looking at figure (5.1)a and b and table 5.1, respectively, which show graphical representations of r.m.s. errors in east, north and height of camera positions and plan position and height of object points with respect to their true values and their numerical representation, the results show a significant improvement in the plan position of exposure stations and we can conclude, in general, that new combined system works well for the plan position of exposure stations in both cases (i.e. different number of ground control points), but not as a big an improvement in height as in plan. These results, which are using two and three control points and for the case after ambiguity fixing, from the height point of the view imply that the number of ground control points in the combined system have a slight direct proportional influence on the height of camera perspective center, however the height is slightly deteriorated in the case of 2 control points. Similar statements can be indicated for the plan position of the camera perspective center for the same cases. The improvements in the plan position and height of the camera perspective center after ambiguity fixing, respectively, are 2 mm and 1.6 mm according to the number of used ground control points. A similar improvement can also be seen in the plan position and height of ground points i.e. 3 mm and 4.5 mm. Therefore, it can be expressed that the differences between the plan positions and height of both exposure stations and ground points after ambiguity fixing are not large considering both cases using 2 and 3 control points. The statements throughout this paragraph imply that coordinates of the camera perspective centre are mostly solved by GPS under the normal conditions.

When a comparison is made for the cases before and after ambiguity fixing, slight improvements are seen in the heights of ground points (2.3 mm and 5.9 mm) although plan positions of them show slightly better improvements (1.16 cm and 2.38 cm), according to the cases using two and three control points respectively. From this outcome, it can also be concluded that, in general, the plan position and height of ground points are mostly independent of phase observables, in fact the plan positions show weaker dependency to phase observables than the heights.

Comparing the results before and after ambiguity fixing in figure (5.2)a, b and table 5.2(a), (b) which are graphical and numerical representations of r.m.s. errors in orientation elements in both cases of three and two ground control points with respect to their true values, significant improvements in the orientation elements can be seen in the case using three ground control points, but not in the case of two ground control points. This might be caused by the sample utilized in this research. The sample used for all the tests carried out consists of a strip with only four photos and four epochs of GPS observables. Anyway it is obvious that this sort of sample would show some statistical variations somehow in some tests, particularly in the tests with less ground control points. Here it is also worth stating that a strip, utilizing just two control points and four photos, cannot find any convenient point on the left and right sides of the strip center line to stabilize itself, although GPS support comes with very weak geometry only along the strip center line. The results of the test using two ground control points show that most effected parameters from the insufficiency of the used sample are orientation elements which causes the combined model not to be able to stabilize itself well.

Figure (5.3)a and b show the deviations in ambiguities from their true values in the case just before ambiguity fixing, while the system is using three and two ground control points respectively. However it can be seen from the both figures that the change in the number of ground control points affects the correct ambiguity solution, this change does not have a strong influence on the coordinates of exposure stations and ground points and we can still get quite a good coordinates for these points. Looking at the case of three ground control points, deviations from the true quantities,

in general, are about 10-15 % of a cycle for both L1 and L2 phases except one L2 phase ambiguity. Considering the fact that the results are produced by the use of simulated data it can be thougth that the L2 phase ambiguities generally show smaller cycle deviations than the L1 phase ambiguities (except in one case mentioned above), even though their magnitudes would be very close to one another in meter units. But in practice, GPS L2 phase observables are much noisier than L1 observables. Therefore, when real data are used, the L2 phase observables might not show such good results. Also, taking into consideration the results in figure (5.3)b and table 5.1 together, it can be pointed out that even if one double difference L1 phase ambiguity is wrongly estimated by one cycle as it was in the test results, the correctly estimated L2 phase ambiguity of the L2 phase observations to the same satellites as the one in L1 phase, and the other correctly estimated L1 and L2 phase ambiguities save the combined system from the danger of coming up with wrong coordinates for exposure stations and ground points. This is also one of the advantages of the new combined system.

Figure (5.4) and table 5.3 show the largest marginally detectable errors in the double difference phase observables, the coordinates of ground control points and the coordinates of new ground points respectively for both cases of two and three ground control points. Small differences between the results for the case of two control points and the case of three control points indicate that the number of ground control points does not have a strong effect on the reliability of new ground points and double difference phase observables, except that on the reliability of ground control points obviously. However, no matter how many ground control points are used, the reliability of ground control points is worse than that of GPS double difference observations, which have direct effect on the coordinates of the antenna used, and therefore on the camera perspective center. According to the conclusions above and the reliability point of view, it can then be stated that the ground control points would not necessarily be used in bundle estimation if GPS phase observables are available, except the reasons for stabilization of the model when such a sample are used as in this research.

The relative difference between largest marginally detectable errors in new ground points for both cases of two and three control points is 9 mm. This difference is very small if it is compared with the original quantities. So, it means that the number of ground control points does not have any significant influence on the reliability of the coordinates of new ground points estimated thorough the collinearity equations using measured photo coordinates of these points. Even this outcome supports the use of few ground control points if GPS phase observables are available to use them together with photo coordinates in a combined bundle estimation model.

5.1.6 SUMMARY

- Quite a good improvement in perspective center local coordinates, especially in the north component after ambiguity fixing, show that the combined system is capable of solving for ambiguities and when the ambiguities are correctly delivered, it also puts forward a good precision for the coordinates of camera perspective center under the normal circumstances.
- Comparing the results in the both cases of different number of control points, it can also be stated that number of ground control points does not have any strong effect on the camera perspective center coordinates.
- Therefore, it might be expressed that first, GPS helps the photogrammetry to have approximate coordinates in sufficient extent for the perspective centers by the antenna on the plane. Then, somewhere in this stage of the process, photogrammetry starts to calculate these coordinates and the coordinates of ground points and orientations of the camera, utilizing from ground control points too, after some iterations, GPS undertakes the entire ambiguity solution. But this last step takes a longer time than that needed to solve other parameters in the used sample, because the sample shows instability since its lack of geometric strength for GPS part, and also photogrammetric part in the case using two control points.
- More sensitive parameters in the new combined system are orientation elements of the camera.
- The insufficient number of ground control points affects to the correct ambiguity solution. But, the use of few ground control points in the model does not have a

strong influence on the coordinates of exposure stations and ground points and we can still get quite good coordinates of these points, even if one ambiguity were solved wrong for one or two cycles. Since the other correctly solved ambiguities help to the model to produce good results for these coordinates.

- The number of ground control points does not have strong effect on the reliability of new ground points and double difference phase observables, and the reliability of ground control points is worse than that of GPS double difference observables. Therefore, it can be implied that the ground control points would not necessarily be used in new combined bundle estimation model if GPS phase observables were available.

5.2 DESCRIPTION OF THE MAXIMUM ERROR LEVELS IN THE NEW COMBINED SYSTEM

5.2.1 TEST OBJECTIVES

The objectives of this test are:

- to determine the maximum errors in both kinds of observations for GPS and photogrammetry that the new combined systems allowed while it delivers the coordinates of all points with acceptable accuracies and with the correct ambiguities, and
- to determine the magnitude of the effect of these maximum errors on the positions of camera perspective centres, assumed as control points moved up into the air in GPS photogrammetry, and object points on the ground. Thus, to look at the reliability and precision of the new combined system under the errors at the level of maximum extent, on the assumption that the system is able to solve the phase ambiguities correctly.

5.2.2 TEST SET-UP

The following were utilised in the test :

- Errors with various standard deviation for both, photo coordinate measurements and phase observables.

5.2.3 PROCEDURE

A test is carried out in order determine the maximum error levels for both parts of the system with which it can cope (i.e. still deliver the correct ambiguities) while it utilises three ground control points. To achieve this, the errors with specified r.m.s.

value were first added to the GPS phase observables and then the program written for new combined system was run several times in order to find out the errors with maximum r.m.s. value in photo coordinates due to the errors with specified r.m.s. value in phase observables while the system still delivers the correct ambiguities. This procedure has been followed to examine the various error levels in specified r.m.s value. Here, correct ambiguities have been chosen as a criterion in order to establish the maximum errors in both systems. The following were then produced during the test:

- Coordinates of antenna positions and orientation elements of the camera at the each exposure time, coordinates of new ground points and ambiguities for dual frequency double difference phases (for the case of three control points before and after ambiguity fixing).
- The root mean square error in each estimated parameter with respect to its true value is used to evaluate the precision of these estimated parameters.
- Marginally detectable errors in the photo coordinates of ground control points and new ground points and GPS phase abservables were separately calculated for the case of three control points.

5.2.4 TEST RESULTS

Figure (5.5) and table 5.4 represents the maximum 95% r.m.s. errors for both components of the system, GPS and photogrammetry, where it can cope with them and still deliver correct ambiguities. The shaded area in the picture means also that if r.m.s errors in both kind of observations in the system fall in this area, the new combined system copes with these errors and delivers correct ambiguities.

Figure (5.6)a and b and table 5.5(a) and (b) are graphical and numerical representations of r.m.s. errors in the coordinates of camera perspective centres and ground points as deviations from their true values respectively, according to the maximum errors, that the combined system allows, in the both system components with respect to the cases before and after ambiguity fixing.

SD of Maximum Errors in Phase observables (mm)	SD of Maximum Errors in Photo Coordinates (μm)
0.2	23
0.4	24
0.6	25
0.8	26
1.0	27
2.0	30
3.0	32
4.0	32
5.0	27
6.0	13
7.0	8
8.0	7
9.0	5

Table 5.4 SD of Maximum errors in both systems that the combined system allows

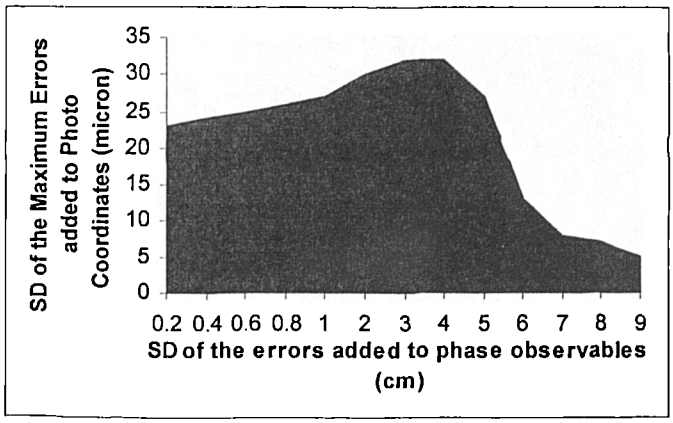

Figure (5.5) Standard Deviations of Maximum errors in both systems that the combined system allows

SD of Max. Errors in Phase Obs.(cm)	SD of Max. Errors in Photo Coor. (μm)	East (BAF) (cm)	East (AAF) (cm)	North (BAF) (cm)	North (AAF) (cm)	Height (BAF) (cm)	Height (AAF) (cm)
0.2	23	0.89	0.64	10.18	0.98	5.54	0.25
0.4	24	1.06	0.66	9.94	0.96	5.45	0.59
0.6	25	1.25	0.69	9.80	0.93	5.38	0.94
0.8	26	1.44	0.72	9.73	0.91	5.34	1.29
1.0	27	1.63	0.75	9.73	0.88	5.33	1.64
2.0	30	2.46	0.88	9.34	0.86	5.21	3.26
3.0	32	3.15	0.99	9.32	0.95	5.40	4.66
4.0	32	3.65	1.06	9.27	1.10	5.57	5.77
5.0	27	3.80	1.06	8.85	1.25	5.13	6.16
6.0	13	3.79	1.40	8.37	1.75	3.73	3.60
7.0	8	4.13	2.00	7.51	2.49	3.51	1.35
8.0	7	4.34	2.38	7.48	3.00	3.50	0.69
9.0	5	3.91	2.51	6.07	3.32	2.84	0.38

Table 5.5(a) Standard Deviations of the errors in camera perspective centre coordinates as deviations from their true values according to the cases before and after ambiguity fixing

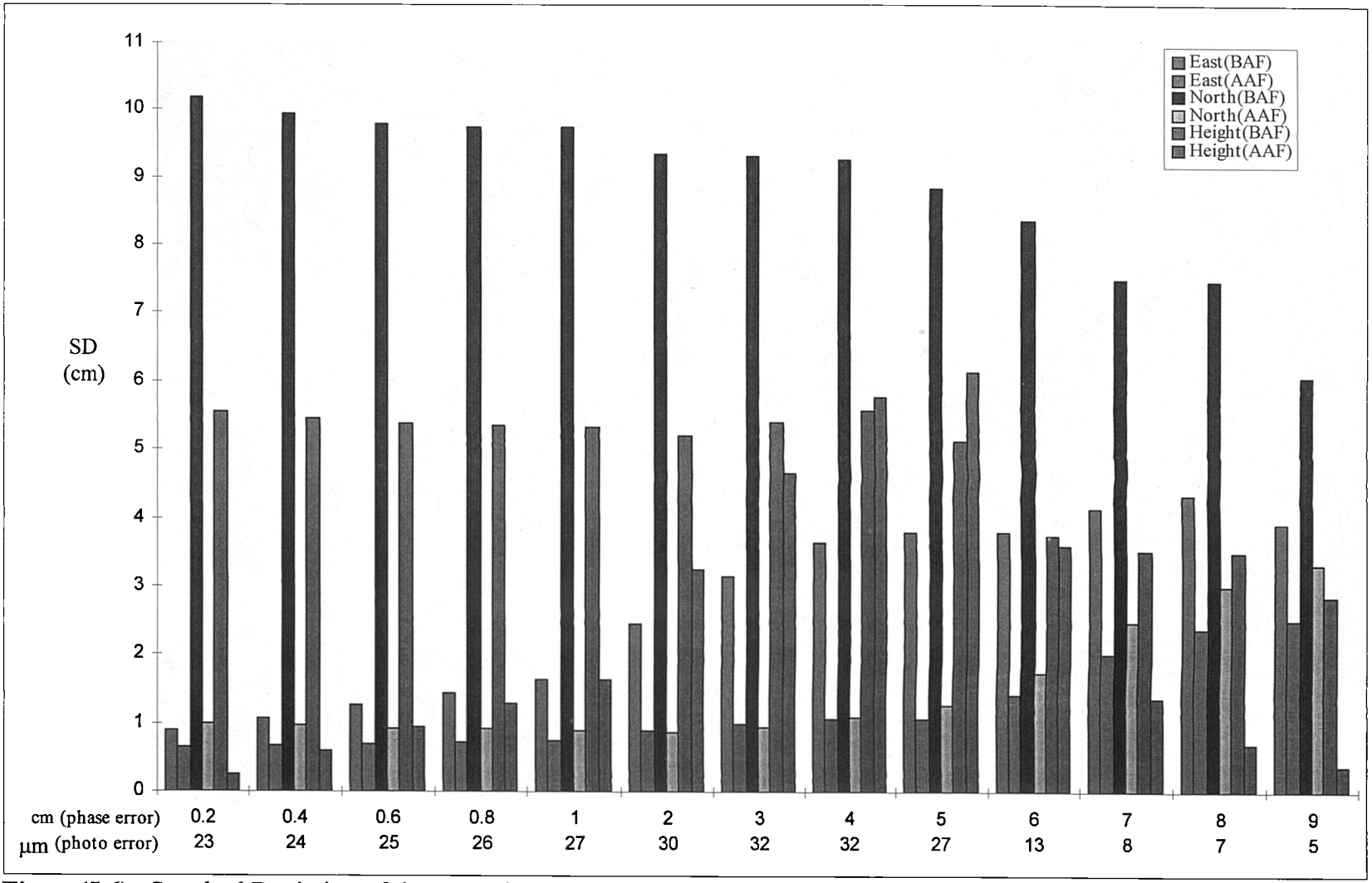

Figure(5.6)a Standard Deviation of the errors in the coordinates of camera perspective centre before and after ambiguity fixing

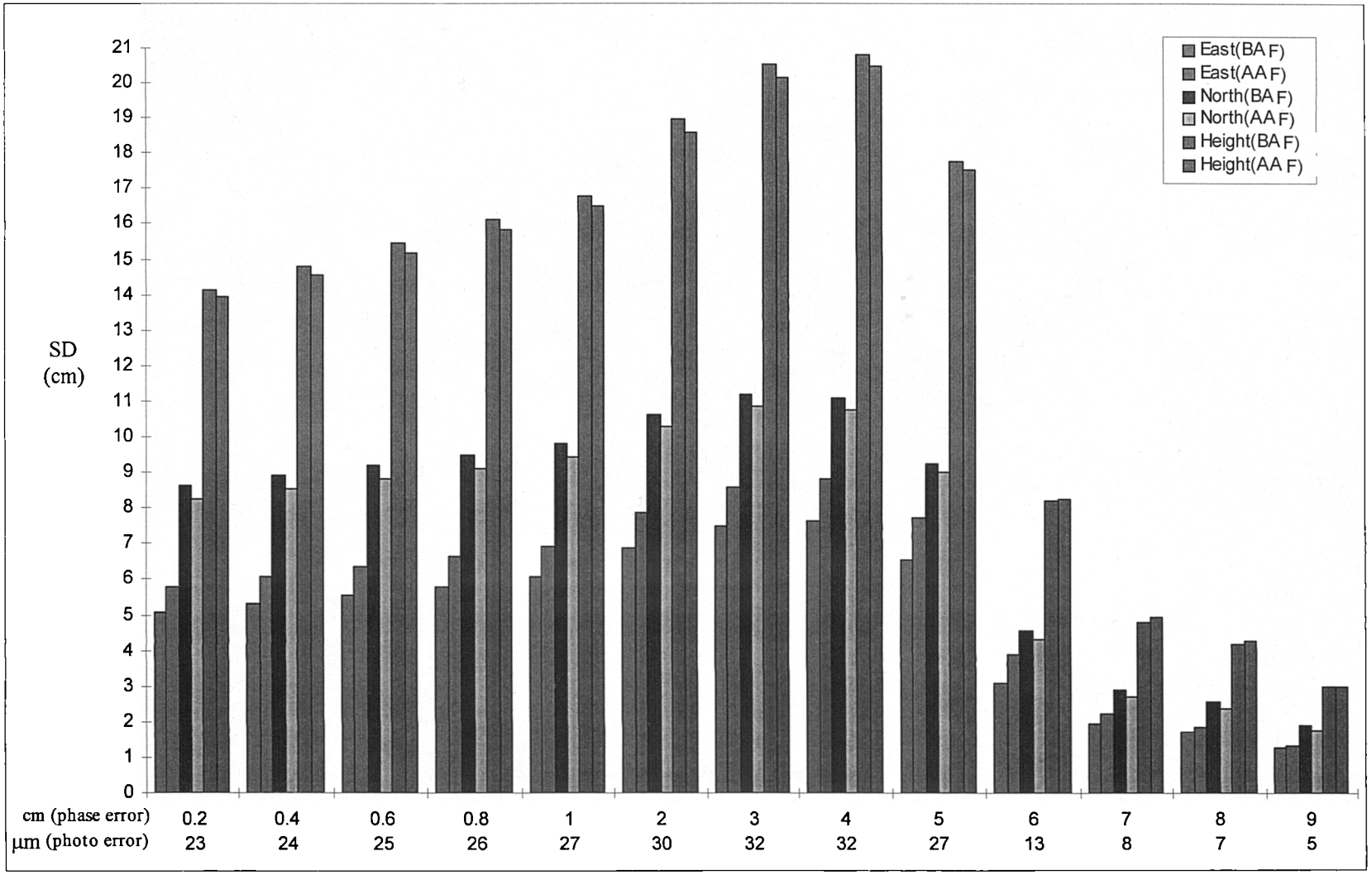

Figure (5.6)b Standard Deviation of the errors in the coordinates of ground points before and after ambiguity fixing

SD of the Errors in Phase Obs. (cm)	SD of the Errors in Photo Coor. (μm)	East (BAF) (cm)	East (AAF) (cm)	North (BAF) (cm)	North (AAF) (cm)	Height (BAF) (cm)	Height (AAF) (cm)
0.2	23	5.06	5.79	8.61	8.23	14.13	13.93
0.4	24	5.31	6.07	8.89	8.53	14.79	14.55
0.6	25	5.55	6.35	9.19	8.82	15.45	15.18
0.8	26	5.80	6.63	9.49	9.12	16.12	15.82
1.0	27	6.05	6.92	9.79	9.43	16.79	16.47
2.0	30	6.88	7.87	10.63	10.29	18.98	18.59
3.0	32	7.49	8.60	11.18	10.85	20.55	20.15
4.0	32	7.64	8.82	11.07	10.76	20.82	20.46
5.0	27	6.55	7.73	9.27	9.01	17.76	17.52
6.0	13	3.10	3.89	4.54	4.33	8.19	8.27
7.0	8	1.92	2.22	2.89	2.70	4.81	4.91
8.0	7	1.70	1.85	2.56	2.39	4.18	4.24
9.0	5	1.29	1.31	1.88	1.77	2.99	2.99

Table 5.5(b) SD of the errors before and after ambiguity fixing in the coordinates of ground points

Table 5.6 and figure (5.7) demonstrate respectively numerical and graphical representations of the largest marginally detectable errors in the coordinates of camera perspective centres, the coordinates of ground control points and the coordinates of new ground points while the combined system is under the effect of maximum errors in both systems.

Maximum R.M.S. Errors in Phase observables (cm)	Maximum R.M.S. Errors in Photo Coordinates (μm)	Camera Perspective Center Coor. (cm)	Ground Control Points Coor. (cm)	New Ground Points Coor. (m)
0.2	23	1.18	62.50	10.21
0.4	24	2.36	65.21	10.64
0.6	25	3.54	67.93	11.08
0.8	26	4.72	70.64	11.52
1.0	27	5.90	73.36	11.96
2.0	30	11.80	81.50	13.30
3.0	32	17.68	86.92	14.21
4.0	32	23.53	86.92	14.27
5.0	27	29.29	73.35	12.21
6.0	13	34.26	35.33	6.30
7.0	8	38.46	21.75	4.14
8.0	7	43.19	19.04	3.71
9.0	5	47.22	13.61	2.77

Table 5.6 Largest marginally detectable errors

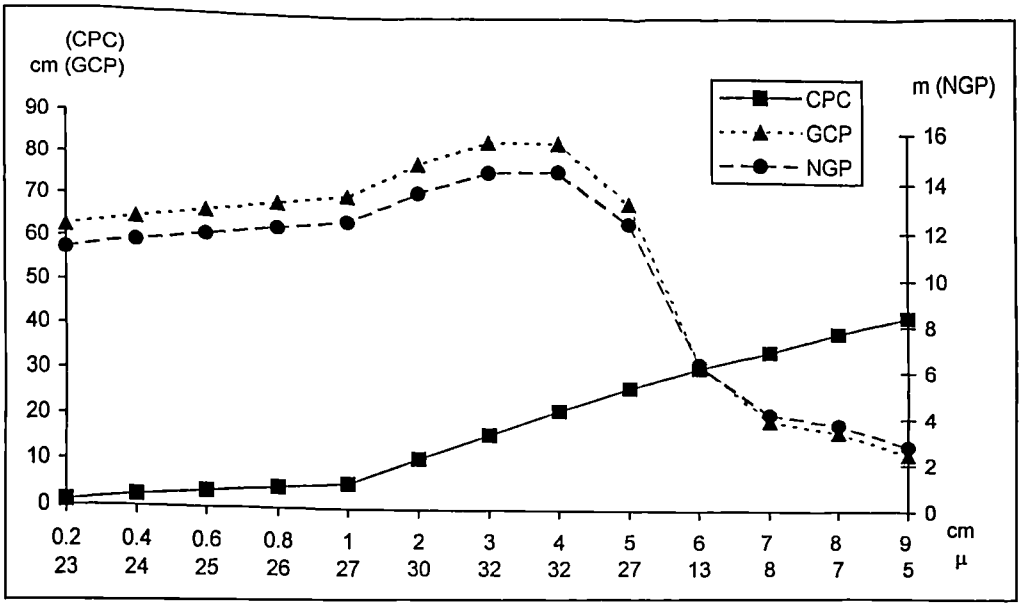

Figure (5.7) Largest marginally detectable errors

5.2.5 DISCUSSION OF RESULTS

Looking at table 5.4, it can be seen that the errors of largest standard deviation in photo coordinates, which are allowed by the new combined system, match with the GPS noises in the interval of 1 to 5 cm standard deviation which is what would be obtained by the antenna on the plane during normal and even extreme conditions (Corbett, 1995). This quantity (5 cm) is also almost the largest multipath error, which would be experienced in any GPS application (Hofmann-Wellenhof et al, 1995). So, while GPS observables are being collected with r.m.s. errors in the range of 1 to 5 cm and even if photo coordinates are measured under the conditions of low precision, (i.e. standard deviation of 20 μm or worse than 20 μm, which fall into the precision rate of traditional second and third order stereo plotter instruments (Wolf, 1983) (Ibrahim, 1995)) the system still delivers correct ambiguities. This fortunately means that both systems, photogrammetry and GPS, can really match and help each other well in the new combined model. In figure (5.5), the decrease in the r.m.s. errors in photo coordinates while GPS is under the errors of 5-6 cm shows that in the new combined system, 5 cm is the critical value for the GPS noises. If the combined system is having an error larger than this extent, it needs photogrammetric coordinates to be measured much more precisely than those in the circumstances with the phase noises which are

less than 5 cm. Therefore, it might be concluded that new combined model would be able to be used confidently and virtually in any conditions, even under severe multipath effect.

The shaded part of the figure (5.5) indicates that if the errors in both systems fall into this area, the combined system would deliver correct ambiguities. If the system delivers correct ambiguities, good improvements in coordinates of camera perspective centres can easily be seen in figure (5.6)a, comparing the results before and after ambiguity fixing. Whereas, the same improvements are not the case for the coordinates of ground points.

It can be seen in figure (5.6)a that before ambiguity fixing, the local coordinate which is worse affected from the errors in the combined system is the north of the camera perspective centre. There could be two reasons for this. The first is that GPS inherently gives best results in east-west direction and worse results in north-south direction because of the geometry of the satellites (Leick, 1995). The second is so that photogrammetry has worse strength in north-south direction and better strength in east-west direction due to that the flown direction was much closer to east-west direction than north-south direction in this research. As can be seen from the results before and after ambiguity fixing when they are compared, the biggest improvement in the coordinates of camera perspective centre is also in the north. Before ambiguity fixing, the largest change in the north is 9 mm in extent thorough the errors added to the system from the beginning up until the critical error, while photo coordinates contain very large errors from $\sigma_o = 23$ μm to $\sigma_o = 32$ μm, and the phase noises change from the smallest to larger, so up until the critical error. Considering this fact as well, even though the effect of GPS noises appear on the north in small extent it can be stated that the north is affected much more from the errors in photo coordinates rather than these phase noises. After ambiguity fixing, the magnitude of the errors in the north changes only 2.7 mm for the phase noises in the range from the beginning to the critical error. In spite of the decreased errors in photo coordinates that are after the critical error, an increase in the size of the errors appearing in the north is seen due to the large phase noises in the system, even if ambiguities are fixed.

Referring to the case before ambiguity fixing in figure (5.6)a and table 5.5(a), it can be concluded that the extent of the error in the east of camera perspective centre changes depending on the magnitude of the phase noises rather than the magnitude of the errors in photo coordinates, even if they are very large, especially up until the critical error. Looking at the part after critical error in the graph and comparing the results before and after ambiguity fixing, it might also be drawn a conclusion as the combined system works well and produces reasonable results even if it is under a pressure of very large phase noises, while the photo coordinates are having reasonable and small size of errors.

Looking at the results produced under the errors applied to the system from beginning to critical error in figure (5.6)a again, the following statements can be written:

- The improvement in the height of camera perspective centre depends mostly on size of the GPS phase noises. If phase noise is small in magnitude, the improvement is significant even if the errors in photo coordinates are very large.
- It can also be pointed out that as the phase noises increases, the relative changes in the r.m.s. errors according to the noises at different sizes applied to the system stand by small magnitudes in all the part through up until the critical error before ambiguity fixing, i.e. maximum change of 4.6 mm.
- After ambiguity fixing, the r.m.s. errors in the height increase direct proportionally with the increase in phase noises, although an improvement are still seen comparing the results for the heights before and after ambiguity fixing, except the last two cases with phase noise of 4-5 cm.
- An improvement in the height are also observed for the cases after critical error. Because the errors in the photo coordinates are pulled down for the sake of obtaining correct ambiguities while the phase noises still increase.
- So, it can be concluded that as long as one of both of the systems has small errors, then the height of the camera perspective centre will be well determined.

From figure (5.6)b, similar conclusions can also be drawn here for the coordinates of ground points as in the previous test. There is not any striking improvement in any one of the coordinates of ground points considering the results before and after ambiguity

fixing. The east even shows a deterioration when these both cases are considered. The height exhibits a slight deterioration instead of an improvement too for the cases with the different errors in size after critical error.

Looking at the magnitudes of the errors produced in each one of the three local coordinates according to the applied noises into both systems, in general it can be pointed out that the size of the errors in the photo coordinates is the major factor describing and affecting the magnitude of errors appearing in the coordinates of ground points. It is also clearly seen that phase noises do not have a significant effect on these coordinates, according to the results produced through the runs for the small noises in photo coordinates, even though the phase noises are very large in size. So, there is no significant interaction between the phase noises and the errors to be appear in the coordinates of ground points, especially in their plan position. The only thing that has a substantial effect on the magnitude of errors in the coordinates of ground points is the precision of the measured photo coordinates of ground points.

The largest marginally detectable errors in the coordinates of camera perspective centre increase linearly, as shown in figure (5.7), depending on the magnitude of the phase noises in the combined system. The results displayed in table 5.6, numerically, and figure (5.7), graphically, also indicate that the most critical effect on the magnitude of these largest marginally detectable errors is from the phase noise levels in the combined system, as has already been expressed.

The largest marginally detectable errors in the coordinates of ground control points and new ground points follow quite similar patterns but the errors are at two different levels. On one hand, those errors vary between 13.61 cm and 86.92 cm for ground control points, on the other hand, the others that are for new ground points vary between 2.75 m and 14.21 m. The numerical results in the table and the graphical results in the figure display that the only effective factor is the size of the errors in the photo coordinates on the size of these largest marginally detectable errors. It can also be concluded from these results that the photogrammetric noises in the combined

system have a direct proportional influence on this sort of errors in the coordinates of both type of the points depending on the size of these photogrammetric noises.

5.2.6 SUMMARY

- It is a necessity for the combined system to work well that photogrammetric measurements must be made more precisely if GPS is under a large phase noises i.e. 5 cm (table 5.4 and figure (5.5)).
- If the errors in both systems falls into the shaded area as shown in figure (5.5), the combined system delivers the ambiguities correctly.
- Figure (5.6)a introduces that the biggest improvement in the coordinates of camera perspective centre is in the north.
- Also the r.m.s. errors in the east and the north of the camera perspective centre show almost constant attitude until the case with the error of 3 cm in GPS, while the errors in both components of the combined system increase after ambiguity fixing.
- After this case with the error of 3 cm, the errors in the both local coordinates start to increase depending on the size of the phase noises in the cases after ambiguity fixing.
- It can also be indicated from figure (5.6)a that the improvement in height of camera perspective centre depends on mostly the GPS phase noise levels.
- When one of both photogrammetry and GPS have large errors, the other one takes care of improving the height unless it has large errors too.
- From figure (5.6)b, it can be pointed out that ,in general, the magnitude of the errors in the photo coordinates is the major factor describing and affecting the magnitude of the errors appearing in the coordinates of ground points.
- The results in figure (5.7) illustrates that the largest marginally detectable errors in the coordinates of camera perspective centre are mostly affected by the magnitude of the phase noises in the combined system.
- The largest marginally detectable errors in the coordinates of ground control points and new ground points follow quite similar paths but in the different level of errors. However, the errors for ground control points and for new ground points vary 13.61 cm to 86.92 cm and 2.75 m to 14.21 m respectively.

6. CHAPTER SIX

6.1 VARIATIONS IN RELIABILITY AND PRECISION OF THE SYSTEM ACCORDING TO THE SPECIFIED VARIOUS ERRORS IN PHOTO MEASUREMENTS AND PHASE OBSERVABLES

6.1.1 TEST OBJECTIVES

- The main objective of this test is to assess the precision of estimated coordinates of new ground points and the camera pespective center produced by the new combined system using the antenna on the aircraft when precision of photo coordinates and phase observables are varied.
- The second is to see whether the mapping specifications would be met by these precisions.

6.1.2 TEST SET-UP

- Errors with standard deviation of ±2, ±5 and ±10 μm for both x and y photo coordinates.
- Noises with standard deviation of ±2, ±5 and ±10 centimeters for all phase measurements.
- Different number of ground control points (2 and 3)
  were exercised.

6.1.3 TEST PROCEDURE

The random numbers were generated for each one of the errors of the specified standard deviation in photo coordinates, then they were added to the true photo coordinates of the points. Therefore, the observed photo coordinates were constituted

for each specified case, the standard deviation of the GPS phase observables is changed one by one to obtain the GPS phase measurements made up for the various specified standard deviation, and then the program was run several time to test each case made up. For this reason, in each run, random numbers were also generated to produce the GPS phase observables with the noises of specified standard deviation made up to test each case, according to the conditions on the plane. These numbers were then added to the calculated true phases to form their respective phase observations and the combined system has been run several times to see the error variations in the estimated parameters due to different conditions which were described according to the each one of different cases using errors with the specified standard deviation for the photo coordinates and the GPS phase observables as well. The system was also run to test the cases mentioned above with different number of ground control points, 2 and 3. In all, 24 runs of the program were put through. In each run, the following reliability and precision indicators are calculated :

- The largest marginally detectable errors in the photo coordinates of ground control points and new ground points and GPS phase abservables with regard to the both cases using two and three control points.
- The root mean square errors in absolute plan position and height of ground control points and new ground points and exposure stations for all the cases tested.

6.1.4 RESULTS OF THE TEST

Figure (6.1)a and b and table 6.1 show graphical and numerical representations of the errors in the coordinates of camera perspective center for the phase noises of standard deviation of ± 2 cm according to the results before and after ambiguity fixing, when the combined system has 2 and 3 ground control points.

BAS and AAS stand for Before Ambiguity Solution and After Ambiguity Solution respectively.

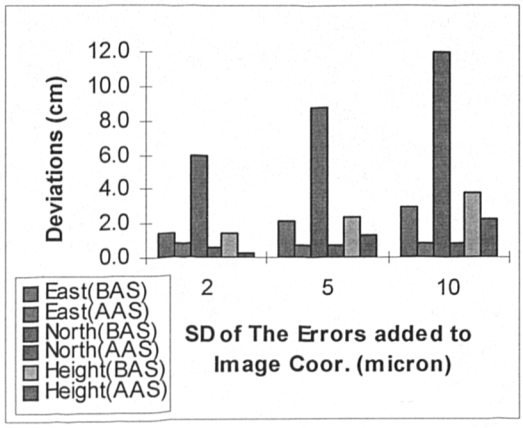

Figure (6.1)a r.m.s. errors in local coordinates of camera perspective center for the GPS phase observables with standard deviation of ±2 cm and using 3 ground control points.

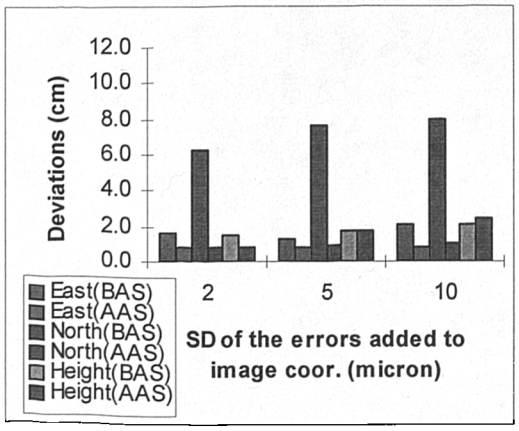

Figure (6.1)b r.m.s. errors in local coordinates of camera perspective center for the GPS phase observables with standard deviation of ±2 cm and using 2 ground control points.

	3 ground control points			2 ground control points		
σ_p (μm)	2	5	10	2	5	10
East (BAS)(cm)	1.44	2.12	2.98	1.62	1.22	2.02
East (AAS)(cm)	0.81	0.75	0.77	0.81	0.81	0.81
North (BAS)(cm)	6.00	8.77	11.90	6.20	7.67	7.92
North (AAS)(cm)	0.64	0.69	0.79	0.84	0.92	1.03
Height (BAS)(cm)	1.38	2.38	3.81	1.48	1.71	2.03
Height (AAS)(cm)	0.28	1.35	2.29	0.84	1.74	2.45

Table 6.1 r.m.s. errors in local coordinates of camera perspective center for the GPS phase observables with standard deviation of ±2 cm.

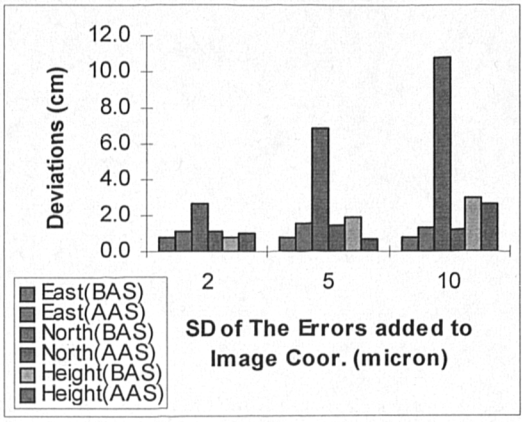

Figure (6.2)a r.m.s. errors in local coordinates of camera perspective center for the GPS phase observables with standard deviation of ±5 cm and using 3 ground control points.

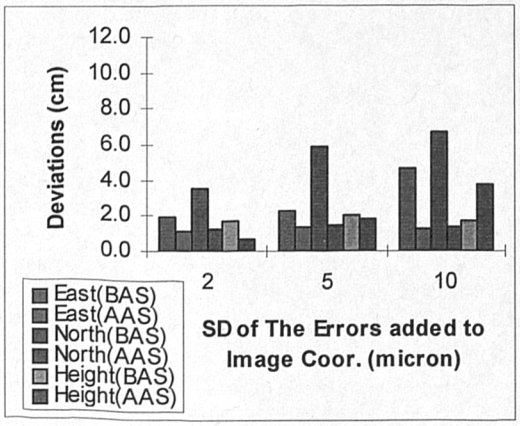

Figure (6.2)b r.m.s. errors in local coordinates of camera perspective center for the GPS phase observables with standard deviation of ±5 cm and using 2 ground control points.

Figure (6.2)a and b and table 6.2 show graphical and numerical representations of the errors in the coordinates of camera perspective center for the phase noises of standard deviation of ± 5 cm according to the results before and after ambiguity fixing, when the combined system has 2 and 3 ground control points.

	3 ground control points			2 ground control points		
σ_p (μm)	2	5	10	2	5	10
East (BAS)(cm)	0.75	0.78	0.75	1.98	2.32	4.65
East (AAS)(cm)	1.13	1.55	1.32	1.09	1.41	1.25
North (BAS)(cm)	2.61	6.93	10.73	3.53	5.87	6.71
North (AAS)(cm)	1.14	1.45	1.26	1.30	1.43	1.32
Height (BAS)(cm)	0.77	1.94	3.04	1.74	1.99	1.66
Height (AAS)(cm)	0.99	0.62	2.67	0.68	1.81	3.70

Table 6.2 r.m.s. errors in local coordinates of camera perspective center for the GPS phase observables with standard deviation of ±5 cm.

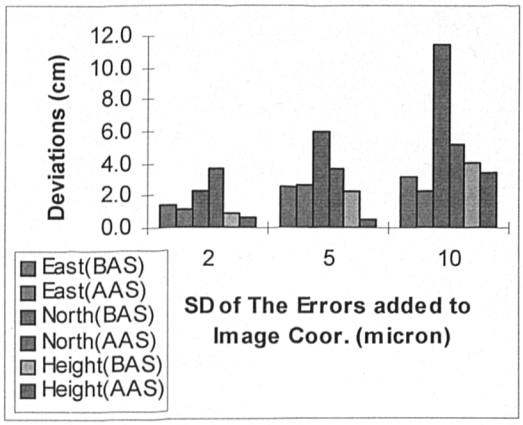

Figure (6.3)a r.m.s. errors in local coordinates of camera perspective center for the GPS phase observables with standard deviation of ±10 cm and using 3 ground control points.

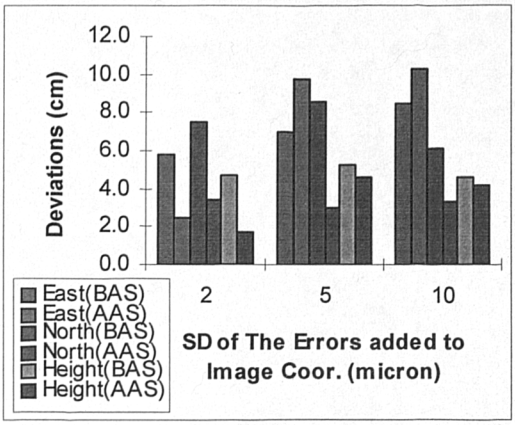

Figure (6.3)b r.m.s. errors in local coordinates of camera perspective center for the GPS phase observables with standard deviation of ±10 cm and using 2 ground control points.

Figure (6.3)a and b and table 6.3 show graphical and numerical representations of the errors in the coordinates of camera perspective center for the phase noises of standard deviation of ± 10 cm according to the results before and after ambiguity fixing, when the combined system has 2 and 3 ground control points.

	3 ground control points			2 ground control points		
σ_p (μm)	2	5	10	2	5	10
East (BAS)(cm)	1.41	2.50	3.24	5.74	6.91	8.41
East (AAS)(cm)	1.16	2.71	2.35	2.45	9.76	10.30
North (BAS)(cm)	2.34	6.04	11.53	7.45	8.56	6.09
North (AAS)(cm)	3.74	3.69	5.27	3.46	2.95	3.30
Height (BAS)(cm)	0.85	2.28	4.13	4.76	5.27	4.61
Height (AAS)(cm)	0.68	0.50	3.43	1.74	4.56	4.21

Table 6.3 r.m.s. errors in local coordinates of camera perspective center for the GPS phase observables with standard deviation of ±10 cm.

Figure (6.4)a and b and table 6.4 show graphical and numerical representation of the errors in the coordinates of new ground points for the phase noises of standard

deviation of ± 2 cm according to the results before and after ambiguity fixing, when the combined system has 2 and 3 ground control points.

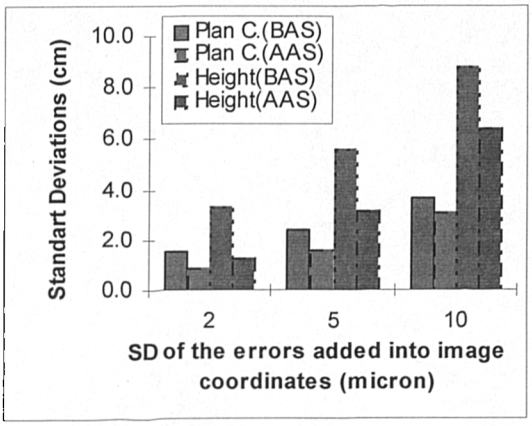

Figure (6.4)a r.m.s. errors in local coordinates of new ground points for the GPS phase observables with standard deviation of ±2 cm and using 3 ground control points.

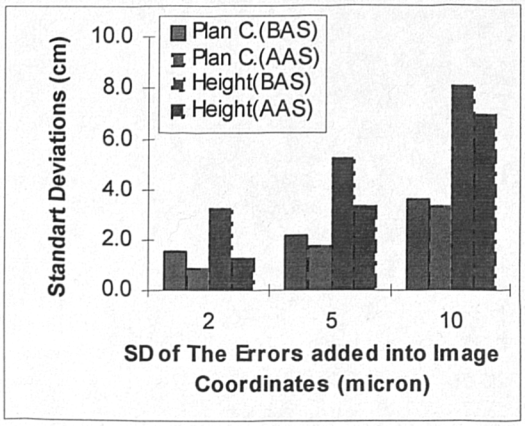

Figure (6.4)b r.m.s. errors in local coordinates of new ground points for the GPS phase observables with standard deviation of ±2 cm and using 2 ground control points.

	3 ground control points			2 ground control points		
σ_p (μm)	2	5	10	2	5	10
Plan (BAS)(cm)	1.47	2.34	3.66	1.48	2.18	3.60
Plan (AAS)(cm)	0.87	1.63	3.07	0.87	1.77	3.37
Height (BAS)(cm)	3.34	5.64	8.85	3.31	5.30	8.08
Height (AAS)(cm)	1.31	3.21	6.47	1.26	3.35	6.92

Table 6.4 r.m.s. errors in local coordinates of new ground points for the GPS phase observables with standard deviation of ±2 cm.

Figure (6.5)a and b and table 6.5 show graphical and numerical representation of the errors in the coordinates of new ground points for the phase noises of standard deviation of ± 5 cm according to the results before and after ambiguity fixing, when the combined system has 2 and 3 ground control points.

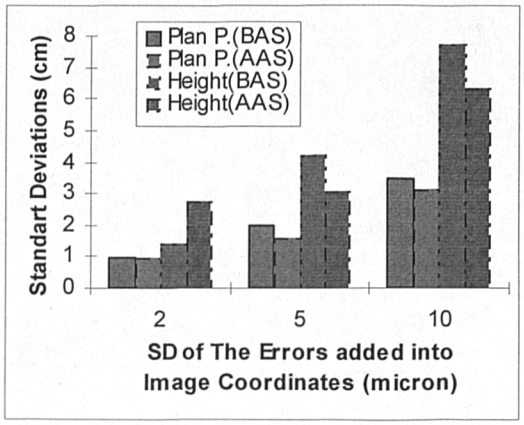

Figure (6.5)a r.m.s. errors in local coordinates of new ground points for the GPS phase observables with standard deviation of ±5 cm and using 3 ground control points.

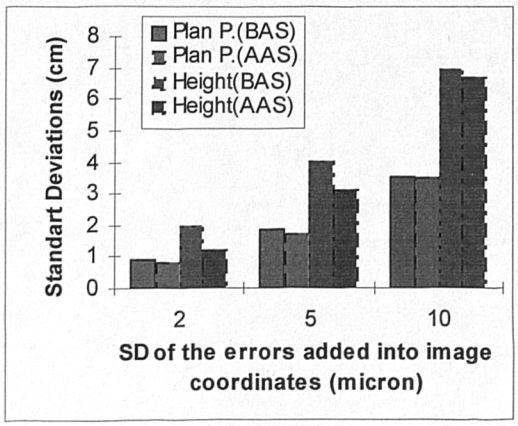

Figure (6.5)b r.m.s. errors in local coordinates of new ground points for the GPS phase observables with standard deviation of ±5 cm and using 2 ground control points.

	3 ground control points			2 ground control points		
σ_p (μm)	2	5	10	2	5	10
Plan P. (BAS)(cm)	0.94	1.97	3.45	0.88	1.84	3.53
Plan P. (AAS)(cm)	0.99	1.57	3.13	0.84	1.73	3.54
Height (BAS)(cm)	1.43	4.25	7.76	1.96	4.02	6.96
Height (AAS)(cm)	2.74	3.07	6.35	1.22	3.16	6.73

Table 6.5 r.m.s. errors in local coordinates of new ground points for the GPS phase observables with standard deviation of ±5 cm.

Figure (6.6)a and b and table 6.6 show graphical and numerical representation of the errors in the coordinates of new ground points for the phase noises of standard deviation of ± 10 cm according to the results before and after ambiguity fixing, when the combined system has 2 and 3 ground control points.

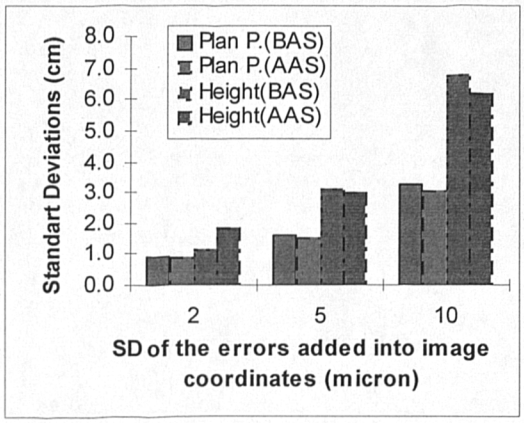

Figure (6.6)a r.m.s. errors in local coordinates of new ground points for the GPS phase observables with standard deviation of ±10 cm and using 3 ground control points.

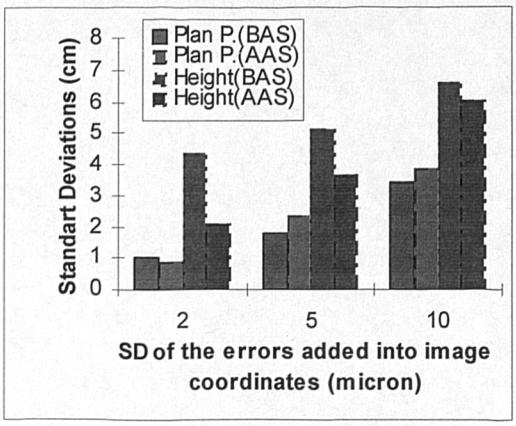

Figure (6.6)b r.m.s. errors in local coordinates of new ground points for the GPS phase observables with standard deviation of ±10 cm and using 2 ground control points.

	3 ground control points			2 ground control points		
σ_p (μm)	2	5	10	2	5	10
Plan P. (BAS)(cm)	0.87	1.63	3.23	1.03	1.76	3.44
Plan P. (AAS)(cm)	0.91	1.54	3.07	0.89	2.36	3.87
Height (BAS)(cm)	1.14	3.12	6.81	4.40	5.11	6.63
Height (AAS)(cm)	1.86	3.00	6.19	2.10	3.66	6.01

Table 6.6 r.m.s. errors in local coordinates of new ground points for the GPS phase observables with standard deviation of ±10 cm.

Table 6.7(a) shows the accuracy specifications for mapping purposes at selected scales ranging from 1:500 to 1:20000. In the table, under the accuracy columns for both plan and height, the first column gives the maximum tolerance and the second column gives the relative tolerance (IRCS, 1988).

map scale	photo scale	H (m)	Accuracy in plan (m)		Accuracy in height (m)	
1:500	1:2500	380.0	0.03	0.03	0.17	0.05
1:2000	1:5000	760.0	0.12	0.10	0.33	0.10
1:2500	1:10000	1500.0	0.15	0.13	0.67	0.20
1:10000	1:25000	3800.0	0.60	0.50	1.67	0.50
1:20000	1:50000	7600.0	1.20	1.00	3.33	1.00

Table 6.7(a) Accuracy specifications for mapping at selected scale

Table 6.7(b) represents the size of the errors in plan position and height of the ground points calculated from the outcomes delivered by the several runs of the combined system under the various conditions, i.e. with the r.m.s. phase noises of ± 2 cm, ± 5 cm and ± 10 cm, the r.m.s photo coordinate errors of ± 2 μm, ± 5 μm and ± 10 μm and 2-3 ground control points, according to several photo scales.

		Errors in plan position (cm)						Errors in height (cm)					
		3 ground control points			2 ground control points			3 ground control points			2 ground control points		
Photo scales	Phase noises (cm)	photo noise ±2 μ	photo noise ±5 μ	photo noise ±10μ	photo noise ±2 μ	photo noise ±5 μ	photo noise ±10μ	photo noise ±2 μ	photo noise ±5 μ	photo noise ±10 μ	photo noise ±2 μ	photo noise ±5 μ	photo noise ±10μ
1: 2500	± 2	0.73	1.38	2.59	0.73	1.49	2.85	1.11	2.71	5.46	1.06	2.83	5.84
1: 2500	± 5	0.84	1.33	2.64	0.71	1.46	2.99	2.31	2.59	5.36	1.03	2.67	5.68
1: 2500	± 10	0.77	1.30	2.59	0.75	1.99	3.27	1.57	2.53	5.23	1.77	3.09	5.07
1: 5000	± 2	1.46	2.76	5.18	1.46	2.98	5.7	2.22	5.42	10.92	2.12	5.66	11.68
1: 5000	± 5	1.68	2.66	5.28	1.42	2.92	5.98	4.62	5.18	10.72	2.06	5.34	11.36
1: 5000	± 10	1.54	2.6	5.18	1.5	3.98	6.54	3.14	5.06	10.46	3.54	6.18	10.14
1: 10000	± 2	2.92	5.52	10.36	2.92	5.96	11.4	4.44	10.84	21.84	4.24	11.32	23.36
1: 10000	± 5	3.36	5.32	10.56	2.84	5.84	11.96	9.24	10.36	21.44	4.12	10.68	22.72
1: 10000	± 10	3.08	5.2	10.36	3	7.96	13.08	6.28	10.12	20.92	7.08	12.36	20.28
1: 25000	± 2	7.3	13.8	25.9	7.3	14.9	28.5	11.1	27.1	54.6	10.6	28.3	58.4
1: 25000	± 5	8.4	13.3	26.4	7.1	14.6	29.9	23.1	25.9	53.6	10.3	26.7	56.8
1: 25000	± 10	7.7	13	25.9	7.5	19.9	32.7	15.7	25.3	52.3	17.7	30.9	50.7
1: 50000	± 2	14.6	27.6	51.8	14.6	29.8	57	22.2	54.2	109.2	21.2	56.6	116.8
1: 50000	± 5	16.8	26.6	52.8	14.2	29.2	59.8	46.2	51.8	107.2	20.6	53.4	113.6
1: 50000	± 10	15.4	26	51.8	15	39.8	65.4	31.4	50.6	104.6	35.4	61.8	101.4

Table 6.7(b) r.m.s. errors in the coordinates of ground points at the selected scales

Table 6.7(c) shows r.m.s. errors in the plan position and the height of the camera perspective centres using camera lenses of 0.152 m, flying height of 450 m, the r.m.s. phase noises of ± 2 cm, ± 5 cm and ± 10 cm, the r.m.s photo coordinates errors of ± 2 μm, ± 5 μm and ± 10 μm and 2-3 ground control points.

	Errors in plan positions (cm)						Errors in height (cm)					
	3 ground control points			2 ground control points			3 ground control points			2 ground control points		
Phase noises (cm)	photo noise ±2 μ	photo noise ±5 μ	photo noise ±10μ	photo noise ±2 μ	photo noise ±5 μ	photo noise ±10μ	photo noise ±2 μ	photo noise ±5 μ	photo noise ±10 μ	photo noise ±2 μ	photo noise ±5 μ	photo noise ±10μ
± 2	0.88	0.86	0.94	0.98	1.03	1.11	0.23	1.14	1.93	0.70	1.47	2.07
± 5	1.36	1.79	1.54	1.44	1.70	1.54	0.83	0.52	2.25	0.57	1.53	3.12
± 10	3.31	3.87	4.87	3.58	8.61	9.14	0.57	0.42	2.90	1.47	3.85	3.55

Table 6.7(c) r.m.s. errors in the coordinates of camera perspective centre

Figure (6.7)a through to (6.9)b and table 6.8, respectively, show graphical and numerical representations of largest marginally detectable errors in the coordinates of ground control points, camera perspective centre and new ground points using various size of errors in both photogrammetric and phase measurements according to the cases using 2 and 3 ground control points.

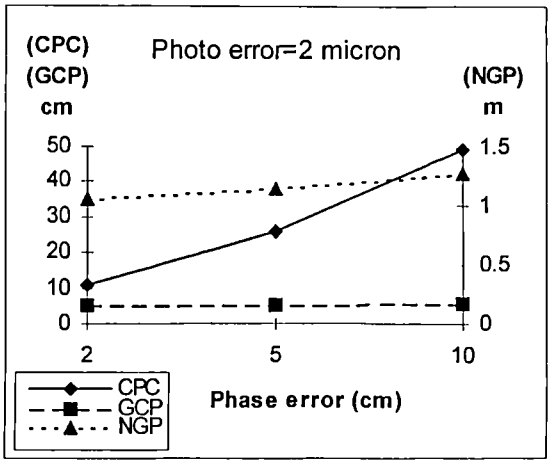

Figure (6.7)a Largest marginally detectable errors. In the case using 3 control points and r.m.s photo errors of ±2 micron.

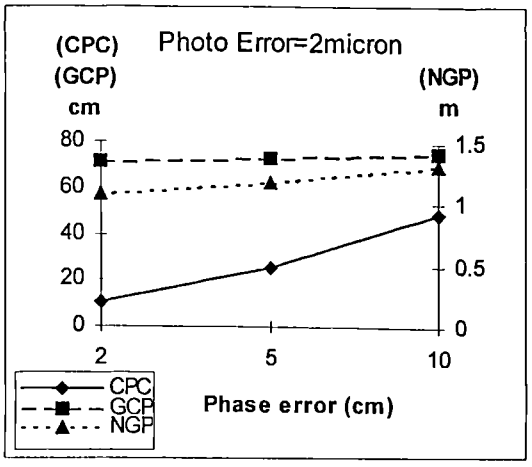

Figure (6.7)b Largest marginally detectable errors. In the case using 2 control points and r.m.s photo errors of ±2 micron.

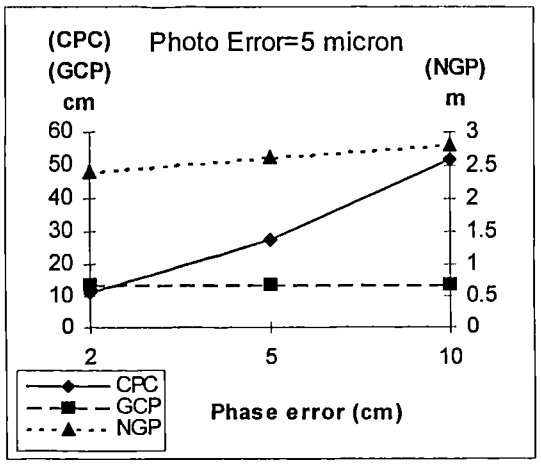

Figure (6.8)a Largest marginally detectable errors. In the case using 3 control points and r.m.s photo errors of ±5 micron.

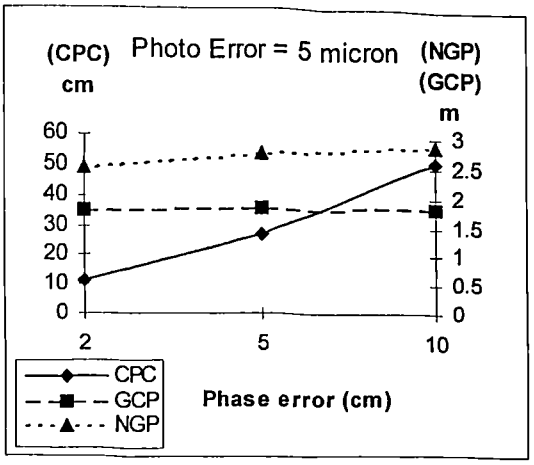

Figure (6.8)b Largest marginally detectable errors. In the case using 2 control points and r.m.s photo errors of ±5 micron.

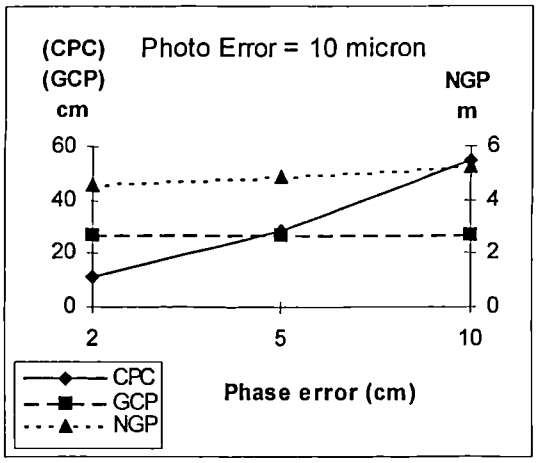

Figure (6.9)a Largest marginally detectable errors. In the case using 3 control points and r.m.s photo errors of ±10 micron.

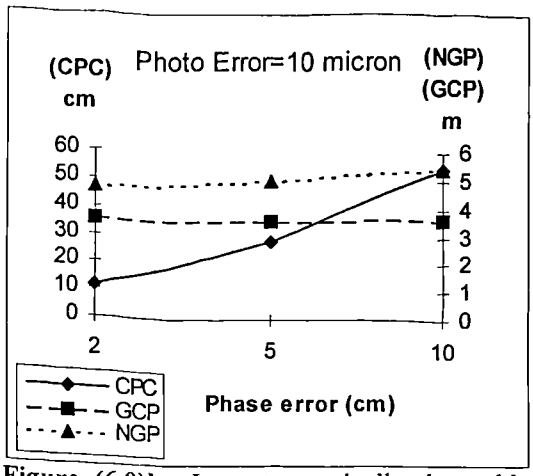

Figure (6.9)b Largest marginally detectable errors. In the case using 2 control points and r.m.s photo errors of ±10 micron.

		3 control points			2 control points		
photo noise (μ)	phase noise (cm)	Camera perspective centre (cm)	Ground control points (cm)	New ground points (m)	Camera perspective centre (cm)	Ground control points (cm)	New ground points (m)
2	2	11	5.4	1.046	10.9	71	1.071
2	5	26	5.5	1.144	25.7	72.9	1.178
2	10	49	5.5	1.273	49.2	76	1.325
5	2	12	14	2.398	11.5	176.8	2.444
5	5	27	14	2.617	27.2	178.2	2.68
5	10	52	14	2.798	52.1	181.6	2.879
10	2	12	27	4.574	11.7	354.9	4.665
10	5	28	27	4.89	28.4	356.3	5.006
10	10	54	27	5.241	54.5	360.2	5.409

Table 6.8 Largest marginally detectable errors

6.1.5 DISCUSSION OF RESULTS

In figure (6.1)a and b and table 6.1, it can be seen that the errors in the photo coordinates of the ground points have a directly proportional effect on the east, north and the height of the camera perspective centre according to their respective size in the case of 3 control points, while before ambiguity fixing GPS phase measurements have errors with standard deviation of 2 cm. In addition, an improvement is seen on the east in the both cases using 2 and 3 control points when the results before and after ambiguity fixing are compared. The magnitude of the errors appearing in the east after ambiguity fixing considering the both cases of 2 and 3 control points almost remain constant for all the errors in various sizes applied to the photo coordinates of the ground points. Besides this, the same conclusion can be drawn for the north as well. It exhibits a quite good improvement relative to the size of the errors in it before ambiguity fixing. The height also shows an improvement, which is proportional to the size of the errors in the photo coordinates of the ground points, according the case of three control points. However the sizes of the errors appearing in the height before and after ambiguity fixing are again proportional to the size of the errors in the photo coordinates of the ground points. In the case of two control points, a slight deterioration is seen in the height, after ambiguities are fixed. The magnitudes of the errors in it are quite reasonable for mapping purposes, that they varies from 0.8 cm to 2.5 cm depending on the size of the errors in the photo coordinates of the ground points.

Figure (6.2)a and b and table 6.2 show r.m.s. errors in the local coordinates of perspective centre for the cases using 2-3 control points, the phase noises of ± 5 cm standard deviation and the errors (in photo coordinates of the ground points) of ± 2 μm, ± 5 μm and ± 10 μm standard deviations. From these results, similar conclusions can be drawn especially for the cases of after ambiguity fixing, except the size of the errors appeared in the local coordinates that are slightly worse. It can be seen when the results obtained for this test are compared with those in previous test mentioned in the previous paragraphs. An obvious deterioration can also be seen in the east of the

camera perspective centre comparing the results before and after ambiguity fixing in the case of 3 control points.

Figure (6.3)a and b and table 6.3 represent the results with different pattern than the ones given above for the local coordinates of the camera perspective centre, especially those in the case using 2 ground control points produced by the run for the phase noise of ± 10 cm and the errors (in photo coordinates of the ground points) of standard deviations of ± 2 μm, ± 5 μm and ± 10 μm. These results were represented here to show that how large GPS phase noises can be coped with by the combined system, while it still delivers good results for the coordinates of the camera perspective centre and the ground points for the seek of proving its powerfulness since one of the objectives of this thesis is to represent capability of the new system. ±10 cm noise is not the usual case for the GPS phase measurements under any conditions, e.g. even under a normal multipath of ± 2 cm or under the very severe multipath which is around ± 5 cm on plane (Corbett, 1994). As can be seen from the figure (6.3)b representing the results in the case of 2 control points, the errors appeared in the north of the camera perspective centre in the cases with the r.m.s. errors of 5-10 μm are larger than the half of the wavelength of L1 phase after ambiguity solution. Since some of the ambiguities are wrongly solved by 1 or 2 cycles. Here, it can also be indicated that the results after ambiguity fixing in figure (6.3)a for the case of 3 control points still show reasonable outcomes obtained for the coordinates of camera perspective centre while the system is under the conditions of photogrammetric errors in three different levels and phase noises of ± 10 cm standard deviation. So, this again proves that the coordinates of the camera perspective centre will be well determined as long as one of the systems has small errors (i.e. ± 2 μm in the cases of 2-3 control points and ± 2 μm or ± 5 μm in the case of three control points for photogrammetry) while the other has large error (i.e. ±10 cm for GPS).

All the figures showing r.m.s. errors in the local coordinates of new ground points suggest that these errors introduce similar trends for each different phase errors, except the small differences in their sizes (in some cases they are ignorable), considering the results before and after ambiguity fixing in the cases using 2-3 control points and the three different photogrammetric errors. The largest differences are

- 9.1 mm, 5.0 mm and 8.8 mm in height and
- 8.0 mm, 5.0 mm and 1.2 mm in plan position

in the cases of 2 ground control points and

- 2.8 mm, 2.1 mm and 14.3 mm in height and
- 0.6 mm, 0.9 mm and 1.2 mm in plan position

in the cases of 3 ground control points for the cases of the r.m.s errors of ± 10 μm, ± 5 μm and ± 2 μm in photo coordinates respectively, comparing the results after ambiguity fixing for GPS phase noises of ± 10 cm, ± 5 cm and ± 2 cm. These differences indicate that variations in the size of GPS phase noises do not show a significant effect on the coordinates of new ground points treated as one set of unknown parameters in the new combined model. It can clearly be seen from the results in figure (6.4)a and b, (6.5)a and b, (6.6)a and b and Table 6.4, 6.5 and 6.6 that the size of the errors in the plan position and the height of new ground points mostly depend on the magnitude of the errors in photo coordinates of these ground points which were applied as ± 2 μm, ± 5 μm and ± 10 μm in the tests. Considering the different number of ground control points, the differences after ambiguity fixing, which are

- 3 mm, 1.4 mm and 0.0 mm in plan position and
- 4.5 mm, 1.4 mm and 0.5 mm in height

for the case using GPS phase noise of ± 2 cm standard deviation,

- 4.1 mm, 1.6 mm and 1.5 mm in plan position and
- 3.8 mm, 0.9 mm and 15.2 mm in height

for the case using GPS phase noise of ± 5 cm standard deviation and

- 8 mm, 8.2 mm and 0.2 mm in plan position and
- 1.8 mm, 6.6 mm and 2.4 mm in height

for the case using GPS phase noise of ± 10 cm standard deviation in the cases using the r.m.s errors of ± 10 μm, ± 5 μm and ± 2 μm in photo coordinates respectively, indicate that in the new combined system the number of ground control points does not have a strong influence on the coordinates of new ground points.

Comparing the results in Table 6.7(a) and 6.7(b) in terms of relative tolerance, the errors in the plan position of the ground points meet with the technical mapping specifications laid down, under all the conditions tested, except where the system are having the phase noise of ± 10 cm in phase observations and r.m.s. errors of ± 10 μm in photo coordinates and 2 control points altogether at the same time. Similarly, when a comparison is made in terms of maximum tolerance the results even in the exceptional cases meet the mapping specifications as well. Looking at the errors in the height of ground points produced by the runs set up for different cases, it can be seen that they are also within the technical mapping specifications for all the circumstances tested when the maximum tolerances are taken into consideration.

In general, no matter how many ground control points are used, the results in Table 6.7(b) displaying the precision of the plan position of ground points are within the mapping specifications for all the scales represented in Table 6.7(a) and for all the conditions made up and tested, i.e. for phase errors with ± 2 cm, ± 5 cm and ± 10 cm standard deviation and photo noises of ± 2 μm, ± 5 μm and ± 10 μm standard deviation. Precision of the height of ground points are affected slightly more than the plan position by the errors in photo coordinates. Therefore, more care is needed to get the precision that can meet the mapping specifications in Table 6.7(a). In this connection, the system with the errors of ± 2 μm and ± 5 μm standard deviation in the photo coordinates gives reasonable precision for the height as well according to the results for both cases using 2 and 3 ground control points.

Looking at Table 6.7(c), the largest difference between the r.m.s. errors in the plan and height coordinates of camera perspective centre in cases using 2 and 3 ground control points are 0.2 cm and 1.0 cm respectively, considering the cases with phase noises of ± 2 cm and ± 5 cm standard deviation and with the errors of ± 2 μm, ± 5 μm and ± 10 μm standard deviation in photo coordinate. The system with 3 control points also produces good results for both coordinates, the plan and height of exposure station while it is having phase observations with the noises of ± 10 cm standard deviation. With 2 control points the results are still good for the height, but not for the plan

position except the case under the photogrammetric noise of ± 2 μm standard deviation.

The differences are quite small, comparing the results for plan positions in the cases using different photogrammetric errors if the system is having phase noises of the same standard deviation except the cases using photogrammetric noise of ± 5 μm, ± 10 μm standard deviation under the phase noise of ± 10 cm standard deviation. But in the height, similar differences become a bit larger. The precision of the plan coordinates of exposure stations goes worse direct proportionally by the size of the phase noises considering the results for both cases using 2-3 control points. The same effect can not be seen upon the height. It is affected by photogrammetric noise rather than phase noise. This statement also parallels to the expressions in the part concerning exposure station in the first test. In short, the errors appearing in the plan and height of the camera perspective centre under the various conditions as those in the tests here lie within the mapping specifications except the circumstances mentioned above.

Comparing the results in Table 6.8 and figure (6.7)a through figure (6.9)b that concern the largest marginally detectable errors in camera perspective centre for the cases using 3 and 2 control points, the results for the same phase noises in the case of 3 control points show almost the same reliability for the camera perspective centre for all the precision of photo coordinates tested. When the size of the phase noises is increased, the reliability of exposure stations become worse proportionally depending on the magnitude of the applied phase noises. Looking at the results for both cases using 2 and 3 ground control points in the table and the figures again and taking into consideration the conclusions above, it can clearly be implied that the only dominant factor is the precision of phase observables on the reliability of camera perspective centre if the very slight influences of the photo noises are ignored especially where the system is having large phase noises.

The reliability of ground control points can be investigated in the following way, looking at the results in Table 6.8 and figures (6.7)a through figure (6.9)b. According to the results in the cases using 3 ground control points, the error level in photo

coordinates are the major active factor describing the reliability of ground control points proportionally by its respective size, instead of phase noises being different than the case in the camera perspective centre. In this case, i.e. using 3 control points, phase noises do not involve into the reliability of ground control points at all. In the case using 2 control points, both type of errors in photo coordinates and in phase observables together become active factors describing the reliability of ground control points. But the effect of phase noises in the system is much stronger than the effect of the errors in photo coordinates. From these outcomes, it can be stated that if the model have a good strength, i.e. with 3 control points, the reliability of ground control points is only under the pressure of the errors in photo coordinates. If strength of the model is weak, phases noises also starts to affect the reliability of ground control points in small sizes relative to the effect of the photogrammetric noise.

No matter how many ground control points are used, the factor showing the strongest effect on the reliability of new ground points is the errors in the measured photo coordinates of these points. The effect also comes direct proportionally on them by the size of these errors. However the phase noises in the system have a slight influence on this reliability proportionally with its size. The magnitude of this effect is relatively small, therefore it is negligible, comparing with the strong influence formed by the errors in photo coordinates.

6.1.6 SUMMARY

- It can be concluded that in general, the errors before ambiguity fixing in the photo coordinates of the ground points according to the cases using 2 and 3 ground control points have an effect on the east, north and height of camera perspective centre direct proportionally by their respective sizes.
- Quite a good improvement is seen on the north, while the others are generally having reasonable improvement as well for both cases using 2 and 3 control points, except the results for the east and the height in some cases with large errors, when the results before and after ambiguity fixing (in figure (6.1)a and b and Table 6.1) are compared.

- The variations in the size of GPS phase noises do not show a significant effect on the coordinates of new ground points.
- It can clearly be indicated from the results in figure (6.4)a and b, (6.5)a and b, (6.6)a and b and Table 6.4, 6.5 and 6.6 that the size of the errors in the plan position and height of new ground points mostly depends on the measurement precision of the photo coordinates of ground points.
- The results after ambiguity fixing using different number of ground control points introduce that the number of ground control points does not have a strong influence on the coordinates of new ground points, in the new combined system.
- The results in Table 6.7(a) and 6.7(b) show that the errors in the plan position of the ground points meet the technical mapping specifications laid down, under all the conditions to be experienced in practice.
- All the errors appearing in the plan and height of a camera perspective centre regarding the various cases lie within the mapping specifications except a few extreme circumstances.
- If the precision of photogrammetric measurements is good, ± 2 μm standard deviation or better, photogrammetry takes care of the reliability of exposure stations. Phase noises do not exhibit any significant effect on the reliability in these circumstances. When the size of photogrammetric noise gets larger, the phase noise in the system starts to affect the reliability itself even in both cases using 2 and 3 control points.
- If the model is of good strength, i.e. with 3 control points, the effect of phase noises is blanketed by the photogrammetric component of the combined system on the reliability of ground control points and the errors in photo coordinates become unique active factor affecting the reliability proportionally with its size.
- No matter how many ground control points are used, the factor showing a strong effect on the reliability of new ground points is the errors in the photo coordinates. The effect also comes direct proportionally on them by the size of these errors.

6.2 VARIATIONS IN THE RELIABILITY AND PRECISION OF THE SYSTEM WITH ADDITIONAL AMBIGUITY PARAMETERS

6.2.1 Test Objectives

Test objective is

- The main objective of this test is to assess whether the combined system can cope with additional ambiguity parameters and can still deliver good results for all the estimated parameters or not.
- The second is to analyze the precision of estimated coordinates of new ground points and the camera perspective centre produced by the new combined system with additional ambiguity unknowns while the photo coordinates and phase observables are under the errors of various precision.
- The third is to see whether these precisions would be met with the mapping specifications.

6.2.2 Test Set-up

- Errors of ±2, ±5 and ±10 microns standard deviation for both x and y photo coordinates.
- Noise of ±2, ±5 and ±10 centimeters standard deviation for all phase measurements.
- Different numbers of ground control points (2 and 3) were used.

6.2.3 Procedure

A similar procedure has been carried out for this test as for the previous one. The only difference is that a few new ambiguities are added into the system as new unknown parameters. To do this, the design and parameter matrices of the model constituted for

parameters. To do this, the design and parameter matrices of the model constituted for the combined system are modified and rearranged in the C computer program. Afterward, it becomes ready to produce the results for the estimated parameters in the condition of the new test. In each run, the following reliability and precision indicators were calculated :

- The largest marginally detectable errors in the photo coordinates of ground control and new ground points and also GPS phase abservables for the both cases of two and three control points.
- The root mean squares error in plan position and height of ground control and new ground points and exposure stations as deviations from their respective absolute values under the all test conditions.

6.2.4 Results of the test

Figure (6.10)a and b and Table 6.9 show graphical and numerical representations of the errors in the coordinates of camera perspective center for the phase noises of standard deviation of ± 2 cm according to the results before and after ambiguity fixing, when the combined system has 2 and 3 ground control points.

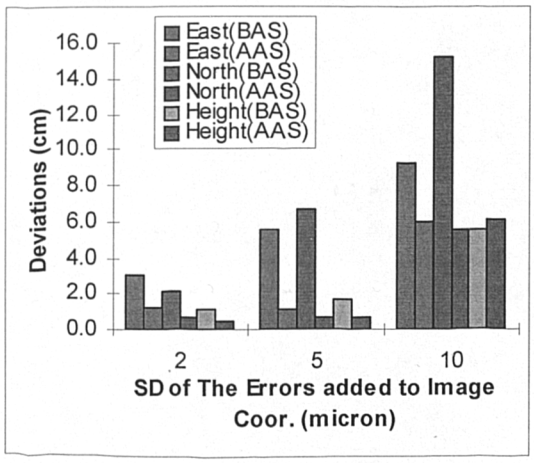

Figure (6.10)a r.m.s. errors in local coordinates of camera perspective center for the GPS phase observables with standard deviation of ±2 cm and using 3 ground control points.

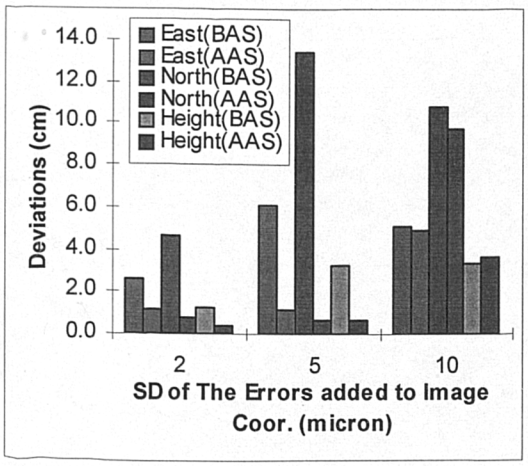

Figure (6.10)b r.m.s. errors in local coordinates of camera perspective center for the GPS phase observables with standard deviation of ±2 cm and using 2 ground control points.

	3 ground control points			2 ground control points		
σ_p (μm)	2	5	10	2	5	10
East (BAS)(cm)	3.07	5.50	9.25	2.64	6.05	5.16
East (AAS)(cm)	1.28	1.17	5.95	1.20	1.13	4.95
North (BAS)(cm)	2.09	6.60	15.22	4.61	13.40	10.83
North (AAS)(cm)	0.71	0.70	5.47	0.74	0.68	9.80
Height (BAS)(cm)	1.09	1.67	5.54	1.29	3.25	3.41
Height (AAS)(cm)	0.40	0.63	6.05	0.39	0.65	3.62

Table 6.9 r.m.s. errors in local coordinates of camera perspective center for the GPS phase observables with standard deviation of ±2 cm.

Figure (6.11)a and b and table 6.10 show graphical and numerical representations of the errors in the coordinates of camera perspective center for the phase noises of standard deviation of ± 5 cm according to the results before and after ambiguity fixing, when the combined system has 2 and 3 ground control points.

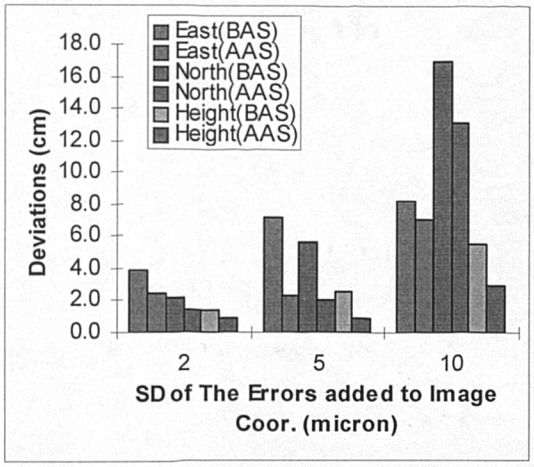

Figure (6.11)a r.m.s. errors in local coordinates of camera perspective center for the GPS phase observables with standard deviation of ±5 cm and using 3 ground control points.

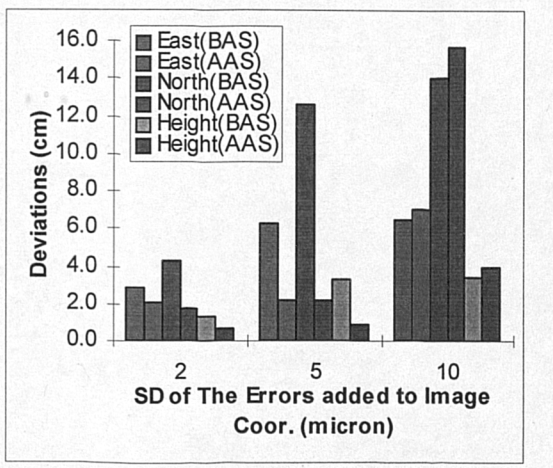

Figure (6.11)b r.m.s. errors in local coordinates of camera perspective center for the GPS phase observables with standard deviation of ±5 cm and using 2 ground control points.

	3 ground control points			2 ground control points		
σ_p (μm)	2	5	10	2	5	10
East (BAS)(cm)	3.81	7.23	8.24	2.83	6.27	6.50
East (AAS)(cm)	2.40	2.25	7.10	2.13	2.16	7.04
North (BAS)(cm)	2.14	5.68	17.00	4.23	12.63	14.07
North (AAS)(cm)	1.47	1.99	13.08	1.79	2.14	15.72
Height (BAS)(cm)	1.46	2.57	5.59	1.28	3.25	3.38
Height (AAS)(cm)	0.91	0.92	2.99	0.68	0.82	3.91

Table 6.10 r.m.s. errors in local coordinates of camera perspective center for the GPS phase observables with standard deviation of ±5 cm.

Figure (6.12)a and b and table 6.11 show graphical and numerical representations of the errors in the coordinates of camera perspective center for the phase noises of standard deviation of ± 10 cm according to the results before and after ambiguity fixing, when the combined system has 2 and 3 ground control points.

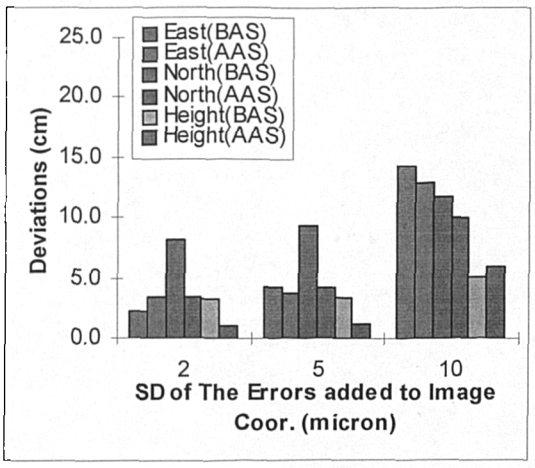

Figure (6.12)a r.m.s. errors in local coordinates of camera perspective center for the GPS phase observables with standard deviation of ±10 cm and using 3 ground control points.

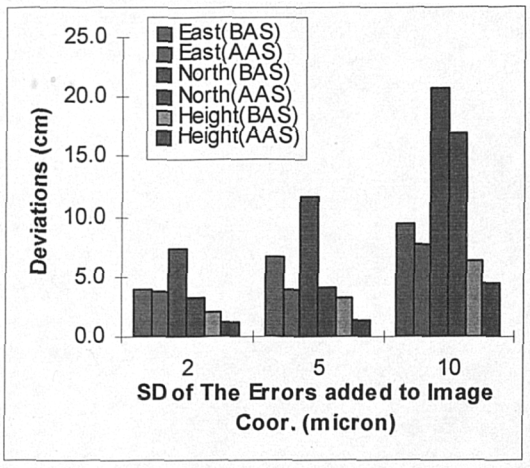

Figure (6.12)b r.m.s. errors in local coordinates of camera perspective center for the GPS phase observables with standard deviation of ±10 cm and using 2 ground control points.

	3 ground control points			2 ground control points		
σ_p (μm)	2	5	10	2	5	10
East (BAS)(cm)	2.23	4.27	14.22	3.93	6.71	9.36
East (AAS)(cm)	3.43	3.74	12.87	3.69	3.90	7.64
North (BAS)(cm)	8.13	9.40	11.66	7.29	11.67	20.77
North (AAS)(cm)	3.34	4.22	10.09	3.20	4.11	16.87
Height (BAS)(cm)	3.27	3.43	5.05	2.11	3.20	6.38
Height (AAS)(cm)	1.07	1.27	5.93	1.24	1.29	4.41

Table 6.11 r.m.s. errors in local coordinates of camera perspective center for the GPS phase observables with standard deviation of ±10 cm.

Figure (6.13)a and b and table 6.12 show graphical and numerical representation of the errors in the coordinates of new ground points for the phase noises of standard deviation of ± 2 cm according to the results before and after ambiguity fixing, when the combined system has 2 and 3 ground control points.

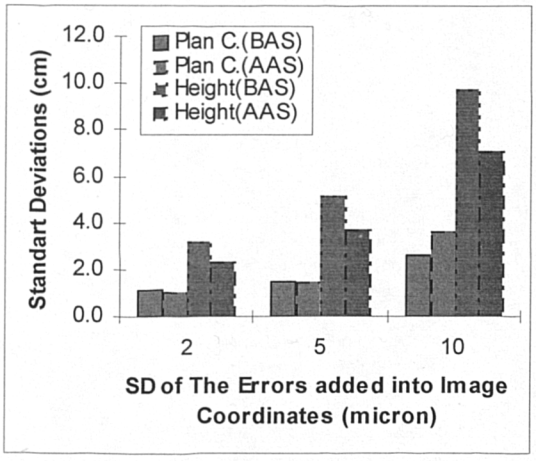

Figure (6.13)a r.m.s. errors in local coordinates of new ground points for the GPS phase observables with standard deviation of ±2 cm and using 3 ground control points.

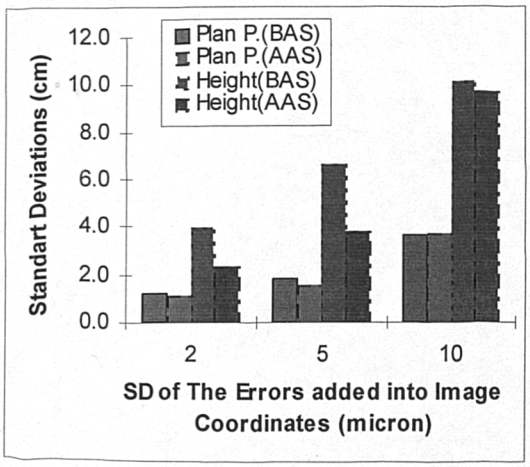

Figure (6.13)b r.m.s. errors in local coordinates of new ground points for the GPS phase observables with standard deviation of ±2 cm and using 2 ground control points.

	3 ground control points			2 ground control points		
σ_p (μm)	2	5	10	2	5	10
Plan (BAS)(cm)	1.09	1.50	2.62	1.21	1.79	3.61
Plan (AAS)(cm)	1.07	1.49	3.65	1.08	1.52	3.70
Height (BAS)(cm)	3.20	5.21	9.80	3.95	6.58	10.15
Height (AAS)(cm)	2.32	3.73	7.11	2.34	3.79	9.68

Table 6.12 r.m.s. errors in local coordinates of new ground points for the GPS phase observables with standard deviation of ±2 cm.

Figure (6.14)a and b and table 6.13 show graphical and numerical representation of the errors in the coordinates of new ground points for the phase noises of standard deviation of ± 5 cm according to the results before and after ambiguity fixing, when the combined system has 2 and 3 ground control points.

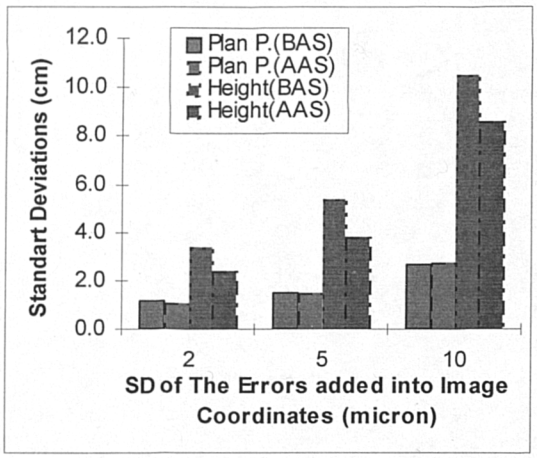

Figure (6.14)a r.m.s. errors in local coordinates of new ground points for the GPS phase observables with standard deviation of ±5 cm and using 3 ground control points.

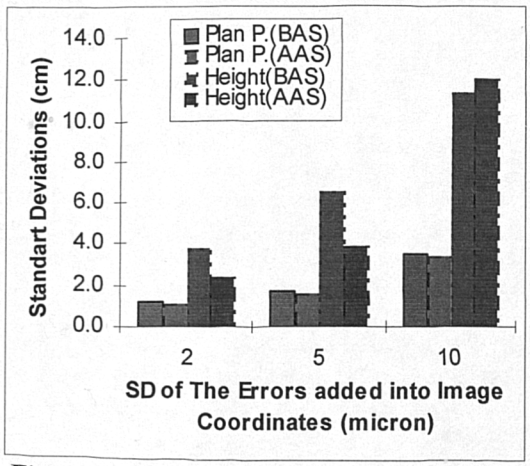

Figure (6.14)b r.m.s. errors in local coordinates of new ground points for the GPS phase observables with standard deviation of ±5 cm and using 2 ground control points.

	3 ground control points			2 ground control points		
σ_p (μm)	2	5	10	2	5	10
Plan (BAS)(cm)	1.12	1.50	2.63	1.17	1.72	3.46
Plan (AAS)(cm)	1.12	1.52	2.69	1.11	1.54	3.39
Height (BAS)(cm)	3.39	5.38	10.52	3.74	6.50	11.37
Height (AAS)(cm)	2.39	3.82	8.64	2.40	3.85	12.03

Table 6.13 r.m.s. errors in local coordinates of new ground points for the GPS phase observables with standard deviation of ±5 cm.

Figure (6.15)a and b and table 6.14 show graphical and numerical representation of the errors in the coordinates of new ground points for the phase noises of standard deviation of ± 10 cm according to the results before and after ambiguity fixing, when the combined system has 2 and 3 ground control points.

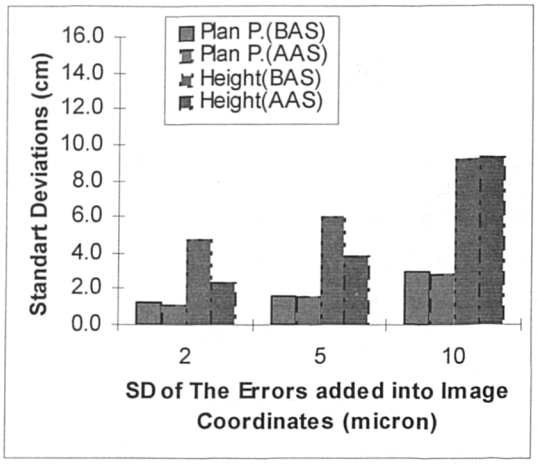

Figure (6.15)a r.m.s. errors in local coordinates of new ground points for the GPS phase observables with standard deviation of ±10 cm and using 3 ground control points.

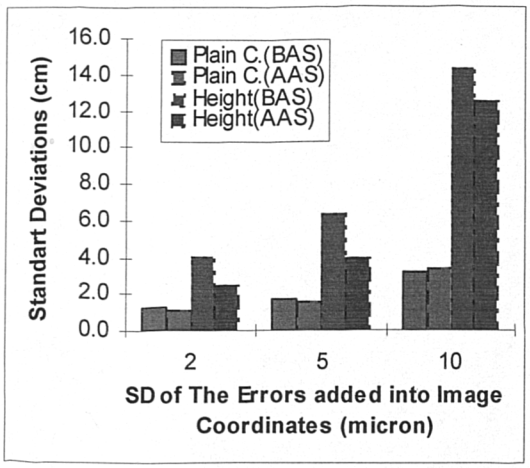

Figure (6.15)b r.m.s. errors in local coordinates of new ground points for the GPS phase observables with standard deviation of ±10 cm and using 2 ground control points.

	3 ground control points			2 ground control points		
σ_p (μm)	2	5	10	2	5	10
Plan (BAS)(cm)	1.27	1.61	2.94	1.18	1.67	3.17
Plan (AAS)(cm)	1.15	1.60	2.84	1.13	1.60	3.33
Height (BAS)(cm)	4.75	5.99	9.23	4.05	6.29	14.32
Height (AAS)(cm)	2.40	3.90	9.36	2.44	3.94	12.56

Table 6.14 r.m.s. errors in local coordinates of new ground points for the GPS phase observables with standard deviation of ±10 cm.

Table 6.15(a) represents the size of the errors in plan position and height of the ground points calculated from the outcomes delivered by the several runs of the combined system under the various different conditions, i.e. with the r.m.s. phase noises of ± 2 cm, ± 5 cm and ± 10 cm, the r.m.s. photo coordinate errors of ± 2 μm, ± 5 μm and ± 10 μm and 2-3 ground control points, according to several photo scales.

		Errors in plan position (cm)						Errors in height (cm)					
		3 ground control points			2 ground control points			3 ground control points			2 ground control points		
Photo scales	Phase noises (cm)	photo noise ±2 μm	photo noise ±5 μm	photo noise ±10μm	photo noise ±2 μm	photo noise ±5 μm	photo noise ±10μm	photo noise ±2 μm	photo noise ±5 μm	photo noise ±10μm	photo noise ±2 μm	photo noise ±5 μm	photo noise ±10μm
1: 2500	± 2	0.90	1.25	2.90	0.91	1.28	2.99	1.95	3.13	5.97	1.96	3.18	8.12
1: 2500	± 5	0.94	1.28	2.26	0.93	1.29	2.84	2.01	3.21	7.25	2.01	3.23	10.09
1: 2500	± 10	0.96	1.34	2.38	0.95	1.34	2.79	2.01	3.27	7.85	2.05	3.31	10.54
1: 5000	± 2	1.80	2.50	5.83	1.81	2.55	6.01	3.89	6.26	11.93	3.93	6.36	16.24
1: 5000	± 5	1.88	2.55	4.51	1.86	2.58	5.69	4.01	6.41	14.50	4.03	6.46	20.19
1: 5000	± 10	1.93	2.69	4.77	1.90	2.69	5.59	4.03	6.54	15.71	4.09	6.61	21.08
1: 10000	± 2	3.59	5.00	12.05	3.62	5.10	12.12	7.79	12.52	23.86	7.85	12.72	32.49
1: 10000	± 5	3.76	5.10	9.03	3.73	5.17	11.38	8.02	12.82	29.00	8.06	12.92	40.38
1: 10000	± 10	3.86	5.37	9.53	3.79	5.37	11.18	8.06	13.09	31.42	8.19	13.22	42.16
1: 25000	± 2	8.98	12.50	30.63	9.06	12.75	31.05	19.47	31.30	59.66	19.63	31.80	81.22
1: 25000	± 5	9.40	12.75	22.57	9.31	12.92	28.44	20.05	32.05	72.50	20.14	32.30	100.94
1: 25000	± 10	9.65	13.43	23.83	9.48	13.43	27.94	20.14	32.72	78.54	20.47	33.06	105.39
1: 50000	± 2	17.96	25.00	61.25	18.12	25.51	62.09	38.93	62.60	119.32	39.27	63.60	162.45
1: 50000	± 5	18.80	25.51	45.14	18.63	25.84	56.89	40.11	64.11	144.99	40.28	64.61	201.88
1: 50000	± 10	19.30	26.85	47.66	18.96	26.85	55.88	40.28	65.45	157.08	40.95	66.12	210.78

Table 6.15(a) r.m.s. errors in the coordinates of ground points at the selected scales

Table 6.15(b) shows r.m.s. errors in the plan position and the height of the camera perspective centres using camera lenses of 0.152 m, flying height of 450 m, the r.m.s. phase noises of ± 2 cm, ± 5 cm and ± 10 cm, the r.m.s photo coordinates errors of ± 2 μm, ± 5 μm and ± 10 μm and 2-3 ground control points.

	Errors in plan positions (cm)						Errors in height (cm)					
	3 ground control points			2 ground control points			3 ground control points			2 ground control points		
Phase noises (cm)	photo noise ±2μm	photo noise ±5μm	photo noise ±10μ	photo noise ±2μm	photo noise ±5μm	photo noise ±10μ	photo noise ±2μm	photo noise ±5μm	photo noise ±10μ	photo noise ±2μm	photo noise ±5μm	photo noise ±10μ
± 2	1.46	1.36	8.08	1.41	1.32	10.98	0.40	0.63	6.05	0.39	0.65	3.62
± 5	2.81	3.00	15.52	2.78	3.04	17.22	0.91	0.92	2.99	0.68	0.82	3.91
± 10	4.79	5.64	16.35	4.88	5.67	18.52	1.07	1.27	5.93	1.24	1.29	4.41

Table 6.15(b) r.m.s. errors in the coordinates of camera perspective centre

Figure (6.16)a through to (6.18)b and table 6.16, respectively, show graphical and numerical representations of largest marginally detectable errors in the coordinates of ground control points, camera perspective centre and new ground points using various size of errors in both photogrammetric and phase measurements according to the cases using 2 and 3 ground control points.

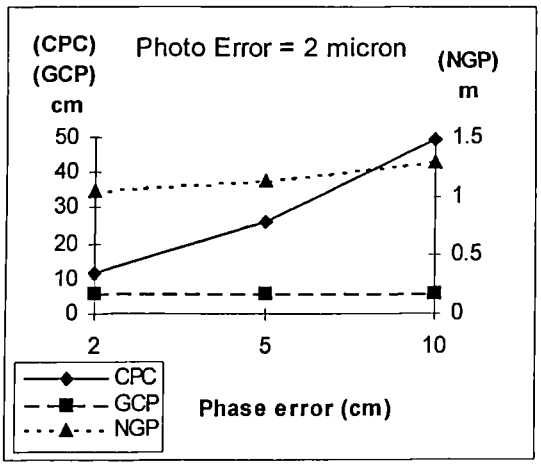

Figure (6.16)a Largest marginally detectable errors. In the case using 3 control points and r.m.s photo errors of ±2 micron.

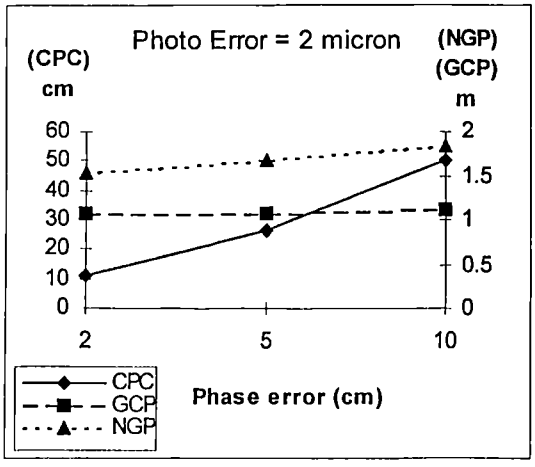

Figure (6.16)b Largest marginally detectable errors. In the case using 2 control points and r.m.s photo errors of ±2 micron.

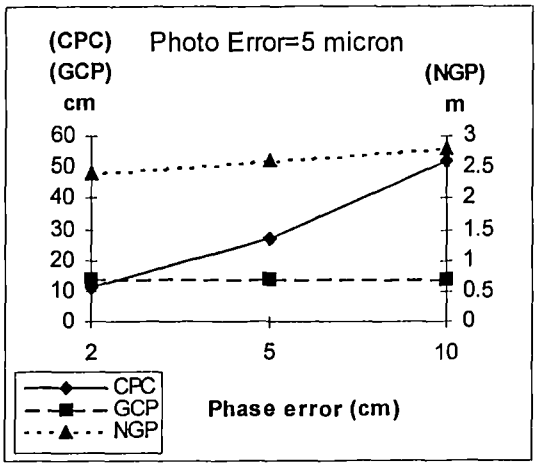

Figure (6.17)a Largest marginally detectable errors. In the case using 3 control points and r.m.s photo errors of ±5 micron.

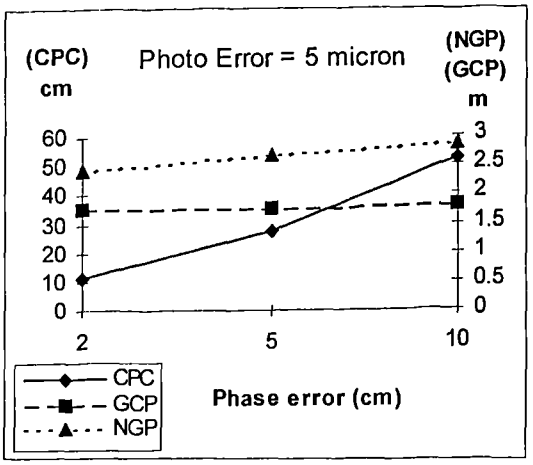

Figure (6.17)b Largest marginally detectable errors. In the case using 2 control points and r.m.s photo errors of ±5 micron.

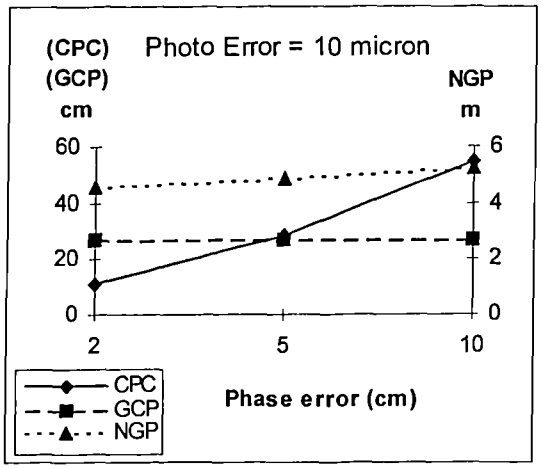

Figure (6.18)a Largest marginally detectable errors. In the case using 3 control points and r.m.s photo errors of ±10 micron.

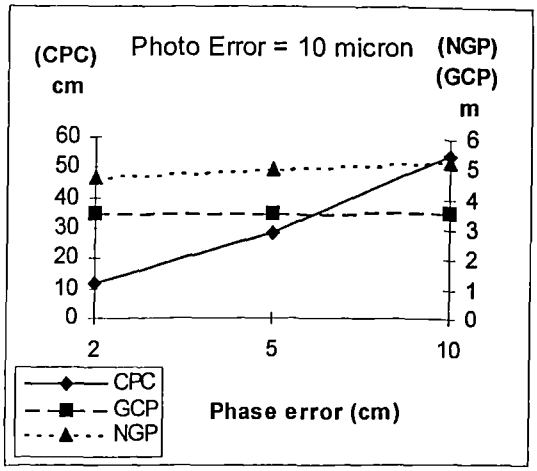

Figure (6.18)b Largest marginally detectable errors. In the case using 2 control points and r.m.s photo errors of ±10 micron.

		3 control points			2 control points		
photo noise (μm)	phase noise (cm)	Camera perspective center (cm)	Ground control points (cm)	New ground points (m)	Camera perspective center (cm)	Ground control points (m)	New ground points (m)
2	2	11.53	5.60	1.05	11.18	1.06	1.55
2	5	26.20	5.60	1.13	26.35	1.07	1.69
2	10	49.61	5.82	1.29	50.57	1.11	1.84
5	2	12.32	14.20	2.42	11.48	1.76	2.45
5	5	27.50	14.63	2.62	27.24	1.77	2.68
5	10	52.48	14.31	2.80	52.11	1.80	2.86
10	2	12.10	27.37	4.54	11.70	3.50	4.65
10	5	28.30	27.29	4.94	28.38	3.51	4.98
10	10	54.41	27.20	5.23	54.44	3.53	5.23

Table 6.16 Largest marginally detectable errors

6.2.5 Discussion of Results

From the graphs in figure (6.10)a and b and figure (6.11)a and b, a directly proportional relationship can be seen between the size of the errors in three local coordinates of camera perspective center and the precision of observed photo coordinates in both cases of 2 and 3 control points referring to the results after ambiguity fixing, where photo coordinates and phase observables are measured in precision of 2, 5 and 10 μm and 2 and 5 cm respectively. Comparing the results for 2 and 3 control points after ambiguity fixing, using 2 and 5 μm precision of photo coordinates and 2 and 5 cm precision of phase observables, quite good improvements are seen in the precision of each one of local coordinates of the camera perspective center. On the other hand, when the errors appeared in the mutually same coordinates are compared according to the both cases using 2 and 3 ground control points and the results after ambiguity fixing are considered, the relative differences between these coordinates, respectively, are 0.8 mm and 0.4 mm in the east, 0.3 mm and 0.2 mm in the north and 0.1 mm and 0.2 mm in the height regarding to the cases using photo coordinates of 2 and 5 μm precision with phase measurements of 2 cm precision. In the cases using photo coordinates of 10 μm precision, the differences become larger, i.e. 10 mm, 45.3 mm and 24.3 mm in east, north and height respectively. These small differences in the cases using photo coordinates of 2 and 5 μm precision put forward that the number of ground control points do not have any significant effect on the coordinates of camera perspective center, if the precision of photo coordinates are efficiently good (i.e. 2 or 5 μm). A slight increase is seen in the magnitude of the errors in the local coordinates of camera perspective center after ambiguity fixing, due to the phase measurements of 5 cm standard deviation rather than those in the case with 2 cm. Although the graphs in figure (6.11)a and b show an improvement in the coordinates of camera perspective center comparing the results before and after ambiguity fixing.

In the case of 3 control points with photo coordinates of 10 μm precision, the errors in the coordinates of exposure station are very large before ambiguity fixing. However, the results introduce some improvements in these coordinates after ambiguity fixing,

although they are not noteworthy improvements. The results for the case using 2 control points with the photo coordinates at the same size precision even show that there is some deterioration in the precision of all the coordinates of exposure stations when the outcomes before and after ambiguity fixing are compared.

As can be seen from figure (6.12)a and b, similar statements can also be made here as in the previous case. So, the results produced under the large phase noises with standard deviation of 10 cm, manifest a different pattern from the above. The size of the errors in the all coordinates become much larger. On the other hand, the results, especially after ambiguity fixing, demonstrate the acceptable sizes of the precision for all the three coordinates of exposure station in the cases using 2 and 5 μm precision of photo coordinates. Application of the errors of 10 μm standard deviation caused system failure while it is delivering ambiguities. The reason to this is the errors in the some coordinates of camera perspective center running over by half of the wavelengths of L1 and/or L2 phases.

If we review all the results in figures from figure (6.10)a to figure (6.12)b, it can be suggested that there is an increase in the sizes of the errors appeared in the coordinates of camera perspective center when the photo coordinates of 10 μm precision are used to test the system. This increase shows that size of the errors in both phase and photo measurements have a considerable effect on the precision of the coordinates of camera perspective center, especially on the plan positions (east and north), as final results regarding the combined system with additional ambiguity parameters. In a comparison with the other coordinates, the best improvements are seen in the height under the all conditions tested.

The results concerning the errors in the coordinates of ground points represented in figure (6.14)a through (6.16)b display a quite similar pattern for all the tested standard deviation of phase noises. The sizes of the errors appearing in the coordinates of ground points in the cases with different phase noises imply that the most sensitive coordinate to the changes in the precision of photo coordinates is the height. When the error sizes in the cases before and after ambiguity fixing are compared in term of

number of ground control points, it can easily be seen that the differences are slight for 2 μm and 5 μm precision of photo coordinates, but not for the 10 μm precision. The differences in the cases of 10 μm precision exhibit a dissimilar picture with those of the higher precisions. The divergences are respectively, for the photo coordinates of 2, 5 and 10 μm precision and for the phase observables of 2 cm precision,

- 1.2 mm, 2.9 mm and 9.9 mm in the plan and
- 7.5 mm, 13.7 mm and 0.5 mm in the height

before ambiguity fixing,

- 0.1 mm, 0.3 mm and 3.5 mm in the plan and
- 0.2 mm, 0.6 mm and 25.7 mm in the height

after ambiguity fixing, for the phase observables of 5 cm precision,

- 0.5 mm, 2.2 mm and 8.3 mm in the plan and
- 3.5 mm, 11.2 mm and 7.0 mm in the height

before ambiguity fixing and

- 0.1 mm, 0.2 mm and 8.5 mm in the plan and
- 0.1 mm, 0.3 mm and 33.9 mm in the height

after ambiguity fixing and for the phase observables of 10 cm precision,

- 0.9 mm, 0.6 mm and 2.3 mm in the plan and
- 7 mm, 3 mm and 4.9 mm in the height

before ambiguity fixing and

- 0.2 mm, 0.0 mm and 50.9 mm in the plan and
- 0.4 mm, 0.4 mm and 32.0 mm in the height

after ambiguity fixing. From these outcomes, it can be concluded that the number of ground control points does not have a noteworthy influence on the coordinates of ground points especially on the plan positions, unless the system is having large photo noises, e.g. 10 μm. Where the system is under large photo noises, the height of ground points starts to be worse, but not the plan position of these points. If we look carefully at the results produced for the photo coordinates of 10 μm precision, it is worthless to say that the same conclusion can be drown for the plan position produced in the all circumstances tested in this research as well. According to the outcomes describing the errors in the height and stated above that was calculated for the cases after ambiguity solution, it can be expressed that these differences, which are produced by comparing

the results for the both cases of 2 and 3 ground control points, are large. In addition to this, it is important to see that the differences between those differences for the cases before and after ambiguity fixing are also large, where the outcomes derived for the phase observations of 2 cm and 5 cm precision are taken into consideration. According to these last two statements, it can be suggested that the number of ground control points become an important issue affecting the precision of the height of ground points where the system was having large size of photo noise, i.e. 10 μm.

The another point to be mentioned here is that an improvement can clearly be seen in the height coordinate of ground points, but not in the plan position, considering the cases using the photo coordinates of 2 μm and 5 μm precision for all the three phase noises applied to the system where the results are compared for the cases before and after ambiguity fixing. Thus, it can be suggested that the noise in the phase observables does not show any significant effect on the plan position, though an improvement in the height is seen.

Despite the fact that the system shows a deterioration in the plan or in the height under some conditions in the cases using 10 μm photo noise. When the results are compared in terms of the number of ground control points used in the tests, it can be seen that the size of the errors in the height in the cases where 3 control points are used is relatively smaller than those in the cases where 2 control points are used, the errors in the plan position also show a deterioration even if they are small. This supports the suggestion for the necessity to improve the strength of the system where the system is having a large size of photo noise, i.e. 10 μm.

Phase noise does not have a strong influence on the plan positions of the ground coordinates. However a slight effect can be seen on the height, depending on how large phase noise the system is, and how many ground control points were used.

Comparing the results in table 6.15(a) in terms of relative tolerance and maximum tolerance for mapping in table 6.7(a), it can be seen that the errors in the plan position of the ground points meet the technical mapping specifications laid down under the all

conditions tested. Looking at the errors in the height of ground points produced the same conditions, it can be seen that they are also within the technical mapping specifications for all these circumstances tested if the maximum tolerances are taken into consideration. They are even within relative tolerances specified for mapping purposes when photo coordinates of 2 μm and 5 μm precision are used. Since the height of the ground points is affected more than the plan position by the errors in photo coordinates, the height needs a bit more attention to improve its precision. Then it can meet the mapping specifications in table 6.7(a). In connection with this, the system with the errors of ± 2 μm and ± 5 μm standard deviation in the photo coordinates gives reasonable precision for the height according to even relative tolerances of mapping specifications as well in the both cases using 2 and 3 ground control points.

As can be seen in table 6.15(c), the largest differences between the r.m.s. errors in the plan and height coordinates of camera perspective centre according to the number of ground control points used are respectively 0.5 mm and 2.3 mm, considering the cases using phase noises of ± 2 cm and ± 5 cm standard deviation for the errors of ± 2 μm and ± 5 μm standard deviation in photo coordinate. In the cases with photo coordinates of 10 μm precision and where 3 ground control points are used, the results for plan position are not good, they are even worse where 2 ground control points are used if they are examined in terms of all the phase noises tested in the research. The height exhibits a different style of the results than those in the plan position.

Looking at the results in the cases using photo coordinates of 2 μm and 5 μm precision, it can be seen that style of the errors are quite similar for the plan positions and the height, where the system is having the same phase noise. According to this outcome, it can be concluded that the precision of the coordinates of camera perspective centre are affected propotionally by the size of the errors in phase observables rather than the size of the errors in photo coordinates while the system that uses additional ambiguity parameters is having a good precision of photo coordinates, i.e. 2 μm or 5 μm. In general, the results for the height of camera perspective centre introduce a better precision than for the plan position in the cases using photo

coordinates of 2 μm and 5 μm precision where the phase noises are varying 2 cm to 10 cm. Thus, the conclusion that the precision of the height of camera perspective centre depends on precision of photo coordinates rather than the precision of phase observables in the combined system can also be drown here as in the previous tests. For the plan position of the camera perspective centre, in the contrary, it is other way around. Considering the results in the cases with 2 and 5 μm precision of photo coordinates using 2 and 5 cm precision of phase observables, all the errors appeared in the plan position and the height coordinate of camera perspective centre lie within the mapping specifications except those for the circumstances using large phase and photo noises.

If the outcomes for the largest marginally detectable errors in the previous test and in the test here of the combined system are compared in terms of the phase observables, the ground control points and the new ground points, except the results in the cases shown in figure (6.16)b, quite similar outcomes can be seen in Table 6.16 for all the conditions tested as they were presented in the previous test. The outcomes in the exceptional cases, i.e. for the photo coordinates of all three precisions using phase observables of 2 cm precision and 2 ground control points, also indicate parallel conclusions as those in the previous test, with only difference. So the difference appears in the size of the largest marginally detectable errors for ground control points and for new ground points too. Therefore, the same conclusions are valid for the new combined system with additional ambiguity parameters as well.

6.2.6 Summary

- Quite good improvements are seen in the precision of all local coordinates of camera perspective center with photo coordinates of 2 and 5 μm precision and phase observables of 2 and 5 cm precision for the cases after ambiguity fixing.
- The number of ground control points does not have any significant effect on the coordinates of camera perspective center, if the precision of photo coordinates are sufficiently good (i.e. 2 or 5 μm).

- The phase noise shows only a very tiny influence on the coordinates of camera perspective center for the case after ambiguity solution, when the system is having a large size of standard deviation of phase noises, i.e. 5 cm.
- If the errors in photo coordinates are large, the errors appearing in the local coordinates of exposure station also increase in the case that 3 control points are used. When 2 control points are used, the system starts to fail to deliver ambiguities.
- Even when the system has large phase noise, the precision of the local coordinates of camera perspective center is still acceptable with photo coordinates of 2 and 5 μm precisions, but not with 10 μm precision.
- The conclusion that the best improvements is in the height of camera perspective center for all the conditions tested becomes clear when the results are compared for the other coordinates.
- The errors appearing in the coordinates of ground points produced under various conditions with different phase noises indicate that the most sensitive coordinates to the changes in the precision of photo coordinates is the height.
- It can be expressed that the number of ground control points does not have any noteworthy influence on the coordinates of ground points especially on the plan positions, unless the system is having large photo noises, e.g. 10 μm. Where the system is under large photo noises, the height starts to be worse, but not the plan position of ground points.
- The number of ground control points, namely the strength of the system, becomes an important issue effecting the precision of the height of ground points where the system are having photo noises of large size, e.g. 10 μm.
- The noise in the phase observables does not show any significant effect on the plan position of ground points. In addition to this, an improvement in the height of ground points can also be seen.
- It is necessary to improve the strength of the system where the system has large photo noise, e.g. 10 μm.
- Phase noise does not have a strong influence on the plan positions of ground points. However a slight effect can be seen on the height, depending on how large phase noises the system is under and how many ground control points are used.

- The errors in the plan position of the ground points meet the technical mapping specifications, laid down, under all the conditions tested. The errors in the height are also within the technical mapping specifications for all these circumstances tested if the maximum tolerances are taken into consideration. The system with the errors of ± 2 μm and ± 5 μm standard deviation in the photo coordinates gives reasonable precision for the height according to the relative tolerances of mapping specifications as well in the both cases using 2 and 3 ground control points.
- It can be concluded that the precision of the coordinates of camera perspective centre are indirectly proportionally affected by the size of the errors in phase observables, rather than the size of the errors in photo coordinates while the system that uses additional ambiguity parameters has photo coordinates of good precision, e.g. 2 μm or 5 μm.
- In general, the results for the height of camera perspective centre introduce a better precision than those for the plan position with photo coordinates of 2 μm and 5 μm precision where the phase noise varies 2 cm to 10 cm. Thus, the precision of the height of camera perspective centre depends on the precision of measured photo coordinates rather than the precision of phase observables in the new combined system with additional unknowns. For the plan position of camera perspective centre is, on the contrary, the other way around.
- In the cases using photo coordinates of 2 μm and 5 μm precision for phase observables of 2 cm and 5 cm precision, all the errors appeared in the plan position and the height coordinate of camera perspective centre lie within the mapping specifications except those for the circumstances using large phase and photo noises.
- The outcomes for the largest marginally detectable errors in this test show a similar picture as in the previous test.

7. CHAPTER SEVEN

7.1 IDENTIFICATION OF CYCLE SLIPS AND PRECISION ANALYSIS OF THE SYSTEM

7.1.1 Test Objectives

The objectives of this test are

- to determine how big an effect cycle slips have on the parameters in the new combined system,
- to show that the combined system is capable of identifying, placing, solving and correcting cycle slips in GPS phase observables,
- after correcting cycle slips, to show the precision improvements in the parameters of new combined system and analyze them for mapping purposes.

7.1.2 Test Set-up

- One or two cycle slips in different sizes were added into the raw (and artificial) GPS phase observables.
- This adding process has been performed by choosing the candidate phases in both L1 and L2 at different epochs.
- The errors in the system for GPS phase observables and photo measurements were set up according to the normal conditions met on the aircraft, i.e. that have been constituted by using phase observables having noises of 2 cm standard deviation and photo coordinates having errors of 10 μm standard deviation.
- 3 ground control points were used.

7.1.3 Test Procedure

First, the random numbers generated for the errors were added to the phase and the photo measurements. In addition to this, one or two cycle slips of different sizes were put into the phase observables having the errors in the normal conditions, depending on what tests were being undertaken. Then the bundle estimation with GPS phase observables was run. At the end of first stage of the run, a statistical test has been used to identify the cycle slips and determine their sizes. Then the phase observables contaminated by cycle slips were corrected and the bundle adjustment was run once more to deliver the correct ambiguity parameters. Then, a final run with fixed ambiguities and cycle slips took place to analyze the final precision of the photogrammetric parameters. The same procedure was followed to analyze the precision of the parameters delivered by the system with different numbers of cycle slips of different sizes, in different epochs, in different type of phase observables, i.e. L1 and L2. Several runs were undertaken to produce the following as precision indicators:

- The root mean square errors of absolute plan positions and heights of camera perspective centers and new ground points.

7.1.4 Results of the test

The results in figure (7.1) and Table 7.1 are respectively graphical and numerical representations of the effect of a cycle slip of 2 cycles in extent in one L2 phase observable, which is in the third epoch, on the coordinates of camera perspective center in the cases before and after cycle slip detection and after ambiguity and cycle slip fixing (BCSD, ACSD and CSAwFA&CS).

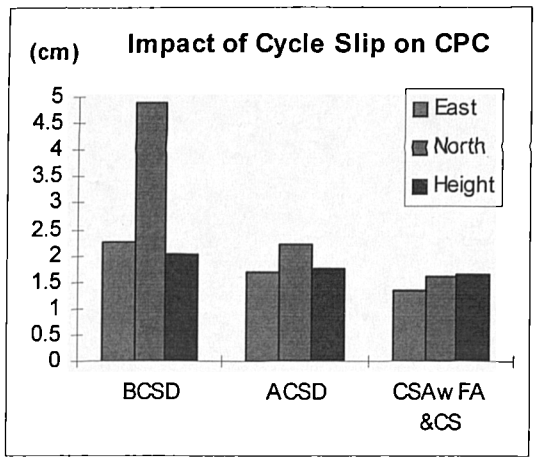

Figure (7.1) The effect of a cycle slip of 2 cycle in one L2 phase observable of the third epoch on the coordinates of camera perspective center

cm	*Before* cycle slip detection	After cycle slip detection	After cycle slip&amb. fixing
East	2.25	1.67	1.35
North	4.89	2.20	1.60
Height	2.02	1.75	1.65

Table 7.1

The results in figure (7.2) and Table 7.2 are respectively graphical and numerical representations of the effect of a cycle slip of 7 cycles in extent in one L2 phase observable, which is in the third epoch, on the coordinates of camera perspective centre before and after cycle slip detection and after ambiguity and cycle slip fixing.

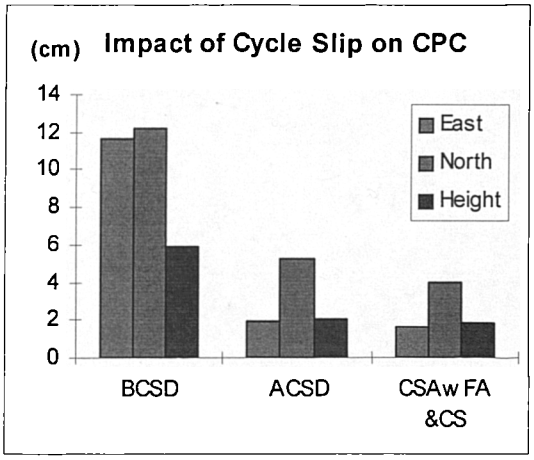

Figure (7.2) The effect of a cycle slip of 7 cycle in one L2 phase observable of the third epoch on the coordinates of camera perspective center

cm	Before cycle slip detection	After cycle slip detection	After cycle slip&amb. fixing
East	11.69	1.93	1.56
North	12.17	5.23	3.97
Height	5.88	2.04	1.81

Table 7.2

The results in figure (7.3) and Table 7.3 are respectively graphical and numerical representations of the effect of a cycle slip of 2 cycles in extent in one L1 phase observable, which is in the fourth epoch, on the coordinates of camera perspective center before and after cycle slip detection and after ambiguity and cycle slip fixing.

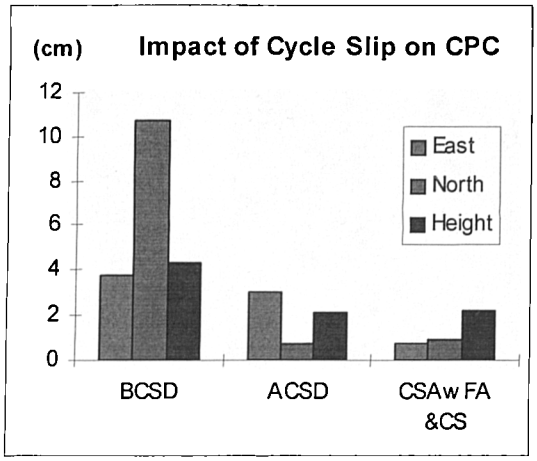

Figure (7.3) The effect of a cycle slip of 2 cycle in one L1 phase observable of the 4th epoch on the coordinates of camera perspective center

cm	Before cycle slip detection	After cycle slip detection	After cycle slip&amb. fixing
East	3.75	2.98	0.71
North	10.76	0.73	0.94
Height	4.27	2.10	2.23

Table 7.3

The results in figure (7.4) and Table 7.4 are respectively graphical and numerical representations of the effect of a cycle slip of 2 cycles in extent in one L1 phase observable, which is in the second epoch, on the coordinates of camera perspective center before and after cycle slip detection and after ambiguity and cycle slip fixing.

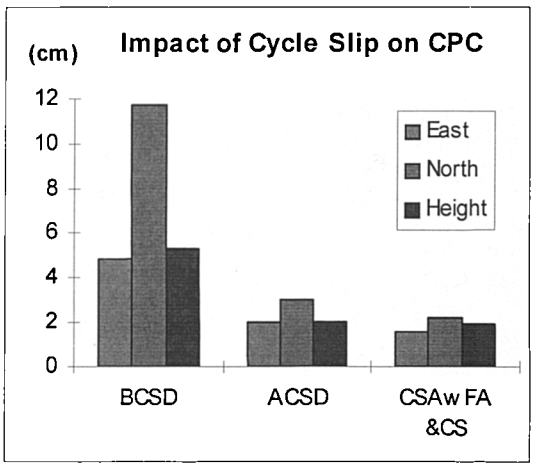

Figure (7.4) The effect of a cycle slip of 2 cycle in one L1 phase observable of the 2nd epoch on the coordinates of camera perspective center

cm	Before cycle slip detection	After cycle slip detection	After cycle slip&amb. fixing
East	4.85	2.01	1.60
North	11.77	2.99	2.22
Height	5.27	2.02	1.89

Table 7.4

The results in figure (7.5) and Table 7.5 are respectively graphical and numerical representations of the effect of a cycle slip of 2 cycles in extent in one L1 phase

observable, which was observed for the reference satellite in second epoch, on the coordinates of camera perspective center before and after cycle slip detection and after ambiguity and cycle slip fixing.

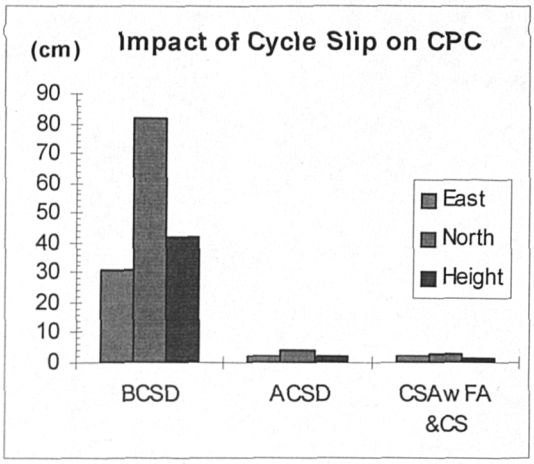

Figure (7.5) The effect of a cycle slip of 2 cycle in one L1 phase observable of the 2nd epoch on the coordinates of camera perspective center

cm	Before cycle slip detection	After cycle slip detection	After cycle slip&amb. fixing
East	30.60	2.39	1.94
North	81.49	4.17	2.88
Height	42.02	2.18	1.63

Table 7.5

The results in figure (7.6) and Table 7.6 are respectively graphical and numerical representations of the effect of a cycle slip of 2 cycles in extent in one L1 phase observable which was observed for the reference satellite in fourth epoch, on the coordinates of camera perspective center before and after cycle slip detection and after ambiguity and cycle slip fixing.

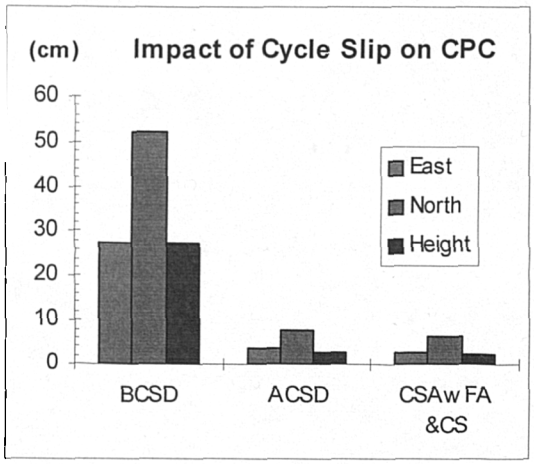

Figure (7.6) The effect of a cycle slip of 2 cycles in one L1 phase observable of the 4th epoch on the coordinates of camera perspective center

cm	Before cycle slip detection	After cycle slip detection	After cycle slip&amb. fixing
East	27.27	3.65	2.93
North	52.28	7.60	6.63
Height	27.57	2.55	2.07

Table 7.6

The results in figure (7.7) and Table 7.7 are respectively graphical and numerical representations of the effect of two cycle slips in two L1 phase observable, which are in the same epoch, on the coordinates of camera perspective center before and after cycle slip detection and after ambiguity and cycle slip fixing.

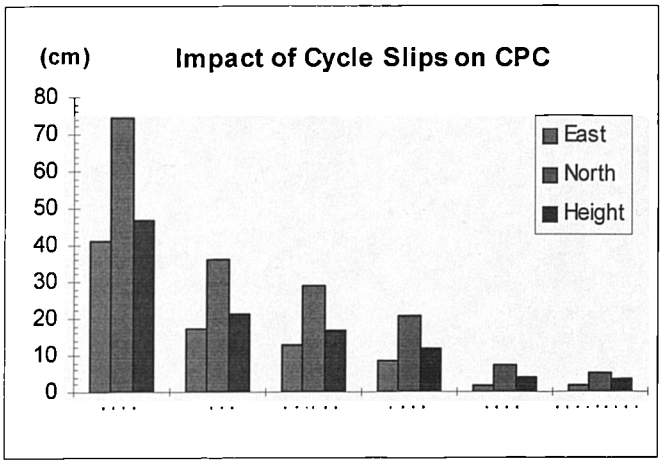

Figure (7.7) The effect of two cycle slips in two L1 phase observable on the coordinates of camera perspective centre

cm	Before cycle slips detection	Detection of first cycle slip	False detection of second cycle slip	Detection of second cycle slip	After cycle slips detection	After cycle slips&amb. fixing
East	41.15	17.17	12.74	8.53	1.65	1.47
North	74.69	35.88	28.71	20.45	7.01	5.27
Height	46.46	21.23	16.61	11.64	3.86	3.38

Table 7.7

The results in figure (7.8) and Table 7.8 are respectively graphical and numerical representations of the effect of two cycle slips in two L1 phase observable, which are in different epochs, on the coordinates of camera perspective center before and after cycle slip detection and after ambiguity and cycle slip fixing.

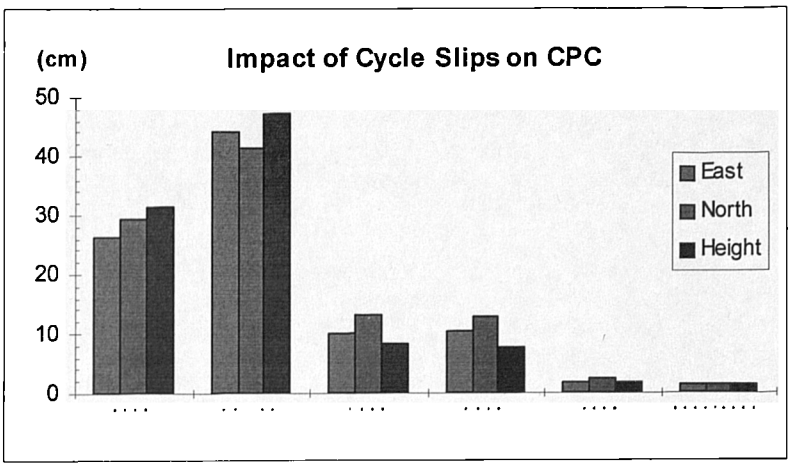

Figure (7.8) The effect of two cycle slips in two L1 phase observable on the coordinates of camera perspective center

cm	Before cycle slips detection	False detection of first cycle slip	Detection of first cycle slip	Detection of second cycle slip	After cycle slips detection	After cycle slips&amb. fixing
East	26.09	43.99	10.17	10.41	1.84	1.52
North	29.41	41.48	12.98	12.87	2.24	1.43
Height	31.49	47.13	8.24	7.56	1.85	1.26

Table 7.8

The results in figure (7.9) and Table 7.9 are respectively graphical and numerical representations of the effect of a cycle slip of 2 cycles in extent in one L2 phase observable, which is in the third epoch, on the coordinates of ground points before and after cycle slip detection and after ambiguity and cycle slip fixing.

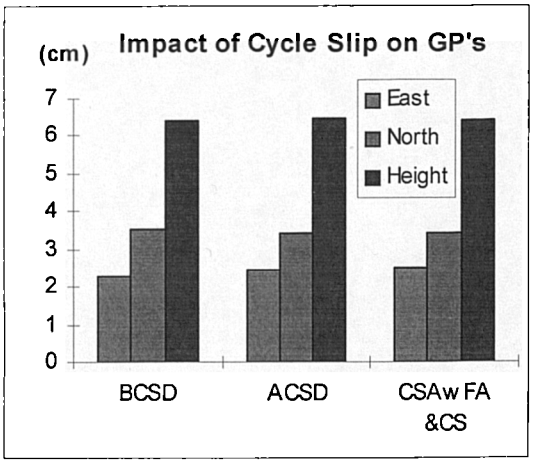

Figure (7.9) The effect of a cycle slip of 2 cycles in one L1 phase observable on the coordinates of ground points

cm	Before cycle slip detection	After cycle slip detection	After cycle slip&amb. fixing
East	2.28	2.42	2.51
North	3.54	3.42	3.40
Height	6.39	6.44	6.38

Table 7.9

The results in figure (7.10) and Table 7.10 are respectively graphical and numerical representations of the effect of a cycle slip of 7 cycles in extent in one L2 phase observable, which is in the third epoch, on the coordinates of ground points before and after cycle slip detection and after ambiguity and cycle slip fixing.

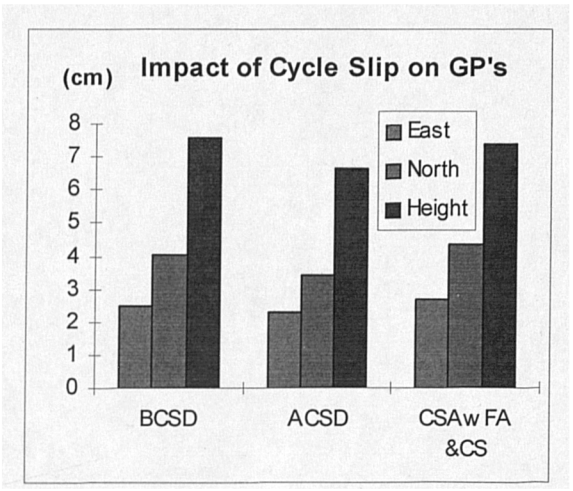

Figure (7.10) The effect of a cycle slip of 7 cycles in one L1 phase observable on the coordinates of ground points

cm	Before cycle slip detection	After cycle slip detection	After cycle slip&amb. fixing
East	2.46	2.31	2.65
North	4.05	3.40	4.36
Height	7.57	6.62	7.37

Table 7.10

The results in figure (7.11) and Table 7.11 are respectively graphical and numerical representations of the effect of a cycle slip of 2 cycles in extent in one L1 phase observable, which is in the fourth epoch, on the coordinates of ground points before and after cycle slip detection and after ambiguity and cycle slip fixing.

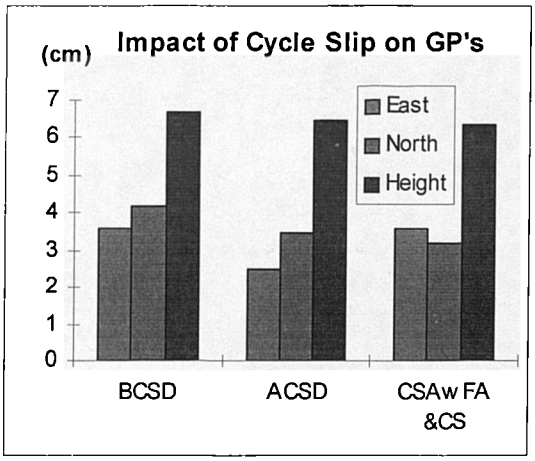

Figure (7.11) The effect of a cycle slip of 2 cycles in one L1 phase observable on the coordinates of ground points

cm	Before cycle slip detection	After cycle slip detection	After cycle slip&amb. fixing
East	3.57	2.47	3.59
North	4.19	3.49	3.21
Height	7.07	6.64	7.55

Table 7.11

The results in figure (7.12) and Table 7.12 are respectively graphical and numerical representations of the effect of a cycle slip of 2 cycle in extent in one L1 phase observable, which is in the second epoch, on the coordinates of ground points before and after cycle slip detection and after ambiguity and cycle slip fixing.

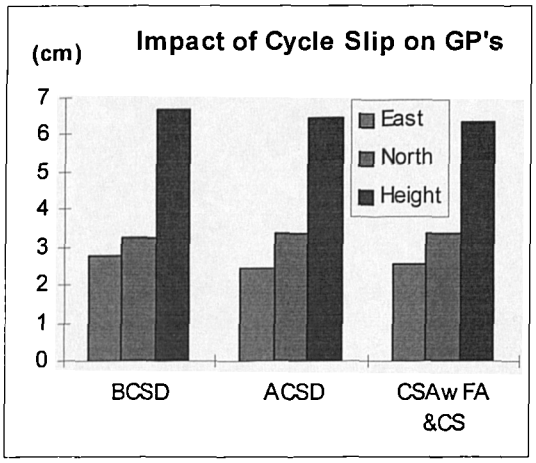

Figure (7.12) The effect of a cycle slip of 2 cycles in one L1 phase observable on the coordinates of ground points

cm	Before cycle slip detection	After cycle slip detection	After cycle slip&amb. fixing
East	2.76	2.45	2.54
North	3.26	3.39	3.37
Height	6.66	6.44	6.36

Table 7.12

The results in figure (7.13) and Table 7.13 are respectively graphical and numerical representations of the effect of a cycle slip of 2 cycles in extent in one L1 phase observable, which was observed for the reference satellite in the second epoch, on the coordinates of ground points before and after cycle slip detection and after ambiguity and cycle slip fixing.

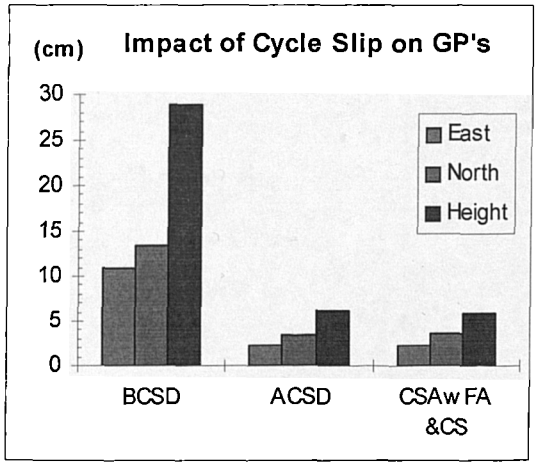

Figure (7.13) The effect of a cycle slip of 2 cycles in one L1 phase observable on the coordinates of ground points

cm	Before cycle slip detection	After cycle slip detection	After cycle slip&amb. fixing
East	10.92	2.35	2.38
North	13.47	3.45	3.54
Height	28.93	6.24	6.00

Table 7.13

The results in figure (7.14) and Table 7.14 are respectively graphical and numerical representations of the effect of a cycle slip of 2 cycles in extent in one L1 phase observable which was observed for the reference satellite in fourth epoch, on the coordinates of ground points before and after cycle slip detection and after ambiguity and cycle slip fixing.

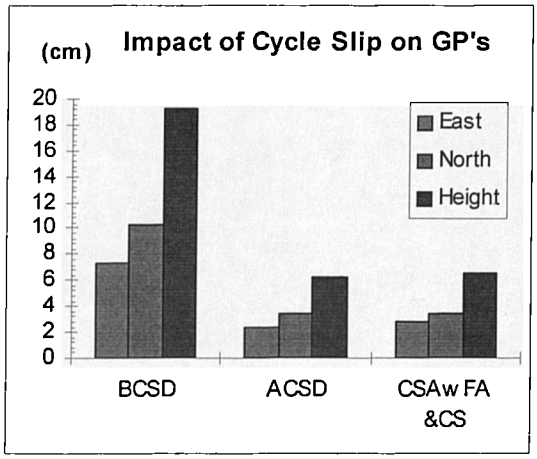

Figure (7.14) The effect of a cycle slip of 2 cycles in one L1 phase observable on the coordinates of ground points

cm	Before cycle slip detection	After cycle slip detection	After cycle slip&amb. fixing
East	7.24	2.35	2.74
North	10.22	3.34	3.42
Height	19.23	6.14	6.50

Table 7.14

The results in figure (7.15) and Table 7.15 are respectively graphical and numerical representations of the effect of two cycle slips in two L1 phase observable, which are in the same epoch, on the coordinates of ground points before and after cycle slip detection and after ambiguity and cycle slip fixing.

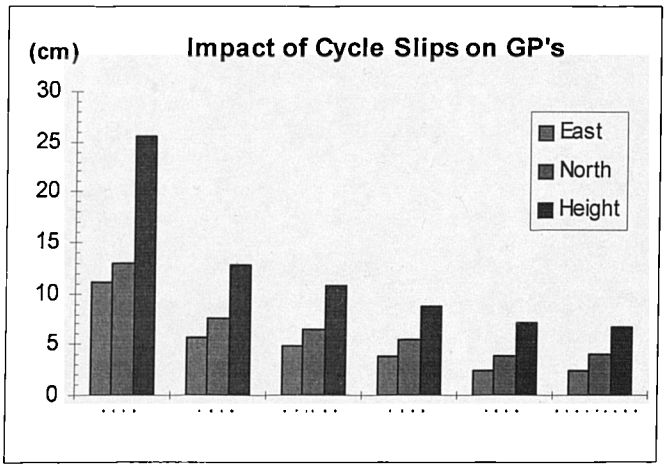

Figure (7.15) The effect of two cycle slips in two L1 phase observable on the coordinates of ground points

cm	Before cycle slips detection	Detection of first cycle slip	False detection of second cycle slip	Detection of second cycle slip	After cycle slips detection	After cycle slips&amb. fixing
East	11.20	5.76	4.81	3.79	2.34	2.47
North	12.94	7.40	6.45	5.41	3.88	4.06
Height	25.61	12.83	10.74	8.63	6.99	6.76

Table 7.15

The results in figure (7.16) and Table 7.16 are respectively graphical and numerical representations of the effect of two cycle slips in two L1 phase observable, which are in different epochs, on the coordinates of ground points before and after cycle slip detection and after ambiguity and cycle slip fixing.

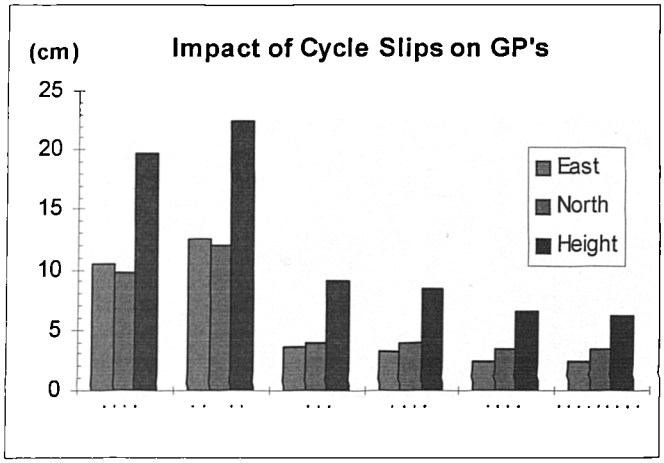

Figure (7.16) The effect of two cycle slips in two L1 phase observable on the coordinates of ground points

cm	Before cycle slips detection	False detection of first cycle slip	Detection of first cycle slip	Detection of second cycle slip	After cycle slips detection	After cycle slips&amb. fixing
East	10.37	12.53	3.64	3.19	2.44	2.44
North	9.78	12.07	3.87	3.86	3.42	3.49
Height	19.75	22.48	9.12	8.41	6.46	6.16

Table 7.16

Two cases where the system produced maximum errors in the coordinates of camera perspective center and ground points were chosen for precision analysis. Table 7.17 shows the coordinate precisions of camera perspective center and ground points for the

selected mapping scales. The cases arisen with the maximum errors are those involving the results in Tables 7.6 and 7.7 for camera perspective center and Tables 7.10 and 7.15 for ground points.

		Camera Perspective Center				Ground Points			
Scales		Plan Positions (cm)		Height (cm)		Plan Positions (cm)		Height (cm)	
Photo	Map	1.Case	2. Case	1.Case	2.Case	1.Case	2. Case	1.Case	2.Case
1:5000	1:2000	11.75	9.18	3.47	5.67	8.56	7.98	12.37	11.34
1:25000	1:10000	58.74	45.91	17.37	28.36	42.81	39.88	61.84	56.72
1:50000	1:20000	117.47	91.82	34.74	56.72	85.62	79.75	123.68	113.44

Table 7.17 r.m.s. errors in the coordinates of camera perspective centre and ground points at the selected scales

7.1.5 Discussion of Results

As will be seen from figure (7.1) and Table 7.1, the results before cycle slip detection show relatively larger errors in the coordinates of camera perspective center than those in the case after cycle slip detection. If we look at the results before cycle slip detection and after cycle slip fixing, it can be seen that the biggest improvement is in the north while the others, east and height, have smaller improvements. So, comparing the results before cycle slip detection and after cycle slip and ambiguity fixing, it will be seen that the improvements are 40% in the east, 67% in the north and 18% in the height. Actually the size of these errors is not worse than those after cycle slip detection, since the magnitude of the cycle slip is not large, namely 2 cycles. Figure (7.2) and Table 7.2 show the results for the case using a cycle slip in larger size than previous one, i.e. 7 cycles. The results also exhibit larger errors in the coordinates of camera perspective center before cycle slip detection relatively to those after cycle slip fixing. The errors after cycle slip fixing are quite reasonable and close to the errors in the previous case. Although it appears as if the size of the cycle slip directly effects the size of the errors appeared in the coordinate of camera perspective center when the results for both cases mentioned above are compared, it does not mean that. Cycle slips cause large errors in the coordinates of exposure station before cycle slip fixing. This is right. But, when the cycle slip is detected and fixed the size of the errors in the coordinates goes down to the sizes that are close to those in the case using smaller size of cycle slip. So, looking at the results after cycle slip and ambiguity fixing, it can be

noticed that the effect resulting from cycle slip on the east and on the height are almost cleaned up if it is fixed. But if we look at the errors in the north after cycle slip fixing, it seems that a piece of this effect remains in the north or the improvement in the north is less than those in the other coordinates. Graphs in the figures from figure (7.1) to (7.4) show that the most influenced one is the east from the cycle slip in large size in the case before cycle slip detection. The results before cycle slip detection in several cases represented in figures (7.2), (7.3) and (7.4) also demonstrate similar outcomes for the precision of the north and the height, no matter where the cycle slip is and how large the size of it is. The results after cycle slip and ambiguity fixing in figures (7.1), (7.2) and (7.4) exhibit quite similar outcomes for the precision of the east and the height and almost similar outcomes for the north. It can be concluded from the outcomes given above that the system is capable of solving the cycle slip, no matter which epoch it is in and how big it is.

If a cycle slip arises in the observation, that is to the reference satellite, in any epoch, this cycle slip would affect entire double difference observations in this particular epoch. If we look at figures (7.5) and (7.6), this effect can obviously be seen on the results representing the errors in the coordinates of camera perspective center before cycle slip and ambiguity fixing. The size of the errors in this case are quite larger than those in the other cases. After fixing the cycle slip, they drop down to the reasonable sizes, as can be seen from the figures. So, comparing the results before cycle slip detection and after cycle slip fixing in figures (7.5) and (7.6), the improvements are respectively 94% and 89% in the east, 95% and 87% in the north and 96% and 92% in the height. These results suggest that the system can correctly solve the cycle slip, even it is under the conditions as above.

Figures (7.7) and (7.8) and Table 7.7 and 7.8 show the results obtained for two different cases which are using 2 cycle slips in the same epoch and in different epochs. First three bars in figure (7.7) display the precision for the coordinates of camera perspective center before any cycle slip detection or correction. Their sizes are almost similar with those in the cases using one cycle slip. The second three bars show those after first cycle slip detection. The third three bars show those in the case with wrongly

placed second cycle slip, however first cycle slip was already fixed, and the fourth three bars represent those after the detection of second cycle slip. Then, the last three bars show the results after ambiguity and cycle slip fixing. Therefore, these last three bars display the final precision for the coordinates of camera perspective center delivered by the system while it is having 2 cycle slips in an epoch.

Figure (7.8) and Table 7.8 also show the results for a case similar to that given above, except that two cycle slips are being used in different epochs. As can be seen from the figure, second three bars display the precision for the coordinates of camera perspective center before any cycle slip detection and even, where the first cycle slip was wrongly placed, differing from the case stated above. In these both cases using 2 cycle slips, no matter they are in the same epoch or different, the final precision for the coordinates of camera perspective center are in acceptable sizes, after cycle slips were fixed. Thus, it is suggested that the system is also capable of solving cycle slips even if it has more than one, no matter where they are.

The figures from (7.9) to (7.12) show the precision results for the coordinates of ground points in the cases using one cycle slip, under the different conditions set up in this research. Comparing the results before cycle slip detection and after cycle slip fixing in the cases set up for different conditions as represented at these figures, it can clearly be seen that the errors in each individual coordinate of ground points are very close to each other. Comparing the results for the cases in the figures again, it can be noticed that the size of the errors in each coordinates of ground points are also very close to each other. If the results after cycle slip fixing in figures (7.13) and (7.14), which are for the cases using one cycle slip in the phase observation to the reference satellite, and those in the cases mentioned above are compared, it can be seen that the system produces very similar precision for the coordinates of ground points under every conditions tested for cycle slip detection in the research. If we look at the results before cycle slip detection, a large deterioration in the precision of the coordinates of ground points can be seen, which is opposite to those in the cases not using a cycle slip appeared in the phase observable to the reference satellite in an epoch. This deterioration is caused by the large errors in the coordinates of camera perspective

center. Because the cycle slip in the phase observable to the reference satellite affects not only this phase observation but also all the others in the epoch due to the structure of differential GPS (using double difference equations). So the source of these errors in the coordinates of camera perspective center is this sort of cycle slips. Considering the conclusions about precision of ground points so far, it can be suggested that cycle slips do have a significant influence in the precision of the coordinates of ground points in any case. However subsequent fixing of ambiguities does not lead to any improvement.

Figures (7.15) and (7.16) and Table 7.15 and 7.16 show the results for the cases using 2 cycle slips in the same epoch and in different epochs. The outcomes after cycle slip fixing in both figures exhibit similar precision for the coordinates of ground points. They are also very close to those in the previous cases. First three bars in figure (7.15) are for the precision of the coordinates of ground points before any cycle slip detection. So, in this case, it can be seen from the figure that the coordinate are having large errors. The sizes of these errors go down 50% after detection of first cycle slip, as will be seen from the second three bars in the figure. The third, fourth and fifth three bars respectively show the precision where the second cycle slip was wrongly placed, where second cycle slip are detected and then where after detecting and fixing the second cycle slip as well. The only difference between figures (7.16) and (7.15) is that first cycle slip has wrongly been placed in figure (7.15) instead of second one in figure (7.16). Looking at the precision for the coordinates of ground points after cycle slip and ambiguity fixing in all cases tested so far, it can be concluded that the cycle slips do not leave any significant remaining errors in the coordinates of ground points if they were detected and fixed. If they were able to be fixed, it means that their influences on the precision of ground points were removed in the all cases.

All the precision for the coordinates of camera perspective center and ground points after cycle slip fixing in Table 7.17 meet the whole maximum accuracy specifications for mapping at the selected scales if they are compared with the accuracies for the same purposes in Table 6.7(a). Looking at the precision after cycle slip fixing in Table 7.17 as final results in this test, it is seen that all of the precision for the plan position

and the height of both, camera perspective center and ground points meet maximum and relative or at least maximum accuracy specifications for mapping at selected scales.

7.1.6 Summary

For the cases having one cycle slip, following can be summarized:

- Looking at the results before cycle slip detection and after cycle slip fixing, it can be seen that the biggest improvement on the coordinates of camera perspective center is in the north while the others, east and height, have smaller improvements.
- The size of the errors in the coordinates of camera perspective center increases, depending on the size of the cycle slip in the case before cycle slip detection.
- When a cycle slip with large size is detected and fixed, the size of the errors in the coordinates of camera perspective center goes down until the sizes that are close to those in the case using smaller size of cycle slip. So, the effect resulting from cycle slip on the east and on the height of the camera perspective center is almost removed if it is fixed. But a piece of this effect remains in the north or the improvement in the north is less than those in the other coordinates.
- The most affected coordinate from a large cycle slip is the east.
- The results before cycle slip demonstrate similar outcomes for the precision of the north and the height, no matter where the cycle slip is and how large the size of it is.
- So, the results after cycle slip and ambiguity fixing exhibit quite similar outcomes for the precision of the east and the height and almost similar outcomes for the north under the various conditions.
- It can be concluded from the outcomes given previously that the system is capable of solving the cycle slip, no matter which epoch it is in and how big it is.
- The sizes of the errors in the case of a cycle slip in an observation to the reference satellite in any epoch are larger than those in the other cases. After fixing the cycle slip, they drop down to the reasonable sizes. So this means that the system can correctly solve for cycle slip, even under the above conditions.
- The errors in each individual coordinate of ground points are very close to each other in all the cases tested. It can be suggested that the system produces very

similar precision for the coordinates of ground points in every conditions tested for cycle slip detection.

- The large deterioration in the precision of the coordinates of ground points before cycle slip detection is caused by the large errors in the coordinates of camera perspective center.
- Cycle slips do also significantly influence the precision of the coordinates of ground points.

For the cases having two cycle slips, the following can be given as summary:

- When the system has 2 cycle slips at the same time, no matter where they are in the same epoch or different, the precision for the coordinates of camera perspective center are in acceptable sizes after cycle slips were fixed. Thus, it is suggested that the system is also capable of solving cycle slips even if it is having more than one, no matter where they are.
- The precision after cycle slip fixing in the cases having 2 cycle slips exhibit similar precision for the coordinates of ground points. They are also very close to those in the cases using one cycle slip.

In general:

- It can be concluded that cycle slips do not leave any significant remaining errors in the coordinates of ground points if they were detected and fixed.
- All of the precision for the plan position and the height of both, camera perspective center and ground points meet maximum and relative or at least maximum accuracy specifications for mapping at selected scales.

CHAPTER EIGHT

8. CONCLUSIONS AND SUGGESTIONS FOR FURTHER WORK

This thesis has been concentrated on the development of the algorithms and a research software necessary to perform the combination of GPS dual frequency phase observations and photogrammetric coordinates in observation space, being different than the recent adopted approaches which combine photogrammetric coordinates of image points with the camera perspective center coordinates derived from GPS.

The key results from this work is a demonstration that the combination of GPS and photogrammetry in observation space is fully capable of yielding a correct solution. The coordinates of the ground points and camera stations are recoverable, as are values for the GPS integer ambiguities, and any cycle slips can be detected and repaired. This is an important conclusion because the viability of the method has never been shown before. If the method can be adopted in practice it could potentially result in less expensive and faster photogrammetric surveys - mainly because the need to fly and measure cross strips to control GPS drift errors will be eliminated. It is also possible that the method could lead to higher quality results as more sophisticated data cleaning procedures could be adopted and small GPS errors (due to multipath) could be eliminated (the photogrammety increases the redundancy).

The following specific conclusions may also be drawn:

- An algorithm, that estimates the position and the attitude of the camera at each exposure and the coordinates of the object points, recovers the correct integer ambiguities and identifies and then compensates cycle slips by using the bundle adjustment combining dual frequency GPS phase observations and photogrammetric coordinates in observation space has been developed. Since the processing involves all the parameters above there is no need to add drift parameters to the estimation process to cover the shifts in the coordinates of camera perspective centers.

- The method effectively computes the baseline components between a stationary receiver with known coordinates and a moving receiver with unknown coordinates under the normal conditions. This baseline must be less than twenty kilometers, since beyond this distance the ionosphere becomes a significant part of the GPS error budget (Leick, 1995). The trails have shown that the new method can give positional accuracies of 11 mm and 13 mm (95th percentile) in the horizontal and 23 mm and 25 mm (95th percentile) in the vertical for an about 600 meter baseline using 6 satellites and 3 and 2 control points respectively.

- Considering that the multipath is one of the limiting factors on the achievable accuracy with the GPS-aerotriangulation, the results of 13 mm and 11 mm r.m.s errors in plan and 25 mm and 23 mm r.m.s errors in height for exposure stations and 34 mm and 31 mm r.m.s errors in plan and 69 mm and 65 mm in height for object points in strips that use 2 and 3 ground control points respectively have been achieved. This was with dual frequency phase data with errors of 2 cm standard deviation which describes the most severe multipath, together with noise, to be experienced and photogrammetric data with the errors of 10 μm standard deviation, and indicates that the new combined system may produce good results even under severe multipath conditions. This circumstance may also be accepted as a normal condition, that the new system challenges, referring to the results in figure 5.5 and table 5.4.

- Although the noise in GPS observations is described as a limiting factor by the research and the approximate position of the used antenna is described as another requirement in the earlier researches on GPS-aerotriangulation, since the approximate values for the ambiguities have been taken as zero in this research the size of the noise in the phase measurements caused by multipath and by the used receiver for short baselines is not a limitative factor on the solution of the correct ambiguity and the correct coordinate of the antenna onboard the aircraft.

- In the first test, the final results for the camera perspective center local coordinates show that the combined system is capable of solving the ambiguities. Then, since the ambiguities are correctly delivered, it also provides coordinates with good precision for camera perspective centers under the circumstances which have been described as normal in this research.

- Comparing the results in first test carried out for control points with different numbers, it can be stated that the number of ground control points does not have a strong influence on camera perspective center coordinates.

- According to the comparison of the results for the different number of ground control points in the third test, the differences, which are 3 mm, 1.4 mm and 0.0 mm in plan position and 4.5 mm, 1.4 mm and 0.5 mm in height for the GPS phase noise of standard deviation of ± 2 cm, 4.1 mm, 1.6 mm and 1.5 mm in plan position and 3.8 mm, 0.9 mm and 15.2 mm in height for the GPS phase noise of standard deviation of ± 5 cm and 8 mm, 8.2 mm and 0.2 mm in plan position and 1.8 mm, 6.6 mm and 2.4 mm in height for the GPS phase noise of standard deviation of ± 10 cm in the cases of the r.m.s errors of ± 10 μm, ± 5 μm and ± 2 μm in photo coordinates respectively, indicate that the number of ground control points does not have a strong influence on the quality of the coordinates of new ground points, in the new combined system. In addition the number of ground control points affecting the correct ambiguity solution does not also have a strong influence on the coordinates of the exposure stations and ground points. Having quite good coordinates of these points at the end of the adjustment process, even if one ambiguity were wrongly estimated by one or two cycles since the other correctly solved ambiguities help the model to produce good results for these coordinates shows that the ground control points are not strictly necessary in bundle estimation if GPS phase observations are available. This is also confirmed by the results of reliability analysis for new ground points, ground control points and double difference phase observations. Because the reliability of ground control points is worse than that of GPS double difference observations. The results using different numbers of ground control points in the third test confirms this statement as well. At least two control points were necessarily used in the tests carried out during the entire research since such a small sample which consists of one strip with four photographs and GPS phase data from only four epochs with weak geometry were used. With only one strip of four photos and epochs, GPS help only comes on to the strip center line with weak geometry. So that the model constituted by such a sample could not find any point to base on the orthogonal direction to the strip line unless there are sufficient number of ground control points. This explains why at least two ground control points were necessarily used in all the tests.

- Looking at figure 5.5 and 5.6, when either photogrammetry or GPS have large errors, the other one takes care of improving the coordinates of camera perspective centre and improve their precision unless it also has large errors. This also means

that it is a necessity for the combined system to work well for either photogrammetric or GPS measurements to be carried out precisely if the other one has any large errors. In the whole system, reliability and error analysis show that the precision of the camera perspective centres obtained from the new combined bundle estimation depends mostly on the noise size in the GPS phase observations, however the magnitude of the errors in the photo coordinates is the major factor describing and affecting the size of the errors appearing in the coordinates of ground points.

- The error analysis for the positions of new ground points in the third test show that the measurement precision is the most important factor affecting the precision of the position of these points, and have a directly proportional influence on position precision of the camera perspective centers.

- According to the comparison of the results using a GPS phase noise of ± 10 cm, ± 5 cm and ± 2 cm, as the largest differences between these results are 9.1 mm, 5.0 mm and 8.8 mm in height and 8.0 mm, 5.0 mm and 1.2 mm in plan position for the cases of 2 ground control points and 2.8 mm, 2.1 mm and 14.3 mm in height and 0.6 mm, 0.9 mm and 1.2 mm in plan position for the cases of 3 ground control points for the r.m.s errors in photo coordinates of ± 10 μm, ± 5 μm and ± 2 μm respectively, it has been found that the variations in the size of GPS phase noises do not show a significant effect on the coordinates of new ground points.

- On the one hand, looking at the results in the table 6.8 it can clearly be implied that the only dominant factor is measurement precision of the phase observations on the reliability of camera perspective centre derived by the means of new estimation model if the very slight influence of the photo noise is ignored, especially where the system has large phase noise. On the other hand, if the precision of photogrammetric measurements is good, ± 2 μm standard deviation or better, photogrammetry takes care of solving the correct coordinates of the exposure stations. Phase noises do not exhibit any significant effect on the reliability in this circumstance. When the size of photogrammetric noise gets larger, the phase noise in the system becomes effective on the reliability and even the precision of these points. Besides these, the factor showing a strong effect on the reliability of new ground points is the precision of the photo coordinates. Therefore using diapositives and modern analytical instruments will increase the reliability of the system, the precision of the products of the new system and the system quality for

solving the ambiguities and identifying the cycle slips. Since measurement precision of these points are directly effective on obtaining of these quantities.

- Comparing the results represented in table 6.7(b) and 6.7(c) with the mapping specifications in table 6.7(a) the precision of the coordinates of ground points and the coordinates of the camera perspective center derived from the new combined GPS-aerotriangulation estimation meets the maximum tolerances given as mapping specifications for all scales under the tested conditions. This precision also lies within the relative tolerances as mapping specifications except those derived whilst under some extreme conditions, i.e. with the photogrammetric error of 10 μm in the case of phase noise of 10 cm using 2 ground control points for plan position of ground points and with the photogrammetric error of 10 μm in the case of all phase noises tested using 2 and 3 ground control points for height of ground points and with the phase noise of 10 cm in the cases of all photogrammetric errors tested using 2 and 3 ground control points for the plan positions of camera perspective centers (this last one can be ignored because it is an extreme case).

- During practical photography, some satellites will come into view or vanish from view. So if some satellites come into view, they will introduce new ambiguities to be solved for in the new combined bundle estimation. The results derived from the test set up to examine such circumstances show in general that no matter how many ground control points are used, accuracies of the coordinates of camera perspective centers and the ground points meet the maximum and the relative tolerances as mapping specifications for all the scales represented in table 6.7(a) under the all circumstances tested even with large phase noises, e.g. 10 cm, except those whilst photogrammetric coordinates have large measurement error with standard deviation of 10 μm. This represents an encouraging capacity of the new system, despite the fact that the used sample is very small. It can also be seen from these results that the system also produces coordinates with sufficient precision for these points for all the conditions tested, even for the exceptional one, where the maximum tolerances for the mapping specifications are taken into consideration.

- In addition to the above, it can be concluded that the number of ground control points does not have any noteworthy influence on the coordinates of ground points especially on their plan positions, unless the system has large photo noise, e.g. 10 μm. Where the system has large photo noise, the height starts to degrade, but not the plan position of ground points. The number of ground control points, namely

the strength of the system, then become an important issue affecting the precision of the height of ground points. Therefore it can be suggested that the use of precise instruments as analytical plotters whilst measuring photo coordinates and as CCD cameras whilst taking photographs shored overcome the high precision problem required for photogrammetric measurements by the system which has extra unknown parameters, i.e. new ambiguities to be solved for the new satellites in view.

- Comparing and analyzing the results produced for the cases before and after cycle slip detection in the test set up to examine the case with cycle slips, it can be said that if the size of the cycle slip in the phase observation is small, the improvements in the coordinates of camera perspective center are small as well. If it is large, much bigger improvements can then be seen in these coordinates. From this point of view, it can be concluded that firstly the new system is capable of detecting and fixing the cycle slips, and secondly the sizes of the errors in the coordinates of the camera perspective center before cycle slip detection increase directly proportional with regard to the size of the cycle slip. But it can also be stated that no matter how big or small cycle slip the new system has and where it is, the system produces good results since these coordinates have similar residual errors after cycle slip fixing even in both cases. Although, the size of the errors in these coordinates in the case using a cycle slip in the observation to the base satellite in any epoch are quite larger than those in the other cases before cycle slip detection. After fixing the cycle slip, they drop down to the reasonable sizes. So this means that the system can correctly solve for cycle slips, even if it is under the conditions as above, and produce coordinates with sufficient precision for camera perspective centers and ground points under the normal conditions, i.e. as described earlier with phase noise of 2 cm standard deviation and photogrammetric errors of 10 μm standard deviation.

- Similar conclusions can be given for the accuracy of ground points after cycle slip fixing, however they have large size of errors before cycle slip fixing, not directly because of the cycle slip but also the deterioration in the camera perspective center coordinates caused by the cycle slip.

- When the system has 2 cycle slips, no matter if they are at the same epoch or different, the precision for the coordinates of camera perspective center are of acceptable sizes after cycle slips have been fixed. Thus, it is suggested that the system is also capable of solving cycle slips even if there are more than one. The

accuracies for the coordinates of ground points after cycle slip fixing exhibit similar results with those using one cycle slip.

- It can be concluded that cycle slips do not leave any significant remaining errors in the coordinates of ground points if they were detected and fixed. Also, the plan position and the height of both, camera perspective center and ground points meet maximum and relative accuracy specifications for mapping at selected scales or at least maximum accuracy specifications for mapping if the image coordinates can be obtained with 5 micron precision or better.

- Using the new combination method, there is no necessity to solve for the initial ambiguities before kinematic positioning starts, as these ambiguities are solved for in the estimation process simultaneously together with the other parameters in the combined system.

- If the target of the aerial-triangulation is to obtain the camera perspective center positions, the new combined system can produce these positions with sufficient precision to meet the mapping specification for any scales even under the conditions with multipath for GPS and with measurement precision of worse than 20 micron for image coordinates in photogrammetry. If the aim is to produce precise ground points, the observations in both system must be obtained precisely, especially the image coordinates.

The new system combining GPS and photogrammetric measurements in observation space is capable of overcoming of the redundancy problem which has generally been experienced in the early research, and provides for the determination of integer ambiguities thereby saving a lot of effort and time. As a result of the new combined GPS-aerotriangulation, it can be concluded that the system therefore provides a two-way benefit. The first is for photogrammetrists who can benefit from the use of GPS products thereby solving the ground control problem and the second is for the users of the GPS who can benefit from the large number of photogrammetric measurements thereby solving the redundancy problem for point coordinates determination. Therefore a simultaneous solution is possible.

The used model in these tests for the new combined GPS-aerial triangulation bundle estimation is a simplified one in which it is assumed that the aerial camera is operated in a strapped-down mode, all known systematic errors in both GPS and

photogrammetry has been removed or modeled well and observations as the image coordinates of points observed are not correlated within themselves or with the other observation data sets, i.e. the available coordinates of ground points and the GPS phase observations, except the GPS phase observations of the same frequency in the same epoch. Considering the statements above, and the work already done, further work should be carried out along the following lines.

- Enabling the camera in strapped-down mode means that the components of the eccentricity vector between the camera perspective center and the antenna onboard the aircraft to be resolved into three components are parallel to the camera axes in the camera coordinate system. If the camera is let to rotate freely, then the components of the eccentricity vector will no longer be constant with respect to the camera coordinate system. This has to be modeled taking into consideration the relative rotations between the camera coordinate system and the local coordinate system. This point is worth considering in future work which might lead to an understanding of which mode is appropriate under given circumstances and requirements. These eccentricity vector components can also be resolved in the new combined GPS-aerial triangulation bundle estimation process by introducing them into the adjustment as new unknown parameters to estimate since the redundancy of the model for new system is sufficient.

- Attitude determination of the camera is one of the major research area in aerial triangulation. There are several research carried out using different methods and instruments. The recent one employs the GPS to determine this attitude using several GPS antennas onboard the aircraft. Then it provides reasonably accurate camera attitude, after post-processing the data collected during a photogrammetric mission. In order for precise point coordinate determination using analytical aerial triangulation, the new combined GPS-aerotriangulation bundle estimation functional model can be expanded to incorporate this attitude information as additional observations. Then the reliability expected from such a system with additional observations and precision of the estimated coordinates of new ground points will possibly increase. This could only be confirmed by the tests which may also reveal that the amount of money and time spent on the computational task involved in determination of these parameters is actually worthwhile compared with the improvement in system reliability and precision of estimated coordinates of new ground points.

- So far, the tests carried out are based on a strip with photogrammetric data of four photographs and with GPS data of four epochs. Therefore the new system has to be tested for samples with data in practice. More tests are also required examining the different block sizes experienced in the practice in order to provide a sufficient confidence for the system and to obtain more knowledge on the reliability of the system.

- The order of GPS phase noises that the new system allows while photogrammetric noises are small, i.e. 3 microns or better than this size of error, might encourage researchers to study the new system for long baselines.

- As the use of more than one antenna onboard the aircraft will increase the redundancy of the new combined model this will give a chance to introduce and to resolve some new unknowns, e.g. the offset components between camera perspective center and the antennas on the wings at each exposures. Although the model would become much more sophisticated than the one used.

- In the strap-down mode, the use of two antennas on the one wing, i.e. one at the end of the wing and the other one on the half way of the same wing might help to model or to resolve the error caused by the vibration or/and the flexibility of the wing. Once this is achieved the new system produces more precise results and becomes more reliable while the wing antennas are used for any reason. There is also no need to keep camera in strap-down mode. Since the camera orientation elements are solved for in the estimation process of the new system independently from the aircraft attitude.

8.1 SUMMARY

- An algorithms and a research software to perform these algorithms have been developed to combine GPS dual frequency phase observations and photogrammetric coordinates in observation space.
- The combination of GPS and photogrammetry in observation space is fully capable of yielding a correct solution.
- The coordinates of the ground points and camera stations are simultaneously recoverable, as are values for the GPS integer ambiguities, and any cycle slips can be detected and repaired by the new combined estimation method.

- The need to fly and measure cross strips to control GPS drift errors can be eliminated.
- The size of the noise in the phase measurements caused by multipath and by the used receiver for short baselines is not a limitative factor on the solution of the correct ambiguity and the correct coordinate of the antenna onboard the aircraft.
- The tests carried out for control points with different numbers show that the number of ground control points does not have a strong influence on the coordinates of camera perspective centers and ground points.
- It can also be stated that even if one ambiguity were wrongly estimated by one or two cycles since the other correctly solved ambiguities help the model to produce good results for these coordinates shows that the ground control points are not strictly necessary in bundle estimation if GPS phase observations are available.
- When either photogrammetry or GPS have large errors, the other one takes care of improving the coordinates of camera perspective centre and improve their precision unless it also has large errors.
- It is a necessity for the combined system to work well for either photogrammetric or GPS measurements to be carried out precisely if the other one has any large errors.
- The precision of the camera perspective centres obtained from the new combined bundle estimation depends mostly on the noise size in the GPS phase observations, however the magnitude of the errors in the photo coordinates is the major factor describing and affecting the size of the errors appearing in the coordinates of ground points.
- The variations in the size of GPS phase noises do not show a significant effect on the coordinates of new ground points.
- The factor showing a strong effect on the reliability of new ground points is the precision of the photo coordinates.

- No matter how big or small cycle slip the new system has and where it is, the system is capable of detecting and fixing the cycle slips and produces good results for exposure stations and ground points.

REFERENCES AND BIBLIOGRAPHY

Abidin HZ (1993) *Computational and Geometrical Aspects of On-The-Fly Ambiguity Resolution,* Ph.D. dissertation, Department of Surveying Engineering Technical Report No. 164, University of Newbrunswick, 314 pp

Ackermann F (1990) *Kinematic GPS camera positioning for aerial triangulation,* Proceedings of the Second International Symposium on Precise Positioning with the GPS, Ottowa, 13 pp

Ackermann F (1992a) *Kinematic GPS control for photogrammetry,* Photogrammetric Record, Vol. 14(80), pp 261-276

Ackermann F (1992b) *Prospects of kinematic GPS for aerial triangulation,* ITC Journal 1992-4, 13 pp

Ackermann F and Schade H (1993) *Application of GPS for aerial triangulation,* Photogrammetric Engineering and Remote Sensing, Vol 59(11), 8 pp

Ackermann F (1994) *Practical experience with GPS supported aerial triangulation,* Photogrammetric Record, Vol. 14(84), pp 861-874

Alobaida A (1993) *Design and simulation of a real time mapping satellite for the Kingdom of Saudi Arabia,* Dept. of Geodetic Science and Surveying, The Ohio State University, Ph.D. Dissertation

Amer F (1978) *Adjustment of aerial triangulation,* Institute of Aerial Survey and Earth Science (ITC) Lecture Notes, Enschede

Andersen O (1989) *Experiences with kinematic GPS during aerial photography in Norway,* 42nd Photogrammetric Week, Stuttgart

Becker RD and Barriere JP (1993) *Airborne GPS for photo navigation and photogrammetry: An integrated approach,* Photogrammetric Engineering & Remote Sensing, Vol. 59, No. 11, pp 1659-1665

Beutler G (1992) *The 1992 activities of the International GPS Geodynamics Service (IGS),* Geodesy and Physics of the Earth, IAG Symposium No. 112, Potsdam, Germany, 5-10 October

Blankenberg LE (1993) *GPS-supported aerial triangulation - state of art,* The Photogrammetric Journal of Finland, 13(1), pp 4-16

Blewitt G (1989) *Carrier phase ambiguity resolution for the global positioning system applied to geodetic baselines up to 2000 km,* Journal of Geophysical Research, 94B, pp 10187-10203

Bock Y, Gourewitch SA, Counselman CC, King RW, and Abbot RI (1986) *Interferometric analysis of GPS phase observations,* Manuscripta Geodetica, Vol. 11, No. 4, pp 282-288

Braasch MS (1992) *Characterization of GPS multipath errors in the final approach environment,* Proceedings of ION GPS-92, Albuquerque, 12 pp

Brossier R, Million C (1990) *Use of external data for aerial triangulation at the institute geogaphique national*, ISPRS Com I, Manaus

Brown RA (1992) *Instantaneous GPS attitude determination*, Proceedings of the IEEE Position Location and Navigation Symposium, Monterey, California, USA

Burnside CD (1979) *Mapping from aerial photographs*, Collins Professional and Technical Books, pp 348

Colomina I (1993) *A note on the analytics of aerial triangulation with GPS aerial control*, Photogrammetric Engineering & Remote Sensing, Vol. 59, No. 11, pp 1619-1624

Connan ME, Schwarz KP, Wei M, and Delikaraoglu D (1992) *A consistency test of airborne GPS using multiple monitor stations*, Bulletin Geodesique 66, pp 2-11

Corbett SJ (1993) *GPS for attitude determination and positioning in airborne remote sensing*, University of Newcastle Upon Tyne, UK

Corbett SJ (1994) *GPS single epoch ambiguity resolution for airborne positioning and orientation,* PhD Thesis, University of Newcastle Upon Tyne, UK

Corten FLJH (1984) *Navigation and sensor orientation systems in aerial photography*, ITC Journal, Vol. 1984(4), 9 pp

Cortes P, Heimes FJ (1988) *A comparative study of dynamic positioning by GPS*, ISPRS, Kyoto

Cross PA (1983) *Advanced least-squares applied to positing-fixing - Working paper No 6,* North East London Polytechnic, Department of Surveying, UK

Cross PA (1994) *Satellite position fixing systems,* Engineering Surveying Technology, Jonn Wiley & Sons, pp 111-145

Cross PA (1994) *DGPS - Has it come of age?,* Paper represented at the 3th differential GPS user and operators seminar, Hydrographic Society, Aberdeen, 10 pp

Crowl J, and Merchant D *Airborne GPS photogrammetric calibration and test ranges at Madison county, Ohio*

Curry S, and Schuckman K (1993) *Practical considerations for the use of airborne GPS for photogrammetry*, Photogrammetric Engineering & Remote Sensing, Vol. 59, No. 11, pp 1611-1617

Curry S, Salsig G and Whittaker K *A practical test of a photogrammetric project controlled with airborne GPS*

de Jong CD (1991) *GPS-Satellite Orbits and Atmospheric Effects,* Report of the Faculty of Geodetic Engineering, Mathematical and Physical Geodesy, No. 91.1, Delft University of Technology, The Netherland

Euler HJ and Landau H (1992) *Fast GPS ambiguity resolution on-the-fly for real time applications,* Proceeding of the Sixth International Geodetic Symposium on Satellite Positioning, Columbus, Ohio, USA, 10pp

Faig W and Shih TY (1989) *Should one consider combining kinematic GPS with aerial photogrammetry?*, Photogrammetric Engineering & Remote Sensing, Vol. 55, No. 12, pp 1723-1725

Frieβ P (1990) *Kinematic GPS for aerial photogrammetry - Empirical results*, Proceedings of the Second International Symposium on Precise Positioning System, Ottawa, Canada, 3-7 September, 16 pp

Frieβ P (1991) *Aerotriangulation with GPS - Methods, experience, expectation*, Proceedings of the 43rd Photogrammetric Week, Stuttgart, 7 pp

Georgiadou Y (1990) *Ionospheric delay modeling for GPS relative positioning.* Proceedings of the Second International Symposium on Precise Positioning System, Ottawa, Canada, 3-7 September, pp 466-476

Georgiadou Y, and Kleusberg A (1988a) *On the Effect of Ionospheric Delay on Geodetic Relative Positioning,* Manuscripta Geodetica, Vol 13, pp 8

Georgiadou Y, and Kleusberg A (1988b) *On carrier signal multipath effects in relative GPS positioning,* Manuscripta Geodetica, Vol 13

Griffiths H, Hilton PJ (1970) *A comprehensive textbook of classical Mathematics. A contemporary Interpretation,* Springer-Verlag, New York, 637 pp

Gruen A, Cocard M, and Kahle HG (1993) *Photogrammetry and kinematic GPS: Results of a high accuracy test,* Photogrammetric Engineering and Remote Sensing, Vol. 59, No. 11, pp 1643-1650

Habib A and Novak K *GPS controlled aerial triangulation of single flight lines*

Hatch R, Larsn K (1985) *MAGNET-4100 GPS survey program processing techniques and test results,* Proceedings of The First International Symposium on Precise Positioning with GPS, Rockville, Maryland, April 15-19, Vol. 1, pp 285-297

Hein GW (1989) *Precise kinematic GPS/INS positioning: A discussion on affiliations in aerophotogrammetry,* 42nd Photogrammetric Week, Stuttgart

Hoffmann-Wellenhof B, Lichtenegger H, and Collins J (1994) *GPS Theory and practice,* Springer-Verlag Wien, 355 pp

Hogholen A (1993) *Kinematic GPS in aerotriangulation in Finland,* Reports of The Finish Geodetic Institute 93:5

Ibrahim A M (1995) *Reliability analysis of combined GPS-aerial triangulation system,* PhD Thesis, University of Newcastle Upon Tyne, UK

Jacobsen K (1990) *European progress on GPS photogrammetry,* ASPRS, Denver

Jacobsen K, Li K (1990) *Bundle block adjustment using kinematic GPS positioning,* ISPRS Com I, Manaus

Jacobsen K (1991) *Trends in GPS photogrammetry,* ASPRS Baltimore 1991

Jacobsen K (1993) *Experience in GPS photogrammetry*, Photogrammetric Engineering and Remote Sensing, Vol. 59, No. 11, pp 1651-1658

Khalid MA (1990) *Post-processing strategies for precise static surveying,* PhD Thesis, University of Newcastle Upon Tyne, UK

King RW, Masters EG, Rizos C, Stolz E, Collins J (1987) *Surveying with Global Positioning System,* Dummler, Bonn

Lachapelle G, Cannon ME, Lu G (1992) *Ambiguity resolution on-the-fly a comparison of a P code and a high performance C/A code receiver technologies*, In Proceedings of ION GPS-92, Fifth International Technical Meeting of the Satellite Division of the Institute of Navigation, Albuquerque, New Mexico, pp 1025-1032

Landau H, Hundt R, Pagels C, Vollath U (1994) *Aircraft positioning and guidance with the global positioning system*, Proceedings of KIS-94, Banff, 8 pp

Lapine L (1992) *Analytical calibration of the airborne photogrammetric system using a priori knowledge of the exposure station obtained from GPS technique*, Dept. of Geodetic Science and Surveying, The Ohio State University, UMI Dissertation Services, Publication No. 9111738, Ann Arbor, MI 48109

Leatherdale JD (1988) *Requirements for photo control*, Photogrammetric Record, Vol.12 (71), 15 pp

Leick A (1995) *Satellite Surveying,* John Wiley and Sons, 560 pp

Melbourne WG (1985) *The case for ranging in GPS based geodetic system,* First International Symposium on Precise Positioning with GPS, Rockville

Merchant DC (1993) *GPS controlled aerial photogrammetry*, Photogrammetric Engineering & Remote Sensing, Vol. 59, No. 11, pp 1633-1636

Microsoft Cooperation (1990) C for yourself, 418 pp

Mrstik T and Kusevic K (1994) *Kinematik and On-The-Fly software for a 1:500 GPS photogrammetry application*, Proceedings of KIS-94, Banff, 11 pp

Nesbo I and Canter P (1990) *GPS attitude determination for navigation*, GPS World, October 1990, pp 36-39

Nolan JM, Gourevitch SA, Ladd JW (1992) *Geodetic processing using full dual band observables*, In Proceedings of ION GPS-92, Fifth International Technical Meeting of the Satellite Division of the Institute of Navigation, Albuquerque, New Mexico, pp 1033-1041

Press WH, Teukolsky SA, Vetterling WT and Flannery BP (1992) *Numerical recipes in C: The art of scientific computing*, (second edition) Cambridge [Cambridgeshire], New York, Cambridge University Press, 994 pp

Quinn PG (1993) *Instantaneous attitude determination*, Proceedings of ION GPS-93, Salt Lake City, Utah, USA, Vol. 1, pp 603-615

Rath J and Ward P (1989) *Attitude estimation using GPS*, Proceedings of the National Technical Meeting of the Institution of Navigation, San Mateo, California, USA,

Remondi BW (1984) *Using the global positioning system (GPS) phase observables for relative geodesy: Modeling, Processing, and Results,* PhD Dissertation, U. of Texas at Austin.

Remondi BW, Hofmann-Wellenhof B (1989) *GPS broadcast orbits versus precise orbits: A comparison study. Global Positioning System: An overview,* IAG Symposium No. 102, Edinburgh, Scotland, 7-8 August, pp 203-217

Rochen C, Meertens C (1991) *Monitoring selective availability dither frequenciesand their effect on GPS data.* Bulletin Geodesique 65(3), pp 162-169

Roth BD (1986) *Application of Navstar GPS to precision attitude determination,* Proceedings of the Fourth International Geodetic Symposium on Satellite Positioning, Austin, Texas, USA, Vol. 2, pp 1345-1359

Royal Institution of Chartered Surveyors (1988) *Specifications for mapping at scales between 1:1000 and 1:10000*, Second Edition, Surveyors Publication, 20 pp

Santerre R (1991) *Impact of GPS satellite sky distribution.* Manuscripta Geodetica 16(1), pp 28-53

Schade H (1992) *Reduction of systematic errors in GPS based photogrammetry for fast ambiguity resolution techniques*, International Archive of Photogrammetry and Remote Sensing, Commission I, Vol. XXIX, Part B1, pp 223-228

Schade H, Cramer M (1994) *Airborne kinematic attitude determination with GPS for photogrammetry and remote sensing*, Proceedings of KIS-94, Banff, 8 pp

Schwarz KP, Chapman MA, Cannon MW, Gong P (1993) *An integrated INS/GPS approach to the georeferencing of remotely sensed data,* Photogrammetric Engineering and Remote Sensing, Vol. 59(11), 8 pp

Teunissen PJG, de Jonge PJ, and Tiberius CCJM (1995) *The Lambda-Method for fast GPS surveying,* Proceedings International Symposium GPS Technology Applications, Bucharest, Romania, pp 203-210

Tolman BW, Clynch JR, Coco DS, Leach MP (1990) *The effect of selective availabilty on differential GPS positioning.* Proceedings of the (U.S.) Institute of Navigation ION GPS-90, Colorado Springs, U.S.A., 19-21 September, pp 579-586

van der Vegt HJM, Boswinkel D, Witmer R (1988) *Utilisation of GPS in large scale photogrammetry*, ISPRS, Kyoto

van Graas F and Braasch MS (1991) *GPS interferometric attitude and heading determination: Initial flight test results*, Proceedings of the 47th Annual Meeting of the Institute of Navigation, Williamsburg, VA, USA

Wild U, Beutler G, Gurtner W, Rothacher M (1989) *Estimating the Ionosphere using one or more dual frequency GPS receivers,* Proceedings of the Fifth International Geodetic Symposium on Satellite Positioning, Las Cruces, U.S.A., 13-17 March, pp 724-736

Wolf R P, (1983) *Elements of photogrammetry*, McGraw-Hill, 628 pp

Wubbena G (1985) *Software development for geodetic positioning with GPS using TI 4100 code and carrier measurements,* First International Symposium on Precise Positioning with GPS, Rockville, Maryland, April 15-19.

APPENDIX A

A. DERIVATION OF COLLINEARITY EQUATIONS

A.1 PHOTOGRAMMETRIC COORDINATE SYSTEM

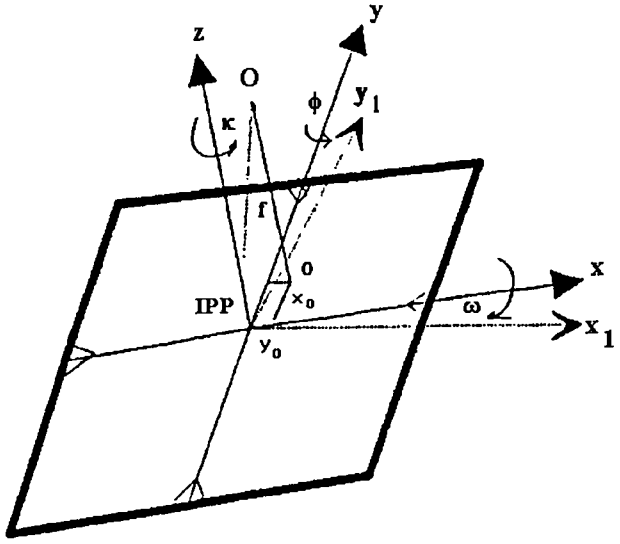

Figure A.a Photo and image coordinate systems

For cameras with side fiducial marks, the commonly adopted reference system for photogrammetric coordinates is the rectangular axis system formed by joining opposite fiducial marks with straight lines. The intersection point of these lines is the origin of this system (i.e. indicated principal point: IPP in the figure). The **x** axis is usually arbitrarily designated as the fiducial line most nearly parallel with the direction of flight, positive in the direction of flight. The positive **y** axis is 90^0 counterclockwise from positive **x**. These two axes constitute the two dimensional photogrammetric coordinate system. In the three dimensional photogrammetric coordinate system (the image coordinate system), in addition to these **x** and **y** axes the **z** axis is considered to be positive upward to constitute a right-handed coordinate system **xyz**. If the camera is perfect, the calibrated principal point (**o** in the figure) will coincide with the indicated principal point. The calibrated principal point is geometrically defined as the foot of the perpendicular dropped from the perspective center (**O** in the figure) to the plane of photograph and its coordinates in the image coordinate system are x_0 and y_0 (the third

coordinate being zero). The coordinates of the perspective center in the **xyz** image coordinate system are therefore x_0, y_0, **f**, where **f** is the camera principal distance.

A.2 THREE DIMENSIONAL COORDINATE ROTATION

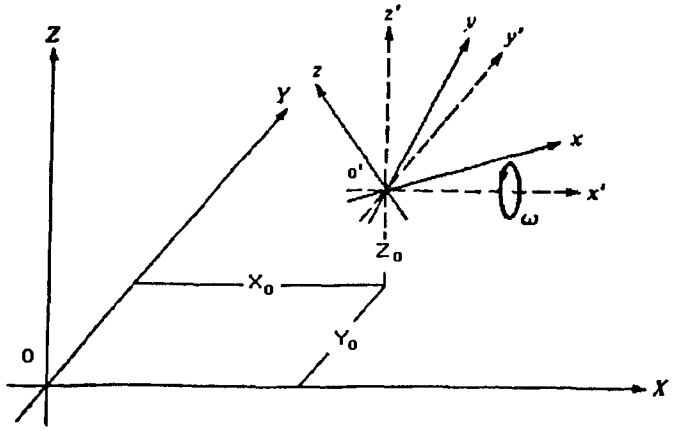

Figure A.b XYZ and **xyz** right-handed three-dimensional coordinate system

In figure A.b an **x'y'z'** coordinate system parallel to the **XYZ** object system is constructed with its origin at the origin of the **xyz** system. In the development of rotation formulas, it is customary to consider the three rotations as taking place so as to convert from the **x'y'z'** system to the **xyz** system. The rotation equations are developed in a sequence of three independent two-dimensional rotations. These rotations are first, ω rotation about the **x'** axis which converts coordinates from the **x'y'z'** system into an $\mathbf{x_1y_1z_1}$ system; second, ϕ rotation about the once rotated $\mathbf{y_1}$ axis which converts coordinates from the $\mathbf{x_1y_1z_1}$ system into an $\mathbf{x_2y_2z_2}$ system; second, κ rotation about the twice rotated $\mathbf{z_2}$ axis which converts coordinates from the $\mathbf{x_2y_2z_2}$ system into an **xyz** system of figure A.b. The exact amount and direction of the rotations for any three-dimensional coordinate transformation will depend upon the orientation relationship between the **xyz** and **XYZ**.

The development of the rotation formulas is as follows:

First rotation through the angle ω about the **x'** axis, as illustrated in figure A.c. The coordinates of any point A in the once rotated $\mathbf{x_1y_1z_1}$ system, as shown graphically in figure A.c, are

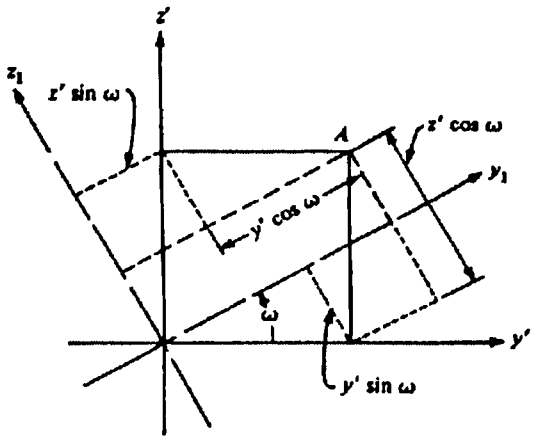

Figure A.c Omega rotation about the x' axis.

$$x_1 = x'$$

$$y_1 = y' \cos\omega + z' \sin\omega \qquad (A.1)$$

$$z_1 = -y' \sin\omega + z' \cos\omega$$

Since this rotation was about x', the x' and x_1 axes are coincident and therefore the x coordinate of A is unchanged.

Second, rotation through the angle ϕ about the $\mathbf{y_1}$ axis, as illustrated in figure A.d. The coordinates of A in the twice rotated $\mathbf{x_2y_2z_2}$ system, as shown graphically in figure A.d, are

$$x_2 = -z_1 \sin\phi + x_1 \cos\phi$$

$$y_2 = y_1 \qquad (A.2)$$

$$z_2 = z_1 \cos\phi + x_1 \sin\phi$$

Since this rotation was about y_1, the y_1 and y_2 axes are coincident and therefore the y coordinate of A is unchanged. Substituting equations (A.1) into (A.2):

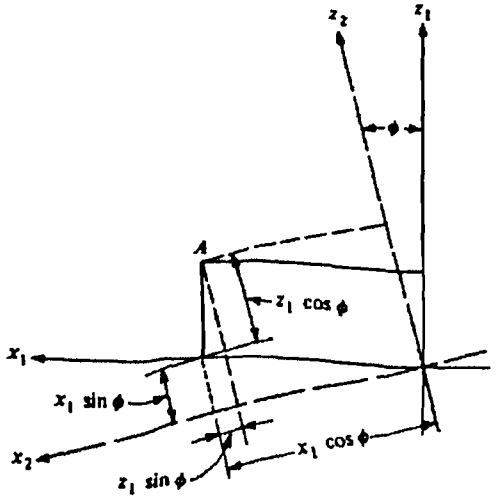

Figure A.d Phi rotation about the y_1 axis.

$$x_2 = -(-y' \sin\omega + z' \cos\omega)\sin\phi + x' \cos\phi$$
$$y_2 = y' \cos\omega + z' \sin\omega \qquad (A.3)$$
$$z_2 = (-y' \sin\omega + z' \cos\omega)\cos\phi + x' \sin\phi$$

Third, rotation through the angle κ about the z_2 axis, as illustrated in figure A.e. The coordinates of A in the three times rotated coordinate system, which has now become the **xyz** system as shown graphically in figure A.e, are

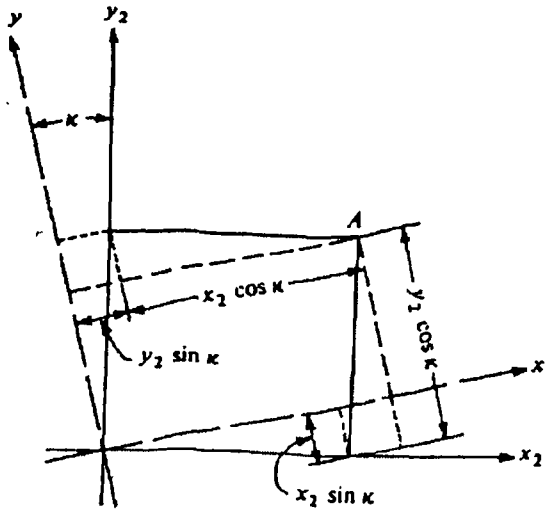

Figure A.e Kappa rotation about the z_2 axis.

$$x = x_2 \cos\kappa + y_2 \sin\kappa$$
$$y = -x_2 \sin\kappa + y_2 \cos\kappa \qquad (A.4)$$

$$z = z_2$$

Since this rotation was about z_2, the z_2 and z axes are coincident and therefore the z coordinate of A is unchanged. Substituting equations (A.3) into (A.4):

$$\begin{aligned} x &= [(y' \sin\omega - z' \cos\omega) \sin\phi + x' \cos\phi] \cos k \\ &\quad + (y' \cos\omega + z' \sin\omega) \sin\kappa \\ y &= [(-y' \sin\omega + z' \cos\omega) \sin\phi - x' \cos\phi] \sin\kappa \\ &\quad + (y' \cos\omega + z' \sin\omega) \operatorname{con}\kappa \\ z &= (-y' \sin\omega + z' \cos\omega) \cos\phi + x' \sin\phi \end{aligned} \qquad (A.5)$$

Factoring equations (A.5)

$$\begin{aligned} x &= x' (\cos\phi \cos\kappa) + y' (\sin\omega \sin\phi \cos\kappa + \cos\omega \sin\kappa) \\ &\quad + z' (-\cos\omega \sin\phi \cos\kappa + \sin\omega \sin\kappa) \\ y &= x' (-\cos\phi \sin\kappa) + y' (-\sin\omega \sin\phi \sin\kappa + \cos\omega \cos\kappa) \\ &\quad + z' (\cos\omega \sin\phi \sin\kappa + \sin\omega \cos\kappa) \\ z &= x' (\sin\phi) + y' (-\sin\omega \cos\phi) + z' (\cos\omega \cos\phi) \end{aligned} \qquad (A.6)$$

Substituting m's for the coefficients of x', y', and z' in equation (A.6), these equations are

$$\begin{aligned} x &= m_{11} x' + m_{12} y' + m_{13} z' \\ y &= m_{21} x' + m_{22} y' + m_{23} z' \\ z &= m_{31} x' + m_{32} y' + m_{33} z' \end{aligned} \qquad (A.7)$$

where

$$\begin{aligned} m_{11} &= \cos\phi \cos\kappa \\ m_{12} &= \sin\omega \sin\phi \cos\kappa + \cos\omega \sin\kappa \\ m_{13} &= -\cos\omega \sin\phi \cos\kappa + \sin\omega \sin\kappa \end{aligned}$$

$$
\begin{aligned}
m_{21} &= -\cos\phi \sin\kappa \\
m_{22} &= -\sin\omega \sin\phi \sin\kappa + \cos\omega \cos\kappa \\
m_{23} &= \cos\omega \sin\phi \sin\kappa + \sin\omega \cos\kappa \\
m_{31} &= \sin\phi \\
m_{32} &= -\sin\omega \cos\phi \\
m_{33} &= \cos\omega \cos\phi
\end{aligned}
\qquad (A.8)
$$

Equations (A.8) may be expressed in matrix form as

$$X = M X'$$

where

$$X = \begin{bmatrix} x \\ y \\ z \end{bmatrix} \quad M = \begin{bmatrix} m_{11} & m_{12} & m_{13} \\ m_{21} & m_{22} & m_{23} \\ m_{31} & m_{32} & m_{33} \end{bmatrix} \quad \text{and} \quad X' = \begin{bmatrix} x' \\ y' \\ z' \end{bmatrix} \qquad (A.9)$$

The matrix M is commonly called the **rotation matrix**.

A.3 DEVELOPMENT OF THE COLLINEARITY CONDITION EQUATIONS

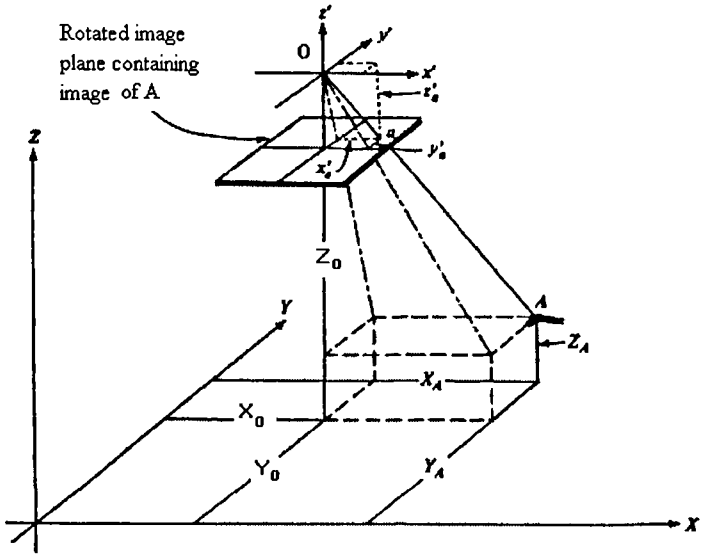

Figure A.f Image coordinate system rotated such that it is parallel to the object space coordinate system.

$$y_a' = \left(\frac{Y_A - Y_O}{Z_A - Z_O}\right) z_a' \qquad \text{(A.11)b}$$

Also, by identity

$$z_a' = \left(\frac{Z_A - Z_O}{Z_A - Z_O}\right) z_a' \qquad \text{(A.11)c}$$

Substituting (A.11)a, (A.11)b, and (A.11)c into equations

$$x_a = m_{11}\left(\frac{X_A - X_O}{Z_A - Z_O}\right) z_a' + m_{12}\left(\frac{Y_A - Y_O}{Z_A - Z_O}\right) z_a' + m_{13}\left(\frac{Z_A - Z_O}{Z_A - Z_O}\right) z_a' \qquad \text{(A.12)}$$

$$y_a = m_{21}\left(\frac{X_A - X_O}{Z_A - Z_O}\right) z_a' + m_{22}\left(\frac{Y_A - Y_O}{Z_A - Z_O}\right) z_a' + m_{23}\left(\frac{Z_A - Z_O}{Z_A - Z_O}\right) z_a' \qquad \text{(A.13)}$$

$$z_a = m_{31}\left(\frac{X_A - X_O}{Z_A - Z_O}\right) z_a' + m_{32}\left(\frac{Y_A - Y_O}{Z_A - Z_O}\right) z_a' + m_{33}\left(\frac{Z_A - Z_O}{Z_A - Z_O}\right) z_a' \qquad \text{(A.14)}$$

Factoring the term (z'_a / Z_A - Z_O) from equations A.12 through A.14, dividing A.12 and A.13 by A.14, and substituting (- f) for z_a , the following collinearity equations result:

$$x_a = -\mathrm{f}\left[\frac{m_{11}(X_A - X_O) + m_{12}(Y_A - Y_O) + m_{13}(Z_A - Z_O)}{m_{31}(X_A - X_O) + m_{32}(Y_A - Y_O) + m_{33}(Z_A - Z_O)}\right] \qquad \text{(A.15)}$$

$$y_a = -\mathrm{f}\left[\frac{m_{21}(X_A - X_O) + m_{22}(Y_A - Y_O) + m_{23}(Z_A - Z_O)}{m_{31}(X_A - X_O) + m_{32}(Y_A - Y_O) + m_{33}(Z_A - Z_O)}\right] \qquad \text{(A.16)}$$

APPENDIX B

B. LINEARISATION OF THE MODIFIED COLLINEARITY EQUATIONS

Dropping the subscripts for a moment, equations (3.25) and (3.26) (see section 3.4.3) can be written as:

$$x = -\mathrm{f}\frac{\mathrm{R}_1 X + x_a}{\mathrm{R}_3 X + z_a} \qquad (\mathrm{B.1})$$

$$y = -\mathrm{f}\frac{\mathrm{R}_2 X + y_a}{\mathrm{R}_3 X + z_a} \qquad (\mathrm{B.2})$$

where:

$$\mathrm{R} = [\,\mathrm{R}_1\ \mathrm{R}_2\ \mathrm{R}_3\,]^{\mathrm{T}}; \qquad \mathbf{R} = \begin{bmatrix} r_{11} & r_{12} & r_{13} \\ r_{21} & r_{22} & r_{23} \\ r_{31} & r_{32} & r_{33} \end{bmatrix} \qquad (\mathrm{B.3})$$

$$\mathbf{X} = \begin{bmatrix} X - X_A \\ Y - Y_A \\ Z - Z_A \end{bmatrix}$$

where

$[\,X\ Y\ Z\,]^{\mathrm{T}}$ are the ground coordinates of the point whose image coordinates are measured.

$[\,X_A\ Y_A\ Z_A\,]^{\mathrm{T}}$ are the antenna coordinates associated with the photo in which the point whose coordinates are measured appears in.

x_a , y_a and z_a are the antenna offset components in the camera coordinate system.

Equation B.1 can be written as:

$$\bar{\ell} = \mathbf{F}(\bar{x})$$

or

$$\ell + \mathbf{v} = \mathbf{F}(x^0 + x) \qquad (B.4)$$

where:

$\ell = \begin{bmatrix} x_i & y_i \end{bmatrix}^T$; vector containing the observed photo coordinates of points corrected for the known systematic errors and for the offset of the principal point (i = 1 to n and n is the total number of points in the block whose image coordinates are measured).

$v = \begin{bmatrix} v_{x_i} & v_{x_i} \end{bmatrix}^T$; vector containing the true residuals of the observed photo coordinates of points.

x^0 is vector containing the approximate values of the unknown parameters.

x is vector containing the true corrections to be applied to the approximate parameters.

Expanding equation B.4 using Taylor's series to first order results in the following:

$$\ell + v = \mathbf{F}(x^0) + \frac{\partial \mathbf{F}}{\partial \mathbf{x}} x \Big| \bar{x} = x^0$$

or

$$\ell - \mathbf{F}(x^0) + v = + \frac{\partial \mathbf{F}}{\partial \mathbf{x}} x \Big| \bar{x} = x^0$$

i.e.

$$b + v = Ax \qquad (B.5)$$

where:

$\mathbf{F(x^0)}$ is the function evaluated using the approximate values of the unknown parameters, $A = \partial F/\partial \bar{x}$ is the design matrix evaluated using the approximate values of unknown parameters and the observations and it takes the form given by equation 3.8 of section 3.4.2 and ***b*** takes the general form below.

$$\mathbf{b} = \begin{bmatrix} \ell_1 - f_1(x^0) \\ \ell_2 - f_2(x^0) \\ \cdots \\ \cdots \\ \ell_{2n} - f_{2n}(x^0) \end{bmatrix} \qquad (B.6)$$

Using equations B.1, we can write:

$$\frac{\partial x}{\partial \omega} = \frac{-f}{(R_3X + z_a)^2}\{[R_3X + z_a][\frac{\partial(R_1X + x_a)}{\partial \omega}] - [R_1X + x_a][\frac{\partial(R_3X + z_a)}{\partial \omega}]\} \qquad (B.7)a$$

Writing the partial derivatives of ***R*** with respect to ω as $\frac{\partial R}{\partial \omega} = [R_{\omega 1} \quad R_{\omega 2} \quad R_{\omega 3}]$

where $R_{\omega 1}$, $R_{\omega 2}$, $R_{\omega 3}$ are column matrices, (B.7)a can be written as:

$$\frac{\partial x}{\partial \omega} = \frac{-f}{(R_3X + z_a)^2}[(R_3X + z_a)(R_{\omega 1}X + x_a) - (R_1X + x_a)(R_{\omega 3}X + z_a)] \qquad (B.7)b$$

From equation (B.1), we can write:

$$R_1X + x_a = \frac{-x}{f}(R_3X + z_a) \qquad (B.7)c$$

which when substituted into (B.7)b yields:

$$\frac{\partial x}{\partial \omega} = -[f(R_{\omega 1}X + x_a) + x(R_{\omega 3}X + z_a)]/q \qquad (B.8)$$

where:

$$q = R_3 X + z_a$$

Similarly

$$\frac{\partial x}{\partial \phi} = -[\mathbf{f}(R_{\phi 1} X + x_a) + x(R_{\phi 3} X + z_a)]/q \qquad (B.9)$$

$$\frac{\partial x}{\partial \kappa} = -[\mathbf{f}(R_{\kappa 1} X + x_a) + x(R_{\kappa 3} X + z_a)]/q \qquad (B.10)$$

also

$$\frac{\partial x}{\partial X_A} = \frac{-f}{(R_3 X + z_a)^2}\{[R_3 X + z_a][\frac{\partial(R_1 X + x_a)}{\partial X_A}] - [R_1 X + x_a][\frac{\partial(R_3 X + z_a)}{\partial X_A}]\}$$

$$= \frac{-f}{(R_3 X + z_a)^2}[-(R_3 X + z_a) r_{11} + (R_1 X + x_a) r_{31}]$$

which when the value of $R_1 X + x_a$ (equation (B.7)c) is substituted into it yields:

$$\frac{\partial x}{\partial X_A} = [\mathbf{f} r_{11} + x r_{31}]/q \qquad (B.11)$$

and similarly

$$\frac{\partial x}{\partial Y_A} = [\mathbf{f} r_{12} + x r_{32}]/q \qquad (B.12)$$

$$\frac{\partial x}{\partial Z_A} = [\mathbf{f} r_{13} + x r_{33}]/q \qquad (B.13)$$

$$\frac{\partial x}{\partial X} = -[\mathbf{f} r_{11} + x r_{31}]/q \qquad (B.14)$$

$$\frac{\partial x}{\partial Y} = -[\mathbf{f} r_{12} + x r_{32}]/q \qquad (B.15)$$

$$\frac{\partial x}{\partial Z} = -[\mathbf{f} r_{13} + x r_{33}]/q \qquad (B.16)$$

In a similar way

$$\frac{\partial y}{\partial \omega} = -[\mathbf{f}(R_{\omega 2}X + y_a) + y(R_{\omega 3}X + z_a)]/q \qquad (B.17)$$

$$\frac{\partial y}{\partial \phi} = -[\mathbf{f}(R_{\phi 2}X + y_a) + y(R_{\phi 3}X + z_a)]/q \qquad (B.18)$$

$$\frac{\partial y}{\partial \kappa} = -[\mathbf{f}(R_{\kappa 2}X + y_a) + y(R_{\kappa 3}X + z_a)]/q \qquad (B.19)$$

$$\frac{\partial y}{\partial X_A} = [\mathbf{f}r_{21} + yr_{31}]/q \qquad (B.20)$$

$$\frac{\partial y}{\partial Y_A} = [\mathbf{f}r_{22} + yr_{32}]/q \qquad (B.21)$$

$$\frac{\partial y}{\partial Z_A} = [\mathbf{f}r_{23} + yr_{33}]/q \qquad (B.22)$$

$$\frac{\partial y}{\partial X} = -[\mathbf{f}r_{21} + yr_{31}]/q \qquad (B.23)$$

$$\frac{\partial y}{\partial Y} = -[\mathbf{f}r_{22} + yr_{32}]/q \qquad (B.24)$$

$$\frac{\partial y}{\partial Z} = -[\mathbf{f}r_{23} + yr_{33}]/q \qquad (B.25)$$

If the rotation matrix, **R**, given by equation (B.3) is written as:

$$\mathbf{R} = \begin{bmatrix} r_{11} & r_{12} & r_{13} \\ r_{21} & r_{22} & r_{23} \\ r_{31} & r_{32} & r_{33} \end{bmatrix}$$

then the partial derivatives of **R** with respect to the three rotations ω, ϕ and κ can be written as:

$$\frac{\partial R}{\partial \omega} = \begin{bmatrix} 0 & \cos\omega \sin\phi \cos\kappa - \sin\omega \sin\kappa & \sin\omega \sin\phi \cos\kappa + \cos\omega \sin\kappa \\ 0 & -\cos\omega \sin\phi \sin\kappa - \sin\omega \cos\kappa & -\sin\omega \sin\phi \sin\kappa + \cos\omega \cos\kappa \\ 0 & -\cos\omega \cos\phi & -\sin\omega \cos\phi \end{bmatrix}$$

$$= \begin{bmatrix} 0 & -r_{13} & r_{12} \\ 0 & -r_{23} & r_{22} \\ 0 & -r_{33} & r_{32} \end{bmatrix} \qquad (B.26)$$

$$\frac{\partial R}{\partial \phi} = \begin{bmatrix} -\sin\phi \cos\kappa & \sin\omega \cos\phi \cos\kappa & -\cos\omega \cos\phi \cos\kappa \\ \sin\phi \sin\kappa & -\sin\omega \cos\phi \sin\kappa & \cos\omega \cos\phi \sin\kappa \\ \cos\phi & \sin\omega \sin\phi & -\cos\omega \cos\phi \end{bmatrix} \qquad (B.27)$$

$$\frac{\partial R}{\partial \kappa} = \begin{bmatrix} -\cos\phi \sin\kappa & -\sin\omega \sin\phi \sin\kappa + \cos\omega \cos\kappa & \cos\omega \sin\phi \sin\kappa + \sin\omega \cos\kappa \\ -\cos\phi \cos\kappa & -\sin\omega \sin\phi \cos\kappa - \cos\omega \sin\kappa & \cos\omega \sin\phi \cos\kappa - \sin\omega \sin\kappa \\ 0 & 0 & 0 \end{bmatrix}$$

$$= \begin{bmatrix} r_{21} & r_{22} & r_{23} \\ -r_{11} & -r_{12} & -r_{13} \\ 0 & 0 & 0 \end{bmatrix} \qquad (B.28)$$

Substitution of the relevant values of the partial derivatives of **R** with respect to the rotational elements (i.e. ω, ϕ, κ) in to equation (B.8), (B.9), (B.10), (B.17), (B.18) and (B.19) finally gives the partial derivatives of **F** with respect to the unknown parameters as:

$$\frac{\partial x}{\partial \omega} = [x\,(r_{33}\,dY - r_{32}\,dZ + z_a) + f(r_{13}\,dY - r_{12}\,dZ + x_a)]/q$$

$$\frac{\partial x}{\partial \phi} = [x\,(\cos\omega \sin\phi\,dZ - \cos\phi\,dX - \sin\omega \sin\phi\,dY + z_a) +$$
$$f(\sin\phi \cos\kappa\,dX - \sin\omega \cos\phi \cos\kappa\,dY + \cos\omega \cos\phi \cos\kappa\,dZ + x_a)]/q$$

$$\frac{\partial x}{\partial \kappa} = -f/q\,(r_{21}\,dX + r_{22}\,dY + r_{23}\,dZ + x_a)$$

$$\frac{\partial x}{\partial X_A} = (r_{11}\ \mathrm{f} + r_{31}\, x)/q$$

$$\frac{\partial x}{\partial Y_A} = (r_{12}\ \mathrm{f} + r_{32}\, x)/q$$

$$\frac{\partial x}{\partial Z_A} = (r_{13}\ \mathrm{f} + r_{33}\, x)/q$$

$$\frac{\partial x}{\partial X} = -(r_{11}\ \mathrm{f} + r_{31}\, x)/q$$

$$\frac{\partial x}{\partial Y} = -(r_{12}\ \mathrm{f} + r_{32}\, x)/q$$

$$\frac{\partial x}{\partial Z} = -(r_{13}\ \mathrm{f} + r_{33}\, x)/q$$

and similarly

$$\frac{\partial y}{\partial \omega} = [y (r_{33}\, \mathrm{dY} - r_{32}\, \mathrm{dZ} + z_a) + \mathrm{f} (r_{23}\, \mathrm{dY} - r_{22}\, \mathrm{dZ} + y_a)]/q$$

$$\frac{\partial y}{\partial \phi} = [y (\cos\omega \sin\phi\, \mathrm{dZ} - \cos\phi\, \mathrm{dX} - \sin\omega \sin\phi\, \mathrm{dY} + z_a) +$$
$$\mathrm{f} (\sin\omega \cos\phi \sin\kappa\, \mathrm{dY} - \cos\omega \cos\phi \sin\kappa\, \mathrm{dZ} + \sin\phi \sin\kappa\, \mathrm{dX} + y_a)]/q$$

$$\frac{\partial y}{\partial \kappa} = \mathrm{f}/q (r_{11}\, \mathrm{dX} + r_{12}\, \mathrm{dY} + r_{13}\, \mathrm{dZ} + y_a)$$

$$\frac{\partial y}{\partial X_A} = (r_{21}\ \mathrm{f} + r_{31}\, y)/q$$

$$\frac{\partial y}{\partial Y_A} = (r_{22}\ \mathrm{f} + r_{32}\ y)/q$$

$$\frac{\partial y}{\partial Z_A} = (r_{23}\ \mathrm{f} + r_{33}\ y)/q$$

$$\frac{\partial y}{\partial X} = -(r_{21}\ \mathrm{f} + r_{31}\, y)/q$$

$$\frac{\partial y}{\partial Y} = -(r_{22}\ \mathrm{f} + r_{32}\ y)/q$$

$$\frac{\partial y}{\partial Z} = -(r_{23}\ \mathrm{f} + r_{33}\ y)/q$$

where

$$q = r_{31}\,\mathrm{dX} + r_{32}\,\mathrm{dY} + r_{33}\,\mathrm{dZ} + z_a$$

$$\mathrm{dX} = X - X_A\,,\quad \mathrm{dY} = Y - Y_A\,,\quad \mathrm{dZ} = Z - Z_A$$

Each image points in each photograph will have a ray represented by two equations of the general form shown by equation (B.29) below.

$$A_{ij}\delta R_j + B_{ij}\delta P_j + C_{ij}\delta G_i = b_{ij} + v_{ij} \qquad (\mathrm{B.29})$$

where:

subscript i refers to the point number and subscript j refers to the photo number.

δR_j, δP_j and δG_j are corrections to be added to the approximate values of the rotation elements of photo j, the antenna coordinates associated with photo j and the ground coordinates of point i respectively.

A_{ij} , B_{ij} and C_{ij} , given by equations (B.30)a, (B.30)b and (B.30)c, are the partial derivatives of the functions with respect to the rotation elements of photo j, antenna coordinates associated with photo j and the ground coordinates of the ith point respectively evaluated using the approximate values of parameters and the observations. It is worth noting here that the above mentioned matrices form the design matrix (A) partitioned into these three matrices.

$$A_{ij} = \begin{bmatrix} \dfrac{\partial x_{ij}}{\partial \omega_j} & \dfrac{\partial x_{ij}}{\partial \phi_j} & \dfrac{\partial x_{ij}}{\partial \kappa_j} \\ \dfrac{\partial y_{ij}}{\partial \omega_j} & \dfrac{\partial y_{ij}}{\partial \phi_j} & \dfrac{\partial y_{ij}}{\partial \kappa_j} \end{bmatrix} \qquad (\mathrm{B.30})\mathrm{a}$$

$$B_{ij} = \begin{bmatrix} \frac{\partial x_{ij}}{\partial X_{Aj}} & \frac{\partial x_{ij}}{\partial Y_{Aj}} & \frac{\partial x_{ij}}{\partial Z_{Aj}} \\ \frac{\partial y_{ij}}{\partial X_{Aj}} & \frac{\partial y_{ij}}{\partial Y_{Aj}} & \frac{\partial y_{ij}}{\partial Z_{Aj}} \end{bmatrix} \qquad \text{(B.30)b}$$

$$C_{ij} = \begin{bmatrix} \frac{\partial x_{ij}}{\partial X_{i}} & \frac{\partial x_{ij}}{\partial Y_{i}} & \frac{\partial x_{ij}}{\partial Z_{i}} \\ \frac{\partial y_{ij}}{\partial X_{i}} & \frac{\partial y_{ij}}{\partial Y_{i}} & \frac{\partial y_{ij}}{\partial Z_{i}} \end{bmatrix} \qquad \text{(B.30)c}$$

$$b_{ij} = \begin{bmatrix} x_{ij} + \mathrm{f}\dfrac{r^0_{11j}(X^0_i - X^0_{Aj}) + r^0_{12j}(Y^0_i - Y^0_{Aj}) + r^0_{13j}(Z^0_i - Z^0_{Aj}) + x_a}{r^0_{31j}(X^0_i - X^0_{Aj}) + r^0_{32j}(Y^0_i - Y^0_{Aj}) + r^0_{33j}(Z^0_i - Z^0_{Aj}) + z_a} \\ y_{ij} + \mathrm{f}\dfrac{r^0_{21j}(X^0_i - X^0_{Aj}) + r^0_{22j}(Y^0_i - Y^0_{Aj}) + r^0_{23j}(Z^0_i - Z^0_{Aj}) + y_a}{r^0_{31j}(X^0_i - X^0_{Aj}) + r^0_{32j}(Y^0_i - Y^0_{Aj}) + r^0_{33j}(Z^0_i - Z^0_{Aj}) + z_a} \end{bmatrix} \qquad \text{(B.31)}$$

$$\nu_{ij} = \begin{bmatrix} \nu_{x_{ij}} \\ \nu_{y_{ij}} \end{bmatrix} \qquad \text{(B.32)}$$

With a slight modification, the same matrices can be used for the case when no antenna coordinates are available by substituting zero for the antenna offset components and replacing the antenna coordinates (X_{Aj} , Y_{Aj} , Z_{Aj}) by the coordinates of the perspective center (X_{0j} , Y_{0j} , Z_{0j}).